



**HAL**  
open science

# Investigation of mechanochemical synthesis of condensed 1,4-diazines and pharmaceutically attractive hydrazones

Paulo Filho Marques de Oliveira

## ► To cite this version:

Paulo Filho Marques de Oliveira. Investigation of mechanochemical synthesis of condensed 1,4-diazines and pharmaceutically attractive hydrazones. Chemical and Process Engineering. Ecole des Mines d'Albi-Carmaux, 2015. English. NNT : 2015EMAC0007 . tel-01271090

**HAL Id: tel-01271090**

**<https://theses.hal.science/tel-01271090>**

Submitted on 8 Feb 2016

**HAL** is a multi-disciplinary open access archive for the deposit and dissemination of scientific research documents, whether they are published or not. The documents may come from teaching and research institutions in France or abroad, or from public or private research centers.

L'archive ouverte pluridisciplinaire **HAL**, est destinée au dépôt et à la diffusion de documents scientifiques de niveau recherche, publiés ou non, émanant des établissements d'enseignement et de recherche français ou étrangers, des laboratoires publics ou privés.



# THÈSE

En vue de l'obtention du

## DOCTORAT DE L'UNIVERSITÉ DE TOULOUSE

Délivré par :

École Nationale Supérieure des Mines d'Albi-Carmaux conjointement avec l'INP Toulouse

---

**Présentée et soutenue par :**  
**Paulo Filho MARQUES de OLIVEIRA**

le vendredi 30 octobre 2015

**Titre :**

Investigation of mechanochemical synthesis of condensed 1,4-diazines and pharmaceutically attractive hydrazones

---

**École doctorale et discipline ou spécialité :**

ED MEGEP : Génie des procédés et de l'Environnement

**Unité de recherche :**

Centre RAPSODEE, CNRS UMR 5302 - École des Mines d'Albi-Carmaux

**Directeur/trice(s) de Thèse :**

Directeur : Michel BARON

Co-directeur : Michel BALTAS

**Jury :**

Sylviane GIORGI-RENAULT - Professeur, Université de Paris Descartes

Marc DESCAMPS - Professeur, Université de Lille I

Jean MARTINEZ - Professeur, Université de Montpellier I

Michel BALTAS - Directeur de Recherche, Université de Toulouse III, UPS

Michel BARON - Professeur, École des Mines d'Albi-Carmaux

Alain CHAMAYOU - Maître-assistant, École des Mines d'Albi-Carmaux

Tomislav FRIŠČIĆ - Professeur, McGill University, Montréal (CA)

Brigitte GUIDETTI - Maître de conférences, Université de Toulouse III, UPS

Présidente

Rapporteur

Rapporteur

Examineur

Examineur

Examineur

Examineur

Examineur



*“...Imagination is more important than knowledge.  
Knowledge is limited. Imagination encircles the  
world.”*

*Albert Einstein (Berlin, 1929)*



*Ao meus pais... aos meus primeiros mestres. Àqueles que não me ensinaram matemática ou português, mas coisas que o ser humano nunca poderá aprender com a ciência racional. Como ser gente, como ser humilde, como ser digno, como ser forte e como ser humano... Obrigado Paulo e Iraides por acreditarem em mim e terem me dado a oportunidade de seguir os caminhos que escolhi.*



## Remerciements

It is not possible to develop or evolve in anything on your own. This thesis was raised by essential contributions from different people from different countries. The support, the help, the analyses and characterizations, but the most important, the smiles I have found, the coffee breaks and the words of encouragement. I hope that those people could find in these words my sincerest gratitude.

Je remercie l'École des Mines d'Albi-Carmaux et le centre de Recherche d'Albi en génie des Procédés des Solides Divisé, de l'Énergie et de l'Environnement (RAPSODEE) de m'avoir donné la possibilité de développer les travaux inclus dans ce manuscrit. Également, je remercie le Laboratoire de Synthèse et Physico-chimie de Molécules d'Intérêt Biologique (LSPCMIB) à l'Université Paul Sabatier (Toulouse III), d'avoir permis l'accès sans restrictions à leurs moyens. J'étais aussi un doctorant de chez vous.

Je tiens à remercier très chaleureusement mes encadrants de thèse de m'avoir accompagné tout au long de ces trois années, pour leur aide et compétence, mais aussi pour leur patience et leur encouragement à finir ce travail. Un très grand merci à mon directeur Michel Baron pour son soutien inestimable. Merci pour m'avoir appris que la science se fait aussi avec beaucoup d'imagination, et qu'il faut respecter, mais jamais nous limiter à des règles qui sont connues ou acceptées dans le domaine scientifique, si on veut vraiment avancer. Merci à mon co-encadrant Alain Chamayou pour son apport en Génie de Procédés, lequel a élargi encore plus le cadre des travaux multidisciplinaires de ces études. De la même façon, mes remerciements s'adressent à mon co-directeur Michel Baltas pour la vision sur la chimie thérapeutique, très nouvelle pour moi, mais que j'ai pu un peu apprendre, et de m'avoir ouvert la porte du LSPCMIB pour cette thèse. Finalement, je voudrais remercier vivement ma co-encadrante Brigitte Guidetti, ma professeure de caractérisation des molécules organiques, pour sa précieuse disponibilité, sa patience et sa sympathie.

Mes remerciements sont aussi destinés aux rapporteurs et aux autres membres du jury pour l'honneur qu'ils m'ont fait en évaluant mes travaux de thèse.

Nous devons remercier le CNRS-JSPS (Projet n° PRC0709, 2013-2014) pour le support financier du projet consacré à l'étude des mécanismes. Merci au Pr. Tohru Sato et à Naoki Haruta de l'Université de Kyoto pour notre collaboration très importante et fructueuse.

Durant ma thèse, j'ai eu le plaisir de travailler aux côtés des personnes qui ont été fondamentales pour l'évolution et la conclusion de mon doctorat. Je remercie Sylvie Delconfetto, bien sûr pour toutes les DSC, mais également il faut la remercier pour les



corrections du français, sa patience et son attention. Merci à Séverine Patry, Laurent Devrient (avec qui j'ai partagé le Labo 0C11), Philippe Accart pour la gentillesse et l'aide au quotidien au laboratoire et aussi pour les « bonjours » de tout les jours donnant plus d'énergie et de motivation. Un merci destiné à Nathalie Lyczko pour les marathons au DRX, pour son aide, sa disponibilité et ses mots encourageants. Je remercie également Bruno Boyer, Celine Boachon, Jean-Marie Sabatier, Christine Rolland et Véronique Nallet.

Je tiens encore à remercier les autres membres permanents du centre RAPSODEE, les enseignants-chercheurs, en particulier Rachel Calvet, toujours attentionnée, pour sa sympathie, toute l'aide et sa gentillesse. Merci au secrétariat gentil et exceptionnel du centre : Anne-Marie Fontes, Chrystel Auriol et Valérie Veres.

Cette thèse doit beaucoup à la Plateforme Gala, grâce à laquelle la collaboration entre le centre RAPSODEE et le LSPCMIB a pu être mise en place. J'en profite donc pour remercier Maria Inês Ré, tout d'abord d'avoir transmis l'opportunité d'un poste de doctorant au sein du Centre, dans un domaine qu'aujourd'hui je trouve très excitant, mais également de s'intéresser à mon quotidien au laboratoire et en France. Merci à Laurène Haurie, toujours sympathique, pour l'aide et l'accueil sur la Plateforme.

Mes remerciements doivent être aussi adressés à quelques membres du LSPCMIB et de l'Institut de Chimie de Toulouse. Merci à Christiane André-Barrès pour sa collaboration très importante qui a pu compléter et mettre en valeur les résultats de ces recherches. Merci à Caroline Toppa (RMN), Corinne Routaboul (FTIR), Isabelle Fabing (méthodes d'HPLC) et Yannick Coppel (CP-MAS NMR au LCC).

Je suis très reconnaissant des travaux de stage réalisés par Grazielle Aguiar et Marcos Gregório de Oliveira qui ont travaillé sur des sujets inclus dans cette thèse. Merci à vous deux, avec qui j'ai pu développer un peu mon côté encadrant, très important pour la suite de ma carrière, et également d'avoir partagé les difficultés et les réussites de la recherche scientifique.

Merci à mes amis, ceux que j'ai découverts pendant ce séjour en France. Les amis qui ont vécu avec moi chaque avancée, chaque pas, chaque frustration... Ceux que j'aimerai pour toute ma vie et que je dois beaucoup remercier pour le soutien, l'aide, la bonne humeur et les soirées ensemble. Plusieurs nationalités, différentes façons de voir... Les échanges ont été enrichissants !! Merci aux doctorants and post-doctorants. Nous avons pu partager des ambiances très amicales, des moments que je ne souhaite pas oublier. Un remerciement spécial à Claire, Briec, Fanny (aussi pour l'initiation au français), Graciela (et Stéphane), Haithem, Tassadit, Leonard, Margot, Marion, Marta, Marwa et William. Merci Lucía, le

sourire de tous les matins, la vie est vraiment toujours belle à sa vue. Maintenant je connais très bien la carte de l'Espagne... Hugo, avec son humour un peu acide et toute sa personnalité, mais toujours coopératif. Entre l'histoire de la France, les musiques et les films français, je me suis aussi enrichi de la culture française (les corrections de français sont également reconnues).

En parlant des amis, l'amitié d'Andréa était très importante. Nous avons partagé les très bons moments autant que les difficiles. Nous avons commencé cette période ensemble et nous avons fini ensemble. Merci pour ton amitié inconditionnelle. Nous allons beaucoup rigoler des épisodes vécus en France à chaque prochaine retrouvaille.

Aux brésiliens (plutôt brésiliennes) qui m'ont fait sentir un peu de l'air de mon pays. Toujours prêtes à aider, comme si nous nous connaissions des Carnavals d'avant. Merci Sue, mon premier contact en France, la personne la plus lumineuse et généreuse que je connaisse. Zeniths, Nay (et les rencontres dans les couloirs de RAPSODEE), Jacks et Bruna, merci pour l'amitié... également merci à ceux qui ont intégré cette communauté, Rafa et Benjamin.

Je ne peux pas oublier mes amis de toujours. Day, Lê, Robison, Line... Vous êtes à mes côtés depuis toujours. Merci pour votre confiance. Merci d'être mes amis, qui je suis... Lucas, merci pour tous les jours. Barbara et Rodolfo, des amis aussi pour la vie, pour la bonne humeur même dans des situations critiques et pour nos histoires ensemble.

Je dois remercier le laboratoire de polymères de l'EEL-USP, Brésil, où j'ai pris le goût pour la recherche à côté des gens admirables pour différentes raisons. Merci Amilton, Giza et Simone.

Enfin... je remercie ma famille, pour être toujours avec moi. Comme je l'ai dit avant, c'est aussi pour vous.

Amis, famille, les personnes sensationnelles que j'ai connues et qui resteront avec moi pour toujours. Muito obrigado!



## **Investigation of mechanochemical synthesis of condensed 1,4-diazines and pharmaceutically attractive hydrazones.**

**Abstract.** One of the goals of pharmaceutical and chemical industries is the development of green processes that eliminates or reduces the use of solvents. However, avoiding solvents often requires the use of metal catalysts or others, that accelerates chemical reactions, but make the purifications difficult, especially in the case of fine chemical products, such as active pharmaceutical ingredients. The mechanochemistry has emerged as a sustainable way that enables chemical synthesis, including organic molecular transformations, using the mechanical energy. In spite of the recent advances of the methodology, some aspects of the mechanical action still remain to be fully elucidated, mainly concerning the mechanisms. In this thesis, three main axes of mechanochemistry were explored. First, the molecular mechanism of 1,4-diazine mechanosynthesis, mentioning dibenzo[a,c]phenazine (DBPZ) and 2,3-diphenylquinoxaline (DPQ), is investigated by using  $^{13}\text{C}$  CP-MAS NMR that reveals intermediate species for DBPZ, and by calorimetric measurements that show continuation of the reaction after grinding for both reactions. The possibility of a concerted mechanism is considered for dibenzo[a,c]phenazine case. The second focus is on 2,3-diphenylquinoxaline product formation. The process parameters for a vibratory ball mill were studied. Grinding material, size and mass of the balls, granulometry of the starting material were assessed, as well as the temperature of the milling media, providing apparent activation energy ( $E_a$ ). Arrhenius and Eyring-Polanyi plots presented changes in  $E_a$  indicating changes in mechanism, which was attributed to a possible mechanically induced eutectic melting after 30 °C. Finally, after understanding some fundamentals and processes for those model reactions, the mechanochemical route was successfully applied to solid-state synthesis of pharmaceutically attractive phenolic hydrazones and catalyzed isoniazid derivatives synthesis, by reacting solid aldehydes and hydrazines. In general, the products were obtained in shorter times and in higher yields compared to classical thermal route. The roles of electronic and solid-state reactivity of the hydrazines were discussed. Biological assays demonstrated the great activity of isoniazid derivatives in inhibiting *Mycobacterium tuberculosis*. The results presented here cover the mechanochemistry at different levels. The fundamental comprehension is still difficult to access due to the complexity of the system, but some advances could be made such as the detection of intermediate species with significant lifetime. The process parameters are equally important to deduce some mechanism, but also for scale up purposes. At last, the mechanosynthesis of hydrazones showed to be a greener route to produce pharmaceuticals, for high screening of new ones, as well as for the synthesis of others, with great purity and waste reduction.

**Keywords:** Green Chemistry, Mechanochemistry, Mechanism, Kinetics, 1,4-diazine, Hydrazone.



## **Investigation de la synthèse mécano-chimique de 1,4-diazines condensées et d'hydrazones d'intérêt pharmaceutique**

**Résumé.** L'un des objectifs des industries chimique et pharmaceutique est de développer des procédés verts évitant ou réduisant l'utilisation de solvants. Mais ne pas utiliser de solvant nécessite souvent des catalyseurs métalliques ou autre, ce qui rend les purifications délicates, comme dans le cas des synthèses de chimie fine permettant l'obtention de principes actifs pharmaceutiques. C'est ainsi que la mécano-chimie a émergé en tant que voie durable pour la synthèse chimique, y compris dans le cas des transformations moléculaires organiques sous contrainte mécanique. Malgré les progrès récents de cette méthodologie, certains aspects de l'action mécanique ne sont pas totalement élucidés, en particulier ce qui concerne les mécanismes. Dans cette thèse, trois axes principaux de la mécano-chimie ont été explorés. Dans une première partie, le mécanisme moléculaire de la synthèse de deux types de 1,4-diazines, la dibenzo[a,c]phenazine (DBPZ) et la 2,3-diphenylquinoxaline (DPQ), a été investigué. La RMN  $^{13}\text{C}$  CP-MAS a permis de mettre en évidence des intermédiaires de cette synthèse, et des mesures calorimétriques ont révélé que deux réactions se poursuivaient après broyage. La possibilité d'une réaction concertée a également été prise en compte dans le cas de la dibenzo[a,c]phenazine. La seconde partie concerne la formation de la 2,3-diphenylquinoxaline. Les paramètres du procédé ont été étudiés, dans le cas d'un broyeur à bille vibrant. L'influence des matériaux de broyage, de la taille et de la masse des billes, la granulométrie des matières premières, ainsi que la température des media de broyage ont été étudiés, permettant de déterminer une énergie d'activation apparente ( $E_a$ ). Le tracé des courbes selon Arrhenius et Eyring-Polanyi a montré des changements de  $E_a$  caractéristiques de modifications au niveau du mécanisme, attribuées à l'apparition d'un possible eutectique fondant au-dessus de 30 °C, induit mécaniquement. Après cette étude qui a permis la compréhension de certains points fondamentaux, et d'approfondir les procédés de ces réactions modèles, une troisième partie traite de l'application de la mécano-chimie à la synthèse en phase solide d'hydrazones d'intérêt pharmaceutique, et à celle catalysée de dérivés de l'isoniazide obtenus par réaction d'aldéhydes et d'hydrazines. D'une manière générale, les durées de réaction sont plus faibles, et les rendements meilleurs, qu'avec les méthodes classiques. L'influence des réactivités électronique et des hydrazines à l'état solide a été discutée. Les essais biologiques ont démontré une activité avérée des dérivés de l'isoniazide dans l'inhibition de *Mycobacterium tuberculosis*. Les résultats présentés dans cette thèse englobent plusieurs aspects très complémentaires de la mécano-chimie. L'approche fondamentale du mécanisme est d'un accès difficile, en raison de la complexité du système, mais des avancées ont été réalisées comme la mise en évidence d'intermédiaires à longue durée de vie. Les paramètres du procédé apportent une contribution à la compréhension du mécanisme mais aussi en vue du scaling-up. Enfin, la mécanosynthèse s'est révélée être une méthode de chimie verte particulièrement adaptée à la synthèse d'hydrazones d'intérêt pharmaceutique, pour le screening de nouvelles entités ou la synthèse durable de produits de grande pureté.

**Mots clés:** Chimie Verte, Mécano-chimie, Mécanisme, Cinétique, 1,4-diazine, Hydrazone.



# Contents

<b>INTRODUCTION</b> .....	<b>1</b>
<b>CHAPTER 1. LITERATURE REVIEW</b> .....	<b>7</b>
<b>1.1 INTRODUCTION</b> .....	<b>9</b>
<b>1.1.1 Definition and terminology</b> .....	<b>9</b>
<b>1.1.2 Historical overview</b> .....	<b>10</b>
<b>1.1.3 Mechanoactors</b> .....	<b>12</b>
<b>1.2 MECHANOCHEMISTRY AS GREENER ROUTE TO PRODUCE CHEMICALS</b> .....	<b>14</b>
<b>1.3 MECHANOCHEMISTRY OF ORGANIC SYSTEMS</b> .....	<b>15</b>
<b>1.3.1 Mechanochemistry of macromolecules and mechanophores</b> .....	<b>16</b>
<b>1.3.2 Mechanochemistry of ball-milled organic reactions</b> .....	<b>18</b>
<i>1.3.2.1 Mechanochemical preparation of cocrystals</i> .....	<i>18</i>
<i>1.3.2.2 Mechanochemical preparation of metal-organic frameworks</i> .....	<i>19</i>
<i>1.3.2.3 Organic ball milling reactions with covalent C-C and C-X bond formation</i> .....	<i>20</i>
<b>1.4 PHYSICOCHEMICAL MECHANISTIC ASPECTS</b> .....	<b>36</b>
<b>1.4.1 Molecular transport</b> .....	<b>37</b>
<b>1.4.2 Formation of a liquid phase</b> .....	<b>39</b>
<b>1.4.3 Mediation by an amorphous phase or polymorphic transition</b> .....	<b>40</b>
<b>1.5 THE EFFECTS OF MECHANICAL ACTION ON MOLECULAR AND ORBITAL LEVELS</b> .....	<b>43</b>
<b>1.6 REFERENCES</b> .....	<b>46</b>
<b>CHAPTER 2. EXPERIMENTAL PROCEDURES AND CHARACTERIZATION</b>	
<b>TECHNIQUES</b> .....	<b>55</b>
<b>2.1 INTRODUCTION</b> .....	<b>57</b>
<b>2.2 THE EXPERIMENTAL APPARATUS</b> .....	<b>57</b>
<b>2.2.1 The vibratory ball mill Pulverisette 0</b> .....	<b>57</b>
<i>2.2.1.1 Setting the milling temperature (<math>T_m</math>)</i> .....	<i>59</i>
<b>2.3 CHARACTERIZATION AND ANALYTICAL TECHNIQUES</b> .....	<b>60</b>
<b>2.3.1 Kinetic monitoring by high-performance liquid chromatography (HPLC)</b> .....	<b>60</b>
<i>2.3.1.1 Method and calibration curves</i> .....	<i>60</i>
<i>2.3.1.2 Kinetic monitoring - sample preparation and quantification</i> .....	<i>62</i>
<b>2.3.2 Techniques for solid-state characterization and analysis</b> .....	<b>63</b>
<i>2.3.2.1 Differential scanning calorimetry (DSC) analysis</i> .....	<i>64</i>



2.3.2.2 Differential scanning calorimetry (DSC) and hot-stage microscopy (HSM) .....	64
2.3.2.3 Calorimetric measurements.....	65
2.3.2.4 X-ray diffraction (XRD).....	66
2.3.2.5 Solid-State <sup>13</sup> C CP-MAS NMR.....	66
2.3.2.6 Raman spectroscopy .....	66
2.3.2.7 Absolute density.....	67
<b>2.3.3 Classical techniques for molecule characterization.....</b>	<b>67</b>
2.3.3.1 <sup>1</sup> H NMR and <sup>13</sup> C NMR .....	67
2.3.3.2 Fourier Transformed Infrared Spectroscopy (FTIR) .....	67
2.3.3.3 UV-vis spectroscopy .....	67
2.3.3.4 Mass Spectrometry and High Resolution Mass Spectrometry (MS/HRMS).....	68
2.3.3.5 Melting point determination .....	68
<b>2.4 REFERENCES.....</b>	<b>68</b>
<b>CHAPTER 3. THE INVESTIGATION OF THE MECHANISMS OF 1,4-DIAZINES</b>	
<b>MECHANOSYNTHESIS .....</b>	<b>69</b>
<b>3.1 INTRODUCTION.....</b>	<b>71</b>
<b>3.1.1 Mechanochemical reactions pathways .....</b>	<b>71</b>
<b>3.1.2 Previous results on the investigation of dibenzo[a,c]phenazine mechanosynthesis .....</b>	<b>71</b>
<b>3.2 EXPERIMENTAL SECTION.....</b>	<b>73</b>
<b>3.2.1 Materials.....</b>	<b>73</b>
<b>3.2.2 General procedure for synthesis .....</b>	<b>73</b>
<b>3.3 RESULTS AND DISCUSSION.....</b>	<b>74</b>
<b>3.3.1 The mechanosynthesis of dibenzo[a,c]phenazine (DBPZ).....</b>	<b>74</b>
3.3.1.1 Kinetics of DBPZ reaction.....	75
3.3.1.2 Heat release quantification based on the reactions continuation .....	78
3.3.1.3 <sup>13</sup> C CP-MAS NMR investigations.....	81
3.3.1.4 XRD records .....	85
<b>3.3.2 The mechanosynthesis of 2,3-diphenylquinoxaline (DPQ) .....</b>	<b>89</b>
3.3.2.1 Kinetic of DPQ synthesis.....	90
3.3.2.2 Heat release quantification based on the reactions continuation .....	91
3.3.2.3 <sup>13</sup> C CP-MAS NMR investigations.....	94
3.3.2.4 X-ray diffraction records .....	96
3.3.2.5 Remarks about the reaction continuation.....	100
<b>3.4 CONCLUSIONS.....</b>	<b>101</b>
<b>3.5 REFERENCES.....</b>	<b>103</b>

<b>CHAPTER 4. KINETIC STUDIES OF MECHANICALLY-INDUCED 2,3-DIPHENYLQUINOXALINE SYNTHESIS .....</b>	<b>105</b>
<b>4.1 INTRODUCTION.....</b>	<b>106</b>
<b>4.1.1 Kinetics investigation of mechanochemical reactions .....</b>	<b>106</b>
<b>4.1.2 The temperature dependence of rate constant and the activation energy .....</b>	<b>109</b>
4.1.2.1 Arrhenius equation .....	109
4.1.2.2 Eyring-Polanyi equation.....	109
4.1.2.3 The activation energy for mechanically-induced transformations.....	112
<b>4.2 EXPERIMENTAL SECTION.....</b>	<b>113</b>
<b>4.2.1 Materials.....</b>	<b>113</b>
4.2.1.1 Reagents.....	113
4.2.1.2 Milling device .....	113
<b>4.2.2 General procedure for 2,3-diphenylquinoxaline (DPQ) synthesis.....</b>	<b>113</b>
<b>4.3 RESULTS AND DISCUSSION .....</b>	<b>114</b>
<b>4.3.1 Parameters assessment for DPQ synthesis in vibratory ball mill .....</b>	<b>115</b>
4.3.1.1 Effect of the ball material .....	115
4.3.1.2 Effect of the ball weight .....	117
4.3.1.3 Effect of the ball diameter .....	118
4.3.1.4 Effect of the particle size .....	119
<b>4.3.2 Temperature effect on the DPQ synthesis.....</b>	<b>120</b>
4.3.2.1 The temperature dependence of the reaction rate constant and estimation of activation energies.....	128
<b>4.4 CONCLUSION.....</b>	<b>133</b>
<b>4.5 REFERENCES.....</b>	<b>136</b>
<b>CHAPTER 5. THE APPLICATION OF MECHANOCHEMISTRY AS A GREENER ROUTE FOR SYNTHESIS OF PHARMACEUTICALLY ATTRACTIVE MOLECULES: HYDRAZONES MECHANOSYNTHESIS AND THEIR ANTITUBERCULOSIS ACTIVITY .....</b>	<b>141</b>
<b>5.1 INTRODUCTION.....</b>	<b>143</b>
<b>5.1.1 The pharmaceutical interest for mechanochemistry.....</b>	<b>143</b>
<b>5.1.2 Hydrazones.....</b>	<b>144</b>
<b>5.1.3 Targeting tuberculosis disease.....</b>	<b>146</b>
5.1.3.1 Treatment and antituberculosis drugs .....	149
5.1.3.2 Antituberculosis drugs targeting the cell wall biosynthesis – Isoniazid (INH) .....	150
<b>5.1.4 Hydrazine- Hydrazone derivatives targeting <i>M. tuberculosis</i> .....</b>	<b>151</b>

<b>5.2 EXPERIMENTAL SECTION.....</b>	<b>155</b>
<b>5.2.1 Chemistry .....</b>	<b>155</b>
5.2.1.1 <i>Materials for synthesis.....</i>	155
5.2.1.2 <i>General procedure for phenolic hydrazones synthesis.....</i>	155
5.2.1.3 <i>General procedure for isoniazid nitrogen-containing heterocycles derivatives .....</i>	155
<b>5.2.2 Biological assays.....</b>	<b>156</b>
5.2.2.1 <i>Growth conditions of M. tuberculosis H<sub>37</sub>Rv.....</i>	156
5.2.2.2 <i>MIC determinations .....</i>	156
5.2.2.3 <i>M. tuberculosis clinical isolate and drug susceptibility testing .....</i>	156
5.2.2.4 <i>InhA expression and purification .....</i>	157
5.2.2.5 <i>InhA activity inhibition .....</i>	157
<b>5.3 RESULTS AND DISCUSSION .....</b>	<b>158</b>
<b>5.3.1 Mechanosynthesis of phenolic hydrazones.....</b>	<b>158</b>
5.3.1.1 <i>Electronic effects .....</i>	161
5.3.1.2 <i>The solid-state role.....</i>	162
<b>5.3.2 Mechanosynthesis of isoniazid hydrazone derivatives.....</b>	<b>166</b>
<b>5.3.3 The structural analysis of isonicotinoyl hydrazones by DFT and NMR.....</b>	<b>169</b>
5.3.3.1 <i>(E)-N'-(4-hydroxybenzylidene)isonicotinohydrazide (1c) .....</i>	170
5.3.3.2 <i>(E)-N'-((2H-indazol-6-yl)methylene)isonicotinohydrazide (7d).....</i>	175
<b>5.3.4 Biological activities of mechanochemically synthesized hydrazones against M. tuberculosis.....</b>	<b>180</b>
5.3.4.1 <i>Biological evaluation of phenolic hydrazones (1-5a-d) .....</i>	180
5.3.4.2 <i>Biological activity evaluation of isoniazid-nitrogen heterocyclic hydrazones (7a-j).....</i>	182
5.3.4.3 <i>InhA inhibition assay.....</i>	183
5.3.4.4 <i>Cytotoxicity and Selectivity Index determination .....</i>	184
<b>5.3.5 Hydrolytic stability and pK<sub>a</sub> determination of most active hydrazones .....</b>	<b>185</b>
5.3.5.1 <i>pK<sub>a</sub> determination .....</i>	186
<b>5.4 CONCLUSIONS.....</b>	<b>188</b>
<b>5.5 REFERENCES.....</b>	<b>190</b>
<b>GENERAL CONCLUSIONS AND PERSPECTIVES .....</b>	<b>197</b>
<b>GENERAL CONCLUSIONS.....</b>	<b>199</b>
<b>PERSPECTIVES.....</b>	<b>203</b>
<b>RESUME LONG EN FRANÇAIS .....</b>	<b>205</b>
<b>APPENDIX .....</b>	<b>217</b>
<b>APPENDIX I – KINETIC MODELS FOR SOLID-STATE REACTIONS .....</b>	<b>219</b>

<b>APPENDIX II – CHARACTERIZATION DATA .....</b>	<b>223</b>
<b>APPENDIX III – FTIR STUDIES .....</b>	<b>244</b>
<b>ACRONYMS, ABBREVIATIONS AND SYMBOLS .....</b>	<b>246</b>
<b>LIST OF FIGURES, SCHEMES AND TABLES.....</b>	<b>249</b>
<b>STRUCTURES OF HYDRAZONES .....</b>	<b>257</b>



---

# **INTRODUCTION**

---



---

## CONTEXT AND RELEVANCE

In this present era, one of the most important subjects for academics and industrials is related to environmental issues. There is a widespread mobilization in favor to the development with preservation of the natural resources. The chemical and pharmaceutical industries are directly concerned since their production can potentially impact the environment in short- and long-terms, which make them turning to the development of nonpolluting processes. The eco-design of chemicals is formalized in the *Green Chemistry principles*<sup>1</sup> that intend to guide towards the design of chemicals and chemical processes, focusing on the pollution prevention or that are benign or not hazardous from the conception, development, manufacture and applications. In this context, technologies have been developed and implemented in order to reduce the use of solvents in the chemical production, since they represent the main source of waste generation. Thereby, solventless protocols are prominent routes for *sustainable development*.

Mechanochemistry has been presented as an alternative to classical methodologies to transform chemicals without using solvents or only in very small amounts. The use of mechanical energy over the thermal one in solution has been successfully used, with intense scientific production and industrial interest in the last fifteen years for organic mechanochemistry.

In the pharmaceutical area, where the concept of *Green Pharmacy* is more newsworthy than ever<sup>2</sup>, the mechanochemistry are currently applied for the improvement of physicochemical properties of the active pharmaceutical ingredients (APIs) such as tableting and solubility through intermolecular interactions. Notwithstanding, an API is mainly still nowadays, primarily, an issue of fine chemistry, and thus, some examples of drugs or drug candidates synthesis has also been subject of mechanochemistry.

*Pharmaceutical mechanochemistry as a way of sustainable chemistry* is the central theme of the present work, which is motivated by the needs of environmentally friendly protocols to produce chemicals, associated to the run for drug discovery.

Noteworthy, the studies on mechanochemistry presented herein are not limited to the synthesis of such therapeutically attractive molecules, but also using their syntheses as models

---

<sup>1</sup> Anastas, P. T., Warner, J. C., *Green Chemistry : Theory and Practice*, Oxford University Press, New York, 1998.

<sup>2</sup> Baron, M. Towards a greener pharmacy by more eco design. *Waste Biomass Valor* **2012**, *3*, 395–407.



for deeper understanding of the possible phenomena that happens when the matter is perturbed by mechanical action inducing chemical reactions.

The potential of mechanochemistry goes far beyond its greenness as it has been demonstrated by unexpected reaction pathways upon application of mechanical stresses. For the case of single molecular manipulations, such stress allows the circumvention of energetic barriers in specific manners, sometimes different from thermal and photochemical activations.<sup>3</sup> In the other side is placed the ball milling reactions, enabling to perform organic reactions with solid materials in excellent yields, with also their particularities.

Truly progress has been made in these both aspects, but unfortunately, there is a gap between them, which can retard further advances and enrichment of the field. On one hand, the investigations are dedicated to controlled manipulations of covalent bonds, and on the other one, the objective is to access products and architectures from solid forms. Much has been done concerning intermolecular interactions and the physicochemical transformations of the powder, but the electronic states remains to be further studied. Apart from the discussions of Gilman<sup>4</sup> and Senna<sup>5</sup> about the HOMO-LUMO gap closure in mechanically stressed molecules, hardly anything can be found in the literature. The investigations of the reaction mechanism of the mechanically-induced dibenzo[a,c]phenazine synthesis initiated and developed by Baron and collaborators<sup>6</sup>, including a project in collaboration with the Kyoto University<sup>7</sup>, have been also demonstrating some particularities of the mechanically activated systems.

This doctoral research has been developed at RAPSODEE Center (Centre de Recherche d'Albi en génie des Procédés des Solides Divisés, de l'Énergie et de l'Environnement) with co-supervision of LSPCMIB (Laboratoire de Synthèse et Physico-Chimie de Molécules d'Intérêt Biologique). This collaboration has been essential associating the competences of these two laboratories. Powder technology, processing and mechanochemistry for the former, and for the latter, the experience in designing and synthesizing molecules presenting potential biological interest. These laboratories are

---

<sup>3</sup> Hickenboth, C. R.; Moore, J. S.; White, S. R.; Sottos, N. R.; Baudry, J.; Wilson, S. R. Biasing reaction pathways with mechanical force. *Nature* **2007**, *446*, 423–427.

<sup>4</sup> Gilman, J. J. Mechanochemistry. *Science (80-. )*. **1996**, *274*, 65.

<sup>5</sup> Senna, M. Consequences of molecular strain on the solid state addition reaction. *J. Mater. Sci.* **2004**, *39*, 4995–5001.

<sup>6</sup> Carlier, L.; Baron, M.; Chamayou, A.; Couarraze, G. Use of co-grinding as a solvent-free solid state method to synthesize dibenzophenazines. *Tetrahedron Lett.* **2011**, *52*, 4686–4689. Carlier, L.; Baron, M.; Chamayou, A.; Couarraze, G. Greener pharmacy using solvent-free synthesis: Investigation of the mechanism in the case of dibenzophenazine. *Powder Technol.* **2013**, *240*, 41–47.

<sup>7</sup> CNRS/JSPS France-Japan joint research project n° PRC0709 (2013-2014).

members of the Gala Platform in advanced galenic, which was the via for establishing such collaboration.

## **GENERAL OBJECTIVE OF THE RESEARCH**

The object of this thesis lies on the use of mechanochemistry as a sustainable route to produce pharmaceutically interesting molecules while it also aims to contribute to the mechanochemical field by using the reactions carried out in a ball mill device as a mean for understanding the states capable to be attained with mechanical excitation. The thesis intends to bring closer the studies on different reaction pathways and the overall transformation obtained in the mechanoreactors.

### **Specific objectives**

- To synthesize molecules obtained straightforward from the solid reactants in agreement with the *Green Chemistry* principles;
- To design according to these principles compounds bearing basic structures frequently described for their therapeutic activities;
- To determine the intermediates species of chemical or physical nature that can be possibly generated during milling;
- To investigate the processes parameters of the ball milling device and estimate the activation energy of a mechanochemical reaction;
- To identify the similarities on the transformations observed for mechanochemical reactions in order to establish some aspects that can frequently influence and guide such solid systems.

## **CONTENT AND PRESENTATION**

The following parts, encompassing the fundamental studies of mechanochemical reactions, the processing aspects and the application, compose this doctoral thesis.

**Chapter 1.** Literature Review. This first chapter gives an overview of mechanochemistry, including some definitions, a brief history, the insertion in the Green Chemistry framework, and the focus on the organic transformations and the related mechanisms.

**Chapter 2.** The second chapter presents the experimental apparatus and the techniques used for characterizations.

**Chapter 3.** This chapter is dedicated to fundamental investigations of condensed 1,4-diazines mechanosynthesis. The mechanosynthesis of dibenzo[a,c]phenazine (DBPZ) is revised and compared with 2,3-diphenylquinoxaline (DPQ). These studies suggest that intermediate species with higher level of excitation can be generated under continuous grinding, which could be detected while in solid state but would be unstable or not formed when in solution.

**Chapter 4.** The kinetics DPQ synthesis is studied in this part. Some parameters of the milling device were assessed, including milling material, size and weight of the milling balls. The effects of the overall temperature of the milling on the kinetics of transformation are evaluated, enabling the first experimental estimation of the activation energy of a mechanochemical organic reaction in the gram scale. These studies reveal two different behaviors as function of temperature, which is equally attributed to a mechanically induced phase transition of the powder mixture.

**Chapter 5.** This chapter demonstrates to the application of the mechanochemistry in the context of a greener pharmacy. A series of hydrazones designed for potential activities against *Mycobacterium tuberculosis (Mtb)* are synthesized using solid reactants. The reactivity of the starting materials is discussed in terms of chemical reactivity associated to the solid contributions in favor or to prevent the reaction. Finally, the biological assays against *Mtb* reveal some molecules with an activity higher than the frontline drug isoniazid.

**General conclusions.** This part summarizes the general observations of the studies reported and presents the events that typically take place during mechanochemical reactions, which could also be concerned to a wider domain in organic mechanochemistry.

**Perspectives.** Some studies than can be further developed in relation to the results obtained are addressed with this in mind.

---

**CHAPTER 1.**

**Literature Review**

---



## 1.1 INTRODUCTION

The fundamentals of mechanochemistry and relevant researches for this thesis are presented in this literature review. The reason for which this field has gained attention comes from the greener approach enabling synthesis without solvents in quantitative yields as well as the uniqueness of some transformations only possible through this route. Therefore, the green framework offered by mechanochemical route is commented, but the main focus is on the mechanistic aspects. The transitions underwent by the powder upon application of mechanical action are discussed as well as the most prominent results related to findings and understandings on mechanochemistry. The objective of this brief review is to give a panorama of the phenomena possibly occurring during mechanical stress or posteriorly, but as consequence of mechanical action. Also, it aims to open a critical regard on the points not elucidated yet.

### 1.1.1 Definition and terminology

*Mechanochemistry is a branch of chemistry that is concerned with chemical and physicochemical transformations of substances in all states of aggregation produced by the effect of mechanical energy.* Heinicke (1984) gave this definition, which is widely accepted nowadays. However, mechanochemistry is currently most referred to the reaction between solids induced by mechanical energy such as by grinding or milling in ball mills.

In turn, grinding is a general term related to the mechanical action by hard surfaces on materials in order to break them, reducing the particle size, typically used for mortar and pestle. Here, grinding and milling are employed as synonyms.

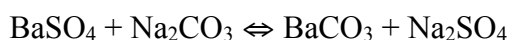
Another term associated to mechanochemistry is for the intentionally addition of liquids the solid system, normally sub-equimolar amounts. In these cases the acronyms LAG and ILAG may appear and mean, Liquid Assisted Grinding and, Ion and Liquid Assisted Grinding, respectively. Kneading is also a kind of solvent assisted grinding.

A mechanochemical reaction does not mean that the reaction is solvent-free; despite in most of the cases, mechanochemical reactions be performed for solid reactants without adding solvents. Liquids can be formed, added as for LAG and ILAG, or already be within the solids as the case of hydrates.

Further definitions are presented where they are most concerned.

### 1.1.2 Historical overview

Mortar and pestle were already used in the Stone Age and, certainly, generated some unknown chemical changes (Lynch and Rowland, 2005). In Greece, in 315 B.C., in a book titled “On Stones” Theophrastus of Eresus makes a reference on the reduction of cinnabar to mercury by grinding it in a mortar and pestle of copper (Takacs, 2013). This is which now is called a mechanochemical reaction. Since then, about 2000 years passed, without any remarkable development or mention to a reaction induced by mechanical action. But, it does not mean that these kinds of reactions were not performed, especially when grinding minerals and pharmaceuticals. In the end of 19<sup>th</sup> century the things began to change through the first extensive investigations on chemical effects produced by mechanical action carried out by Walthère Spring in Liège, Belgium and by M. Carey Lea in Philadelphia, USA (Takacs, 2013). The first was interested in the effect of pressure on phase transformations and chemical reaction to understand the formation of minerals on earth. Spring’s best-known experiment involves the metathesis reaction with barium sulfate and sodium carbonate induced by repeated compression and pulverization (Spring, 1885).



Despite some doubts raised about the results of Spring, it is undeniably that it was the first systematic investigation of the effects of mechanical action on the chemistry of materials, which stimulated further researches.

Almost at the same time, M. Carey Lea in USA was investigated the transformation of “allotropic” silver. He studied some silver halogenated under static pressure as well as trituration in a mortar (Lea, 1893). For the surprise, the weak shearing forces applied during trituration were much more active chemically than the large static force from the press. In addition, Lea observed that mechanical grinding could bring reactions that are different from the thermochemical reactions in the same system. The most noteworthy examples are related to mercuric chloride and silver chloride, which decompose when trituated in a mortar, while mercuric chloride sublimates and silver chloride melts undecomposed when heated (Lea, 1893). This author not only showed that mechanical action causes chemical changes, but also that the changes may be unique, different from the thermochemical reactions. This result is so important that it is still quoted to illustrate the difference between the effects of heat and mechanical action. For these findings, among others, some consider M. Carey Lea as the “father of mechanochemistry” (Takacs, 2013).

Organic reactions were also reported under mechanical stress in the end of the 19<sup>th</sup> century. In 1893, Ling and Baker prepared halogen derivatives of quinhydrone by several methods, including the grinding of dry mixtures and in the presence of water or light petroleum (nowadays, it would be part of LAG) (Ling and Baker, 1893). It is worth to mention, that the researches of Spring, Lea and, Ling and Baker, represent just a few examples of remarkable contributions for the beginning of a systematic investigation in mechanochemistry. Several other punctual texts can be found, but it is not the scope of this review. However, the missing citation here is the one of Ostwald that systematized the chemical modifications induced by mechanical energy as “mechanochemistry”, together with thermochemistry, electrochemistry and photochemistry, according to the type of energy in the system (Takacs, 2013).

The scenario of slow growth of mechanochemistry during the first half of the 20<sup>th</sup> century, mainly dedicated to high pressure and minerals, began to change in 1960 (Takacs, 2013). The mechanical alloying in metallurgy was the main purpose, followed by mechanochemistry of polymers, generating radicals and crosslinking.

The research in the field intensified and some groups devoted to mechanochemistry were formed (Takacs, 2013). Accompanied to that, the development of characterization techniques, such as microscopy, and the manufacture of more elaborate milling devices by Retsch, Fritsch and also lab-made in Russia, pushed toward the fundamental comprehension of the mechanical energy used for chemical transformations (Takacs, 2013). In 1984 The International Mechanochemical Association was created and in 1993 the first official meeting as part of IUPAC agenda were held in Kosice (Slovakia) – the International Conference on Mechanochemistry and Mechanical Alloying (INCOME), event that is still regular.

Notwithstanding the vast advances for minerals and mechanical alloying, and, the use of mechanical energy in organic reactions had been reported before, only recently the research in the area of organic materials intensified. As said before, the opportunity for new clear and green routes to perform organic reactions put forward the organic mechanochemistry both for reactions with covalent bond formation or supramolecular modifications.

The history of mechanochemistry is very summarized above, but the aim is to show some points that carried the field from the mortar and pestle in the earlier times until very designed supramolecular arrangements in organic-inorganic chemistry. More details about the history and development of mechanochemistry can be found in Boldyrev (2002, 2006) and Baláž (Baláž et al., 2006; Baláž, 2008), for example and, more recently, Takacs (2013) published a very complete and detailed paper on the subject.



### 1.1.3 Mechanochemical Reactors

Mechanochemical reactions can be performed in simple apparatus such as mortar and pestle, but it does not enable systematic investigations because it is function of the manipulator. In addition, human hands cannot apply enough energy to surmount the barrier of energy required to start some kinds of transformations. For this reason, mechanochemical reactions are often performed in ball milling devices in which parameters can be modified and set to ensure the repeatability and investigation of the effect of such parameters on the reaction medium. In this manner, the term “ball milling reactions” is direct related to mechanochemical reactions.

The most studied variables are the material of milling media (balls and vessel), revolution speed, amplitude, frequency, filling factor (balls/vessel volume ratio), reaction time and ball-to-powder mass ratio (BPR), which are not completely independent (Stolle 2015; Stolle et al., 2011). They are specific for each type of equipment and are often adapted to the nature of the powder and the reaction. **Figure 1.1** presents the schemes of different mills, and just below, **Figure 1.2** shows a small set of the most used laboratory scale ball mills and their different types of milling media.

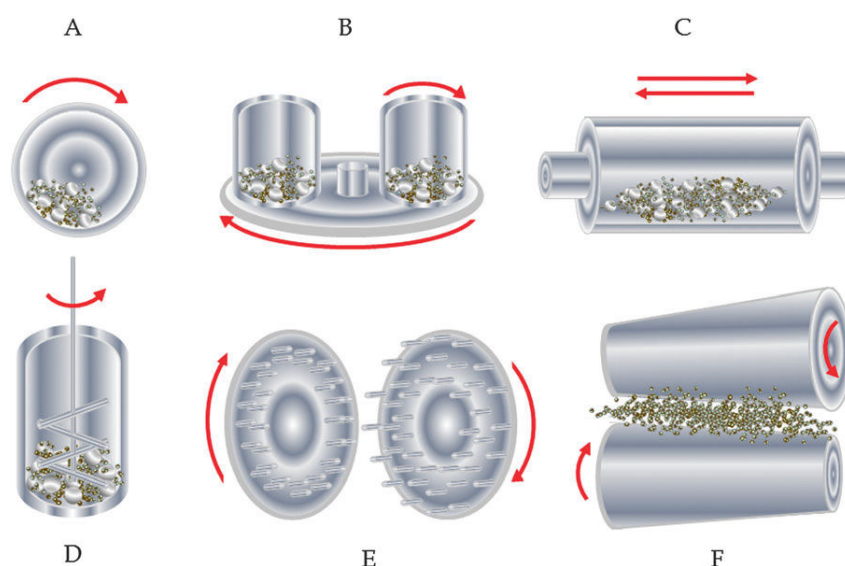


**Figure 1.1.** Types of mills for high-energy milling: A – ball mill, B – planetary mill, C – vibration mill, D – attritor (stirring ball mill), E – pin mill, F – rolling mill (Reproduced from Baláž et al. (2013) by permission of The Royal Society of Chemistry).



**Figure 1.2** Ball mills used in laboratory for mechanosynthesis purpose and their respective milling media: hardened steel, stainless steel, tungsten carbide, agate, zirconium oxide, PTFE. (A) Vibratory mixer mill (MM 400 Restch) and (B) Planetary ball mill (PM Pulverisette 5 Fritsch).

Baláž (2008) pointed out that besides of energy considerations of these machines, known to be great consumers, the form of mechanical activation in milling is important. Each ball mill type can favor specific mechanisms of particle breakage that are mostly shock/impact, friction/shear deformation and, in turn, these deformations are able to favor a specific product formation. Indeed, it has been demonstrated that the way the mechanical energy is inputted, which is function of the milling devices, influences the product obtained.

For example, Boldyreva and co-workers have demonstrated for  $\alpha$ -glycine +  $\beta$ -malonic cocystal formation that sampling from milling jar walls (shear treatment) showed glycinium semi-malonate salt formation, while sampling from the jar top and bottom (impact regime) showed a novel phase formation. The results were confirmed by isolating shear and impact in special devices (Michalchuk et al., 2013, 2014). These materials are very interesting as indicators of mechanical stress regime.

Wang and Liu (2004) studied three different milling devices for pinacol coupling product formation from mechanochemical reaction of aromatic ketones and aldehydes in presence of Zn-ZnCl<sub>2</sub>. Among the three activation methods, high-speed vibration mill, mixer mill and mortar grinder, the latter technique afforded much higher yield and selectivity of the pinacol coupling product, even if it consists in a more gentle milling conditions. The vigorous milling resulted in the partial decomposition.

## 1.2 MECHANOCHEMISTRY AS GREENER ROUTE TO PRODUCE CHEMICALS

Lately the issue of sustainability has grown as the scientific society has become alerted about the impacts of chemicals agents on the environment and human health. Intuitively, the most concerned fields are the fine chemicals and pharmaceutical industries. Furthermore, the pressure from regulatory agencies, especially about waste management, and from the public, made the chemical industry the greatest important subject for chemists, engineers and industrial researchers. The growing number of stipulations and restrictions had forced the industries to adopt measures to minimize the environmental impact. Remediation<sup>8</sup> is the first target solution to reduce pollution; nevertheless, the technologies of processing the residue generated are not so beneficial when compared to the source reduction techniques. This, because a new insight into the problem considers that, fundamentally, is needed to avoid or minimize the production of such waste to the detriment of exclusive concern with the treatment of the chemical residue in the "end of pipe". (Lenardão, 2003) This is the sense of Green Chemistry principles, in which the essential meaning is to design chemicals and chemical routes for pollution prevention and health safety.

In the scientific domain, this subject has gained further attention since the publication of "*Green Chemistry: Theory and Practice*" by Anastas and Warner (1998) with their 12 principles. Surely, before that date there were other studies in this sense, but they simply had not borne the flag of green chemistry principles. For this purpose, the chemists and engineers have engaged in developing or implementing technologies and routes for synthesis and processing of chemicals.

Mainly in organic chemistry, the classical methodologies involve the use of large amounts of solvents in almost steps of preparation and purification, and consequently generate lots of wastes and energy consumption. As mentioned, the most affected industries are for fine chemicals and pharmaceutical production. For the last, more than 85 % of the chemical agents are solvents and the ratio of recycling, which also consumed energy, is not higher than 80 % (Sheldon, 2005). This led to a rigorous discussion and culminated in the foundation of Pharmaceutical Roundtable (PR) together with American Chemical Society Green Chemistry Institute (ACS GCI) and the pharmaceutical industries to treat the subject of Green Chemistry in their corporations. They also use indexes such as E-factor (Sheldon,

---

<sup>8</sup> Environmental remediation deals with the use of techniques to remove, contain, or render harmless environmental contaminants for benefits to human health, as well as to restore the environment. Environmental remediation is carried out on various environmental media, including soil, sediment, groundwater and surface water.

1992, 2007) or process mass intensity (PMI) (Jimenez-Gonzalez et al., 2011) to measure the greenness of their processes.

Therefore, avoiding organic solvents in chemical syntheses is an important part of guidelines towards benign methodologies. New and innovative sustainable reactions and protocols emerged in the last two decades, by using no solvent and catalysts under room or mild conditions, and by using alternative input energies. It is worth to mention that these techniques existed before, but they were not used with a green purpose. The efforts to improve and find alternative sources of energy to perform organic reactions, have stepped up the development and improvement of such solventless technologies. In this manner, photochemistry, microwave irradiation, ultrasound and mechanochemistry are presented as targeted technologies to be implemented. Many publications are dedicated to these techniques that are in general published together as solvent-free or eco-friendly routes of synthesis (Gawande et al., 2014; Baig and Varma, 2012; Martins et al., 2009; Ballini, 2009; Clark and Macquarrie, 2008; Tanaka and Toda, 2000).

This is the position of mechanochemical approaches among the innovative technologies, allowing the transformations of the solid forms, efficiently and quickly without addition of solvents or only nominal amounts. This highlights the mechanochemistry in favor to environmental concerns. It equally represents an opportunity to advance the investigations in field of solid-state chemistry. Nevertheless, it is fundamentally important to understand the mechanisms involved in such mechanically induced transformations, from the solid form and in molecular level, to continue the progress in means of equipment and processing to be directed to scaling-up and industrial applications.

### **1.3 MECHANOCHEMISTRY OF ORGANIC SYSTEMS**

The versatility of mechanochemistry was indirectly introduced on its historical overview. The applications cover all the fields of chemistry. It starts with inorganic solids and goes from mechanical alloying, polymers, manipulation of single molecules attached to polymer chains, several types of well-known organic reactions reaching to supramolecular designs such as cocrystals and three-dimensional metal-organic framework (MOF) architectures.

In spite of the some particularities on each area, the mechanochemistry of organic compounds benefitted from the progress in the mechanochemistry of inorganics, mostly in mechanical alloying, resulting in the extension to more elaborate organic reactions.

Nowadays, a plethora of successful examples of organic reactions carried out under mechanical action are reported (Wang, 2013).

The mechanochemistry concerning the organic synthetic chemistry is illustrated here by the mechanochemistry of polymers, cocrystals and other supramolecular architectures, and the mechanochemical synthesis with covalent bond formation.

### 1.3.1 Mechanochemistry of macromolecules and mechanophores

The application of mechanical stress on polymers has different consequences. In these instances, reactions such as crosslinking of polymer chains (Bridgman, 1935) and molecular weight reduction (Staudinger, 1930) attributed to the C-C homolytic bond cleavage during mechanical action (Kauzmann and Eyring, 1940) can be cited. The facilitated homolytic dissociation can be a result of stretching specific bonds within a molecule, which alters the potential energy surface of a reaction coordinate by lowering the activation barrier. The free radical formation and their subsequent recombination in block, graft chains or conversion in bimolecular reactions (Sohma, 1989) and the polymerization of organic monomers (Kuzuya et al., 1991) are also remarkable results on the mechanochemistry of polymers as well as the degradation of polymers by mechanical action. More detailed reviews can be found in Beyer and Clause-Schaumann (2005), Zharov (1994) and Sohma (1989) for this branch of mechanochemistry of polymers.

The publication of the paper entitled *How Strong is a Covalent Bond?* in 1999 represented a shift on the field of mechanochemistry of macromolecules (Grandbois et al., 1999). In the experiments described in that article, external mechanical forces were controlled applied to covalent bonds by detaching individual macromolecules (polysaccharides) from surfaces in an atomic force microscope (AFM) (**Figure 1.3**). After establishing sufficient statistics based on breaking individual covalent interactions, bond by bond from molecule by molecule, an average breaking (or rupture) force (defined as the maximum measured force before the bond ruptures and the cantilever snaps back to zero force) of  $1.4 \pm 0.3$  nN was determined (Grandbois et al., 1999). This **controlled specific manipulation of covalent interactions** (or chemical bonds) is currently called covalent mechanochemistry (Ribas-Arino et al., 2009; Ribas-Arino and Marx, 2012).

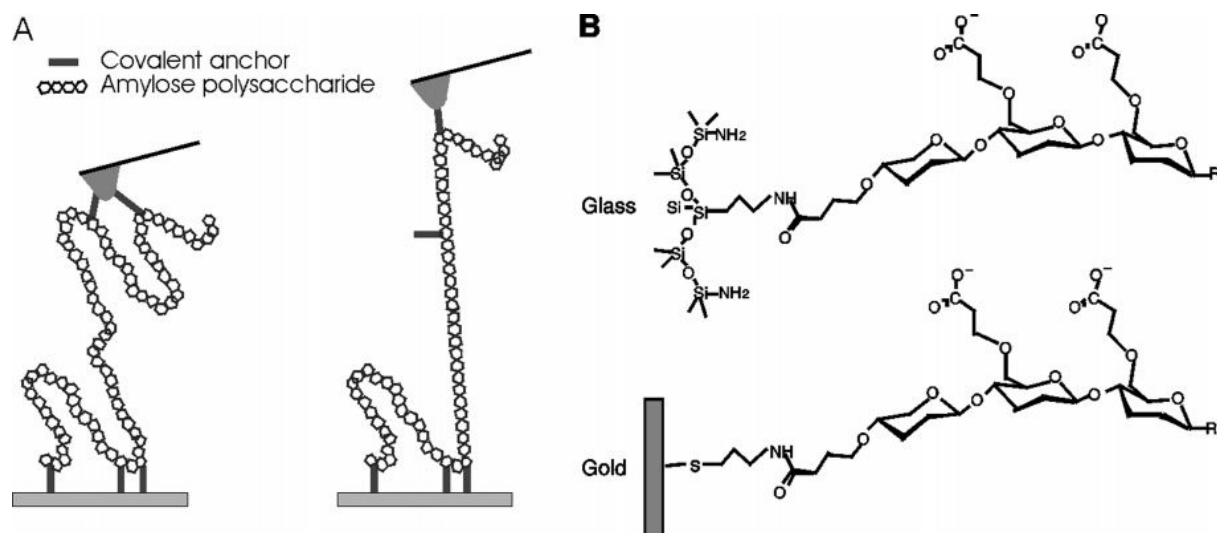


**Figure 1.3.** Stretching of a single polysaccharide chain that is covalently attached between a amino-functionalized glass or gold surface and the AFM tip (Reproduced from Grandbois et al. (1999) with permission of *Science*, American Association for Advancement of Science).

The development of the AFM methodology reported by Grandbois et al. (1999) allowed further manipulation of small molecules attached to macromolecules. Targeted cleavage or intriguing rearrangements of bonds have been demonstrated for these polymer-bound small molecules also for sonochemical conditions (Hickenboth et al., 2007). This chemical entity that poses mechanically labile bonds (mechanoresponsive), i.e., a functional group that changes under the influence of external mechanical forces is defined as mechanophore (Caruso et al., 2009; Brantley et al., 2013).

Mechanochemical activation often arises when the mechanophores are appropriately positioned within a polymer chain to experience tensile forces. The manipulation of these mechanophores has revealed differences between mechanically active reactions in comparison to products thermally or photochemically obtained. This is the case of ring-opening of the small molecules such as benzocyclobutene under mechanical action that circumvents Woodward-Hoffmann rules and rises unexpected products, different from thermo or photochemical implication (Hickenboth et al., 2007; Friedrichs et al., 2010). A number of interesting transformations have been observed including thermally inaccessible isomerizations and cycloreversions (Chen et al., 2002), activation of latent catalysts (Piermattei et al., 2009) and cycloreversions of Diels-Alder adducts (Konda et al., 2013). Caruso et al. (2009), Ribas-Arino and Marx (2012), Brantley et al. (2013) and more recently Li et al. (2015) reviewed this area of mechanochemistry.

More than measuring the force to break bonds, these experiments represented the advances in the fundamental understanding of mechanical effects on molecular orbital level.

### 1.3.2 Mechanochemistry of ball-milled organic reactions

The reactions carried out in ball milling devices represent another face of mechanochemistry. The ball-milling devices presented in the section 1.1.3 have been used in order to perform organic reactions in larger amounts, and additionally, they also allow more rigorous investigations and parameterization of such reactions. Mechanochemical processes have been applied to carbon-carbon and carbon-heteroatom covalent bonds, metal-ligand coordination bonds and non-covalent interactions such as hydrogen bonds, halogen bonds and  $\pi\cdots\pi$  arene stacking interactions. In these instances, cocrystals, coordination polymers and a number of organic reactions with covalent bond formation have been reported.

#### 1.3.2.1 Mechanochemical preparation of cocrystals

The mechanochemical route can be used to prepare supramolecular solid-state structures, such as molecular hydrogen- or halogen-bonded complexes, open frameworks and interlocked architectures (Friščić, 2012). Furthermore, sometimes the use of ball mills to produce such architectures can generate a specific product alternatively to those from solution (Michalchuk et al., 2013).

The cocrystal formation in ball mills represents a wide range of the organic mechanochemistry and has contributed for a deeper understanding of solid-solid transformations induced by mechanical energy. The broadest definition of cocrystal is crystalline molecular solids composed of chemically distinct species (Friščić and Jones, 2009). Braga et al. (2013) regarded a cocrystal as multicomponent crystal formed by two or more different chemical entities, each one possessing a stable crystalline phase, or amorphous solids, at room conditions. Therefore simple solvates and hydrates are excluded from the category of cocrystals but cocrystal solvates and hydrates are included. The cocrystal structure formation involves secondary interactions such as hydrogen bonds, hydrophobic interactions, and also ionic species but not covalent bonds. The components can be organic-organic for molecular cocrystals, organic and an inorganic alkaline or alkaline earth salt to form ionic cocrystals, and also organic-organometallic cocrystals (James et al., 2012; Braga et al., 2013).

The interest for cocrystal design comes surely from their modularity. This property of multicomponent molecular solids provides an opportunity to fine-tune the structural and physical properties of the solid form while the chemical properties are not significantly affected when it is dissolved (Friščić and Jones, 2007). For example, this is the case of modifications of active pharmaceutical active ingredient (API) properties such as tableting

and bioavailability (Delori et al., 2012). **Figure 1.4** shows the example of paracetamol, which has a solid form difficult to be pressed. The problem can be overcome through cocrystallization in LAG conditions with theophylline (Karki et al., 2009).

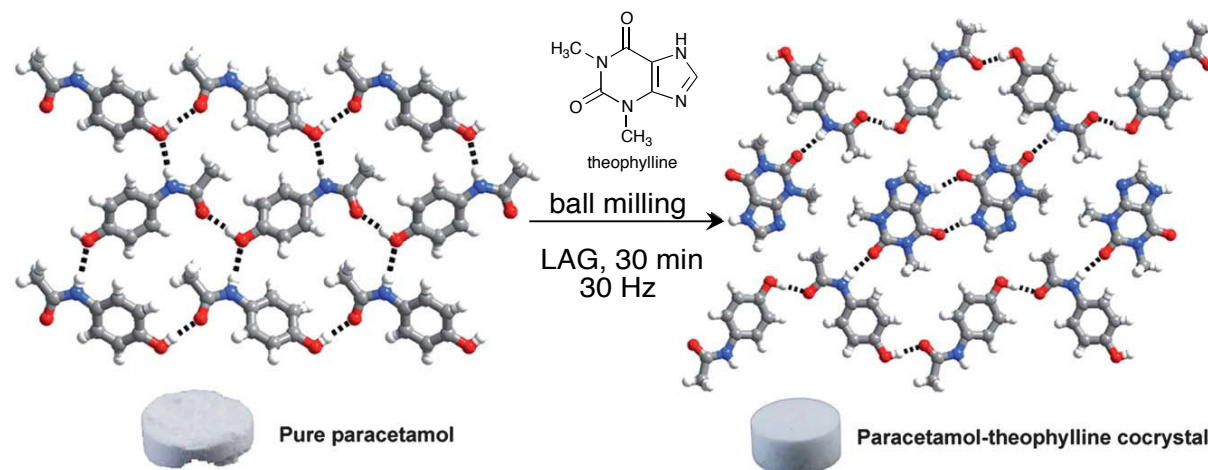


**Figure 1.4.** Paracetamol-theophylline cocrystal formation in ball milling (LAG, MeOH) conditions (Adapted from Delori et al. (2012) with permission of The Royal Society of Chemistry. Original work in Karki et al. (2009))

Several methods have been developed and implemented for cocrystal production in mechanochemical devices, including large-scale continuous extrusion (Medina, 2010). The reviews of Friščić (2012) that includes other supramolecular structures, Braga et al. (2013), Delori et al. (2012) present complete definitions, many examples of cocrystal formation, both in neat or LAG conditions, including API-conformers and suggested mechanisms.

### 1.3.2.2 Mechanochemical preparation of metal-organic frameworks

Another field in mechanochemistry of non-covalent bonds is based in coordination bonds. Metal-organic frameworks (MOFs) are constructed by joining metal-containing units with organic linkers, using strong bonds (reticular synthesis) to create open crystalline frameworks with permanent porosity (Furukawa et al., 2013). These materials have attracted increasing attention due to their potential applications including hydrogen storage and carbon dioxide sequestration as well as for catalytic conversion (Furukawa et al., 2013).

The mechanochemical methodologies to produce coordination polymers (in a more widely definition that includes MOFs) encompasses neat grinding, LAG and ILAG. These protocols can be followed by heating (annealing) (Friščić, 2014). Likewise for cocrystal preparation, MOF synthesis can be performed by manual grinding or in an automated ball mill. The first porous MOF by ball milling was reported by Pichon et al. (2006). The Cu(II)-



isonicotinate water/acetic acid-containing framework was obtained by neat grinding in ten minutes (**Figure 1.5**). More recently, James and co-workers (Crawford et al., 2015) described the continuous, large-scale preparation of  $\text{Ni}^{+2}$  complexes and  $\text{Cu}^{+2}$ ,  $\text{Zn}^{+2}$  and  $\text{Al}^{+3}$  MOFs by extrusion without using solvents or in very small quantities.

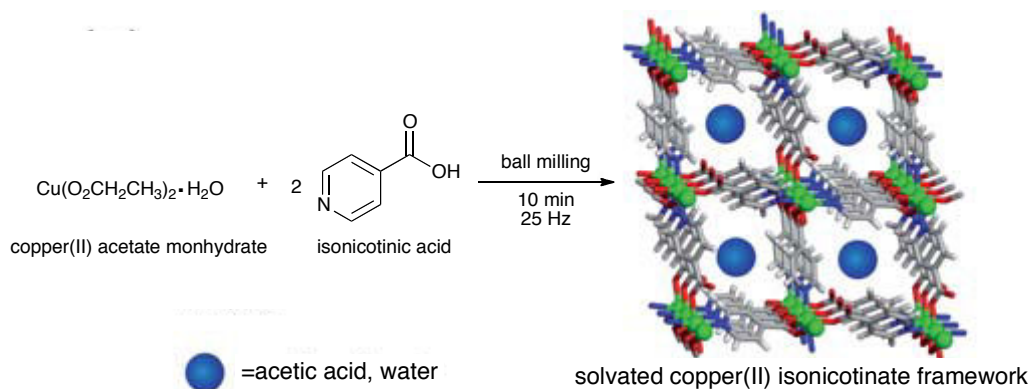


**Figure 1.5.** The first MOFs mechanochemically synthesized (Adapted from Pichon et al. (2006) and Friščić (2010) with permission of The Royal Society of Chemistry).

The mechanochemical synthesis of coordinate polymers and MOFs are reviewed in Garay et al. (2007) and Friščić (2014) as well as in James et al. (2012) and Friščić (2012) that also present other applications of mechanochemistry.

### 1.3.2.3 Organic ball milling reactions with covalent C-C and C-X bond formation

Organic reactions have been almost exclusively carried out in solution-based media under heat. However, the increasing needs for environmental-friendly protocols have opened to the use of different paths to perform organic synthesis. Ball milling reactions may also involve stronger bonds other than coordination and intermolecular interactions. C-C and C-X (X=O, N, S, Cl, Br) bond formation in mechanical devices, catalyzed or not, are briefly described in this section. The number of reactions currently found in the literature is very extensive and thus, the scope of this subsection is not to make an exhaustive review, but to present the possibility of performing organic reactions with solid reactants, including just a few illustrative examples. The review of Rodríguez et al. (2007<sup>a</sup>) was dedicated to C-C bond formation while Wang (2013) reviewed several types of organic mechanochemical reactions.

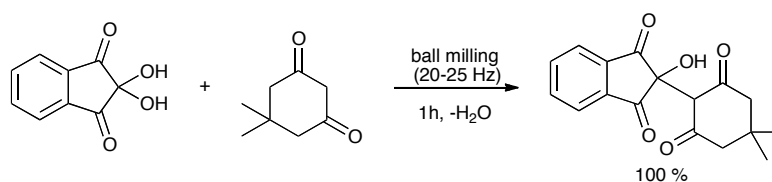
### C-C bond forming reactions

Carbon-carbon bond formation is a fundamental transformation in organic chemistry that allows the construction of the backbone of the organic compounds essential in medicinal chemistry, agrochemicals and to reproduce natural products synthetically. Under mechanochemical conditions, various C-C bond formations have been reported. Table 1 lists some these bond-forming reactions that have been carried out in ball milling devices.

**Table 1.1.** C-C bond forming reactions reported under ball mills conditions.

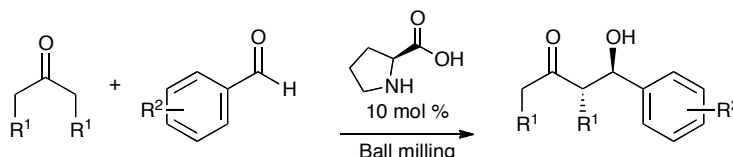
<i>Metal-free C-C bond forming reaction</i>	<i>Metal-catalyzed C-C bond forming reaction</i>
Aldol reaction	Suzuki-Miyaura
Knoevenagel condensation	Sonogashira
Michael addition	Heck
Baylis-Hillman reaction	
Wittig reaction	
Diels-Alder reaction	
Grignard reaction	

**Aldol reaction.** Raston and Scott (2000) reported aldol condensations by grinding solid aldehydes and ketones in the presence of NaOH in a vibratory ball mill for a total of two minutes over a ten-minute period. The melting was observed; the products were obtained in high yields with high chemoselectivity except for the self-condensation of 1-indanone. Kaupp et al. (2002) also performed the quantitative aldol condensation of ninhydrin and dimedone (**Scheme 1.1**). The first dehydration was carried out in a vibratory ball mill (1h, room temperature), but the second elimination of water was possible in solution. More recently, Heintz et al. (2009) reported the aldol self-condensation of valeraldehyde with Al as catalyst, and Waddell et al. (2012) described the unexpected self-condensation of cyclohexanone by milling it with NaOH and ethyl bromide.



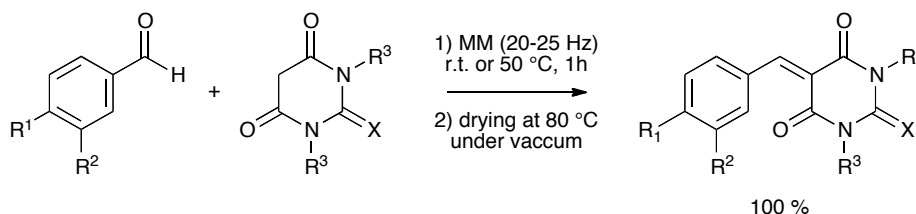
**Scheme 1.1.** Aldol condensation of ninhydrin (Kaupp et al., 2002).

Asymmetric aldol reactions were organocatalyzed by (*S*)-proline (Hernández et al., 2011; Rodríguez et al., 2006, 2007<sup>b</sup>). In particular, Bolm and coworkers reported the first successful asymmetric aldol reaction under ball milling conditions. Various aldehydes and ketones were evaluated and the anticipated aldol products were obtained in good to excellent yields (mostly  $\geq 90\%$ ), high diastereoselectivity (up to 99:1) and excellent stereoselectivities (up to 99% *ee*) (**Scheme 1.2**)(Rodríguez et al., 2006).



**Scheme 1.2.** Proline-catalyzed asymmetric aldol reaction (Rodríguez et al., 2006).

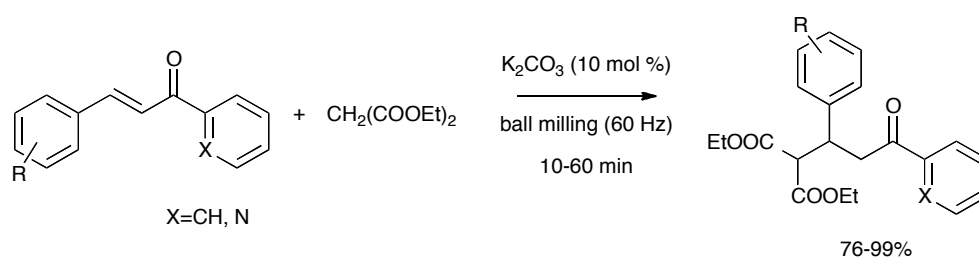
**Knoevenagel condensation.** Knoevenagel condensation is another important reaction for C-C bond formation. Kaupp et al. (2003) used a swing ball mill to prepare diverse compounds using stoichiometric amounts either in solid state (**Scheme 1.3**) or in molten systems. The products from barbituric acid were obtained quantitatively after 1 hour of milling and drying under vacuum at 80 °C.



**Scheme 1.3.** Quantitative uncatalyzed Knoevenagel condensation of aldehydes with barbituric acids (Kaupp et al., 2003).

Trotzki et al. (2008<sup>a</sup>) used malonitrile as methylene component and varied the aldehydes. Soon after 1 h of grinding in planetary mill at 800 rpm, the products were obtained in yields from 5-99%. However, these values could be increased (77-99%) for the less reactive aldehydes by placing the recovered mixture under N<sub>2</sub> atmosphere at room temperature during 24 h. The reaction continuation was ascribed to direct crystallization that is enhanced by seeding with the target product (Trotzki et al., 2008<sup>b</sup>). Stolle and co-workers has used the Knoevenagel condensation of barbituric acid derivatives and aldehydes to assess several parameters of milling devices mentioning rotation frequency, milling ball diameter and milling ball filling degree (Burmeister et al., 2014; Schmidt et al., 2015).

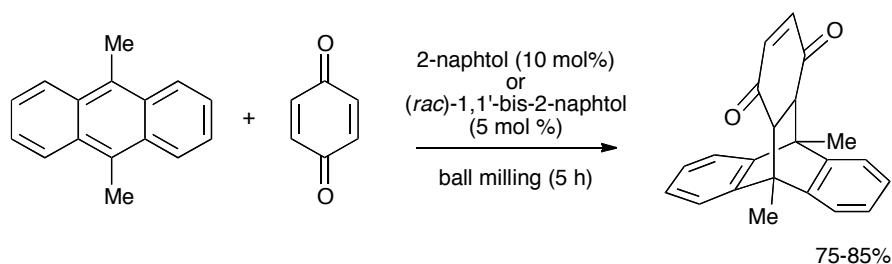
**Michael addition.** Additionally to Knoevenagel condensation reported by Kaupp et al. (2003), they also published the Michael addition, mainly in melt, but one example (4-hydroxybenzylidene malonitrile with dimedone) was ball milled affording the pure product in quantitative yields. Michael addition reaction-type was further described by Zhang et al. (2004<sup>a</sup>, 2004<sup>b</sup>) using a high-speed vibratory ball mill (60 Hz). They explored the addition of 1,3-dicarbonyl compounds to chalcones and azachalcones (**Scheme 1.4**). The presence the weak base  $K_2CO_3$  was essential to achieve good to excellent yields.



**Scheme 1.4.** Michael addition of diethyl malonate to chalcones catalyzed by  $K_2CO_3$  (Zhang et al., 2004<sup>a,b</sup>).

**Diels-Alder.** Diels-Alder type reaction, one of the most popular organic name-reactions, producing two new carbon-carbon bonds, was studied by Senna and co-workers (Watanabe and Senna, 2005; Watanabe et al., 2006) for the case of dimethylantracene and *p*-benzoquinone. The yields could be substantially increased by the addition of phenol derivatives that formed in eutectic complex with the benzoquinone (**Scheme 1.5**).

Another example of Diels-Alder using mechanochemical route is the cycloaddition of cyclopentadiene (liquid) with maleic anhydride or maleimide derivatives (solid) affording only endo-norbornenes with quantitative yield (Zhang et al., 2010). The authors did not use any solvent, catalyst or temperature to obtain the compounds in only 30 min in a mixer mill at 30 Hz. The methodology showed to be superior to the classical route (overnight THF-hexane reflux).

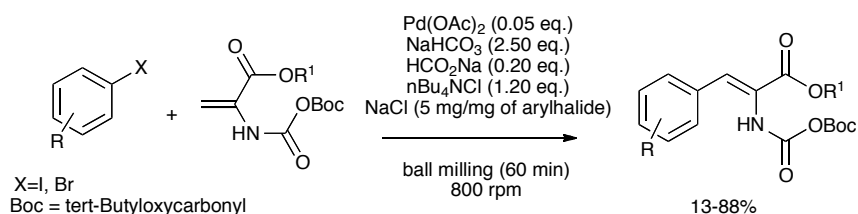


**Scheme 1.5.** Diels-Alder reaction catalyzed by phenol derivatives (Watanabe and Senna, 2005).

More recently, Diels-Alder reaction with 9-substituted anthracenes and maleic anhydride was used to characterize the chemical energetics of a SPEX 8000M mixer mill by comparing the yields mechanochemically obtained with the ones from solution (McKissic et al., 2014).

As summarized in **Table 1.1**, many other reactions involving the formation of bonds between carbon atoms were published and are not limited to the examples discussed above. Baylis-Hillman (Mack and Shumba, 2007) and Wittig (Balema et al., 2002), Grignard reaction (Harrowfield et al., 2001), fullerene cycloadditions (Zhu et al., 2013) and several organocatalytic asymmetric reactions were also investigated under mechanochemical conditions (Chauhan and Chimni, 2012). Cross-couplings palladium-catalyzed reactions such as Suzuki-Miyaura, Sonogashira and Heck reactions are also concerned and constitute a very useful strategy for the synthesis of carbon building blocks such as graphene among other nanomaterials. Metal-catalyzed mechanochemical reactions were recently reviewed, including these C-C bond-forming reactions (Hernández and Friščić, 2015).

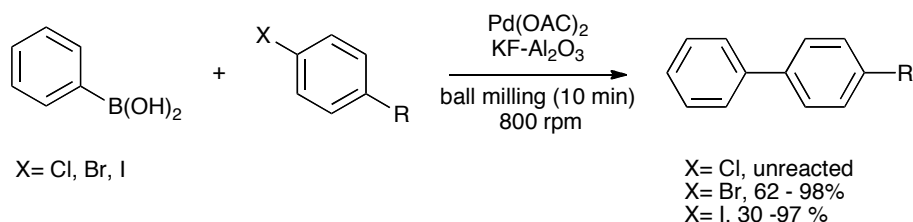
**Heck reaction.** Heck reaction can be used to synthesize many important compounds such as unsaturated amino acids. A carbon-carbon bond is formed between an aryl halide and an olefin. Tullberg et al. (2004) demonstrated the possibility to perform this reaction under solvent-free ball milling conditions. The Pd-catalyzed Heck-Jeffrey reaction of N-substituted amino acrylates with aryl halides gave the cross-coupling products in 13-88 % yields when the syntheses were conducted in a planetary ball mill for 1 h at 800 rpm (**Scheme 1.6**). It was confirmed that only that *Z*-isomer was formed, showing the diastereoselectivity of the method. Similar protocol was used to produce various amino- and hydroxyl-substituted dehydrophenylalanine derivatives (Tulberg et al., 2006).



**Scheme 1.6.** Pd-catalyzed Heck-Jeffrey reaction under ball milling conditions (Tullberg et al., 2004).

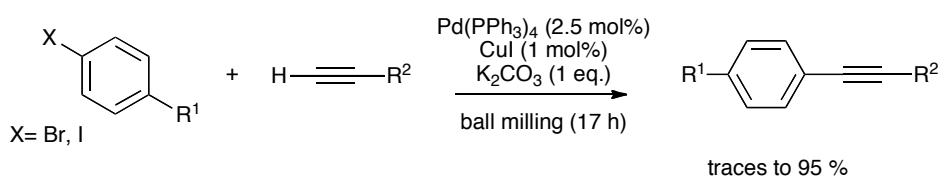
**Suzuki-Miyaura.** Suzuki-Miyaura reaction involves the coupling of boronic acids with aryl halides. Nielson et al. (2000) reported the first Pd-catalyzed Suzuki-Miyaura reaction under solvent-free, mechanochemical method. Technical problems appeared during the milling

experiments due to the stickiness of the reaction mixture. Thus, NaCl was inserted to make the mixture more powdery. More recently, Ondruschka and co-workers studied this type of C-C coupling procedure using KF-supported on Al<sub>2</sub>O<sub>3</sub> (**Scheme 1.7**). The role of water was investigated (Schneider and Ondruschka, 2008; Bernhardt et al., 2010) and, furthermore, this reaction was used to study the effects of the parameter of the milling device (Schneider et al. 2009<sup>a,b</sup>).



**Scheme 1.7.** Pd-catalyzed Suzuki-Miyaura reaction with different aryl halides in the presence of KF-Al<sub>2</sub>O<sub>3</sub> (32 wt% KF) (Schneider and Ondruschka, 2008).

**Sonogashira coupling.** Sonogashira is another reaction to form C-C bonds. It consists in a Pd-catalyzed coupling between terminal alkyne and an aryl halide or aryl triflate. Fulmer et al. (2009) established a solvent-free version of Sonogashira coupling reaction under ball milling conditions (**Scheme 1.8**). The reactions were conducted in the presence of copper iodide in a Spex 8000M mixer mill over 17 h. The substitution of CuI by vial and ball of copper yielded similar results. This work is the first example demonstrating the use of the milling bodies as catalysts in ball milled chemical reactions. Soon afterwards, the weak base 1,4-diazabicyclo[2.2.2]octane (DABCO) was employed in Sonogashira reaction of a variety of aryl halides and acetylenes, in planetary ball mill (800 rpm, 20 min) to afford the products in 45-98% yields (Thorwirth et al., 2010).



**Scheme 1.8.** Sonogashira reaction in high-speed ball milling conditions (Fulmer et al., 2009).

### C-heteroatom bond forming reactions

Carbon-heteroatom bond formation strategies using mechanical energy are overviewed in this subsection. Carbon-nitrogen is specially concerned as well as the synthesis of heterocycles

because they are related a large number of organic moieties of interest for API synthesis. Table 1.2 lists some compounds obtained from C-heteroatom bond formation.

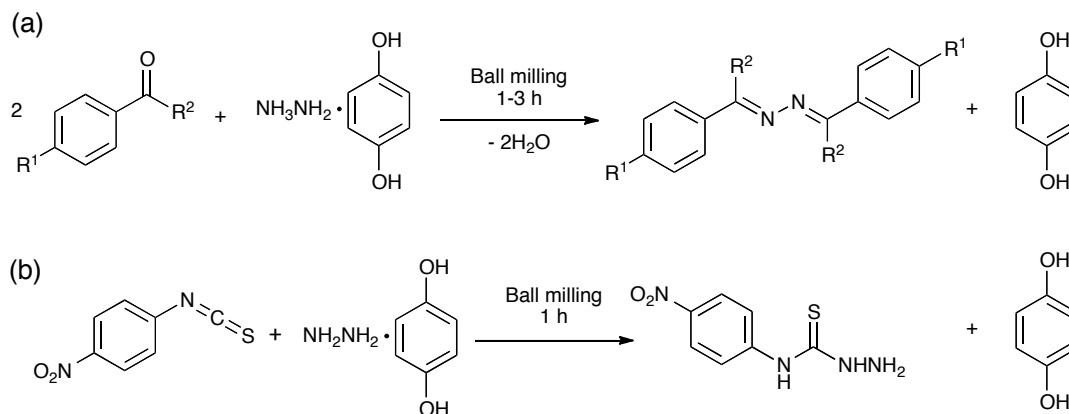
Table 1.2. C-heteroatom bond formation in ball milling conditions.

<i>C-N compounds and derivatives</i>	<i>N-Heterocyclic compounds and derivatives</i>
Imine	Pyrrole
Azine	Pyrazole
Hydrazone	Pyridazine
Amide	Diazepine
Peptide	Triazole
(thio)urea	Quinoxaline
N-protected	Phenazine
<b><i>Other C-heteroatom bond formation</i></b>	
Halogenation	Carbonates
Oxidation	Ester (transesterification)
Ether formation	Sulfides/Selenides

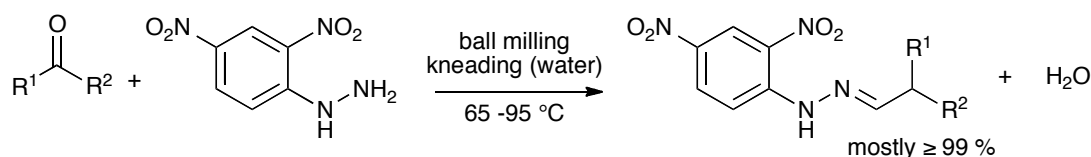
**Imines, azines and hydrazones.** Kaupp and coworkers demonstrated the application of mechanochemistry to prepare several examples of reaction with of C-N and C=N bond formation. They reported the synthesis of imines/azomethines by grinding stoichiometric amounts of aromatic aldehydes and anilines in a mortar and keeping the mixture at room temperature from 2-36 h for reaction completion. Only the reaction between 4-nitrobenzaldehyde and 4-methoxyaniline required heating at 50 °C after mechanical activation. No liquid phase was observed for these systems (Schmeyers et al., 1998). These authors also prepared azines from aldehydes or ketones using the solid complex formed with hydrazine and hydroquinone (**Scheme 1.9-a**) (Kaupp and Schmeyers, 2000). This strategy allowed maintaining the chemical reactivity of the hydrazine in solid state that is reduced when it is transformed in hydrochloride. A thiocyanate compound was treated with the complex to give a thiourea (**Scheme 1.9-b**). The syntheses were performed by ball milling during 1 – 3 h and the transformations were quantitative in all cases.

Various other reactions were carried out by Kaupp and coworkers, mentioning iminum salts and benzoylhydrazones (Kaupp et al., 2000) and the synthesis of 2,4-dinitrophenylhydrazones by kneading method with water to avoid explosion (**Scheme 1.10**)

(Mokhtari et al., 2009). The milling was performed at 65-95 °C with water to give the compounds mostly in quantitative yields.

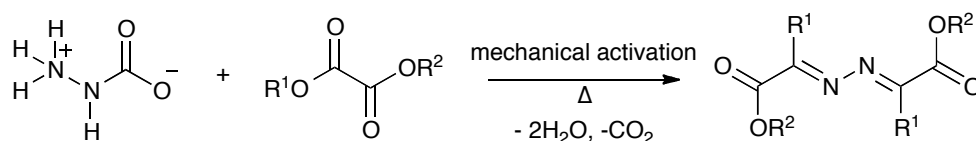


**Scheme 1.9.** (a) azine and (b) thiourea formation in ball mills (Kaupp and Schmeyers, 2000).



**Scheme 1.10.** Kneading ball milling for the preparation of 2,4-dinitrophenylhydrazones in presence of water (Kaupp et al., 2000).

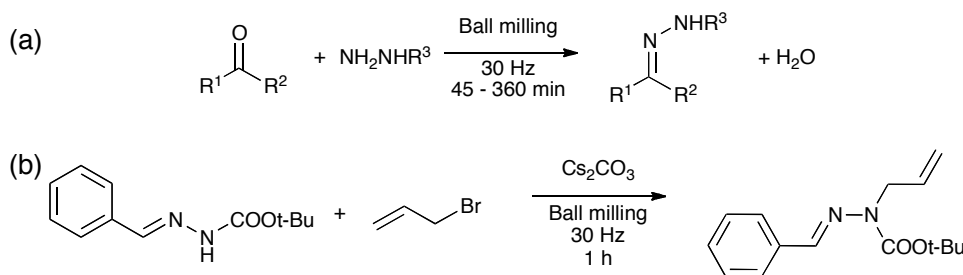
The synthesis of azines in solid state was also reported by reacting a stable solid hydrazine with aldehydes and ketones using manual grinding (Lee et al., 2011<sup>a</sup>). Lee et al. (2011<sup>b</sup>) isolated and characterized the solid hydrazine, which is a zwitterionic product from the reaction of aqueous hydrazine and carbon dioxide in supercritical conditions. Highly conjugated azines could be prepared in 97 % yield or greater (Lee et al., 2011<sup>a</sup>). The same group used the solid form of hydrazine to react with  $\alpha$ -  $\beta$ - and  $\gamma$ -keto derivatives (Lee et al., 2013). The generated products are function of the dicarbonyl compounds, including azines (**Scheme 1.11**).



**Scheme 1.11.** Azine, formation from the reaction of dicarbonyl compounds and the 'solid-hydrazine' (Lee et al., 2011<sup>a</sup>).



A series of protected hydrazones were prepared in a ball mill at 30 Hz by milling the solid reactants, aldehydes or ketones and hydrazines, until the reaction completion (45 – 360 min) (Nun et al., 2011) (**Scheme 1.12-a**). The group also performed N-alkylation using allyl or phenyl bromide as alkylation agent in the same milling device during 1 h in the presence of Cs<sub>2</sub>CO<sub>3</sub> (**Scheme 1.12-b**). The procedure afforded the products in good to excellent yields (85-96%).



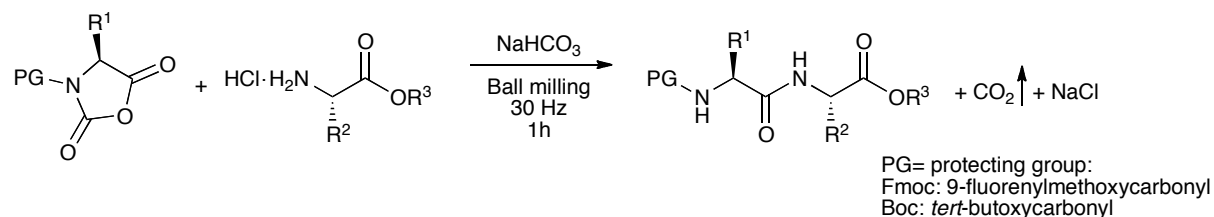
**Scheme 1.12.** (a) Hydrazone formation (b) and an example of N-alkylation in ball mills (Nun et al., 2011).

Other examples of hydrazone formation in ball mill were studied in this thesis. They are related to the mechanochemical synthesis of phenol hydrazones (Oliveira et al., 2015). These compounds with attractive pharmaceutical properties constitute the chapter 5 of this thesis.

**Amides and peptides.** Amides and peptides have also been target compounds to be synthesized mechanochemically. Štrukil et al. (2012<sup>c</sup>) reported the synthesis of aromatic amides and the one-pot synthesis of dipeptides using LAG (Scheme 19). After a screening of the coupling agent and number and size of the milling balls, *N*-ethyl-*N'*-(3-dimethylaminopropyl)carbodiimide (EDC·HCl) was chosen, also due to the easier workup in absence of harmful organic solvents. Chiral bis-amides are included in the examples synthesized, indicating a possible application of the methodology to prepare amide-based chiral ligands. Concerning the dipeptides, the racemization process, which is a typical drawback from solvated methodologies, was not observed for these LAG mechanochemical syntheses.

The solvent-free synthesis of peptides was previously described by Lamaty and coworkers (Declerck et al., 2009). They described the coupling of urethane-protected  $\alpha$ -amino acid *N*-carboxyanhydride (UNCA) derivatives with an amino ester (or amino acid amide) to produce peptides. The solid reactants were milled during 1 h in a mixer mill at 30 Hz in the presence of NaHCO<sub>3</sub> (**Scheme 1.13**). High conversion ratios were generally obtained for Boc-protecting UNCA (often  $\geq 99\%$ ), but they were lower for Fmoc-protecting group. No

racemization was observed. The report includes dipeptides such as Aspartame and also exemplifies the mechanosynthesis of a tripeptide.



**Scheme 1.13.** Synthesis of dipeptides under solvent-free ball milling conditions (Declerck et al., 2009).

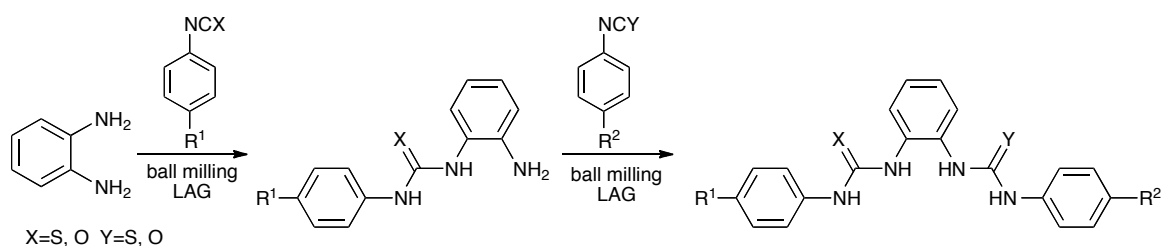
The group proceeded with the mechanosynthesis of peptides and could obtain pentapeptides in an environmentally benign route (Bonnamour et al., 2013). The ball milling (LAG) of stoichiometric amounts of Boc-protected  $\alpha$ -amino acid N-carboxyanhydrides/N-hydroxysuccinimide (Boc-AA-NCA/Boc-AA-OSu) with  $\alpha$ -amino acid alkyl ester salts in the presence of NaHCO<sub>3</sub> afforded the peptides in 83-98 % yields (20 – 60 min). In addition, the amount of liquid for LAG and the number and size of milling balls were studied. They illustrated the potential of the methodology by synthesizing the primary structure of Leu-enkephalin, which was finalized using classical routes. This molecule plays a role in processing sensory information in the brain. Other contribution for API mechanosynthesis reported by the group is the partial synthesis of the amide Teriflunomide (Métro et al., 2012).

**Click mechanochemistry for desymmetrization and thioureas.** Click chemistry can also be promoted with solid reactants in ball mills. Zhang et al. (2013) reported the synthesis of isothiocyanates, symmetrical and non-symmetrical thioureas from anilines using CS<sub>2</sub> and KOH.

Mono- and bis(thio)ureas organocatalysts were successfully prepared using click coupling of aromatic di(amines) with isothiocyanates (Štrukil et al., 2012<sup>a</sup>). Achiral and chiral, symmetrical and non-symmetrical thioureas were obtained by LAG with MeOH in a mixer mill. Subsequently, the organocatalysts were employed for Morita-Baylis-Hillman reaction in the presence of DABCO (Štrukil et al., 2012<sup>a</sup>).

The same group conducted further milling studies on desymmetrizations of aromatic diamines forming non-symmetrical thioureas (**Scheme 1.14**) (Štrukil et al., 2012<sup>b</sup>). The mono-thioureas from *o*-phenylenediamine were obtained in high yields ( $\geq 98\%$ ) in LAG conditions (MeOH,  $\eta = 0.25 \mu\text{g/mL}$ ). Bis-thioureas required longer reaction (milling) times (3 – 9 h) to give the

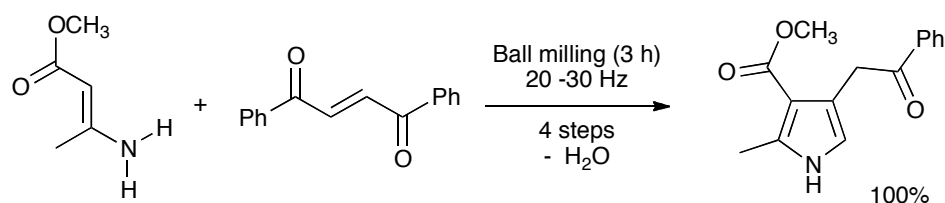
products in high yields. When the *p*-phenylenediamine is used, the desymmetrization is more delicate due to the less steric hindrance of this molecule over the *o*-diamine. After some adjusts such as solvent in LAG and the intensity of milling, reflected by the reduction of milling ball diameter and weight as well as diluting the medium with NaCl, excellent yield was obtained for *p*-methoxy derivative, but it was not successfully applied for the *p*-nitrophenyl isothiocyanate that yielded the symmetrical bis-thioureas. This was attributed to the higher reactivity of the *p*-NO<sub>2</sub> derivative.



**Scheme 1.14.** Synthesis of symmetrical and non-symmetrical *o*-phenylenediamine (thio)urea derivatives by ball milling (LAG) (Štrukil et al., 2012<sup>b</sup>).

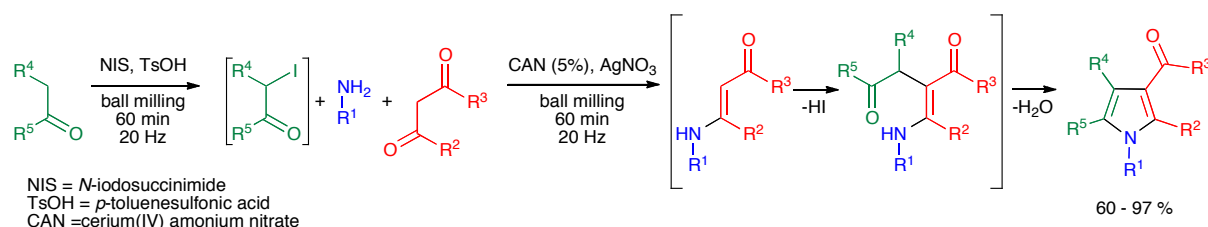
More recently, these collaborators reported the mechanosynthesis of pharmaceutically relevant sulfonyl-(thio)ureas in LAG conditions, both Cu-catalyzed and base-assisted coupling of sulfonamides and iso(thio)cyanates. Some of the compounds are APIs to treat diabetes (Tan et al., 2014).

**N-heterocycles.** Five-membered nitrogen-containing heterocycles such as pyrroles and triazoles can be found in the literature. Kaupp et al. (1999) treated primary/secondary enamine esters/ketones with *trans*-1,2-dibenzoyl ethene in a ball mill running at 20 – 30 Hz for 3 h. The protocol was used for one-pot synthesis of pyrrole derivatives in 100% yield. The four-step cascade reactions encompass a vinylogous Michael addition, imine/enamine rearrangement, cyclisation and elimination (selected example, **Scheme 1.15**).



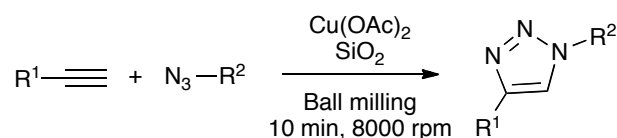
**Scheme 1.15.** Pyrrole derivatives synthesis in ball mill - 4-step reaction (Kaupp et al., 1999).

Polysubstituted functionalized pyrroles were prepared through one-pot solid-state process in a high-speed vibratory mill. The sequential multicomponent process was considered as the coupling of an  $\alpha$ -iodoketone preparation with a general version of the classical Hantzsch pyrrole synthesis (**Scheme 1.16**) (Estévez et al., 2013).



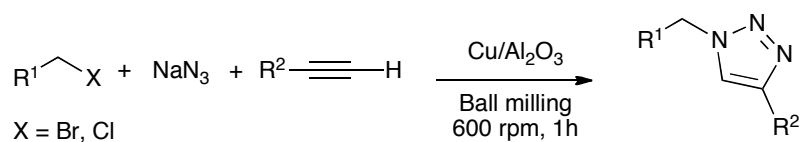
**Scheme 1.16.** Sequential three-component pyrrole synthesis in ball mill (Estévez et al., 2013).

Copper-catalyzed click reactions were carried out in ball milling devices to produce 1,2,3-triazoles (Thorwirth et al., 2011; Mukherjee et al., 2013). The methodology adopted by Thorwirth et al. (2011) gives the 1,4-substituted-1*H*-1,2,3-triazoles from azides and alkynes using a planetary ball mill (**Scheme 1.17**). The protocol was applied to a broad variety of substrates enabling to access a wide range of complex triazoles. Click polymerization in a planetary mill in the presence of SiO<sub>2</sub> using ZrO<sub>2</sub> beaker and balls could be performed as well, without destroying the polymer backbone.



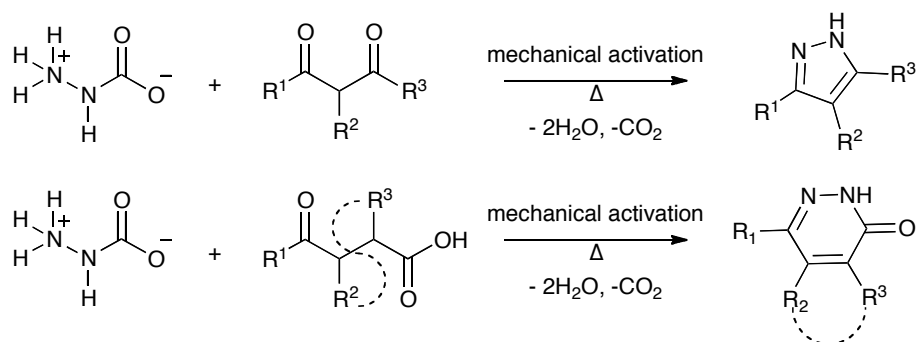
**Scheme 1.17.** Cu-catalyzed 1,3-dipolar cycloaddition of alkynes with azides forming substituted 1,2,3-triazoles in a planetary mill (Thorwirth et al., 2011).

Mukherjee et al. (2013) reported 1,2,3-triazole derivatives obtained from one-pot reaction of sodium azide and terminal alkynes with alkyl halides or aryl boronic acids over Cu/Al<sub>2</sub>O<sub>3</sub> catalytic surface (**Scheme 1.18**). When the halides were used the ball mill vessel was charged as once with the three reactants and the catalyst, while for boronic acids, the aryl azide had to be previously formed and after 1 h at 600 rpm, the alkyne was inserted to proceed the triazole synthesis. In both cases it was possible to afford the products in good to excellent yields.



**Scheme 1.18.** Cu/Al<sub>2</sub>O<sub>3</sub> catalyzed one-pot Click reaction in ball-milling for 1,2,3-triazoles derivative synthesis (Mukherjee et al., 2013).

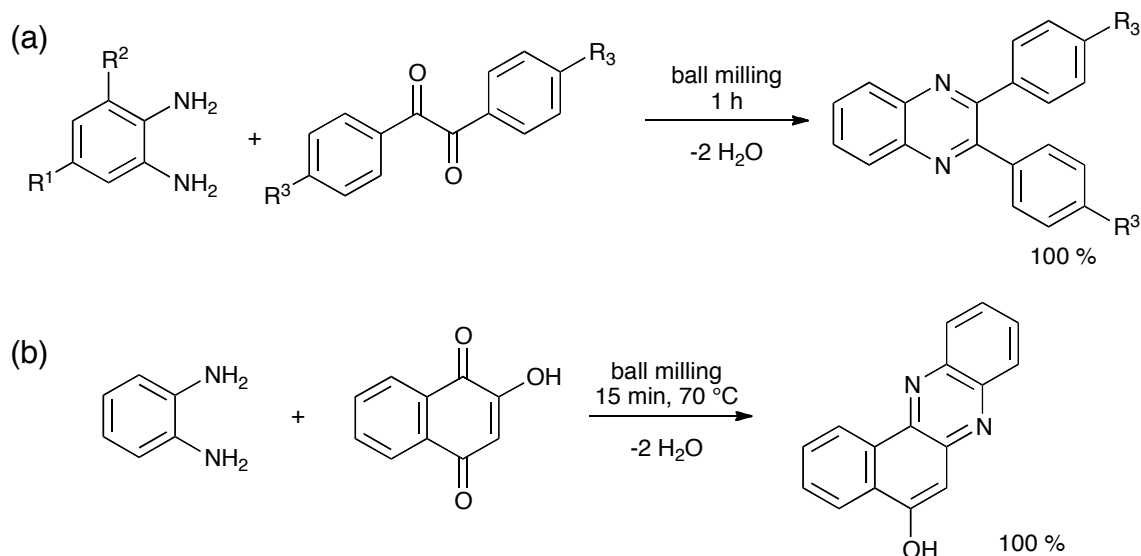
Other examples of five-membered N-containing heterocycle rings are pyrazoline (Zhu et al., 2009) and pyrazole derivatives (Paveglio et al., 2014). Lee et al. (2013) also prepared pyrazoles with the zwitterionic solid form of hydrazine-carbon dioxide as well as six-membered ring pyridazinone (**Scheme 1.19**).



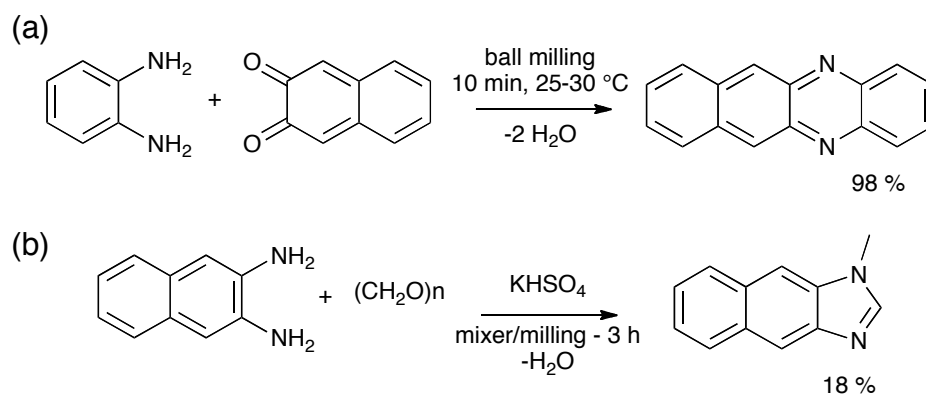
**Scheme 1.19.** Mechanically activated pyrazole and pyridazinone synthesis (Lee et al., 2013).

*o*-Phenylenediamines are good candidates to generate six-membered N-heterocycles other ring-fused structures such as benzimidazole derivatives from the reaction with dicarbonyl compounds. Kaupp and Naimi-Jamal (2002) reported a number of solvent-free reactions, among which, ball milled condensations with this 1,2-diamine. Diphenylquinoxalines were prepared quantitatively by co-grinding the appropriate starting materials in a ball mill for up to 1 h (**Scheme 1.20-a**) while benzo[*a*]phenazin-1-ol was obtained in 15 min of milling at 70 °C (**Scheme 1.20-b**). They also investigated the condensation with *o*-phenylenediamine with oxaglutamic, oxalic and parabanic acids.

Benzophenazines were prepared in ball milling devices by reacting *o*-phenylenediamine with 1,2-diones. Zefirov et al. (1996) prepared benzo[*a*]phenazine in 98 % yield using 2,3-naphthoquinone as dione and a vibrational ball mill (**Scheme 1.21-a**). They also produced two 1-methyl-1*H*-benzimidazoles and 1-methyl-1*H*-naphtho[2,3-*d*]imidazole in a vertical mixer containing steel beads. This last compound could not be produced by the conventional solution procedure (**Scheme 1.21-b**).



**Scheme 1.20.** Quantitative condensations with *o*-phenylenediamine with 1,2-dicarbonyl compounds in ball milling conditions: (a) diphenylquinoxalines and (b) benzo[a]phenazin-1-ol (Kaupp and Naimi-Jamal, 2002).

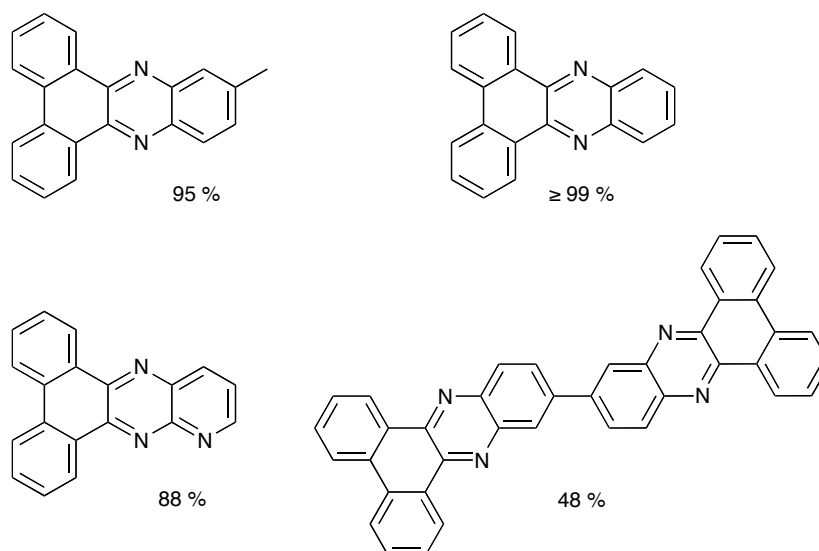


**Scheme 1.21.** (a) benzo[a]phenazine and (b) 1-methylnaphth[2,3-d]imidazole obtained under mechanical action (Zefirov et al., 1996).

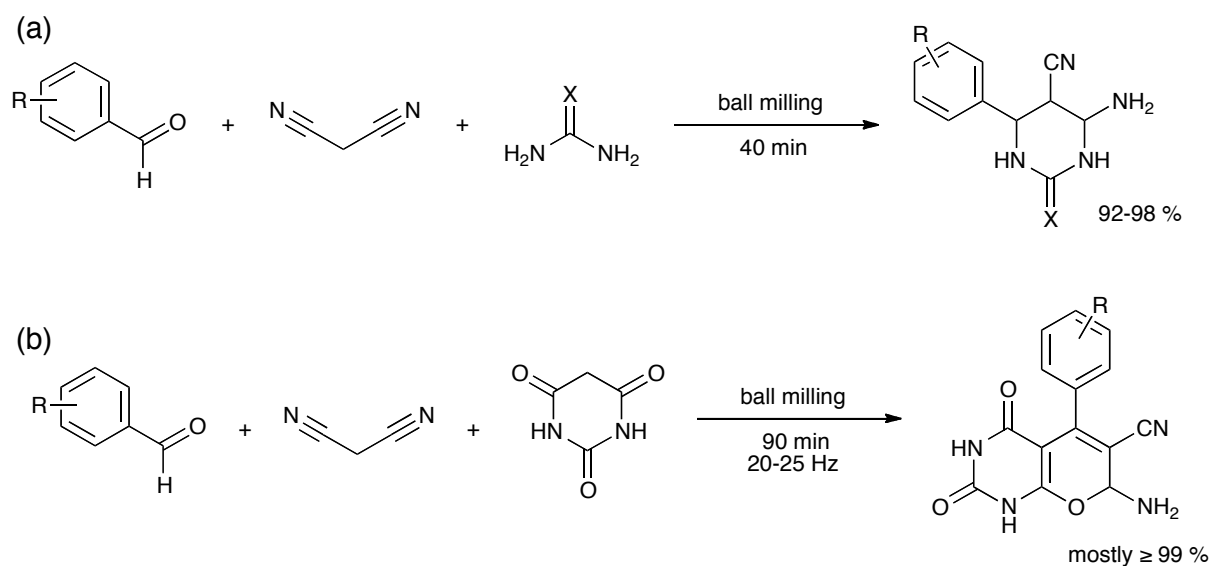
A series of dibenzophenazines was prepared with 9,10-phenanthrenequinone as 1,2-dione with *o*-phenylenediamines (Carlier et al., 2011). The yields ranged from 48 to  $\geq 99$  % as function of the diamine (**Scheme 1.22**) and the electron-donating -withdrawing effects.

The mechanochemistry with *o*-phenylenediamine and 9,10-phenanthrenequinone is further investigated in the chapter 3 of this thesis.

The three-component ball milling reactions afforded a series of 2-thio and 2-oxo-pyrimidine-5-carbonitriles in excellent yields after optimization of the milling parameters, time and total weight of the balls (**Scheme 1.23-a**) (M'hamed and Alduaij, 2014). Mashkouri and Naimi-Jamal (2009) also reported the one-pot synthesis of pyrano[2,3-d]pyridimine-2,4-(1*H*,3*H*)-diones using aryl aldehydes and malononitrile (**Scheme 1.23-b**).

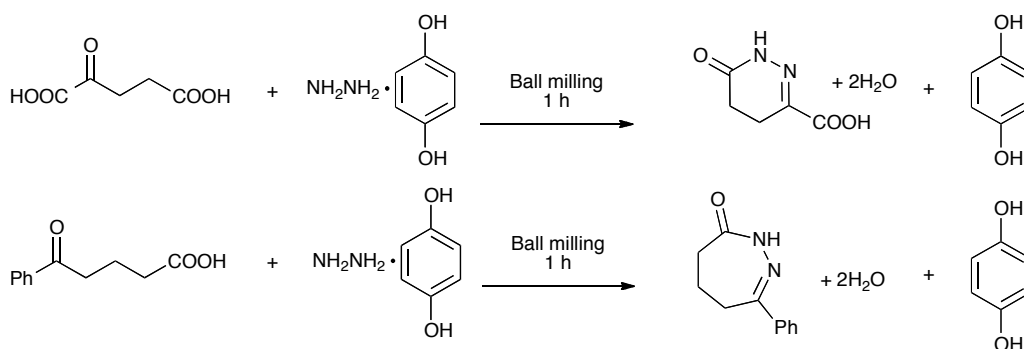


**Scheme 1.22.** Dibenzophenazines obtained by co-grinding of solid 1,2-diamines and 9,10-phenanthrenequinone (Carlier et al., 2011).



**Scheme 1.23.** Three-component reaction in milling devices: (a) (M'hamed and Alduaij, 2014); (b) (Mashkouri and Naimi-Jamal, 2009)

Kaupp and Schmeyers (2000) used the hydrazine-hydroquinone complex to generate heterocyclic structures from dicarbonyl compounds. One six-membered pyridazine and one seven-membered diazepine derivative were obtained in quantitative yields after 1 h of milling (**Scheme 1.24**).



**Scheme 1.24.** Pyridazine and diazepine derivatives prepared by ball milling (Kaupp and Schmeyers, 2000).

As mentioned before, the ball milling reactions developed for carbon-heteroatom bond formation are not limited to these selected examples. It is possible to cite *N*-protecting reactions of amino groups (Siddharth et al., 2006; Konnert et al., 2013), halogenation using *N*-bromosuccinimide in mortar and pestle (Sarma et al., 2000; Pravst et al., 2006) or in ball mill (Rahman et al., 2005) as well as the oxidative halogenation in presence of strong oxidants such as oxones (Schmidt et al., 2012; Hernández et al., 2014). Oxidation procedures in ball mills using Oxone<sup>®</sup> was reported by Collom et al. (2013) that demonstrated different selectivities in comparison to solution for oxidation of methoxylated aromatic compounds. Cravotto et al. (2012) used this reagent for chemoselective oxidation of thioethers and thiophenes. Using KMnO<sub>4</sub>, Szuppa et al. (2010) studied the oxidative cleavage of β-pinene yielding nopinone under ball milling conditions.

For further examples, a very recent book entitled “*Ball Milling Towards Green Synthesis; Application, Projects and Challenges*” (Stolle and Ranu, Eds., 2015) has different chapters dedicated to each type of the reaction cited herein with many other examples, including reactions with covalent bond formation (C-O, N-O, C-B, etc.), cocrystals, MOFs and peptides.

In despite of the few number of reactions discussed in this section in comparison to the possibilities reported in the literature, it is enough to show the potential of mechanochemistry to synthesize organic compounds in excellent, and often, quantitative yields, starting with solid reactants. The methodologies reduce or avoid the use of solvents, at least during the synthesis, which already represents a strong decrease. The most attractive aspect of mechanochemical transformations may lie on the obtainment of unexpected new products not reported under solution-based methodologies. Notwithstanding, the deep understanding of the phenomena figuring upon application of mechanical stresses is very important to allow further advances. The mechanisms of physical transformations such as liquid phase



formation, amorphous intermediate phases, or crystal-to-crystal, are included in different studies. In the other hand, the knowledge of the perturbations caused in the atomic and electronic level for mechanochemical reactions are still limited.

#### 1.4 PHYSICOCHEMICAL MECHANISTIC ASPECTS

The increasing number of publications and the prominent results demonstrate that mechanochemistry is a solid field to be further developed. For such advances, the fundamental understanding of the transformations due to mechanical stress is mandatory.

In mechanochemistry of organic compounds the milling devices are the same as those of inorganic chemistry and metallurgy and same techniques may be used and improved to understand the transformations in organics caused by the milling treatment. Boldyreva (2013) presented some aspects that are similar for all solids, such as local heating, possible eutectic melting, generation of fresh surfaces and various defects as well as the improvement of contacts between the particles. In the other hand, there are particularities of the organic solids such as the mechanical behavior of deformation, the lower vapor pressure and the anisotropy of the organic crystals. The last one is very important because a reaction performed in solid-state may present a specific orientation, different from those in solution and heat, which makes the mechanochemical route, sometimes, the unique way to access a product.

A variety of changes occur during ball milling for both inorganic and organic solids. The role of mechanical action, independently of the nature of the solid is usually (i) to provide better contact between reagents because of mixing, (ii) decreasing the particle size, (iii) generating fresh reactive surfaces and expose them to the contact, (iv) generating defects, that are probably the most reactive sites, and also, (v) the mechanical action can induce phase transitions such as melting and sublimation of one or several reagents and amorphization (James et al., 2012). These steps do not emerge mandatorily in this sequence, but in a proper dynamic of events. The defects and phase transitions are the two stages, if they take place; of the transformations suffered by the solids when milled, which are not completely clarified yet.

The great variety of reaction types, the conditions of synthesis and the differences of the raw materials make the establishment of any general rule difficult. In addition, the stochastic dynamic and the heterogeneity of the media, despite some recent advances in in-situ monitoring, remain as limiting factors for observation of the phenomena happening during the ball milling procedure.

The hot spot and magma plasma models, for friction and impact respectively, are the most cited for inorganic materials such as metals and metal oxides. To be brief, both consider deformations and local temperature rising of hundreds or thousands of degrees Celsius for very short periods ( $10^{-3} - 10^{-4}$  s) during mechanical stress (Baláž, 2008). The magma plasma theory also proclaims the generation of transient plasmas and the ejection of energetic species including free electrons (Baláž, 2008). However, to take up these theories for solid-solid organic reactions seems to be complicated because if that range of temperature were reached, an extensive decomposition would be observed and, no product could be formed.

According to Friščić and Jones (2009) the mechanochemical cocrystal formation, where secondary interactions such as hydrogen bonds, van der Waal's and  $\pi$ - $\pi$  stacking are involved, are assumed to occur, mainly, through three different pathways: (i) molecular transport across surfaces, through the vapor phase or through the bulk of the crystal, (ii) formation of a liquid phase such as eutectic intermediate phases, and (iii) reaction via an amorphous intermediate phase. Nevertheless, these transformations are not limited only to cocrystal formation, but can be also expected for organic reactions including rupture/formation of covalent bonds. Still, it is worth mentioning that a reaction can be perfectly controlled by several or all these mechanisms.

#### 1.4.1 Molecular transport

The first, molecular transport, relates to molecules only loosely held in the lattice, which is likely to occur in case where one or both reactants exhibit significant vapor pressures in solid state. Product formation in such systems is expected to occur readily upon contact between reactant solids, even in the absence of mechanical agitation (Friščić and Jones, 2009). Kuroda and co-workers have extensively studied the cocrystal formation with *p*-benzoquinone (BQ) and phenol derivatives (Kuroda et al., 2002; Cheung et al., 2003; Kuroda et al., 2004). They studied the co-grinding of crystals of racemic-bis- $\beta$ -naphthol, 2,2'-biphenol and 4,4'-biphenol with BQ, and attributed the formation of the cocrystals to molecular diffusion processes. As the BQ is a volatile solid this is the likely mechanism for such case (**Figure 1.6**). Decades before, Rastogi and co-workers had established that surface migration and diffusion through a vapor phase are the main mechanism for picric acid-aromatic hydrocarbons (*e.g.* naphthalene) cocrystal formation (Rastogi et al., 1963). Thereby, the role of mechanochemistry is to accelerate the transport of molecules and to enhance the contact between them.

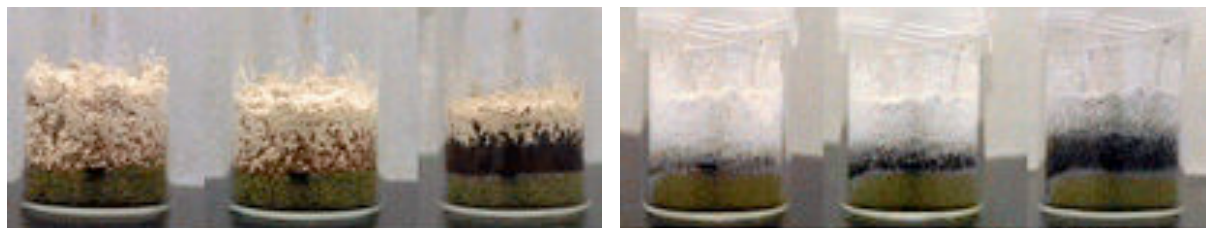


**Figure 1.6.** Softly layered powders: (left) 2,2'-biphenol and benzoquinone; (right) 4,4'-biphenol and benzoquinone (Reproduced from Kuroda et al. (2004) by permission of The Royal Society of Chemistry).

Nevertheless, Kaupp demonstrated that not only the vapor phase is able to move readily, but also the molecules can be detached under mechanical stress and moved through the bulk of the crystal. The experiments were performed by nanoscratching and imaging surfaces of molecular crystals using atomic force microscopy (Kaupp and Naimi-Jamail, 2005; Kaupp, 2003). Thiohydantoin crystal was one of them. The tip that goes down vertically through a specific face ((110)-face) of thiohydantoin crystal apparently breaks hydrogen bonds, and thus, enabling the migration of molecules or small molecular aggregates (Kaupp and Naimi-Jamail, 2005; Kaupp, 2003). This technique and the scanning near-field optical microscopy (SNOM) were also applied for solid-state organic reactions such as for azomethine synthesis. Solid anilines and solid benzaldehydes were co-ground to produce azomethines in 100% yield without passing through liquid phases. The solid-state mechanism was elucidated by AFM and SNOM that indicated long distance migration of the aldehydes into the lattice of anilines derivatives. The reactions took place not only in the points of contacts of the two solids, but also close distance sublimation was detected permitting the reaction to occur in non-contacting interfaces (Schmeyers et al, 1998). Similar observations were made for the case of solid hydrazine (hydrazine-hydroquinone complex) and aldehydes (Kaupp and Schmeyers, 2000). This methodology of investigation was first used for a gas-solid, for which, three-step mechanism was proposed by Kaupp, and then, it was extended to solid-solid reactions. Step 1 is phase rebuilding when the reacted molecules must migrate to great distances forming crystal-correlated surface feature; step 2 is phase transformation when the product lattice discontinuously forms, and it follows step 3; the crystal disintegration with formation of a new surface as the two solid phases have different crystal structures (Kaupp, 2003). The crystal packing also plays a role in how the molecular migrations will occur. However, unlike the observations of Kaupp, Rothenberg et al. (2001) and Dolotko et al. (2010) have demonstrated the formation of liquid phase for some of these reactions.

Mikhailenko, Shakhtshneider and Boldyrev (2004) studied the mechanochemical synthesis of phthalylsulphathiazole. Optical microscopy and differential scanning calorimetry (DSC) were used to elucidate the reaction between sulphathiazole and phthalic anhydride. The results allowed assuming that the main processes determining the synthesis progress are the transport of phthalic anhydride through the gas phase and the reaction of its vapor with the surface of sulphathiazole crystals. The reaction begins before any melting of the reactants, and the mechanical action decreases the temperature of the process inducing the sublimation of the reactant (Mikhailenko et al., 2004).

### 1.4.2 Formation of a liquid phase

The transformations mediated by some liquid phase are the second discussed mechanism for solid mechanochemical reactions. The examples for this kind of pathway are addressed to the product formation that can be facilitated by an intermediate liquid phase that subsequently becomes a part of the product and disappears as the reaction approaches completion (Friščić and Jones, 2009). The cases, in which one reactant is a liquid in the synthesis condition, or the addition of any liquid to be part of the final product such as the formation of hydrates or to integrate the final crystal lattice, will not be discussed here. Likewise, the use of small amount of liquids to enhance or promote molecular diffusion is not the focus. Bowmaker (2013) recently reviewed this last, liquid-assisted grinding (LAG), and it has shown as a great way to increase yields and to reduce grinding times.

Reactants that have low melting points or reaction mixtures, which may form low-melting eutectics, seem to be preferred to explain organic reactions, mainly, in which covalent bonds are formed. The cocrystal formation from benzophenone (BZP) and diphenylamine (DPA) was investigated and revealed nucleation from a submerged eutectic that started forming at 13.3 °C. Further mechanical treatment is thus required to create, by fracture or attrition, fresh BZP/DPA interfaces at which more liquid can form and hence at which more cocrystal can crystallize (**Figure 1.7**) (Chadwick et al., 2007).

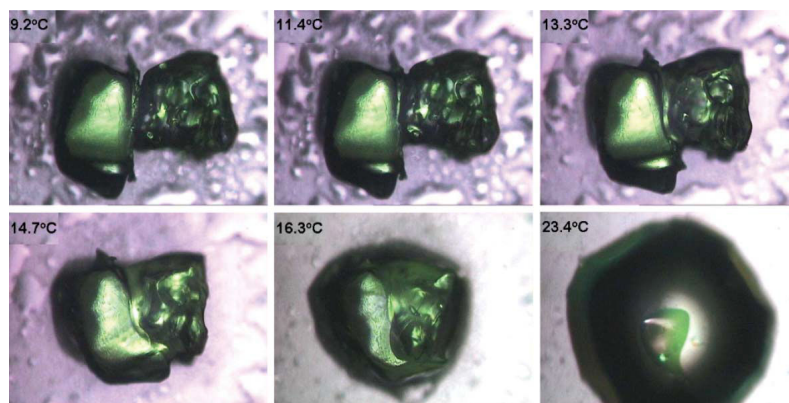


**Figure 1.7.** The eutectic melting of benzophenone and diphenylamine crystals (Reproduced from Chawick et al. (2007) by permission of The Royal Society of Chemistry).

Recently, Boldyreva and co-workers provided DSC and TGA analyses that indicate the formation of eutectic melt during shear treatment of  $\alpha$ -glycine +  $\beta$ -malonic acid forming the glycinium semi-malonate salt (Michalchuk et al., 2014). Rothenberg et al. (2001) demonstrated for a wide range of reactions that before believed to occur in solid phase formed, indeed, eutectic melts. Aldol condensation, ketone oxidation, naphthol coupling, azomethines, phenol bromination, benzhydrol etherification and oligomerization of benzylic alcohols were investigated in a mortar and pestle system and a liquid phase was detected at room temperature or, in some cases, by increasing the temperature, but still lower than the melting points. Dolotko et al. (2010), used  $^1\text{H}$  and  $^{13}\text{C}$  NMR, XRD and DSC analyses to study the reaction between *o*-vanillin and *p*-toluidine and it was showed that they react in a liquid eutectic formed upon grinding. The process of eutectic melts formed during milling is not exclusively for organic systems but also appears for inorganic materials. It still should be noted that some reactions could also form liquid products such as water that also can intervene in the reaction mechanism.

### 1.4.3 Mediation by an amorphous phase or polymorphic transition

The formation of an amorphous intermediate is the most likely mechanism of cocrystal formation in the absence of a special mass transfer pathway that would include a liquid or a gas, but for organic reactions with covalent bond formation it is also suggested the presence of amorphous during grinding. This model relates to molecules relatively strongly held in their lattice positions (*e.g.* through substantial hydrogen bonding) but whose reactivity is increased under mechanochemical conditions (Frišćić and Jones, 2009). The amorphous is expected to be more mobile which might facilitate some solid-state diffusion.

The amorphization of organic molecules, especially an API or excipient, might be a strategy in pharmaceutical industry to increase solubility and bioavailability. The use of mechanical treatment can also induce this kind of transition but also polymorphic transition. Descamps and coworkers have studied and reviewed the amorphization of sugars, sugar hydrates and pharmaceutical compounds including APIs upon milling by using diverse techniques (Descamps et al., 2007; Williard and Descamps, 2008; Williard et al., 2010; Caron et al., 2011). The solid-state amorphization of crystalline  $\alpha$ -lactose was studied structurally and thermodynamically, and, the results reveal that the processes in the course of the milling cannot be described as a simple transformation from crystal to amorphous. Instead of a biphasic system made of perfect crystalline and a genuine amorphous matter, it appears to be constituted of wide panel of structural states more or less disordered and ranging from crystalline to the amorphous state (Caron et al., 2011). Similarly, crystalline  $\alpha$ -lactose monohydrate amorphizes during milling process, but the hydrates of  $\alpha$ -trehalose and  $\alpha$ -glucose do not. The difference between the hydrates and anhydrides of the two last is attributed to the plasticizing effect of the structural water molecules which can often depresses the effective glass transition temperature below the milling temperature (Williard et al., 2010). The glass transition temperature ( $T_g$ ) plays a central role in the possibility of the amorphization of a material. It was demonstrated for pharmaceutical compounds such as lactose, mannitol, sorbitol and the drug budenoside that an amorphization or a crystal-to-crystal transition upon milling or comilling is function of the temperature of milling and their  $T_g$ . Milling crystalline compounds well below the  $T_g$  of the corresponding liquid induces a direct solid state vitrification characterized by the total absence of caramelization, different from thermal quench of the melt. In the other hand, milling crystalline compounds above  $T_g$  may induce polymorphic transformations, which generally place the system in metastable states (Descamps et al., 2007).

Indomethacin drug is another model for investigation. Otsuka et al. (1986) studied the effect of grinding on the physicochemical properties of indomethacin polymorphs. The  $\alpha$ - and  $\gamma$ -forms were converted to a noncrystalline solid during grinding at 4°C, but at 30 °C the  $\gamma$ -form was converted to metastable  $\alpha$ -form and the  $\alpha$ -form remained unchanged. It was suggested that the  $\gamma$  form of indomethacin was converted to a noncrystalline solid by mechanical stress during grinding. This noncrystalline solid was stable at 4°C, but not at 30 °C and crystallized to  $\alpha$ -form (Otsuka et al., 1986). Desprez and Descamps (2006) investigated the evolution of the amorphous state (glassy state) of indomethacin upon milling and the transformation was directly affected by parameters of milling (i.e. the energy of

milling). A glass of high energy and high disorder (absence of dimers) is produced at high milling intensity. Milling at lower intensity is able to drive the initial amorphous system directly to a crystalline organization. The nature of the phase itself depends on the milling intensity: the stable  $\gamma$ -form, which usually crystallizes at low temperature (near  $T_g$ ), is observed at the lowest milling intensity; the metastable  $\alpha$ -form, which crystallize at slightly higher temperature, is observed at higher milling intensity (Desprez and Descamps, 2006).

Finally, Jayasankar et al. (2006) studied carbamazepine-saccharin cocrystal formation during grinding and storage. The amorphous phases generated during cogrinding can lead to a crystal formation during storage. Water has a significant effect and increases the rate of cocrystallization during (1) cogrinding hydrated form of reactants, and (2) storage of co-ground reactants at high humidity. Similarly to the results of Williard et al. (2010) with sugars hydrates, water was found as a potential plasticizer.

The results presented above are not exhaustive but crucial to the comprehension of grinding and/or cogrinding of organic crystals and the transformations generated by the mechanical stress. These same modifications can certainly occur during a mechanochemical reaction. The amorphous, metastable phases, highly disordered states might be produced in the course of the ball-milling of the reactants and, consequently, increasing molecular mobility, increasing free enthalpy and the reactivity of solids. Also, the neglected environmental conditions such as moisture should be studied once it can influence the molecular dynamic transitions.

Until recently, the state of a molecular solid upon milling were sometimes suggested indirectly or not clearly detected. Currently, it can be precisely detected and quantified thanks to the latest implementations of techniques for *in-situ* monitoring.

Friščić and co-workers have focused in metal-organic frameworks, mainly zeolitic imidazolate frameworks (ZIFs), to develop *in-situ* monitoring of the mechanochemical reaction by using high-energy synchrotron X-ray diffraction (Friščić et al., 2013). The experimental setup enabled the detection of crystalline and amorphous intermediates during ball-milling, which were found to be a function of the liquid choice in liquid-assisted grinding (LAG) and ion- and liquid-assisted grinding (ILAG) (Friščić et al., 2013). More recently, they were able to quantify the amount of amorphous in these systems by Rietveld analysis and using an internal standard (Halasz et al., 2014). The method was also applied to pharmaceutical cocrystal formation from carbamazepine-saccharin and nicotinamide-suberic acid (Halasz et al., 2013). Again, amorphous and crystalline intermediates were detected,

confirming the stepwise formation of the product, and also the assessment to the particle sizes of reaction components was possible (Halasz et al., 2013).

Raman spectroscopy has also contributed to mechanistic understanding of mechanochemical reactions (Lin et al., 2013). Phase transformations in pharmaceutical compounds could be detected by using this technique (Lin et al., 2013; Hédoux et al., 2011), and more lately, an *in situ* monitoring of mechanochemical milling reactions to form coordination polymers and organic cocrystals (Gracin et al., 2014). The LAG cocrystal formation monitoring suggested the participation of the liquid in the reaction mechanism.

The last advanced in *in situ* monitoring was performed by combining X-ray diffraction and Raman spectroscopy (Batzdorf et al., 2015). The reaction mechanism of different compounds, including MOF and cocrystals, was elucidated. Theophylline-benzoic acid cocrystal, for example, was formed without any intermediate. This association allows studying milling reactions comprehensively on the molecular and crystalline structure and, therefore, deducing the pathway of mechanochemical transformations. The same group investigated the formation of a theobromine:oxalic acid 2:1 cocrystal using different techniques, but only synchrotron XRD for *in situ* monitoring (Fischer et al., 2015). A self-accelerated process explains the fast transformation from a highly activated species that is completed in 60 s. They assumed this process leads to the direct conversion of the solid reactants to the product in three phases and a diffusion mechanism was postulated (Fischer et al., 2015).

As a matter of fact, the three mechanisms covered, molecular transport across surfaces, liquid phase formation and solid transformations such as amorphous or metastable forms are interested in understanding how the crystals lose crystallinity and reorganize again. However, these physicochemical transformations are not directly addressed to the perturbations suffered in the orbital level, or in how the excitation levels of the electrons are attained to make a reaction possible.

## **1.5 THE EFFECTS OF MECHANICAL ACTION ON MOLECULAR AND ORBITAL LEVELS**

Although it is known the particularities manifested by mechanochemistry that is able to yield unique products, different from those in solution, upon applying specific mechanical energy, the understanding in how this happens is not completely elaborated yet. This is not about the



solid transformations present in the previous section involving molecular diffusion, eutectic contact melts, or some other phase generated during grinding, which are equally important, but the consequences of mechanical interaction in atomic and electronic level.

The findings in the covalent mechanochemistry domain presented in section 1.3.1, pressed forward by product formation forbidden according to Woodward-Hoffman (WH) rules (Woodward and Hoffmann, 1969), indicate different reaction pathways under mechanical stress (Wollenhaupt et al., 2015).

Moore and co-workers demonstrated, including experimental data, that the ring-opening of functionalized benzocyclobutene (BCB) yields the same product, *E,E*-diene, for both *cis*- or *trans*-functionalized BCB. This is unexpected according to WH rules, in which thermochemical excitation would give the *E,E*-diene only for the *trans* isomer, and also contrary to photochemical excitation, so disrotatory, that would raise the *E,E*-diene only for the *cis* isomer (**Figure 1.8**). Their researches have shown that WH rules can be circumvented and that mechanical energy can not only accelerate the reaction but also change the pathways in which it will occur, and then, unexpected, or unique product formation can be observed (Hickenboth et al., 2007).

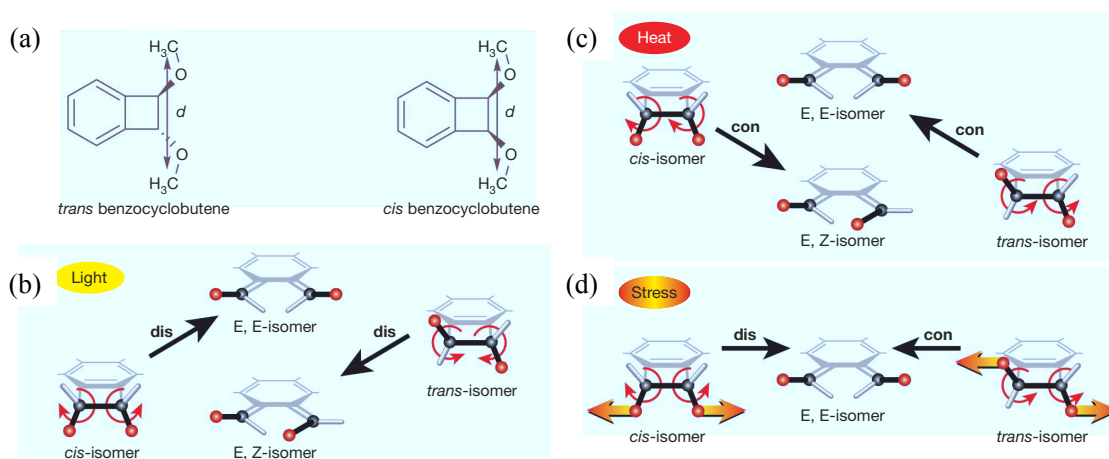


**Figure 1.8.** Electrolytic ring opening of cyclobutene. (a) the mechanical tensile force is applied in the terminal groups. The expected pathways of ring opening for *cis*- and *trans*-BCB isomers as function of the activation source of energy: (b) photochemistry, (c) thermochemistry and (d) mechanical stress (Reproduced from Hickenboth et al. (2007) with permission of Nature Publishing Group)

Gilman has exposed the role of mechanical energy in solid-state reaction mainly directed to HOMO-LUMO (highest occupied molecular orbital-lowest unoccupied molecular orbital) gap closure in molecules suffering shear strain (Gilman, 1996). Other authors confirmed by calculation that lattice deformations can significantly decrease the HOMO-

LUMO gap and also demonstrated that any excess strain, such as that associated to shock wave or defects, can further reduce the gap (Kuklja et al., 2000). These investigations were performed for energetic materials that detonate upon the application of mechanical energy. Luty et al. (2002) also studied energetic materials and looked for determining the first step of shock-induced reaction, which was attributed to a single *N-N* bond breaking for the model molecule. Previous application of their theory of solid-state reactivity showed that completely closure of HOMO-LUMO gap is not necessary for a mechanically induced chemical reaction (Luty and Eckhardt, 1995). They also evoked the concept of distortion-induced electronic degeneracy that is a kind of “inverse Jahn-Teller effect”. This last means that strain induces excitation.

Senna and co-workers investigated the ball-milled systems both inorganic and organic from the perspective of molecular orbital calculations. They analyzed the changes in HOMO-LUMO gap for Diels-Alder reaction between anthracene derivatives and *p*-benzoquinone, by artificially decreasing the dihedral angle of anthracene. It was demonstrated theoretically a decrease of the gap energy calculated for the deformation of  $\pi$  plane of anthracene and substituted-anthracene. This deformation could be a result of mechanical action deforming the molecules in the crystal lattice and favoring the position to form an activated-complex intermediate (Senna, 2004; Pradipta et al., 2004).

The few number of examples given above was used with intent of illustrating the general framework of electronic structure and its deformation induced by mechanical energy, and not to give a specialist insight on the subject. However, they inspire for deeper investigation on the exciting field of mechanochemistry.

It is clear that mechanochemical methodologies for transforming the matter offer a powerful alternative to solution-based techniques. In addition to the environmentally-friendly side due to extreme reduction of the solvents (at least during the synthetic procedures), the energy consumption by the milling devices, generally high, can also be advantageous over the heating processes in reflux, mainly because the reaction time reduction and high yields obtained. Although one can doubt about the scaling up of these systems, large-scale synthesis (Kaupp, 2006) as well as continuous production (Medina et al., 2010; Crawford et al., 2015) in mechanical energy inputting devices have been developed. Thus, industrial applications (Boldyrev, 1996) such as for pharmaceuticals (Delori et al., 2012), mainly for solid properties modification, fine chemicals, which also involve APIs synthesis, and catalysts synthesis (Xu et al., 2015) can be implemented.

Furthermore, mechanochemistry has proved to have its own space among the other domains in chemistry. This becomes clearer when the transformations induced by mechanical stress are different from those obtained from thermal procedures. However, the mechanisms arising from the mechanical stress are not fully clarified yet, probably because the lack of links between single molecular manipulation and the ball-milling mechanochemical reactions between different species.

### 1.6 REFERENCES

- Anastas, P. T., Warner, J. C, Green Chemistry: Theory and Practice, Oxford University Press, New York, 1998.
- Baig, R. B. N.; Varma, R. S. Alternative energy input: mechanochemical, microwave and ultrasound-assisted organic synthesis. *Chem. Soc. Rev.* **2012**, *41*, 1559–1584.
- Baláž, P.; Choi, W. S.; Fabián, M.; Godocikova, E. Mechanochemistry in the preparation of advanced materials. *Acta Montan. Slovaca* **2006**, *11*, 122–129.
- Baláž, P. *Mechanochemistry in Nanoscience and Minerals Engineering*, Springer Verlag, Berlin Heidelberg, 2008.
- Balema, V. P.; Wiench, J. W.; Pruski, M.; Pecharsky, V. K. Mechanically induced solid-state generation of phosphorus ylides and the solvent-free Wittig reaction. *J. Am. Chem. Soc.* **2002**, *124*, 6244–6245.
- Ballini, R., Ed. *Eco-friendly synthesis of fine chemicals*; The Royal Society of Chemistry, Cambridge, UK, 2009.
- Batzdorf, L.; Fischer, F.; Wilke, M.; Wenzel, K.-J.; Emmerling, F. Direct In Situ Investigation of Milling Reactions Using Combined X-ray Diffraction and Raman Spectroscopy. *Angew. Chemie Int. Ed.* **2015**, *54*, 1799–1802.
- Bernhardt, F.; Trotzki, R.; Szuppa, T.; Stolle, A.; Ondruschka, B. Solvent-free and time-efficient Suzuki-Miyaura reaction in a ball mill: The solid reagent system KF-Al<sub>2</sub>O<sub>3</sub> under inspection. *Beilstein J. Org. Chem.* **2010**, *6*, 30–34.
- Beyer, M. K.; Clausen-Schaumann, H. Mechanochemistry: the mechanical activation of covalent bonds. *Chem. Rev.* **2005**, *105*, 2921–2948.
- Boldyrev, V.V., Reactivity of solids: past, present and future – International Union of Pure and Applied Chemistry, Backwell Science, Oxford, 1996.
- Boldyrev, V. V. A Historic View on the Development of Mechanochemistry in Siberia. *Chem. Sus. Dev.* **2002**, *10*, 3–12.
- Boldyrev, V. V. Mechanochemistry and mechanical activation of solids. *Russ. Chem. Rev.* **2006**, *75*, 177–189 DOI: 10.1070/RC2006v075n03ABEH001205.
- Boldyreva, E. Mechanochemistry of inorganic and organic systems: what is similar, what is different? *Chem. Soc. Rev.* **2013**, *42*, 7719–7738.
- Bonnamour, J.; Métro, T.-X.; Martinez, J.; Lamaty, F. Environmentally benign peptide synthesis using liquid-assisted ball-milling: application to the synthesis of Leu-enkephalin. *Green Chem.* **2013**, *15*, 1116–1120.

- Bowmaker, G. A. Solvent-assisted mechanochemistry. *Chem. Commun.*, **2013**, *49*, 334-348.
- Braga, D.; Maini, L.; Grepioni, F. Mechanochemical preparation of co-crystals. *Chem. Soc. Rev.* **2013**, *42*, 7638–7648.
- Brantley, J. N.; Wiggins, K. M.; Bielawski, C. W. Polymer mechanochemistry: The design and study of mechanophores. *Polym. Int.* **2013**, *62*, 2–12.
- Bridgman, P. W. Effects of High Shearing Stress Combined with High Hydrostatic Pressure. *Phys. Rev.* **1935**, *48*, 825–847.
- Burmeister, C. F.; Stolle, A.; Schmidt, R.; Jacob, K.; Breitung-Faes, S.; Kwade, A. Experimental and Computational Investigation of Knoevenagel Condensation in Planetary Ball Mills. *Chem. Eng. Technol.* **2014**, *37*, 857–864.
- Carrier, L.; Baron, M.; Chamayou, A.; Couarraze, G. Use of co-grinding as a solvent-free solid state method to synthesize dibenzophenazines. *Tetrahedron Lett.* **2011**, *52*, 4686–4689.
- Caron, V.; Willart, J. F.; Lefort, R.; Derollez, P.; Dande, F.; Descamps, M. Solid state amorphization kinetic of alpha lactose upon mechanical milling. *Carbohydr. Res.* **2011**, *346*, 2622–2628.
- Caruso, M. M.; Davis, D. a.; Shen, Q.; Odom, S. a.; Sottos, N. R.; White, S. R.; Moore, J. S. Mechanically-induced chemical changes in polymeric materials. *Chem. Rev.* **2009**, *109*, 5755–5798.
- Chadwick, K.; Davey, R.; Cross, W. How does grinding produce co-crystals? Insights from the case of benzophenone and diphenylamine. *CrystEngComm* **2007**, *9*, 732-734.
- Chauhan, P.; Singh Chimni, S. Mechanochemistry assisted asymmetric organocatalysis: A sustainable approach. *Beilstein J. Org. Chem.* **2012**, *8*, 2132–2141.
- Chen, X. A Thermally Re-mendable Cross-Linked Polymeric Material. *Science (80-. )*. **2002**, *295*, 1698–1702.
- Cheung, E. Y.; Kitchin, S. J.; Harris, K. D. M.; Imai, Y.; Tajima, N.; Kuroda, R. Direct Structure Determination of a Multicomponent Molecular Crystal Prepared by a Solid-State Grinding Procedure. *J. Am. Chem. Soc.* **2003**, *125*, 14658–14659.
- Clark, J.; Macquarrie, D. Eds. *Handbook of green chemistry and technology*, Blackwell Science Publishing, 2008.
- Collom, S. L.; Anastas, P. T.; Beach, E. S.; Crabtree, R. H.; Hazari, N.; Sommer, T. J. Differing selectivities in mechanochemical versus conventional solution oxidation using Oxone. *Tetrahedron Lett.* **2013**, *54*, 2344–2347.
- Cravotto, G.; Garella, D.; Carnaroglio, D.; Gaudino, E. C.; Rosati, O. Solvent-free chemoselective oxidation of thioethers and thiophenes by mechanical milling. *Chem. Commun.* **2012**, *48*, 11632.
- Crawford, D.; Casaban, J.; Haydon, R.; Giri, N.; McNally, T.; James, S. L. Synthesis by extrusion: continuous, large-scale preparation of MOFs using little or no solvent. *Chem. Sci.* **2015**, *6*, 1645–1649.
- Declerck, V.; Nun, P.; Martinez, J.; Lamaty, F. Solvent-Free Synthesis of Peptides. *Angew. Chemie Int. Ed.* **2009**, *48*, 9318–9321.
- Delori, A.; Friščić, T.; Jones, W. The role of mechanochemistry and supramolecular design in the development of pharmaceutical materials. *CrystEngComm* **2012**, *14*, 2350-2362.
- Descamps, M.; Willart, J. F.; Dudognon, E.; Caron, V. Transformation of pharmaceutical compounds upon milling and comilling: The role of Tg. *J. Pharm. Sci.* **2007**, *96*, 1398–1407.
- Desprez, S.; Descamps, M. Transformations of glassy indomethacin induced by ball-milling. *J. Non. Cryst. Solids* **2006**, *352*, 4480–4485.

Dolotko, O.; Wiench, J. W.; Dennis, K. W.; Pecharsky, V. K.; Balema, V. P. Mechanically induced reactions in organic solids: liquid eutectics or solid-state processes? *New Journal of Chemistry*, **2010**, *34*, 25-28.

Estévez, V.; Villacampa, M.; Menéndez, J. C. Three-component access to pyrroles promoted by the CAN–silver nitrate system under high-speed vibration milling conditions: a generalization of the Hantzsch pyrrole synthesis. *Chem. Commun.* **2013**, *49*, 591–593.

Fischer, F.; Scholz, G.; Batzdorf, L.; Wilke, M.; Emmerling, F. Synthesis, structure determination, and formation of a theobromine : oxalic acid 2 : 1 cocrystal. *CrystEngComm* **2015**, *17*, 824–829.

Friedrichs, J.; Lüßmann, M.; Frank, I. Conservation of Orbital Symmetry can be Circumvented in Mechanically Induced Reactions. *ChemPhysChem* **2010**, *11*, 3339–3342.

Friščić, T.; Jones, W. Cocrystal architecture and properties: design and building of chiral and racemic structures by solid–solid reactions. *Faraday Discuss.* **2007**, *136*, 167-178.

Friščić, T.; Jones, W. Recent advances in understanding the mechanism of cocrystal formation via grinding. *Crystal Growth and Design*, **2009**, *9*, 1621–1637.

Friščić, T. New opportunities for materials synthesis using mechanochemistry. *J. Mater. Chem.* **2010**, *20*, 7599-7605.

Friščić, T. Supramolecular concepts and new techniques in mechanochemistry: cocrystals, cages, rotaxanes, open metal–organic frameworks. *Chem. Soc. Rev.* **2012**, *41*, 3493-3510.

Friščić, T.; Halasz, I.; Beldon, P. J.; Belenguer, A. M.; Adams, F.; Kimber, S. a J.; Honkimäki, V.; Dinnebier, R. E. Real-time and in situ monitoring of mechanochemical milling reactions. *Nat. Chem.* **2013**, *5*, 66–73.

Friščić, T. Metal-Organic Frameworks: Mechanochemical Synthesis Strategies. In *Encyclopedia of Inorganic and Bioinorganic Chemistry*; John Wiley & Sons, Ltd: Chichester, UK, 2014; pp. 1–19.

Fulmer, D.; Shearouse, W. C.; Medonza, S. T.; Mack, J. Solvent-free Sonogashira coupling reaction via high speed ball milling. *Green Chem.* **2009**, *11*, 1821-1825.

Furukawa, H.; Cordova, K. E.; O’Keeffe, M.; Yaghi, O. M. The Chemistry and Applications of Metal-Organic Frameworks. *Science (80-. )*. **2013**, *341*, 1230444–1 – 1230444–12.

Garay, A. L.; Pichon, A.; James, S. L. Solvent-free synthesis of metal complexes. *Chem. Soc. Rev.* **2007**, *36*, 846-855.

Gawande, M. B.; Bonifácio, V. D. B.; Luque, R.; Branco, P. S.; Varma, R. S. Solvent-Free and Catalysts-Free Chemistry: A Benign Pathway to Sustainability. *ChemSusChem* **2014**, *7*, 24–44.

Gilman, J. J. Mechanochemistry. *Science*, **1996**, *274*, 65.

Gracin, D.; Štrukil, V.; Friščić, T.; Halasz, I.; Užarević, K. Laboratory real-time and in situ monitoring of mechanochemical milling reactions by Raman spectroscopy. *Angew. Chemie - Int. Ed.* **2014**, *53*, 6193–6197.

Grandbois, M.; Beyer, M.; Rief, M.; Clausen-Schaumann, H.; Gaub, H. E. How Strong Is a Covalent Bond? *Science*, **1999**, *283*, 1727–1730.

Halasz, I.; Puškarić, A.; Kimber, S. A. J.; Beldon, P. J.; Belenguer, A. M.; Adams, F.; Honkimäki, V.; Dinnebier, R. E.; Patel, B.; Jones, W.; Štrukil, V.; Friščić, T. Real-time in situ powder X-ray diffraction monitoring of mechanochemical synthesis of pharmaceutical cocrystals. *Angew. Chemie - Int. Ed.* **2013**, *52*, 11538–11541.

Halasz, I.; Friščić, T.; Kimber, S. a. J.; Užarević, K.; Puškarić, A.; Mottillo, C.; Julien, P.; Štrukil, V.; Honkimaki, V.; Dinnebier, R. E. Quantitative in situ and real-time monitoring of mechanochemical reactions. *Faraday Discuss.* **2014**, 203–221.

Harrowfield, J. M.; Hart, R. J.; Whitaker, C. R. Magnesium and Aromatics: Mechanically-Induced Grignard and McMurry Reactions. *Aust. J. Chem.* **2001**, *54*, 423–425.

Hédoux, A.; Guinet, Y.; Descamps, M. The contribution of Raman spectroscopy to the analysis of phase transformations in pharmaceutical compounds. *Int. J. Pharm.* **2011**, *417*, 17–31.

Heinicke, G. *Tribochemistry*, Carl Hanser Verlag, München, 1984.

Heintz, A. S.; Gonzales, J. E.; Fink, M. J.; Mitchell, B. S. Catalyzed self-aldol reaction of valeraldehyde via a mechanochemical method. *J. Mol. Catal. A Chem.* **2009**, *304*, 117–120.

Hernández, J. G.; Juaristi, E. Efficient ball-mill procedure in the “green” asymmetric aldol reaction organocatalyzed by (S)-proline-containing dipeptides in the presence of water. *Tetrahedron* **2011**, *67*, 6953–6959.

Hernández, J. G.; Macdonald, N. A. J.; Mottillo, C.; Butler, I. S.; Frišćić, T. A mechanochemical strategy for oxidative addition: remarkable yields and stereoselectivity in the halogenation of organometallic Re(I) complexes. *Green Chem.* **2014**, *16*, 1087–1092.

Hernández, J. G.; Frišćić, T. *Tetrahedron Lett.*, **2015**, *56*, 4253–4265.

Hickenboth, C. R.; Moore, J. S.; White, S. R.; Sottos, N. R.; Baudry, J.; Wilson, S. R. Biasing reaction pathways with mechanical force. *Nature* **2007**, *446*, 423–427.

James, S. L.; Adams, C. J.; Bolm, C.; Braga, D.; Collier, P.; Frišćić, T.; Grepioni, F.; Harris, K. D. M.; Hyett, G.; Jones, W.; et al. Mechanochemistry: opportunities for new and cleaner synthesis. *Chem. Soc. Rev.* **2012**, *41*, 413–447.

Jayasankar, A.; Somwangthanaroj, A.; Shao, Z. J.; Rodríguez-Hornedo, N. Cocrystal formation during cogrinding and storage is mediated by amorphous phase. *Pharm. Res.* **2006**, *23*, 2381–2392.

Jimenez-Gonzalez, C., Ponder, C. S., Broxterman, Q. B., Manley, J. B. Using the Right Green Yardstick: Why Process Mass Intensity Is Used in the Pharmaceutical Industry To Drive More Sustainable Processes. *Org. Process Res. Dev.* **2011**, *15*, 912–917.

Karki, S.; Frišćić, T.; László, F.; Laity, P. R.; Day, G. M.; Jones, W. Improving Mechanical Properties of Crystalline Solids by Cocrystal Formation: New Compressible Forms of Paracetamol. *Adv. Mater.* **2009**, *21*, 3905–3909.

Kaupp, G.; Schmeyers, J.; Kuse, A.; Atfeh, A. Cascade reactions in quantitative solid-state syntheses. *Angew. Chemie - Int. Ed.* **1999**, *38*, 2896–2899.

Kaupp, G.; Schmeyers, J. Solid-state reactivity of the hydrazine–hydroquinone complex. *J. Phys. Org. Chem.* **2000**, *13*, 388–394.

Kaupp, G.; Naimi-Jamal, M. R. Quantitative Cascade Condensations between o-Phenylenediamines and 1,2-Dicarbonyl Compounds without Production of Wastes. *European J. Org. Chem.* **2002**, *2002*, 1368–1373.

Kaupp, G.; Naimi-Jamal, M. R.; Schmeyers, J. Quantitative Reaction Cascades of Ninhydrin in the Solid State. *Chem. - A Eur. J.* **2002**, *8*, 594–600.

Kaupp, G. Solid-state molecular syntheses: complete reactions without auxiliaries based on the new solid-state mechanism. *CrystEngComm*, **2003**, *5*, 117–133.

Kaupp, G.; Naimi-Jamal, M. R.; Schmeyers, J. Solvent-free Knoevenagel condensations and Michael additions in the solid state and in the melt with quantitative yield. *Tetrahedron* **2003**, *59*, 3753–3760.

Kaupp, G.; Naimi-Jamal, M. R. Mechanically induced molecular migrations in molecular crystals. *CrystEngComm* **2005**, *7*, 402–410.

Kaupp, G. Waste-free large-scale syntheses without auxiliaries for sustainable production omitting purifying workup. *CrystEngComm* **2006**, *8*, 794–804.

Kauzmann, W. and Eyring, H. *J. Am. Chem. Soc.* **1940**, *62*, 3113–3125.

Konda, S. S. M.; Brantley, J. N.; Varghese, B. T.; Wiggins, K. M.; Bielawski, C. W.; Makarov, D. E. Molecular Catch Bonds and the Anti-Hammond Effect in Polymer Mechanochemistry. *J. Am. Chem. Soc.* **2013**, *135*, 12722–12729.

Konnert, L.; Gauliard, A.; Lamaty, F.; Martinez, J.; Colacino, E. Solventless Synthesis of N -Protected Amino Acids in a Ball Mill. *ACS Sustain. Chem. Eng.* **2013**, *1*, 1186–1191.

Kuklja, M. M.; Stefanovich, E. V.; Kunz, a. B. An excitonic mechanism of detonation initiation in explosives. *J. Chem. Phys.* **2000**, *112*, 3417–3423.

Kuroda, R.; Higashiguchi, K.; Hasebe, S.; Imai, Y. Crystal to crystal transformation in the solid state. *CrystEngComm*, **2004**, *6*, 463–468.

Kuroda, R.; Imai, Y.; Tajima, N. Generation of a co-crystal phase with novel coloristic properties via solid state grinding procedures. *Chem. Commun.* **2002**, 2848–2849.

Kuzuya, M.; Kondo, S.; Noguchi, A. A new development of mechanochemical solid-state polymerization of vinyl monomers: prodrug syntheses and its detailed mechanistic study. *Macromolecules* **1991**, *24*, 4047–4053.

Lea, M. C. On endothermic decompositions obtained by pressure; Part II, Transformations of energy by shearing stress. *Am J Sci*, **1893**, *46*, 413–420.

<sup>a</sup> Lee, B.; Kang, S. H.; Kang, D.; Lee, K. H.; Cho, J.; Nam, W.; Han, O. H.; Hur, N. H. Isolation and structural characterization of the elusive 1 : 1 adduct of hydrazine and carbon dioxide. *Chem. Commun.* **2011**, *47*, 11219.

<sup>b</sup> Lee, B.; Lee, K. H.; Cho, J.; Nam, W.; Hur, N. H. Synthesis of Azines in Solid State: Reactivity of Solid Hydrazine with Aldehydes and Ketones. *Org. Lett.* **2011**, *13*, 6386–6389.

Lee, B.; Kang, P.; Lee, K. H.; Cho, J.; Nam, W.; Lee, W. K.; Hur, N. H. Solid-state and solvent-free synthesis of azines, pyrazoles, and pyridazinones using solid hydrazine. *Tetrahedron Lett.* **2013**, *54*, 1384–1388.

Lenardão, E. J.; Freitag, R. A.; Dabdoub, M. J.; Batista, A. C. F.; Silveira, C. da C. “Green chemistry”: os 12 princípios da química verde e sua inserção nas atividades de ensino e pesquisa. *Quim. Nova*, **2003**, *26*, 123.

Li, J.; Nagamani, C.; Moore, J. S. Polymer Mechanochemistry: From Destructive to Productive. *Acc. Chem. Res.* **2015**, 150715154419008.

Lin, H. L.; Zhang, G. C.; Hsu, P. C.; Lin, S. Y. A portable fiber-optic Raman analyzer for fast real-time screening and identifying cocrystal formation of drug-coformer via grinding process. *Microchem. J.* **2013**, *110*, 15–20.

Ling, A. R.; Baker, J. L. XCVI. - Halogen derivatives of quinone. Part III. Derivatives of quinhydrone. *Journal of the Chemical Society, Transactions*, **1893**, *63*, 1314–1327.

Luty, T.; Eckhardt, C. J. General Theoretical Concepts for Solid State Reactions: Quantitative Formulation of the Reaction Cavity, Steric Compression, and Reaction-Induced Stress Using an Elastic Multipole Representation of Chemical Pressure. *J. Am. Chem. Soc.* **1995**, *117*, 2441–2452.

Luty, T.; Ordon, P.; Eckhardt, C. J. A model for mechanochemical transformations: Applications to molecular hardness, instabilities, and shock initiation of reaction. *J. Chem. Phys.* **2002**, *117*, 1775–1787.

Lynch, A. J., Rowland, C. A. *The History of Grinding*, Society of Mining, Metallurgy and Exploration, 2005.

Mack, J.; Shumba, M. Rate enhancement of the Morita-Baylis-Hillman reaction through mechanochemistry. *Green Chem.* **2007**, *9*, 328–330.

- Martins, M. a P.; Frizzo, C. P.; Moreira, D. N.; Buriol, L.; Machado, P. Solvent-free heterocyclic synthesis. *Chem. Rev.* **2009**, *109*, 4140–4182.
- Mashkouri, S.; Naimi-Jamal, M. R. Mechanochemical solvent-free and catalyst-free one-pot synthesis of pyrano[2,3-d]pyrimidine-2,4(1H,3H)-diones with quantitative yields. *Molecules* **2009**, *14*, 474–479.
- McKissic, K. S.; Caruso, J. T.; Blair, R. G.; Mack, J. Comparison of shaking versus baking: further understanding the energetics of a mechanochemical reaction. *Green Chem.* **2014**, *16*, 1628-1632.
- Medina, C.; Daurio, D.; Nagapudi, K.; Alvarez-Nunez, F. Manufacture of pharmaceutical co-crystals using twin screw extrusion: A solvent-less and scalable process. *J. Pharm. Sci.* **2009**, *99*, 1693-1696.
- Méto, T.-X.; Bonnamour, J.; Reidon, T.; Sarpoulet, J.; Martinez, J.; Lamaty, F. Mechanochemical synthesis of amides in the total absence of organic solvent from reaction to product recovery. *Chem. Commun.* **2012**, *48*, 11781-11783.
- Michalchuk, A. a. L.; Tumanov, I. a.; Drebuschak, V. a.; Boldyreva, E. V. Advances in elucidating mechanochemical complexities via implementation of a simple organic system. *Faraday Discuss.* **2014**, *170*, 311–335.
- Michalchuk, A. A. L.; Tumanov, I. A.; Boldyreva, E. V. Complexities of mechanochemistry: elucidation of processes occurring in mechanical activators via implementation of a simple organic system. *CrystEngComm* **2013**, *15*, 6403–6412.
- Mikhailenko, M.; Shakhshneider, T. P.; Boldyrev, V. V. On the mechanism of mechanochemical synthesis of phthalylsulphathiazole. In *Journal of Materials Science*; **2004**, *39*, 5435–5439.
- Mokhtari, J.; Naimi-Jamal, M. R.; Hamzeali, H.; Dekamin, M. G.; Kaupp, G. Kneading Ball-Milling and Stoichiometric Melts for the Quantitative Derivatization of Carbonyl Compounds with Gas-Solid Recovery. *ChemSusChem* **2009**, *2*, 248–254.
- Mukherjee, N.; Ahammed, S.; Bhadra, S.; Ranu, B. C. Solvent-free one-pot synthesis of 1,2,3-triazole derivatives by the “Click” reaction of alkyl halides or aryl boronic acids, sodium azide and terminal alkynes over a Cu/Al<sub>2</sub>O<sub>3</sub> surface under ball-milling. *Green Chem.* **2013**, *15*, 389–397.
- Nielsen, S. F.; Peters, D.; Axelsson, O. The Suzuki Reaction Under Solvent-Free Conditions. *Synth. Commun.* **2000**, *30*, 3501–3509.
- Nun, P.; Martin, C.; Martinez, J.; Lamaty, F. Solvent-free synthesis of hydrazones and their subsequent N-alkylation in a Ball-mill. *Tetrahedron* **2011**, *67*, 8187–8194.
- Otsuka, M.; Matsumoto, T.; Kaneniwa, N. Effect of environmental temperature on polymorphic solid-state transformation of indomethacin during grinding. *Chem. Pharm. Bull. (Tokyo)*. **1986**, *34*, 1784–1793.
- Ould M’hamed, M.; Alduaij, O. K. An Efficient One-Pot Synthesis of New 2- Thioxo and 2-oxo-pyrimidine-5-carbonitriles in Ball-Milling Under Solvent-Free and Catalyst-Free Conditions. *Phosphorus. Sulfur. Silicon Relat. Elem.* **2014**, *189*, 235–241.
- Paveglio, G. C.; Longhi, K.; Moreira, D. N.; München, T. S.; Tier, A. Z.; Gindri, I. M.; Bender, C. R.; Frizzo, C. P.; Zanatta, N.; Bonacorso, H. G.; et al. How Mechanical and Chemical Features Affect the Green Synthesis of 1 H -Pyrazoles in a Ball Mill. *ACS Sustain. Chem. Eng.* **2014**, *2*, 1895–1901.
- Pichon, A.; Lazuen-Garay, A.; James, S. L. Solvent-free synthesis of a microporous metal–organic framework. *CrystEngComm* **2006**, *8*, 211-214.
- Piermattei, A.; Karthikeyan, S.; Sijbesma, R. P. Activating catalysts with mechanical force. *Nat. Chem.* **2009**, *1*, 133–137.
- Pradipta, M.; Watanabe, H.; Senna, M. Semiempirical computation of the solid phase Diels-Alder reaction between anthracene derivatives and p-benzoquinone via molecular distortion. *Solid State Ionics* **2004**, *172*, 169–172.



Pravst, I.; Zupan, M.; Stavber, S. Solvent-free bromination of 1,3-diketones and  $\beta$ -keto esters with NBS. *Green Chem.* **2006**, *8*, 1001-1005.

Rahman, A. N. M. M.; Bishop, R.; Tan, R.; Shan, N. Solid-state regio- and stereo-selective benzylic bromination of diquinoline compounds using N-bromosuccinimide. *Green Chem.* **2005**, *7*, 207-209.

Ranu, B.; Stolle, A., Eds. *Ball Milling Towards Green Synthesis: Applications, Projects, Challenges*; Royal Society of Chemistry: Cambridge, 2014.

Rastogi, R. P.; Bassi, P. S.; Chadha, S. L. Mechanism of the reaction between hydrocarbons and picric acid in the solid state. *J. Phys. Chem.* **1963**, *67*, 2569-2573.

Raston, C. L.; Scott, J. L. Chemoselective, solvent-free aldol condensation reaction. *Green Chem.* **2000**, *2*, 49-52.

Ribas-Arino, J.; Shiga, M.; Marx, D. Understanding Covalent Mechanochemistry. *Angew. Chemie Int. Ed.* **2009**, *48*, 4190-4193.

Ribas-Arino, Jordi; Marx, D. Covalent Mechanochemistry: Theoretical Concepts and Computational Tools with Applications to Molecular Nanomechanics. *Chem. Rev.* **2012**, *112*, 5412-5487.

Rodríguez, B.; Rantanen, T.; Bolm, C. Solvent-free asymmetric organocatalysis in a ball mill. *Angew. Chemie - Int. Ed.* **2006**, *45*, 6924-6926.

<sup>a</sup> Rodríguez, B.; Bruckmann, A.; Rantanen, T.; Bolm, C. Solvent-Free Carbon-Carbon Bond Formations in Ball Mills. *Adv. Synth. Catal.* **2007**, *349*, 2213-2233.

<sup>b</sup> Rodríguez, B.; Bruckmann, A.; Bolm, C. A highly efficient asymmetric organocatalytic aldol reaction in a ball mill. *Chem. - A Eur. J.* **2007**, *13*, 4710-4722.

Rothenberg, G.; Downie, a. P.; Raston, C. L.; Scott, J. L. Understanding solid/solid organic reactions. *J. Am. Chem. Soc.* **2001**, *123*, 8701-8708.

Sarma, J. A. R. P.; Nagaraju, A.; Majumdar, K. K.; Samuel, P. M.; Das, I.; Roy, S.; McGhie, A. J. Solid state nuclear bromination with N-bromosuccinimide. Part 2. Experimental and theoretical studies of reactions with some substituted benzaldehydes. *J. Chem. Soc. Perkin Trans. 2*, **2000**, 1119-1123.

Schmeyers, J.; Toda, F.; Boy, J.; Kaupp, G. Quantitative solid-solid synthesis of azomethines. *J. Chem. Soc., Perkin Trans. 2*, **1998**, *4*, 989-994.

Schmidt, R.; Stolle, A.; Ondruschka, B. Aromatic substitution in ball mills: formation of aryl chlorides and bromides using potassium peroxomonosulfate and NaX. *Green Chem.* **2012**, *14*, 1673-1679.

Schmidt, R.; Burmeister, C. F.; Baláž, M.; Kwade, A.; Stolle, A. Effect of Reaction Parameters on the Synthesis of 5-Arylidene Barbituric Acid Derivatives in Ball Mills. *Org. Process Res. Dev.* **2015**, *19*, 427-436.

Schneider, F.; Ondruschka, B. Mechanochemical solid-state suzuki reactions using an in situ generated base. *ChemSusChem* **2008**, *1*, 622-625.

<sup>a</sup> Schneider, F.; Stolle, A.; Ondruschka, B.; Hopf, H. The Suzuki-Miyaura Reaction under Mechanochemical Conditions. *Org. Process Res. Dev.* **2009**, *13*, 44-48.

<sup>b</sup> Schneider, F.; Szuppa, T.; Stolle, A.; Ondruschka, B.; Hopf, H. Energetic assessment of the Suzuki-Miyaura reaction: a curate life cycle assessment as an easily understandable and applicable tool for reaction optimization. *Green Chem.* **2009**, *11*, 1894-1899.

Senna, M. Consequences of molecular strain on the solid state addition reaction. *J. Mater. Sci.* **2004**, *39*, 4995-5001.

Sheldon, R. A., Organic synthesis: past, present and future. *Chem. Ind. (London)*, **1992**, 903-906.

- Sheldon, R. a. Green solvents for sustainable organic synthesis: state of the art. *Green Chem.* **2005**, *7*, 267–278.
- Sheldon, R. A., The E Factor: fifteen years on. *Green Chem.* **2007**, *9*, 1273–1283.
- Sikchi, S. A.; Hultin, P. G. Solventless Protocol for Efficient Bis- N -Boc Protection of Adenosine, Cytidine, and Guanosine Derivatives. *J. Org. Chem.* **2006**, *71*, 5888–5891.
- Sohma, J. Mechanochemistry of polymers. *Prog. Polym. Sci.* **1989**, *14*, 451–596.
- Spring, W. *Bull. Soc. Chim. Fr.*, **1885**, *44*, 166–169.
- Staudinger, H.; Bondy, H. F. Über Isopren und Kautschuk, 19. Mitteil.: Über die Molekülgröße des Kautschuks und der Balata. *Berichte der Dtsch. Chem. Gesellschaft A B Ser.* **1930**, *63*, 734–736.
- Staudinger, H.; Leupold, E. O. Über Isopren und Kautschuk, 18. Mitteil.: Viscositäts-Untersuchungen an Balata. *Berichte der Dtsch. Chem. Gesellschaft A B Ser.* **1930**, *63*, 730–733.
- Stolle, A.; Szuppa, T.; Leonhardt, S. E. S.; Ondruschka, B. Ball milling in organic synthesis: solutions and challenges. *Chem. Soc. Rev.* **2011**, *40*, 2317–2329.
- Stolle, A. CHAPTER 10. Technical Implications of Organic Syntheses in Ball Mills. In *Ball Milling Towards Green Synthesis*; Stolle, A.; Ranu, B., Eds.; Royal Society of Chemistry: Cambridge, **2015**; pp. 241–276.
- <sup>a</sup> Štrukil, V.; Igrc, M. D.; Eckert-Maksić, M.; Friščić, T. Click Mechanochemistry: Quantitative Synthesis of “Ready to Use” Chiral Organocatalysts by Efficient Two-Fold Thiourea Coupling to Vicinal Diamines. *Chem. - A Eur. J.* **2012**, *18*, 8464–8473.
- <sup>b</sup> Štrukil, V.; Margetić, D.; Igrc, M. D.; Eckert-Maksić, M.; Friščić, T. Desymmetrisation of aromatic diamines and synthesis of non-symmetrical thiourea derivatives by click-mechanochemistry. *Chem. Commun.* **2012**, *48*, 9705–9707.
- <sup>c</sup> Štrukil, V.; Bartolec, B.; Portada, T.; Đilović, I.; Halasz, I.; Margetić, D. One-pot mechanosynthesis of aromatic amides and dipeptides from carboxylic acids and amines. *Chem. Commun.* **2012**, *48*, 12100–12102.
- Szuppa, T.; Stolle, A.; Ondruschka, B.; Hopfe, W. An Alternative Solvent-Free Synthesis of Nopinone under Ball-Milling Conditions: Investigation of Reaction Parameters. *ChemSusChem* **2010**, *3*, 1181–1191.
- Takacs, L. The historical development of mechanochemistry. *Chem. Soc. Rev.* **2013**, *42*, 7649–7659.
- Tan, D.; Štrukil, V.; Mottillo, C.; Friščić, T. Mechanochemistry of pharmaceutically relevant sulfonyl-(thio)ureas. *Chem. Commun.* **2014**, *50*, 5248–5250.
- Tanaka, K.; Toda, F. Solvent-Free Organic Synthesis. *Chem. Rev.* **2000**, *100*, 1025–1074.
- Thorwirth, R.; Stolle, A.; Ondruschka, B. Fast copper-, ligand- and solvent-free Sonogashira coupling in a ball mill. *Green Chem.* **2010**, *12*, 985–990.
- Thorwirth, R.; Stolle, A.; Ondruschka, B.; Wild, A.; Schubert, U. S. Fast, ligand- and solvent-free copper-catalyzed click reactions in a ball mill. *Chem. Commun.* **2011**, *47*, 4370–4372.
- <sup>a</sup> Trotzki, R.; Hoffmann, M. M.; Ondruschka, B. Studies on the solvent-free and waste-free Knoevenagel condensation. *Green Chem.* **2008**, *10*, 767–772.
- <sup>b</sup> Trotzki, R.; Hoffmann, M. M.; Ondruschka, B. The Knoevenagel condensation at room temperature. *Green Chem.* **2008**, *10*, 873–878.
- Tullberg, E.; Peters, D.; Frejd, T. The Heck reaction under ball-milling conditions. *J. Organomet. Chem.* **2004**, *689*, 3778–3781.

Tullberg, E.; Schacher, F.; Peters, D.; Frejd, T. Solvent-Free Heck-Jeffery Reactions under Ball-Milling Conditions Applied to the Synthesis of Unnatural Amino Acids Precursors and Indoles. *Synthesis (Stuttg)*. **2006**, 1183–1189.

Waddell, D. C.; Clark, T. D.; MacK, J. Conducting moisture sensitive reactions under mechanochemical conditions. *Tetrahedron Lett.* **2012**, *53*, 4510–4513.

Wang, G. W., Liu, L. Mechanochemical reaction of aromatic ketones and aldehydes in the presence of Zn-ZnCl<sub>2</sub>. *Chin. Chem. Lett.*, **2004**, *15*, 587-590.

Wang, G.-W. Mechanochemical organic synthesis. *Chem. Soc. Rev.* **2013**, *42*, 7668–7700.

Watanabe, H.; Senna, M. Acceleration of solid state Diels-Alder reactions by incorporating the reactants into crystalline charge transfer complexes. *Tetrahedron Lett.* **2005**, *46*, 6815–6818.

Watanabe, H.; Hiraoka, R.; Senna, M. A Diels-Alder reaction catalyzed by eutectic complexes autogenously formed from solid state phenols and quinones. *Tetrahedron Lett.* **2006**, *47*, 4481–4484.

Willart, J. F.; Descamps, M. Solid state amorphization of pharmaceuticals. *Mol. Pharm.* **2008**, *5*, 905–920.

Willart, J. F.; Dujardin, N.; Dudognon, E.; Danède, F.; Descamps, M. Amorphization of sugar hydrates upon milling. *Carbohydr. Res.* **2010**, *345*, 1613–1616.

Wollenhaupt, M.; Krupička, M.; Marx, D. Should the Woodward-Hoffmann Rules be Applied to Mechanochemical Reactions? *ChemPhysChem* **2015**, *16*, 1593–1597.

Woodward, R. B.; Hoffmann, R. The Conservation of Orbital Symmetry. *Angew. Chemie Int. Ed. English* **1969**, *8*, 781–853.

Xu, C.; De, S.; Balu, A. M.; Ojeda, M.; Luque, R. Mechanochemical synthesis of advanced nanomaterials for catalytic applications. *Chem. Commun.* **2015**, *51*, 6698–6713.

Zefirov, N. S.; Sereda, G. A.; Volkov, V. P.; Tkachenko, S. E.; Zyk, N. V. Solid-phase synthesis of 1,2-benzophenazine and some fused imidazole derivatives. *Chemistry of Heterocyclic Compounds*, **1996**, *32*, 577–579.

<sup>a</sup> Zhang, Z.; Dong, Y.-W.; Wang, G.-W.; Komatsu, K. Highly Efficient Mechanochemical Reactions of 1,3-Dicarbonyl Compounds with Chalcones and Azachalcones Catalyzed by Potassium Carbonate. *Synlett* **2004**, 61–64.

<sup>b</sup> Zhang, Z.; Dong, Y.-W.; Wang, G.-W.; Komatsu, K. Mechanochemical Michael Reactions of Chalcones and Azachalcones with Ethyl Acetoacetate Catalyzed by K<sub>2</sub>CO<sub>3</sub> under Solvent-Free Conditions. *Chem. Lett.*, **2004**, *33*, 168-169.

Zhang, Z., Peng, Z.-W., Hao, M.-F., Gao, J.-G. Mechanochemical Diels-Alder Cycloaddition Reactions for Straightforward Synthesis of *endo*-Norbornene Derivatives. *Synlett* **2010**, *19*, 2895-2898.

Zharov, A. A. in *High Pressure Chemistry and Physics of Polymers*, Kovarskii, A. L., Ed. CRC Press, Boca Raton, FL, 1994, chap 7.

Zhu, X.; Li, Z.; Jin, C.; Xu, L.; Wu, Q.; Su, W. Mechanically activated synthesis of 1,3,5-triaryl-2-pyrazolines by high speed ball milling. *Green Chem.* **2009**, *11*, 163-165.

Zhu, S.-E.; Li, F.; Wang, G.-W. Mechanochemistry of fullerenes and related materials. *Chem. Soc. Rev.* **2013**, *42*, 7535–7570.

---

**CHAPTER 2.**

**Experimental procedures and  
characterization techniques**

---



## 2.1 INTRODUCTION

The reactors used in mechanochemistry are generally ball-milling devices and pressing machines. In the present case the experimental apparatus used throughout the studies is the vibratory ball mill Pulverisette 0 (Fritsch). It is described in the next section followed by the main techniques utilized for analytical and characterization purposes. The specificities of the procedures or syntheses and biological evaluations, in the case of hydrazones, are included in each concerned chapter.

## 2.2 THE EXPERIMENTAL APPARATUS

The ball milling devices used in mechanochemistry are usually equipment capable of high-energy impacts and energy transfer, which named the processes also as high-energy or high-speed ball milling. Section 1.1.3 in the literature review has already presented the most used ball milling devices for laboratory scale, mentioning mixer-mills (MM) and planetary mills (PM), and the parameters that could be adjusted to optimize the operation. Both ball mills, MM and PM, can provide high-energy deformations to the powder, and this reduces the milling time and increase yields. But, as also discussed, these intense processes are also accompanied by temperature rising, affecting directly the kinetics of transformations. This drawback can influence reproducibility as well as some parametric studies that have to be designed to be adapted to mill's specifications and not freely investigated. Thus, a different way could be the use less intense stress to enable greater control of temperature, even if the milling time has to be prolonged. This is particularly relevant for kinetic studies.

### 2.2.1 The vibratory ball mill Pulverisette 0

The ball mill used in this work is the vibratory ball mill Pulverisette 0 – Fritsch (P0) modified for temperature setting. **Figure 2.1** shows the original configuration (a) and a simplified scheme of the apparatus (b).

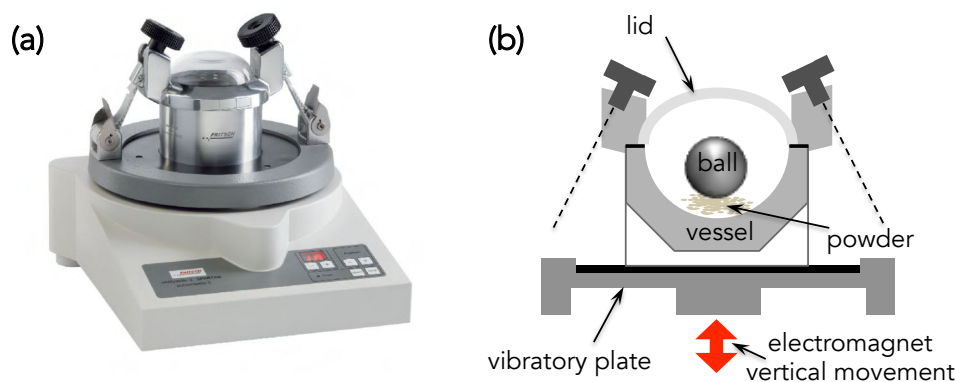


**Figure 2.1.** Vibratory ball mill - Pulverisette 0 (Fritsch) (a) picture, (b) simplified scheme of the apparatus.

The operating principle of P0 is based in impact force. The vibratory plate, bowl or vessel and the milling ball basically compose the vibratory mill P0. The plate vibrates electromagnetically and transfers the oscillatory movement to the vessel and then, to the ball. The vessel has 10 cm of internal diameter and the mass depends on the type of material. Similarly, the milling ball varies according to the type of material but also in diameter. The frequency present is 50 Hz, but the weight of milling system, bowl + ball, changes the natural vibratory frequency. However, the amplitude of the movement can always be adjusted and put constant between 0.1 and 3 mm, but up to 2 mm is recommended for grinding. The amplitude display is based on the persistence of vision of the human eye (**Figure 2.2**), and it must be checked on the amplitude plate on the clamping lid and/or on the bowl. The lines that appear to touch one another display the set amplitude.

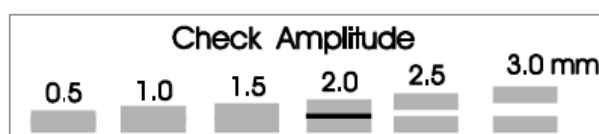


**Figure 2.2.** Amplitude display. The lines that seem to touch each other indicate the amplitude - example for 2 mm.

As mentioned before, one of the important points to study chemical reactions is the temperature of the media. As the most of the milling devices available, P0 is not equipped with a temperature control system, and thereby, a modification was made to equilibrate the temperature inside the milling apparatus, which also allowed the investigation of the mechanosyntheses at different temperatures. For this purpose, a heating/cooling coil, where water could circulate by using a thermostatic bath, was added to the experimental apparatus around the vessel. An insulating material was used to reduce the heat transfer between the

heating coil/vessel and the room. The scheme of the modified vessel and the picture of experimental set are displayed in **Figure 2.3**.

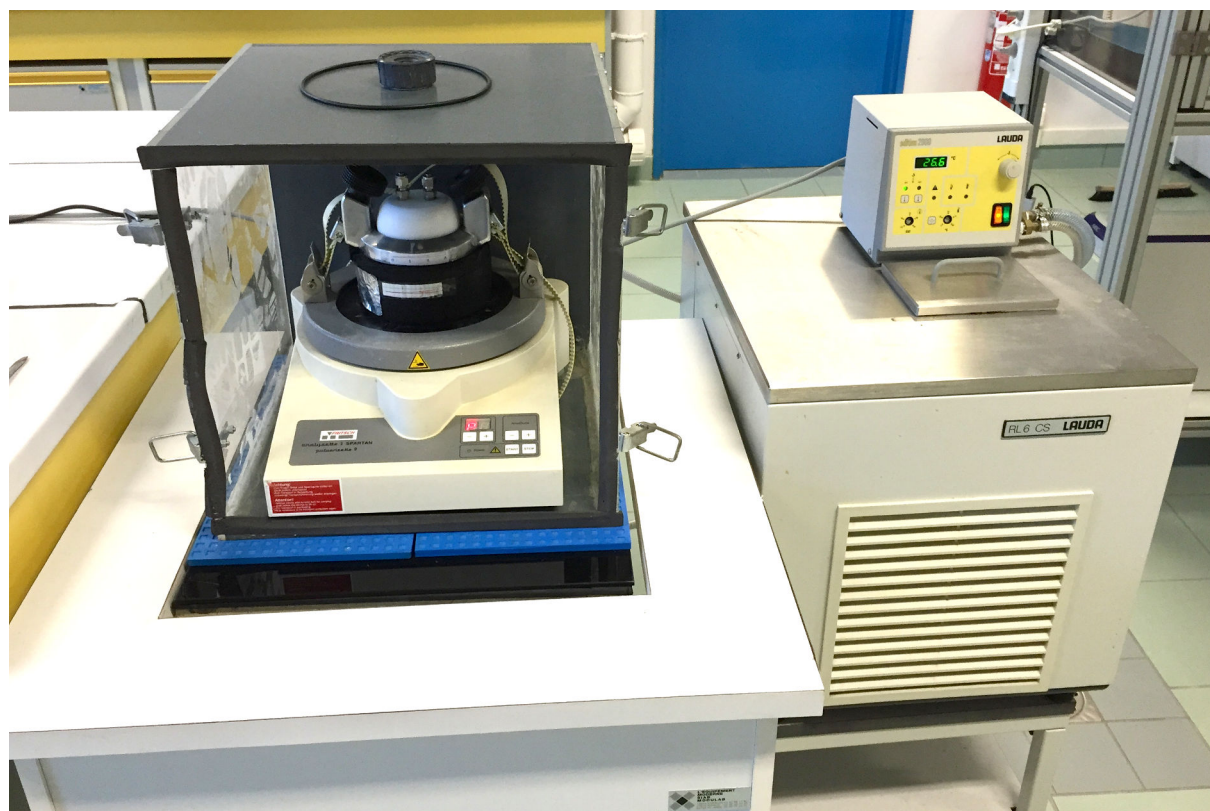


**Figure 2.3.** Picture of the experimental set.

### 2.2.1.1 Setting the milling temperature ( $T_m$ )

Owing the weight of milling media as well as the thickness of the bowl, a minimum time required to reach an equilibrium temperature was about 12 h (this had to be made every time before starting a new experiment). This equilibrium temperature is a result of two different others: the room and the bath temperature. The room temperature was always kept constant at 21 °C, and therefore, the temperature inside the bowl is function of the temperature imposed to the bath. These two temperatures, the temperature inside the bowl, hereafter called milling temperature ( $T_m$ ), and the temperature of the bath ( $T_b$ ) were not the same due to parallel energy losses and transfers. But, the  $T_m$  could be adjusted by changing  $T_b$ , and the pair  $T_m - T_b$  could be reproducible. For example, when the  $T_m$  should be 25 °C,  $T_b$  had to be set to 27 °C. And, every time that  $T_b$  was 27 °C,  $T_m$  was about 25 °C.

The temperature was measured before each run with a thermocouple. During grinding the temperature could not be monitored due to the movement of the ball, which would crash and break the thermocouple. In any case, the temperature control enabled the reproducibility



of the results for a certain temperature, as it will be seen in the Chapter 4, dedicated to kinetic investigations.

## 2.3 CHARACTERIZATION AND ANALYTICAL TECHNIQUES

### 2.3.1 Kinetic monitoring by high-performance liquid chromatography (HPLC)

The HPLC is the most widespread tool for analysis of complex mixtures and the most used in the pharmaceutical domain. HPLC technique was used for quantitative kinetic monitoring of dibenzo[a,c]phenazine (DBPZ) and 2,3-diphenylquinoxaline (DPQ) synthesis (Chapter 3 and 4). HPLC is a separation technique that uses a stationary phase, the column, and a mobile phase or eluent, which generally is a mix of liquid solvents. The system is equipped with a pump that is responsible for the elution and mixing if different components are used as mobile phase. After injection of the sample, it goes into the flowing eluents and then, into the column where the separation based on polarity/affinity between the compounds to be analyzed and the stationary phase will occur. The time required for a compound to come off the column, this is, the time it takes to travel from the injection until the detector, is called retention time. Retention time will increase by increasing the affinity between the solute and the stationary phase or decreasing the affinity between the solute and the mobile phase. When the compound passes again into the eluents, it goes to the detection system, which is generally based on physicochemical properties such as refraction index and UV-vis absorbance. The intensity of response of the detection is directly proportional to the concentration of a certain compound in the sample. It is by using these responses that it is possible to construct the calibration curve; signal as function of concentration.

#### 2.3.1.1 Method and calibration curves

The method for DBPZ and DPQ synthesis were established after a screening of HPLC conditions with different columns, eluents composition and elution conditions (gradient or isocratic, flow rate). The method is fully described in Table 2.1, including the wavelength for each compound for UV-vis detection (predetermined).

The methodology for analysis and quantification of the compounds also includes the sample preparation and the calibration curves. Since the HPLC conditions are determined, the calibration curves are constructed for a specific range of concentrations, being linear in this

range. For the case of DBPZ and DPQ reaction monitoring, these calibration curves were obtained from standard solutions, with known concentrations, of the three components, reactants 1,2-diamine, 1,2-dione and the product, DPQ only. DBPZ is very insoluble and could not be quantified in those conditions. **Figure 2.4** shows the curves that were validated for a range of concentration according to the validation spreadsheet published by Ribeiro et al. (2008). The calibration curves (area under the peak and concentration) were linear presenting accuracy and precision including repeatability that was checked periodically.

Table 2.1 HPLC conditions for DBPZ and DPQ kinetic monitoring.

<b>HLPC equipment</b>	Agilent 1100 series		
<b>Column</b>	Reversed phase Waters Symmetry C <sub>18</sub> (WAT054275) 100 Å, 5 µg, 4.6 mm x 250 mm		
<b>Mobile phase (Rate flow)</b>	ACN <sup>a</sup> /H <sub>2</sub> O (1mL/min)		
<b>Type of elution</b>	<b>Gradient</b>		
	t (min)	ACN/H <sub>2</sub> O (v/v)	
	0 – 4	40/60	
	4 – 4.5	transition to 100/0	
	4.5 – 10.5	100/0	
	10.5 – 11	transition to 40/60	
11 – 18	40/60		
<b>Injection volume</b>	20 µL		
<b>Detection</b>	<b>UV-vis</b>		
	Compound	Wavelength (λ-nm)	Retention time (min)
	PDA <sup>a</sup>	210	3.3
	BZ <sup>a</sup>	260	8.4
	PQ <sup>a</sup>	260	7.9
	DPQ	245	9.6
DBPZ	-	-	
<b>Solvent for the sample</b>	ACN		
<sup>a</sup> ACN = acetonitrile, PDA= o-phenylenediamine, PQ = 9,10-phenanthrenequinone, BZ = benzil			

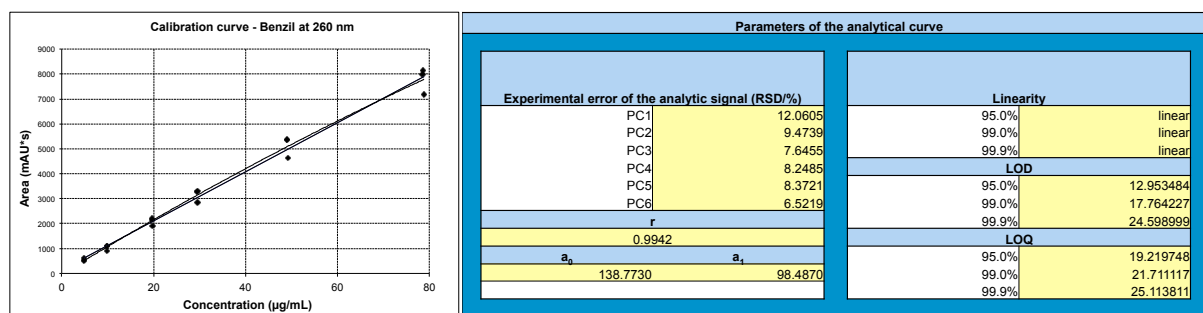


Figure 2.4. Analytical calibration curve and the parameters for benzil (from Ribeiro et al., 2008).

### 2.3.1.2 Kinetic monitoring - sample preparation and quantification

The DBPZ and DPQ syntheses by co-grinding were monitored according to the conditions described above. For a general kinetic experiment, the grinding process was stopped, the powder mixture was put together inside the bowl and then the sample was withdrawn, always about 20 mg, which represents approximately 1 % of the total amount. This amount must be respected because smaller quantities are not representative and more than 20 mg can disturb the system. Immediately, the sample was dissolved in 20 mL of ACN, diluted 10 times and injected, and the grinding was restarted again as well. Figure 2.5 illustrates the sampling procedure from the bowl until injection in the HPLC.

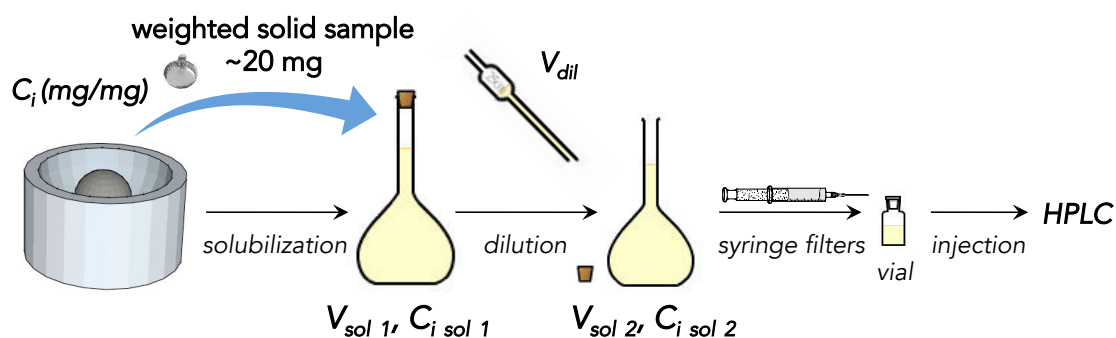


Figure 2.5. Preparation of the samples for HPLC.

The concentration of the compound  $i$  was first determined in  $\mu\text{g/mL}$  by using the equations of the calibration curves (area of the peak as function of the concentration), and then was converted in mg of component  $i$ /mg of the solid sample (Eq. (2.1)).

$$C_i(t) = \frac{C_{i \text{ sol } 2} \cdot V_{\text{sol } 1}}{m_t} \times \frac{V_{\text{sol } 2}}{V_{\text{dil}}} = \frac{m_i}{m_t} \quad (2.1)$$

$C_i$  is the concentration of the compound  $i$  present in the sample that was withdrawn from the milling in any time ( $t$ );

$C_{i\ sol}$  is the concentration of the compound  $i$  in the solution injected for HPLC;

$V_{sol\ 1}$  is the volume of the solution for solubilization of the solid sample;

$V_{sol\ 2}$  is the volume of the diluted solution from solution 1;

$V_{dil}$  is the volume taken from solution 1 to be diluted and form solution 2;

$m_i$  is the weight of the compound  $i$  present in the total weight of the sample ( $m_t$ ).

The reaction conversion was calculated according to Eq. (2.2) with  $C_i(t)$ :

$$X_i = \frac{C_i(t = 0) - C_i(t)}{C_i(t = 0)} \quad (2.2)$$

Note that Eq. (2.2) corresponds to the extent of reaction. This term is used to test the experimental data according to the solid-state kinetic reaction models (Khawan and Flanagan, 2006).

### 2.3.2 Techniques for solid-state characterization and analysis

The use of characterization techniques other than for solid samples to investigate mechanochemical transformations can cover the real events in the solid mixture. Therefore, it is preferred to keep the solid state when it is possible, in spite of the complexity originated from such heterogeneous media that makes very difficult the treatments and interpretations specially for decorrelating different phenomena.

Very outstanding advances to investigate mechanochemical transformations have been reported mainly using synchrotron X-ray diffraction and Raman spectroscopy for *in situ* monitoring (Batzdorf et al., 2015; Frišćić et al., 2013; Halasz et al., 2014). However, some adaptations in the milling devices are mandatory (Halasz et al., 2013) and, sometimes, they are not possible for all kinds of machines.

For the studies reported here, the use of techniques using solid samples is prioritized when possible. Moreover, this was fundamental for understanding some mechanisms of synthesis induced by mechanical action and enabled observing some events not possible in solution. Although they were carried *ex situ*, the analyses were run immediately after milling.

### 2.3.2.1 Differential scanning calorimetry (DSC) analysis

DSC is a thermo-analytical technique based on the difference between the heat required to heat a sample under analysis and a reference, generally an empty crucible, both at the same thermal conditions. As the thermal energy is supplied to the sample, the temperature increases and it is accompanied by changes in enthalpy and specific heat. These changes are slow, but continuous for a certain physical state of the sample, and can be strongly perturbed when the physical state undergoes some transformation. The transitions will be identified due to the pattern of the curves (heat flow as function of temperature) and the enthalpy or the shift on the specific heat can be measured when applicable. The interest of the technique is on these transitions that include polymorphic transitions, crystalline to amorphous, glassy to crystal, the melting point, recrystallization, etc. The analysis can also be performed in the sense of cooling.

DSC analysis was used in order to determine the melting point and heat of fusion of the pure solid compounds, and to investigate the transitions for a mixture of reactive powders (case of *o*-phenylenediamine and benzil).

A DSC Q200 (TA Instrument) and TGA-DSC 11 (Setaram) equipment were used. All the analyses were carried out using nitrogen as purge gas at 50 mL/min at different heating flows, usually 5 or 10 °C/min, as function of sample and measure.

### 2.3.2.2 Differential scanning calorimetry (DSC) and hot-stage microscopy (HSM)

Although DSC analysis has plethora of applications, sometimes DSC measurements are not enough by themselves to conclude about the nature of the thermal event. Eutectic contact melting of reactive powders is an example, in which various events may happen, are superposed and hardly dissociated. This case was observed for the powder mixture of PDA and BZ, which upon reaching a certain temperature, can melt, react and recrystallize. One solution for cases like this is to couple with another technique that gives complementary information such as chemical structure shifts (e.g., FTIR) and morphological changes. This last is the case of hot-stage microscopy (HSM).

Hot-stage microscopy is the result of the combination of the microscope with thermal analysis and it is widely used for visual characterization of thermal transitions. A classical instrument setup is composed by a heating stage, the *hot-stage*, where the sample is deposited, a microscope and, a system that allows measurements of temperature and video/pictures capture.

For PDA:BZ studies, a DSC hot-stage system for direct observations was adapted. A Mettler-Toledo FP900 Thermosystem with a FP90 central processor and a FP84HT measuring cell (the hot-stage) with a transparent window for direct observation were used. The computer program FP99 is able to control the heating rate and to generate the DSC signals. A digital microscope VHX-100 (Keyence) was used for observation, video and picture capture. It was placed right above the glass window of the FP84HT cell. The scheme of the experimental apparatus is shown in **Figure 2.6**.

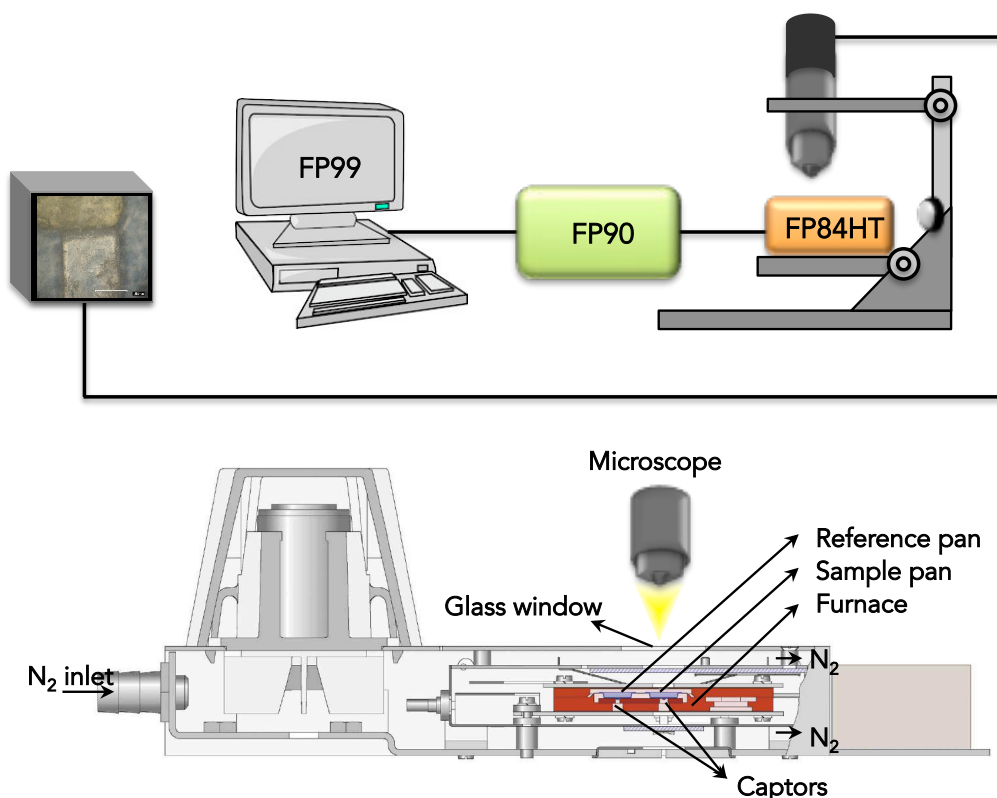


**Figure 2.6.** Experimental apparatus for simultaneously DSC analysis and visual observation of phase transitions: on the top, general scheme and on the bottom, the hot-stage cell (FP84HT).

### 2.3.2.3 Calorimetric measurements

Exploiting the fact that the DBPZ and DPQ reactions continue after grinding, calorimetric measurements were performed using a C80 Calvet Calorimeter (Setaram). For each measure, the powder mixture, always at 1:1 mol/mol (total of 2g), was milled for a certain time at 25 °C. The grinding was stopped; all the powder recovered was put in a stainless steel cell also at 25 °C, and subsequently, into the C80 chamber. The calorimetric monitoring was proceeded isothermally at 25 °C during 24 h. At the end, some samples were taken for

quantification. These measurements enabled the quantification of the heat released by the reaction after grinding.

### 2.3.2.4 X-ray diffraction (XRD)

Solid-state reactions are accompanied by structure changes during reaction. Amorphization during grinding, generation of metastable phases, cocrystals or crystalline intermediates, can be detected by X-ray diffraction. This technique was used to extract information about the solid phases in mechanochemical reaction. The reaction progress was followed qualitatively at different times during reaction and after grinding as well during 24 h. The apparatus used is a Panalytical X'pert Pro MPD (Phillips), with a Cu  $K\alpha$  radiation (1.543 Å) at 45 kV and 40 mA. The reflections were collected in the  $2\theta$  ranging from 6° to 70° with a step size of 0.0668°, a time of 200.025 s per step a scan speed of 0.0424 °/s. This results in 26 min per scan. The phase search was carried out with the JCPDS, COD and CCDC databases when possible.

### 2.3.2.5 Solid-State $^{13}\text{C}$ CP-MAS NMR

A Bruker Avance III 400 MHz WB solid-state spectrometer was used for  $^{13}\text{C}$  cross polarization and magnetic angle spinning (CP-MAS) nuclear magnetic resonance (NMR). This technique was used for possible detection of intermediate and solid transformation monitoring of the reactive solid mixture for DPQ and DBPZ synthesis. For a typical experiment, after grinding during a determined time, a sample was withdrawn and then inserted in the rotor for NMR analysis and accumulated during 20 min. The experiments were performed during grinding at 25 °C, i.e., just like HPLC monitoring, where the grinding was stopped, the sample taken and the grinding restarted, and also after grinding. In this last case, the same sample was kept inside the spectrometer at 25 °C and NMR spectra were taken each hour (20 min of accumulation + 40 min of waiting time) for the next hours (6 h or 24 h) as function of the reaction.

### 2.3.2.6 Raman spectroscopy

The Raman spectra were recorded for the solid sample without further treatment after grinding. The samples were analyzed using a combined Confocal Raman AFM- instrument (WITec alpha 300R, WITec GmbH, Ulm, Germany) operating in Raman mode and in ambient conditions (ca. 22 °C, air). Raman spectra were recorded using a 532 nm frequency-doubled Nd:YAG laser and ultrahigh-throughput (UHTS 300) spectroscopy system with a

CCD (charge-coupled device) as detector. Each spectrum is a result of 10 others at a selected point for an integration time of 1s.

#### 2.3.2.7 Absolute density

The true (absolute) density of the hydrazines was obtained using a Micromeritics AccuPyc II 1340 gas pycnometer with He as gas in 1 cm<sup>3</sup> cell. The measurements were performed two or three times, in which, each one is the average of twenty-five runs. Actually, the volume is measured and the density is calculated with the mass put in the cell.

### 2.3.3 Classical techniques for molecule characterization

After each mechanosynthesis the products were identified and characterized by <sup>1</sup>H NMR, <sup>13</sup>C NMR, FTIR, UV, MS/HRMS and melting point.

#### 2.3.3.1 <sup>1</sup>H NMR and <sup>13</sup>C NMR

The <sup>1</sup>H NMR and <sup>13</sup>C NMR analysis were performed using high-field spectrometers: Bruker AVANCE-300 MHz (2 channels) or a Bruker AVANCE-400 MHz (3 channels) with DMSO-*d*<sub>6</sub> as solvent. Chemical shifts  $\delta$  were expressed in parts per million (ppm), by frequency imposed by the spectrometer, relative to TMS.

#### 2.3.3.2 Fourier Transformed Infrared Spectroscopy (FTIR)

FTIR analysis for identification was performed using KBr pellets on a Thermo Nicolet 5700 spectrometer. The main peaks/bands were identified, specially the -C=N- that is attributed to the hydrazone. FTIR studies with the solid hydrazines as function of temperature were recorded in IN10MX Thermo Scientific FTIR microscope equipped with THMS600 (Linkam Scientific Instruments) heating and freezing stage.

#### 2.3.3.3 UV-vis spectroscopy

UV-Vis spectroscopy was performed using a HP (Hewlett Packard) 8452A diode array spectrophotometer from 200 to 400 nm, with ethanol as a solvent at 20 °C and using quartz cells. The molar absorptivity was determined for the wavelength with the highest absorbance through Lambert-Beer's law with the molar absorptivity  $\epsilon$  in (dm<sup>3</sup> mol<sup>-1</sup> cm<sup>-1</sup>), expressed for the  $\lambda_{\max}$  of the molecule.



### 2.3.3.4 Mass Spectrometry and High Resolution Mass Spectrometry (MS/HRMS)

For determining of the exact mass, MS and HRMS were performed using a Waters Quadrupole Time-of-flight mass spectrometer XEVO G2-S QToF. The samples were dissolved in methanol and Electrospray ionization method was used.

### 2.3.3.5 Melting point determination

The melting points were determined using a Kofler heating bench system Heizbank Type WME (Wagner & Munz GmbH, Germany), with measuring accuracy of  $\pm 1^\circ\text{C}$  in the range of 50-260°C. If the melting point was higher than 260°C or if it could not be exactly determined because of an apparent degradation, the DSC analysis was employed. The analysis was performed in a TGA-DSC 111 (Setaram). The temperature programming was from 20 °C to 200 or 260 °C according to the sample with a constant rate of 5°C /min under nitrogen atmosphere.

## 2.4 REFERENCES

- Batzdorf, L.; Fischer, F.; Wilke, M.; Wenzel, K.-J.; Emmerling, F. Direct In Situ Investigation of Milling Reactions Using Combined X-ray Diffraction and Raman Spectroscopy. *Angew. Chemie Int. Ed.* **2015**, *54*, 1799–1802.
- Friščić, T.; Halasz, I.; Beldon, P. J.; Belenguer, A. M.; Adams, F.; Kimber, S. a J.; Honkimäki, V.; Dinnebier, R. E. Real-time and in situ monitoring of mechanochemical milling reactions. *Nat. Chem.* **2013**, *5*, 66–73.
- Halasz, I.; Friščić, T.; Kimber, S. a. J.; Užarević, K.; Puškarić, A.; Mottillo, C.; Julien, P.; Strukil, V.; Honkimaki, V.; Dinnebier, R. E. Quantitative in situ and real-time monitoring of mechanochemical reactions. *Faraday Discuss.* **2014**, 203–221.
- Halasz, I.; Kimber, S. a J.; Beldon, P. J.; Belenguer, A. M.; Adams, F.; Honkimäki, V.; Nightingale, R. C.; Dinnebier, R. E.; Friščić, T. In situ and real-time monitoring of mechanochemical milling reactions using synchrotron X-ray diffraction. *Nat. Protoc.* **2013**, *8*, 1718–1729.
- Khawam, A.; Flanagan, D. R. Solid-state kinetic models: Basics and mathematical fundamentals. *J. Phys. Chem. B* **2006**, *110*, 17315–17328.
- Ribeiro, F. A. L.; Ferreira, M. M. C.; Morano, S. C.; Silva, L. R.; Scheider, R. P. Planilha de validação: uma nova ferramenta para estimar figuras de mérito na validação de métodos analíticos univariados (Validation spreadsheet: a new tool for estimating the analytical figures of merit for the validation of univariate methods). *Quim. Nova*, **2008**, *31*, 164-17. (spreadsheet available in <http://lqta.iqm.unicamp.br/programasPLAN.html>)

---

## **CHAPTER 3.**

# **The investigation of the mechanisms of 1,4-diazines mechanosynthesis**

---



### 3.1 INTRODUCTION

This first part is dedicated to the fundamental understanding of 1,4-diazine mechanochemical reactions. Dibenzo[a,c]phenazine (DBPZ) and 2,3-diphenylquinoxaline (DPQ) synthesis, which are interesting basic chemical structures for therapeutic molecules (Laursen and Nielsen, 2004; Pereira et al., 2015), are under investigation. These reactions were chosen regarding the previous results and the proposed mechanism published for DBPZ mechanosynthesis (Carlier et al., 2011, 2013 and Haruta et al., 2013) and the similarity of DPQ structure and synthesis to the former. This chapter aims to advance in elucidating some mechanisms of reaction, which could be specific from mechanical activation on solids, performing a comparative study of these two reactions. The kinetic behavior at room temperature, the calorimetric measurements after grinding, X-ray diffraction and solid-state  $^{13}\text{C}$  CP-MAS NMR were used to give new insights in the comprehension of these mechanoreaction pathways.

#### 3.1.1 Mechanochemical reactions pathways

The interaction between the mechanical energy and the electronic state of the molecules undergoing mechanical stresses was presented in the section 1.6 of the literature review. The findings of new reactions pathways such as those described by the experiments in covalent mechanochemistry (Hickenboth et al., 2009) as well as the proposition of HOMO-LUMO gap closure, as a result of mechanical deformation (Senna, 2004; Gilman, 1996), are very interesting and instigate the mechanistic studies of ball milling reactions.

Thereby, the investigation of dibenzo[a,c]phenazine synthesis arises with the purpose to contribute to the understanding of molecular mechanisms during mechanical perturbations as well as its limitations. It has started with the synthesis of different dibenzophenazines and further investigation of reaction mechanism after grinding and finally, with the possibility of a concerted mechanism for the continuous milling period as presented below.

#### 3.1.2 Previous results on the investigation of dibenzo[a,c]phenazine mechanosynthesis

The dibenzophenazines and derivatives are important precursors of therapeutic relevance. The solvent-free mechanochemical synthesis of dibenzo[a,c]phenazine (DBPZ) was reported by Baron and co-workers along with similar molecules, with excellent yield in only 4 h of co-grinding of *o*-phenylenediamine (PDA) and 9,10-phenanthrenequinone (PQ) (Carlier et al.,

2011). Further investigation on kinetics of this synthesis revealed an apparent zero-order reaction when the samples were analyzed immediately after withdrawing, and if they were maintained as powders, i.e., not in solution, the reaction could continue and 24 h after the conversion would evolve. This means that the reaction is spontaneous while in solid-state after a mechanical activation (Carrier et al., 2013). The kinetic behavior instigated a detailed study of the reaction mechanism (See **Figure 3.1**). A stepwise mechanism, push-pull, was proposed using a molecule of water eliminated during the first step as a kind of catalyst for the second addition and, subsequently elimination of water and aromatic ring formation. The results were supported by particle size measurements of the reactants and product (Carrier et al., 2013).

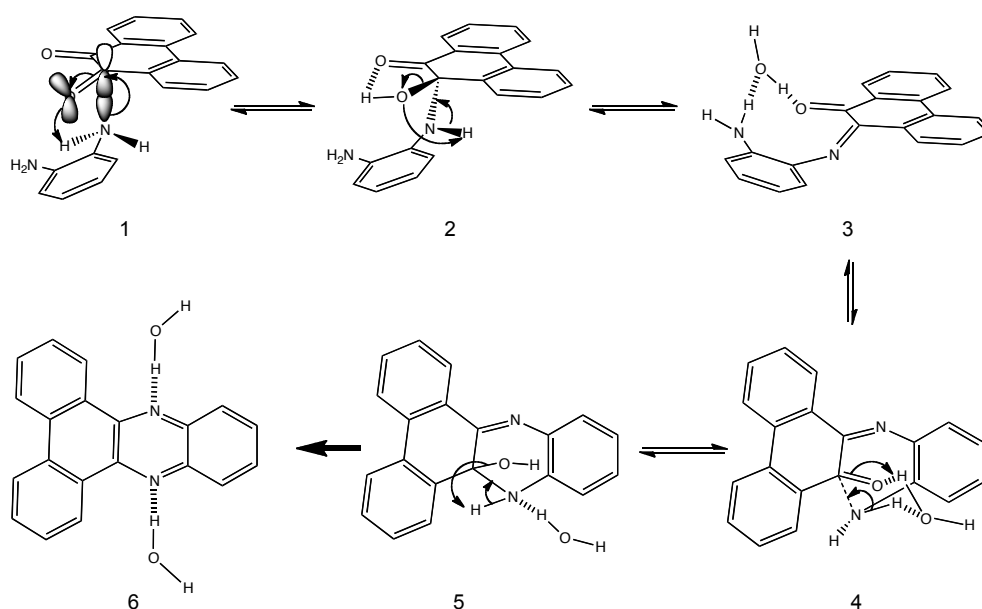


**Figure 3.1** General scheme for DBPZ stepwise formation: (1-3) formation of quinone-imine by addition/elimination; (4-5) transition state, “push-pull” mechanism and the second addition/elimination catalyzed by water and (6) dibenzo[a,c]phenazine (hydrate).

Although this stepwise mechanism proposed is more likely from the organic chemistry point of view, quantum chemistry calculation using frontier orbital theory and vibronic coupling density analysis indicated the possibility of a concerted mechanism as well (Haruta et al., 2013). The results suggested that  $C_2$  symmetry of diamine, which is the most stable isomer, favors the stepwise mechanism, and the  $C_s$  symmetrical isomer favors the concerted mechanism (**Figure 3.2**). However, the  $C_s$  is the most unstable by a difference of 182 meV (4.20 kcal/mol), thus requiring some excitation that cannot be generated thermally, but

possibly mechanically. The reactive site of PQ, the carbonyl, has the symmetrical distribution of the vibronic coupling densities at its reactive site, which also favors the concerted pathway.

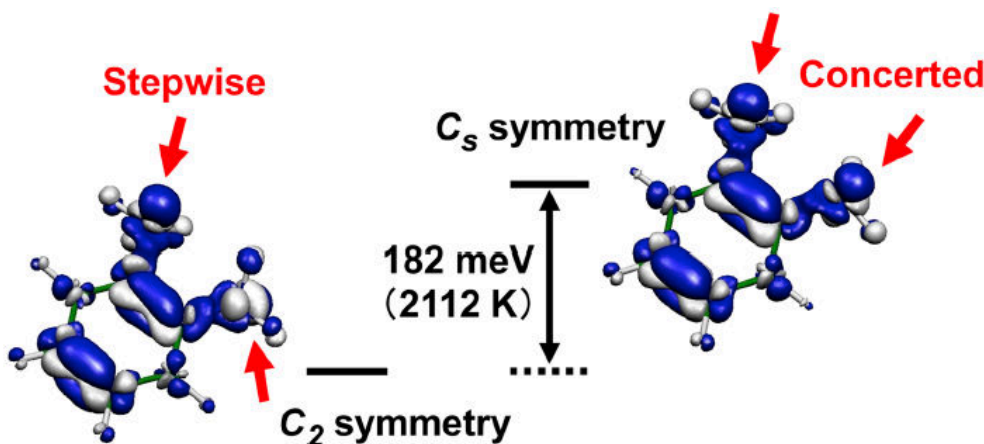


**Figure 3.2.** Vibronic coupling densities for effective vibrations of  $C_s$  and  $C_2$  symmetrical diamine cations and the energy gap between them (Reproduced from Haruta et al., (2013) with permission of Elsevier).

The possibility of a concerted mechanism opened new discussions and further investigation for DBPZ mechanochemical synthesis.

## 3.2 EXPERIMENTAL SECTION

### 3.2.1 Materials

*o*-phenylenediamine (PDA) (Sigma-Aldrich, 98 %), 9,10-phenanthrenequinone (PQ) (abcr GmbH, 95 %) and benzil (BZ) (abcr GmbH, 98 %) were used as received. All the solvents used for analysis, if necessary, have analytical degree. Milli-Q<sup>®</sup> water was used throughout the work.

### 3.2.2 General procedure for synthesis

For a typical experiment, 2 g of powder composed of stoichiometric amounts of 1,2-diamine and 1,2-dione, without previous mechanical treatment, were placed in the bowl of the P0 with the ball at the equilibrium temperature (25 °C), the milling was started and the amplitude adjusted at 2 mm. *o*-phenylenediamine (PDA, 0.6698) and 9,10-phenanthrenequinone (PQ,

1.3204 g) were used for DBPZ synthesis, and PDA (0.6793 g) and benzil (BZ, 1.3207 g) for DPQ synthesis.

The grinding system, bowl + ball, was left to equilibrate at the required temperature (25°C) for at least 12 h before each run. The total weight of the powder of 2 g was maintained for all experiments. The vibratory ball mill is described in the previous chapter.

### 3.3 RESULTS AND DISCUSSION

#### 3.3.1 The mechanosynthesis of dibenzo[a,c]phenazine (DBPZ)

The 1,4-diazine compound, dibenzo[a,c]phenazine (DBPZ) is synthesized through the reaction of a 1,2-diamine with 1,2-dione. **Figure 3.3** schematizes the synthesis of this molecule with *o*-phenylenediamine (PDA) (1,2-diaminobenzene) as diamine and 9,10-phenanthrenequinone (PQ) as dione.

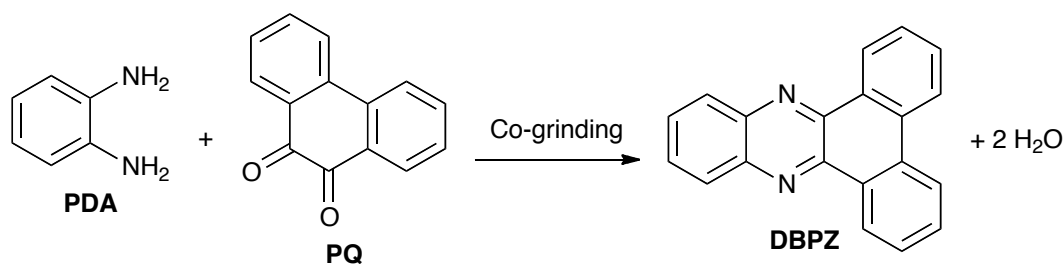


**Figure 3.3.** Synthesis of dibenzo[a,c]phenazine (DBPZ) by co-grinding.

As mentioned before, this reaction was already performed mechanochemically at room temperature. Carlier et al. (2011) reported DBPZ synthesis with quantitative transformations (> 99 %) after 4 h of grinding in the vibratory ball mill P0.

A special characteristic of DBPZ mechanosynthesis is the reaction continuation when the grinding is stopped, but only if the reaction mixture is kept in solid state. If it is dissolved, the reaction will not progress anymore. These characteristics allowed the solid studies such as calorimetric, XRD and <sup>13</sup>C CP-MAS NMR investigations. This was also observed for DPQ mechanosynthesis as it is discussed in its respective sections. It is important to mention that even if the reactions continue after grinding, the interest is on the states achieved during and immediately after grinding.

### 3.3.1.1 Kinetics of DBPZ reaction

The solid-state synthesis of DBPZ was monitored by HPLC. The transformations were followed in means of reactants disappearance due to the very poorly solubility of DBPZ. **Figure 3.4** shows the conversion of PQ during the milling period for DBPZ mechanosynthesis.

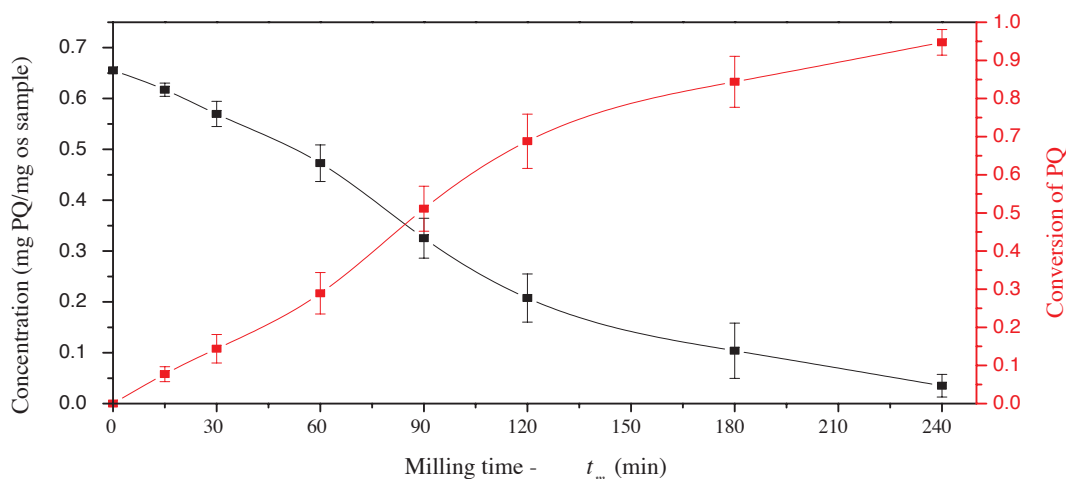


**Figure 3.4.** Kinetic monitoring of PQ transformation for DBPZ synthesis.

The curves from **Figure 3.4** present three different regions, with PQ almost completely transformed after 4 h of milling. The reaction starts slowly with no more than 30 % of conversion from the beginning until 60 min of milling. This period is followed by acceleration of the reaction rate from 60 until 120 min. In this range, the reaction reaches 70 % of conversion for the half time of milling. The last period is marked by the reduction of the reaction rate probably due to concentration effects. From 120 until 240 min, the other half of milling time, the conversion achieved 97 %.

The first slower period could be attributed to physical effects such as particle size reduction that requires part of the mechanical energy, which cannot serve entirely for the reaction. This certainly contributes to retard the reaction, but particle size distribution during milling for the couple PDA and PQ showed that no further reduction takes place after 10 min of grinding (Carlier et al., 2013). Therefore, this part can also correspond to an activation period in which several reactive sites are generated and dispersed in the media. The concentration of the reaction/product formation sites increases and upon reaching a significant concentration the reaction suffers the acceleration observed from 60 until 120 min of grinding due to the several templates of the product already present, in addition to the heat released



from the reaction that can be used to induce further transformation. The deceleratory region from 120 until the reaction completion completely agrees with the low concentration of unreacted species (< 26 % w/w) that are diluted in the powder mixture constituted majorly by the product, which results in physical barriers for reactant contacts to react. Consequently, more two hours of milling are needed to push the reaction forward from 70 % to 97-99%.

The phenomena in solid system reactions diverge from those of homogenous reactions in solution by several factors. The meaning of concentration, the physical species in mechanochemical reactions such as solids, crystalline or amorphous, and the eventual presence of liquids added or formed during milling illustrate such differences. The kinetic data must be carefully analyzed bearing in mind the complexity of mechanochemical reactions. Up to date, there is no kinetic model developed for reaction between solids induced by mechanical action. On the other hand, there are kinetic models for solid-state reactions conducted under thermal conditions. Although these models find some resistance to be applied to mechanochemical reaction, mainly for diffusion in dynamic systems, they can be very useful to give some suggestions of the limiting mechanisms in solid reactions even for mechanically activated media. Reaction-order, nucleation/growth and geometrical models are included in these models that are shown in Appendix I.

For the case of DBPZ synthesis, the models were tested in their integral form. Among the tested models, the Avrami-Eroffeev model (also known as Johnson-Mehl-Avrami-Erofeev-Kolmogorov (JMAEK) models) showed the best fit to experimental data (Cumbrera and Sánchez-Bajo, 1995; Khawam and Flanagan, 2006). The general relation of this model for isothermal transformations is:

$$\alpha = 1 - e^{-kt^n} \quad (3.1)$$

where  $n$  is the Avrami exponent (indicative of transformation process) and  $k$  is the rate constant representing both nucleation and growth. The reaction extent  $\alpha$  is analogous to the conversion, in this case, the conversion of PQ ( $X_{PQ}$ ), and  $t$  is reaction time.

In order to determine  $n$  and  $k$  for DBPZ mechanosynthesis and to evaluate the correlation between experimental points and equation (3.1), the nonlinearized experimental data from **Figure 3.4** were fitted to the general form of Avrami-Erofeev equation and are shown in **Figure 3.5**.

It can be seen that the model is well adjusted to the experimental points ( $R^2 = 0.9926$ ) giving  $n=1.45384$  and  $k=9.93 \times 10^{-4} \text{ min}^{-1}$  or  $5.96 \times 10^{-4} \text{ s}^{-1}$ . The value of  $n$  is consistent with a diffusion-controlled growth. Another form to verify the correspondence between the data and the model is from the linearization of the data (the linearization of equation (3.1)) in the form of Sharp-Hancock plot (not shown) (Hancock and Sharp, 1972). In this case, the  $n$  is obtained from the slope and is equal to 1.30, agreeing with the value found for the nonlinearized data fit. Finally, the general form of the reaction rate for DBPZ in the described conditions at 25 °C is:

$$[-\ln(1 - \alpha)]^{\frac{1}{n}} = kt \quad (3.2)$$

or

$$[-\ln(1 - \alpha)]^{0.688} = 5.96 \times 10^{-4} t \quad (3.2)$$

that is similar to A1.5 kinetic model.

Avrami-Erofeev mathematical model is based on the concept of nucleation and growth of the product within the bulk of the reactant mixture. This is similar to the first discussion of the kinetics of DBPZ of this section and apparently confirms that several nuclei are generated during the first minutes of milling and grow when enough amount of product is formed consuming more reactants.

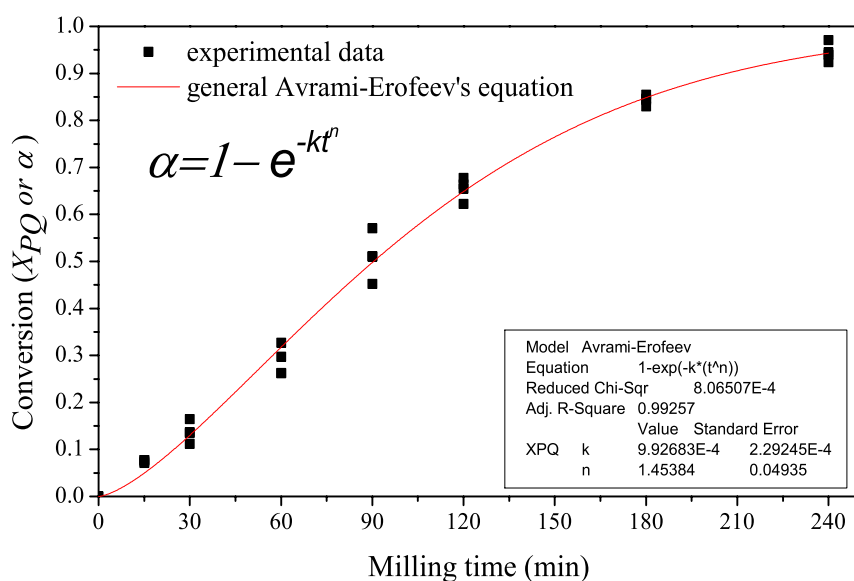


**Figure 3.5.** Nonlinearized data fit to the generalized Avrami-Erofeev's equation for DBPZ synthesis.

Friščić and collaborators (2013) also used this protocol for LAG and ILAG synthesis of metal-organic frameworks. They found that the limiting mechanism is function of the kind of liquid used to assist the grinding. Diffusion (D1) and Avrami (A2) models fitted better for ILAG and LAG respectively.

### 3.3.1.2 Heat release quantification based on the reactions continuation

The fact that the reaction continues after grinding allowed calorimetric measurements and the heat release quantification. The measures were performed isothermally at the same temperature of grinding, i.e. 25 °C, lasted 24 h, and the weight of the powder mixture was always about 1.7 g. These measurements were essential for further understanding of accumulation of any activated species within the solid mixture during grinding and the energy for and from reaction continuation after the grinding time.

The heat flow versus time for different milling times is plotted in **Figure 3.6**. The analyses were repeatable in means of amount of heat released and in the pattern of calorimetric curves.

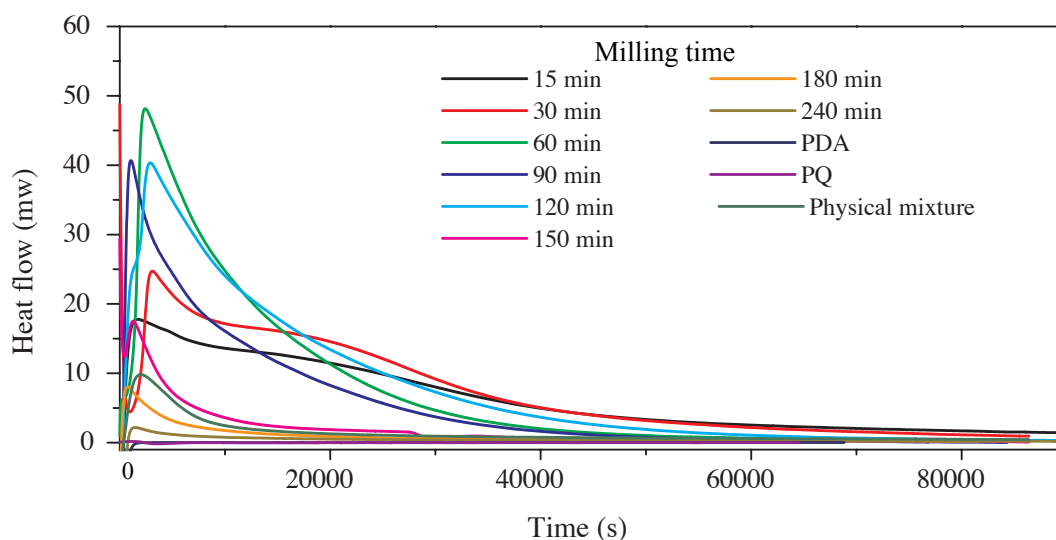


**Figure 3.6.** Heat release patterns for the reaction continuation after grinding for DBPZ synthesis.

As expected, the general curve patterns show that the majority of the heat is released during the first hours of analysis, in which the reaction is still in progress induced by mechanical action. Then, the heat flow starts to decay as the extent of reaction increases and it is almost zero after 24 h of measure. Diffusion limitations are reflected in the curve trends for

these static analyses. As the reaction progresses the product layer hampers the access to inner parts of reactant particles, the contact is more difficult and the reaction becomes much slower.

Regarding the form of the curves, the samples of short milling times, 15 and 30 min are noted by different patterns of heat release. One, in which the heat flow reaches the maximum and starts to decrease, followed by another pattern of almost constant heat flow or very slight decrease, and finally after 7 h the heat flow decreases more rapidly. For the other milling times, only one behavior is observed. After reaching the maximum, the heat flow decreases gradually until the end of analysis. In a first moment, the peak could be attributed to the insertion of the cell into the calorimeter, but nonetheless, the samples of the pure reactant powders, PDA or PQ, did not show any peak or heat released, and thus, the heat flow as well as the curve patterns can be attributed to events from the reactant powder mixture. One possible explanation is that when the grinding is stopped, the reaction continues almost in the same rate for few hours and as the reaction progress the heat is dissipated. Then, to continue without grinding, the mechanism of reaction must change because there is no more induction from external sources of energy. At this moment, the reaction progress slower, probably through diffusion mechanisms. For those presenting only the main higher peak and decay, this second stage of reaction, the slower one, may be hidden into the package of heat released, or it does not appear because enough of product was already generated, releasing heat that induce further reaction. It does not indicate the same mechanism of reaction, but that the product formation, primarily induced by mechanical stress, can supply energy to hold the reaction rate in considerable level. The heat flow and conversion after grinding for the milling time of 30 min is represented in **Figure 3.7**. It shows that after 30 min of grinding the reaction continues approximately at the same rate as during grinding until 120-150 min (7200-9000 s) in the calorimeter. After this time the reaction rate in this static system starts to follow another rate becoming slower after reach 70 % of conversion. This also indicates that the higher peak of heat flow comes from the reaction such as during the grinding period.

In relation to the amount of heat released, during the 24 h followed the milling, the overall values increase when the milling time is increased, achieving the maximum value at 60 min of milling, and then start to decrease. **Table 3.1** contains the overall heat released for the milling times represented by the curves from **Figure 3.6** and other values related to the amount of the powder analyzed or the amount of the powder transformed during grinding. The conversions of PQ at the beginning and at the end of calorimetric measurements were also determined.

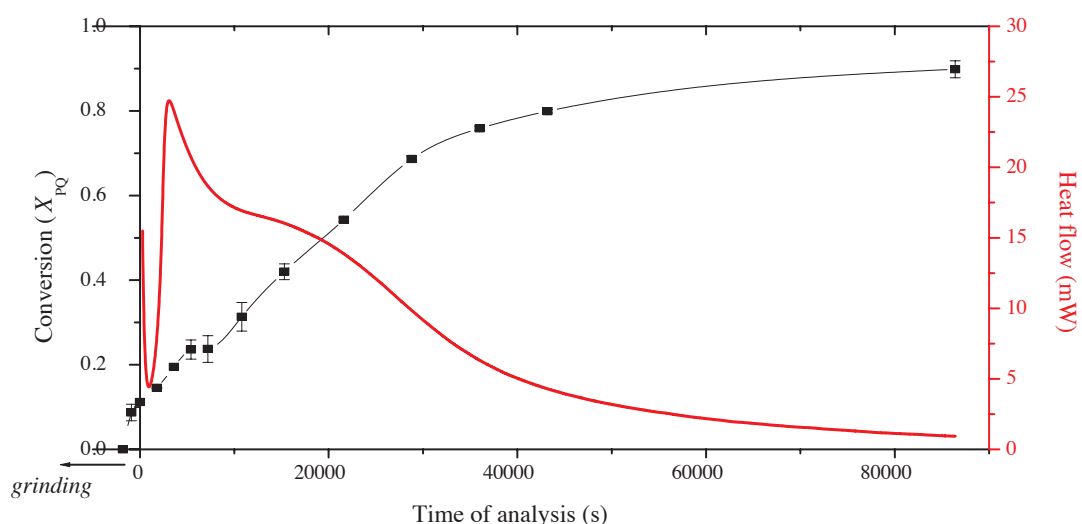


**Figure 3.7.** Heat release and PQ conversion after 30 min of grinding.

**Table 3.1.** Heat released after grinding by the reactant powder mixture for DBPZ synthesis.

<i>t</i>	<i>Overall ΔH</i>	<i>ΔH</i>	$\Delta \text{mol}_{\text{PQ}}^{\text{a}}$	<i>ΔH</i>
min	(J)	(J/g of sample)	(mol/g) $\times 10^3$	(kJ/ $\Delta \text{mol}_{\text{PQ}}^{\text{a}}$ )
15	$-551.76 \pm 11.95$	$-321.38 \pm 6.86$	2.15	$-147.56 \pm 3.20$
30	$-616.02 \pm 11.32$	$-359.77 \pm 6.70$	2.34	$-155.97 \pm 2.86$
60	$-630.23 \pm 2.25$	$-351.02 \pm 1.25$	1.93	$-181.35 \pm 0.65$
90 <sup>b</sup>	-456.92	-269.89	1.16	-233.27
120	$-313.00 \pm 4.96$	$-182.54 \pm 2.89$	0.69	$-263.39 \pm 4.17$
150 <sup>b</sup>	-146.37	-91.49	0.49	-187.68
180	$-75.85 \pm 1.74$	$-45.32 \pm 1.04$	0.31	$-145.17 \pm 3.33$
240 <sup>b</sup>	-38.62	-27.78	-	-148.53
PM <sup>c</sup>	$-120.79 \pm 3.11$	$-61.02 \pm 1.57$	0.8	$-77.52 \pm 3.01$

<sup>a</sup>moles of PQ consumed during analysis, <sup>b</sup>single determination, <sup>c</sup>PM=physical mixture

The values of the measured enthalpies listed in **Table 3.1** are clearly overall values incorporating contributions from all processes including reaction enthalpy and product crystallization. This is clear with regarding the values in kJ/mol of PQ transformed during the analysis. The values are not constant for all the milling times and this confirms that the energy released during the analysis does not come exclusively from the reaction, although it surely represents the majority, because the higher amount released is coincident with the reaction

progress during analysis. This is the most important information from that Table. The differences can be originated from the accumulation of certain species during grinding, before analysis. The nature of this species is unknown, but two possibilities are speculated: the crystallization of the product formed before analysis or the accumulation of an intermediate formed only under mechanical action that leads to the formation of the final product releasing heat, or even a mixture of them.

The fact that the generation and accumulation of such intermediate or product be only possible upon mechanical stress is confirmed by the heat released by the physical mixture of pre-milled reactants. The value per mole of PQ consumed (from 0 to 25 % of conversion) is the lowest one and could be related to the heat of reaction. On the other hand, for the reactant mixture even for short milling periods, the mechanical action is capable to activate or to generate larger amounts of such species and the reaction progresses faster and more heat is released. Still, it is important to mention that the reaction occurring in the physical mixture reaches 25 % because large surface area was generated due to particle size reduction of reactants before being mixed. If the calorimetric measurements were performed with the raw material, only traces of reaction would be observed, and then, the calorimeter would not be able to measure this very low heat flow.

Unfortunately, it was not possible to decorrelate the values subtracting the  $\Delta H$  of DBPZ crystallization (20 kJ/mol) because the point where the crystallization starts was not determined. Therefore, it is also difficult to decorrelate the heat released by each phenomenon.

The calorimetric information is very interesting when coupled with other techniques such as  $^{13}\text{C}$  CP-MAS NMR and XRD. Further discussions of the above results are present in the following sections.

### *3.3.1.3 $^{13}\text{C}$ CP-MAS NMR investigations*

$^{13}\text{C}$  CP-MAS NMR was performed in order to detect intermediates in the solid state, possibly formed during mechanical action. An intermediate detection would be very helpful in elucidating the mechanism of reaction and thus, giving evidences of stepwise or concerted pathways. The experiments were performed immediately after milling at different milling times, for continuous milling and for 30 min of milling in which the NMR spectra was recorded for the same sample.

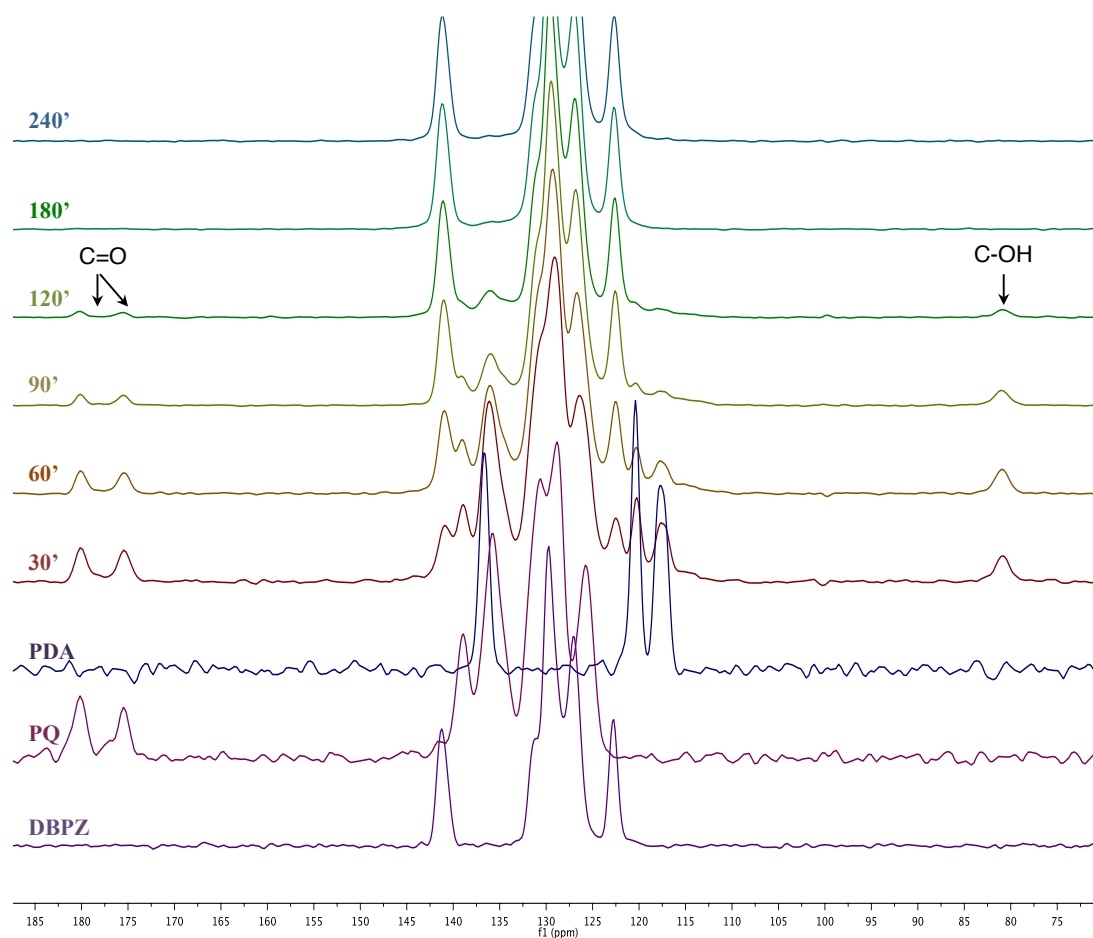


**Figure 3.8.**  $^{13}\text{C}$  CP-MAS NMR spectra for different milling times for DBPZ synthesis. The acquisitions were performed immediately after the milling time.

In **Figure 3.8**, the spectra, recorded as quickly as possible after sampling, are shown for different milling times. The presence of an intermediate is evidenced by the chemical shift at 81 ppm, typically of a C-OH. The  $^{13}\text{C}$  CP-MAS NMR chemical shifts of the carbonyl groups of PQ decreases constantly until 120 min of milling and cannot be detected from 180 min. At the same time, the hemiaminal C-OH signal increases up to 90 min, decreasing at 120 min and disappearing at 180 min. No other intermediate could be detected, including the imine intermediates (expected chemical shift around 160 ppm). This means that under the experimental conditions, the intermediate bearing at the same time a free C=O and a C=N, indicating the stepwise mechanism, as suggested by Carlier et al. (2013) for the static reaction period, was not detected.

It was presented before in the Introduction that Haruta et al. (2013) demonstrated by using DFT calculations and vibronic coupling density theory, the possibility of a concerted mechanism of DBPZ mechanosynthesis. Nevertheless, the concerted mechanism is only

possible through external excitation, in this case, the mechanical energy. Thus, this could be the scenario pointed in  $^{13}\text{C}$  CP-MAS NMR spectra, with both carbonyl groups transformed into hemiaminal C-OH, by direct concerted addition, giving the intermediate **AB** (**Figure 3.9**).

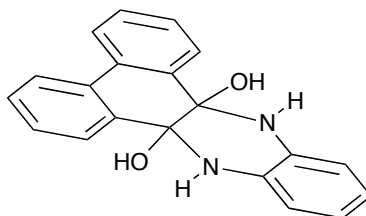


**Figure 3.9.** The possible intermediate (AB) containing C-OH.

The 2C-N formation, i.e., the concerted addition, is the rate-determining step according to calculations schematized in **Figure 3.10-a**, demanding 2.41 eV (232.53 kJ/mol). On the other hand, it is difficult to figure out the elimination of two water molecules concertedly. The energy barrier of 4.42 eV (426.47 kJ/mol) is very high. Since the stepwise elimination requires 2.20 eV and 1.68 eV for the first and second elimination respectively, the two-step elimination mechanism is favored.

It is possible for simplification to consider that if the energy is sufficient for the concerted mechanism, it means that the PQ disappearing in the reactant solid mixture affords at the beginning the intermediate AB that evolves progressively to the final aromatic product DBPZ.

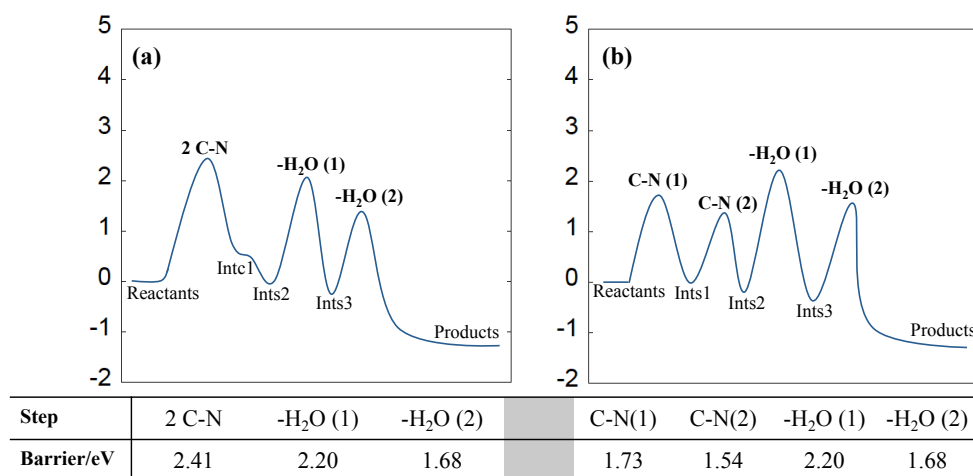


**Figure 3.10.** Energy diagrams representation and the relative energies for the (a) concerted addition mechanism and (b) stepwise mechanism. The calculations were performed using Gaussian 09 Rev C.01 software in the B3LYP/6-311G(d,p) 6D 10 F level of theory (Haruta and Sato, Kyoto University).



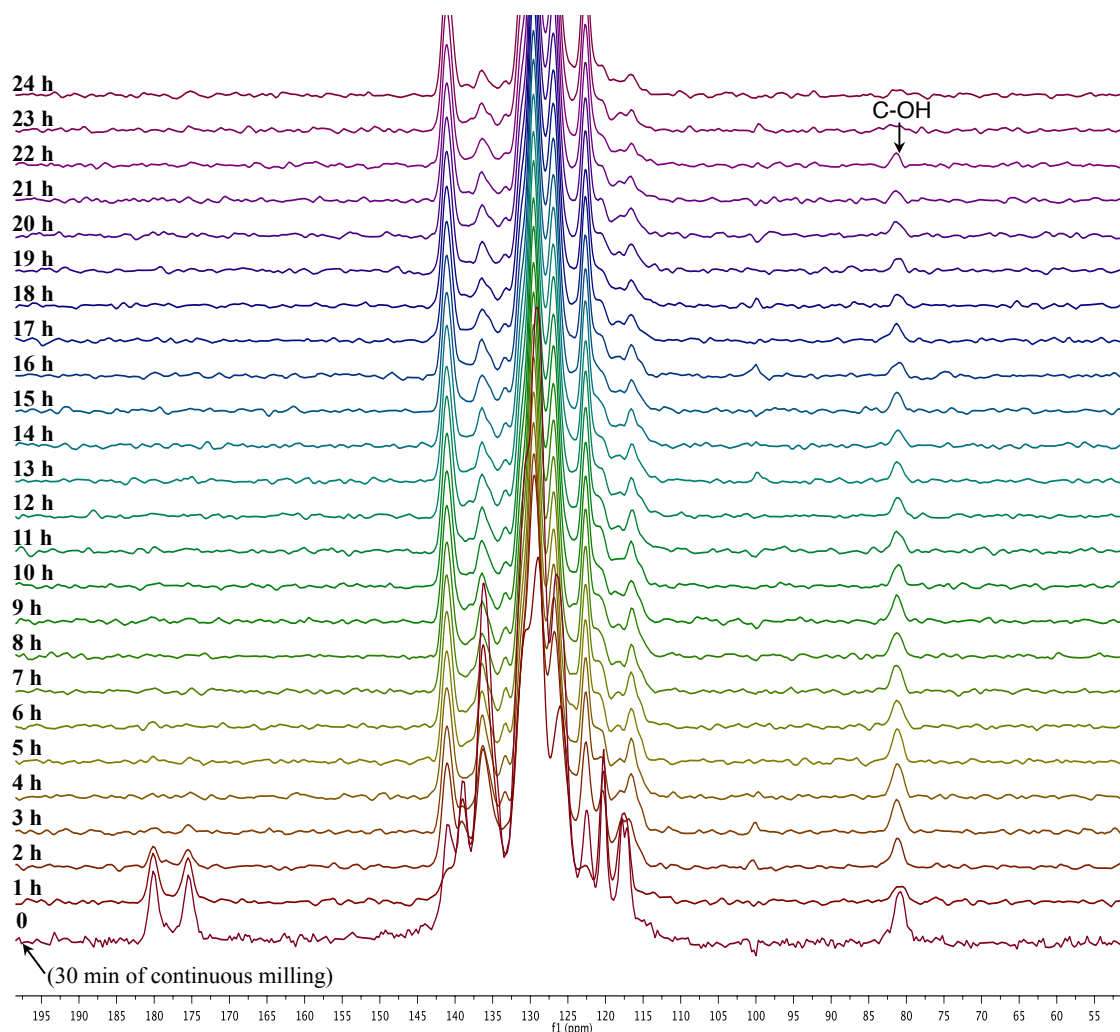


**Figure 3.11.**  $^{13}\text{C}$  CP-MAS NMR spectra after 30 min of grinding for DBPZ synthesis. The acquisitions were performed each hour (20' of integration + 40' waiting) during 24 h.

Unlike the continuous grinding, the reaction cannot continue through a concerted mechanism due to the absence of mechanical excitation. Hence, the stepwise mechanism is expected for the reaction continuation with energy barriers for the first and second additions of 1.73 and 1.54 eV respectively (**Figure 3.10-b**). The  $^{13}\text{C}$  CP-MAS NMR for the post-grinding experiments (**Figure 3.11**) also indicates the presence of the intermediate C-OH and the lack of a non-cyclic imine intermediate. This fact allows implying that the intermediate form AB (**Figure 3.9**) is rapidly formed by the first addition, which requires more energy, followed by the second nucleophile attack, easier than the first. It must be noticed that the rate-determining step for this case is the first elimination of water (2.20 eV) and thus, this process is much longer than for the continuous grinding. This is confirmed by the C-OH, which lasts up to 22 h in the static mode with the disappearance of C=O after 3 h.

Comparing the  $^{13}\text{C}$  CP-MAS NMR results with calorimetric measurements, the higher intensity of C-OH NMR signal is at 60 min (**Figure 3.8**). It is also after this milling time that the higher intensity is observed for the calorimetric curves. In addition, the overall heat released is higher after 60 min of milling for lower reaction extent during analysis ( $\Delta\text{mol}_{\text{PQ}}=1.93\times 10^{-3}\text{mol/g}$ ) compared to 15 min ( $\Delta\text{mol}_{\text{PQ}}=2.14\times 10^{-3}\text{mol/g}$ ) and 30 min ( $\Delta\text{mol}_{\text{PQ}}=2.34\times 10^{-3}\text{mol/g}$ ). If the formation of an intermediate is assumed, part of the heat released could come from the accumulation of such intermediate that after milling is driven by water elimination towards the final product. Further reaction can use this energy, but only the stepwise mechanism is possible as mentioned before. The heat released by the reaction occurring entirely during analysis, i.e., addition and elimination is different from the heat released by the reaction in which the measurements starts with lots of the intermediate AB already formed. In the latter case, the “initial state” is much higher and therefore, releasing more heat. This would result in different amounts of heat and could explain the differences in the heat released per mole of PQ transformed during calorimetric measurements. Moreover, for more prolonged milling times, such difference becomes higher until 120 min, which makes sense because more of the intermediate would be accumulated due to the intense mechanical stress and then more heat would be released even for lower reaction extension. Obviously the heat of crystallization is not being ignored, but the majority could arise from this interpretation.

#### 3.3.1.4 XRD records

The analysis of the X-ray diffractograms may reveal intermediate metastable phases, amorphization and the product crystal formation whether they take place. The DBPZ reaction started with crystalline raw materials, but the state of powder changes during grinding as a consequence of mechanical action and reaction progress, and therefore, the XRD can indicate the possible forms and species present in the solid reactive mixture.

Similarly for the  $^{13}\text{C}$  CP-MAS NMR, two sets of experiments are presented. The X-ray diffractograms recorded immediately after grinding for the continuous milling during 240 min (reaction completion) (**Figure 3.12**) and another series with the same sample from the co-milling of PQ and PDA for 30 min and XRD monitoring for the next 24 h (**Figure 3.13**).

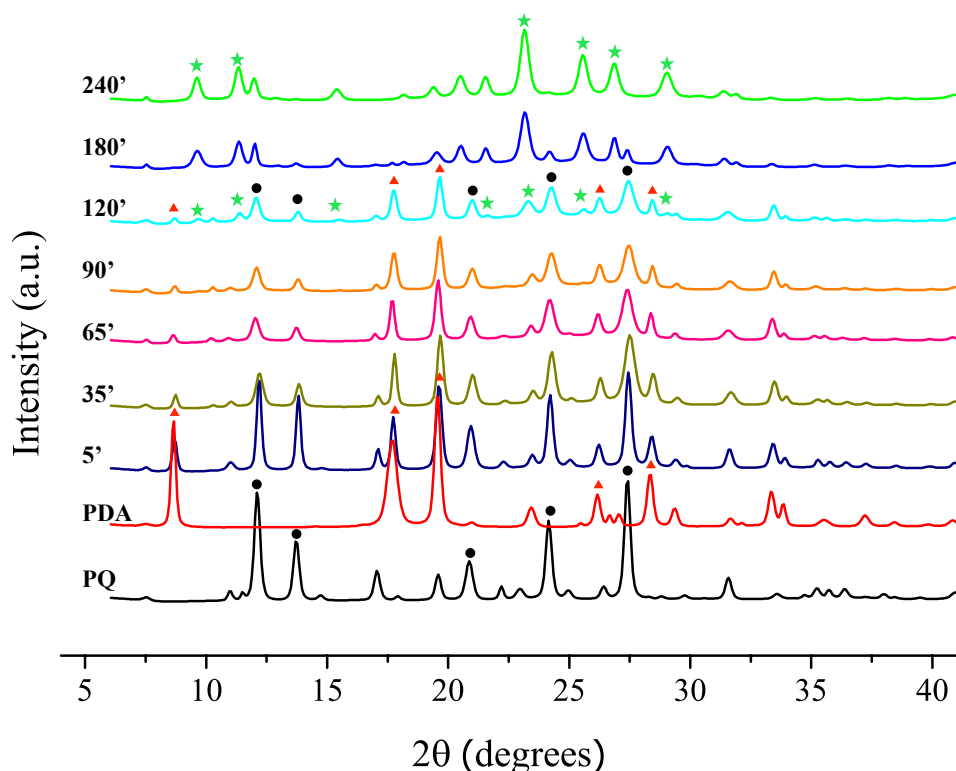


**Figure 3.12.** XRD patterns for solid-state qualitative monitoring of DBPZ synthesis during continuous milling (PQ: black, PDA: red, DBPZ: green). The acquisitions were taken *ex-situ* immediately after the milling times.

The most intense Bragg peaks are identified by color and geometrical form in **Figure 3.12**. At 5 min only the mixture of reactant powders can be observed. From 5 to 180 min the characteristic peaks of the reactant powder decrease in intensity, disappearing at 240 min. At 120 min the main peaks of the product start to be perceptible. The most remarkable change occurs between 120 and 180 min, where several diffraction positions from crystalline reactants become less intense and those from the product rise more intense. This point could correspond to the crystallization of the product formed up to that moment and crystal growth reaching the minimal size for XRD detection. The kinetic curve from **Figure 3.4** shows that at 120 min, the great majority is related to the product. Furthermore, this observation also agrees with the interpretation of the kinetic pattern described by an Avrami-Erofeev model for nucleation and growth.

There was no intermediate peak in XRD patterns, which appears and disappears indicating that the reaction apparently does not go through a discrete intermediate solid form such as a cocrystal formation, or metastable phases, at least, not detectable. It is unlikely that intermediate AB can crystallize. Besides, no amorphization was observed.

The analyses with the sample at 120 min showed that this is the stage of most important transitions. For continuous milling, the product starts to be detectable in XRD patterns at 120 min, probably due to larger crystal size, and it is also at that instant that the C-OH disappears in  $^{13}\text{C}$  CP-MAS NMR spectra.

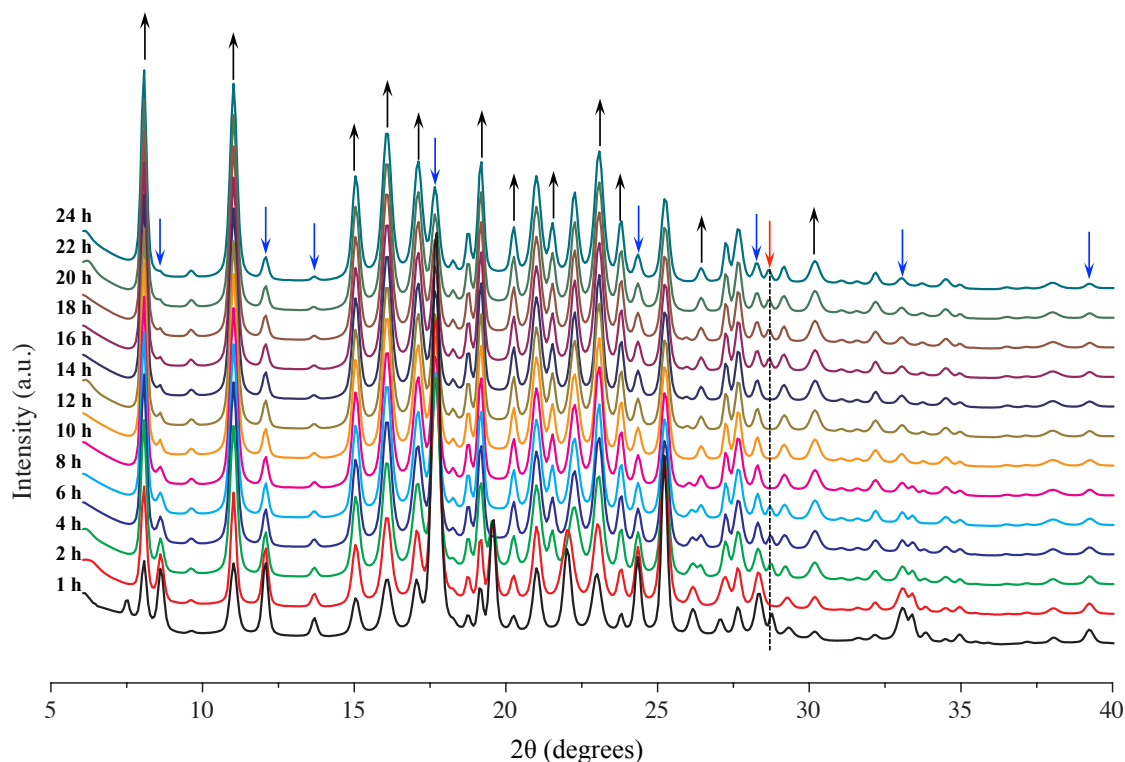


**Figure 3.13.** XRD patterns for solid-state qualitative monitoring of DBPZ synthesis after 30 min of grinding. The acquisitions were taken each hour (26' of acquisition + 34' waiting) during 24 h.

XRD was recorded for the static reaction as well. After 30 min of continuous grinding the same sample was analyzed each hour (26' of acquisition + 34' waiting) during the next 24 h. It can be seen from **Figure 3.13** the reaction progresses with the reduction of peaks in the positions of the reactants (blue arrows) ( $2\theta = 8.6^\circ$ ,  $17.7^\circ$ ,  $19.6^\circ$ ,  $28.2^\circ$  and  $33.3^\circ$  for PDA and  $12.1^\circ$ ,  $13.7^\circ$  and  $24.1^\circ$  for PQ) and others that start increasing from the first hour (black arrows). In fact, no sudden changes were observed after 4 h, probably because the incident X-ray beam itself induced the reaction after repeated records accelerating the transformation, and then, the time cannot be surely compared to  $^{13}\text{C}$  CP-MAS NMR spectra for the static case.

Contrary from diffractograms of continuous milling, a peak at  $2\theta = 28.6^\circ$  (red arrow) appears and disappears dynamically. Probably it comes from a specific association, from an

intermediate crystalline form that, in this case, evolves slowly to the final product. For example, the formation of some hydration with the water eliminated by the reaction could be possible with DBPZ (Dey et al., 2007; Carlier et al., 2013).

Although the product obtained by continuous milling and 24 h in static systems (after 30 min of milling) be chemically the same, the XRD patterns from **Figure 3.13** also reveal that after 24 h the product that has been formed has different structure from the one at the end of 4 h of continuous milling. The small amounts of the remaining reactants can also be associated to the product such as for cocrystals and the resultant diffractograms are different. In addition, the crystallization mechanism can be completely different. In order to compare the XRD patterns of DBPZ prepared by co-milling, part of it was recrystallized from solution. Surprisingly, the recrystallization of DBPZ from EtOH and DMF solution still afforded another structure. This can be seen in **Figure 3.14**, in which XRD patterns for the recrystallized form and for the DBPZ obtained by milling are also displayed after heat or moisture treatment in order to induce structure changes.

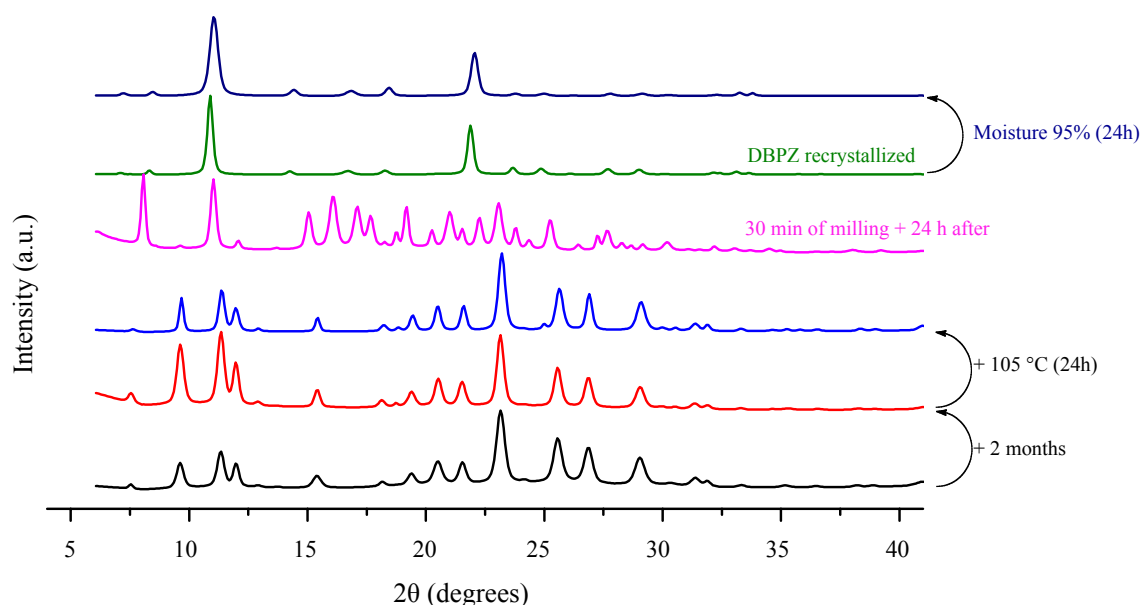


**Figure 3.14.** XRD patterns of DBPZ obtained in different conditions.

Actually, the XRD pattern of DBPZ produced during the 24 h followed from the milling presents in addition to the unknown peaks, some that overlap the DBPZ recrystallized and DBPZ entirely produce by milling. For example, the positions  $2\theta = 9.6^\circ$ ,  $18.2^\circ$  and  $23.1^\circ$  in **Figure 3.14** are characteristic from the DBPZ obtained by constant milling and at  $2\theta = 10.9^\circ$  it is found the most intense diffracted signal of DBPZ from recrystallization in solution.

At  $2\theta = 18.8^\circ$ , a very weak peak is coincident in all diffractograms. It is further noted that the peaks of left reactants are very weak when they can be observed. The rest of the peaks can be a result of undefined interaction as well as another crystalline form. Nonetheless, these considerations must be seen with attention because the other unknown structures could diffract in the same  $2\theta$  leading to misleading conclusion.

The storage time and heat treatment did not alter the crystal structure of the DBPZ prepared mechanochemically. The same was observed when the recrystallized form was exposed to moisture with no changes in the XRD patterns.

The possible structures were not found in CCDC. Unfortunately, it was not possible to proceed with the structure refinement from those records either. In any case, it is clear that the structures obtained mechanochemically under continuous milling or for short time milling and left static to react are more complex and probably more than one are present, mainly for the latter. The static conditions for reaction progress probably do not drive the reaction properly to one structure formation. In the case of continuous milling, the mechanical energy induces the product formation by renewing the surfaces and even destroying less stable arrangements, which results in the most stable form under mechanical stress. As mentioned before, the crystalline reactants can also contribute to have different XDR patterns.

### 3.3.2 The mechanosynthesis of 2,3-diphenylquinoxaline (DPQ)

The investigations carried out for DBPZ synthesis revealed interesting behaviors such as the detection of the intermediate containing the C-OH function, the different solid forms and the heat released after milling. It goes without mentioning the great data fitting of the kinetic results. Part of the discussion was based on the assumption of an intermediate formed upon application of mechanical stress. In the case of DPQ synthesis, the reaction pathway is expected to be different due to use of a different 1,2-dione, in which the two carbonyl groups are not positioned in favor to a concerted addition. Therefore, in order to perform a comparative study between DBPZ and DPQ synthesis by co-grinding, the same analyses were performed.

The DPQ is also 1,4-diazine compound synthesized through the reaction of an aromatic 1,2-diamine with 1,2-dione. **Figure 3.15** schematizes the synthesis of this molecule with *o*-phenylenediamine (PDA) (1,2-diaminobenzene) as diamine and benzil (BZ) (diphenylethanedione) as dione.

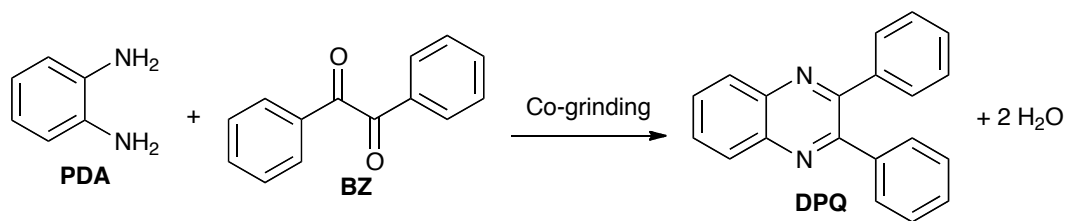


**Figure 3.15.** Synthesis of 2,3-diphenylquinoxaline (DPQ) by co-grinding.

As for the case of DBPZ, this reaction was already performed mechanochemically at room temperature. Kaupp and Naimi-Jamal (2002) presented DPQ synthesis highlighting that the reactants were completely consumed in one hour of ball milling. Again, similar to DBPZ synthesis, the reaction to produce DPQ also continues after grinding. Calorimetric measurements, XRD and <sup>13</sup>C CP-MAS NMR investigations after grinding could be performed thanks to this characteristic.

### 3.3.2.1 Kinetic of DPQ synthesis

The kinetic quantitative monitoring for DPQ synthesis was performed quantitatively by using HPLC. Differently from DBPZ that is poorly soluble in acetonitrile, the product DPQ could also be quantified. The complete transformation was achieved after one hour of continuous milling in the P0 with 2 mm of amplitude and at 25 °C. The simultaneous quantification allowed to confirm that each mole of reactant disappeared affords one mole of product as showed in **Figure 3.16** (bottom).

The reaction clearly follows a zero-order reaction type. The constant input of mechanical energy could be the rate-determining step in these conditions. Zero order reactions for mechanically induced transformations were already reported (Branković et al., 1998; Lin et al., 2012; Kaupp, 2003; Declerck et al., 2009). Further discussions on the kinetic aspect of DPQ synthesis are held in the next chapter.

The quantitative conversion of BZ is obtained after one hour. That is, the milling is four-time reduced for BZ conversion to yield the DPQ compared to DBPZ synthesis. Firstly, the difference must be attributed to the chemical reactivity of PQ and BZ. The carbon of the C=O group of benzil has higher electrophilic character compared to that C=O of PQ, and consequently, the carbonyl carbons atoms, C=O, of the benzil are more attractive for nucleophiles such as amines (Muddasir et al, 2009).

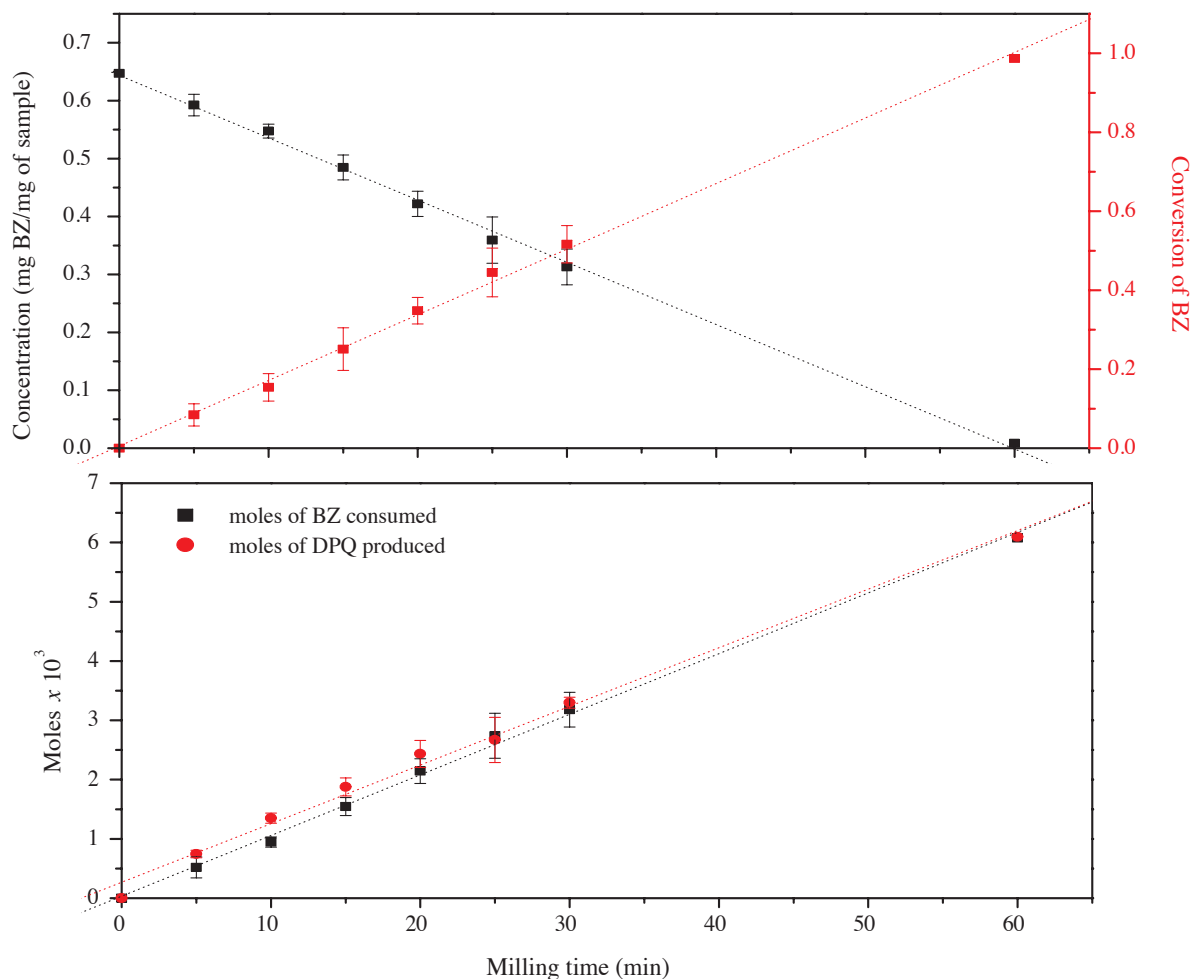


**Figure 3.16.** Kinetic monitoring of BZ transformation for DBPZ synthesis: concentration and conversion of benzil (top) and moles of product and reactant (down).

The reaction between BZ and PDA also continues after grinding. This is an indication that PDA probably diffuses into the crystal lattice of the PQ and BZ and, since the reaction started, the heat released can serve to promote further transformations. For the moment, the fact that reaction continues was used to perform other analyses such as for DBPZ.

### 3.3.2.2 Heat release quantification based on the reactions continuation

Calorimetric measurements were carried out in isothermal conditions at the same milling temperature (25 °C). Before analysis, the reactants were co-milled for different times, immediately recovered from the milling bowl and placed in the cell for heat release quantification. **Figure 3.17** displays the heat release patterns for DPQ synthesis during next 24 h after continuous milling.



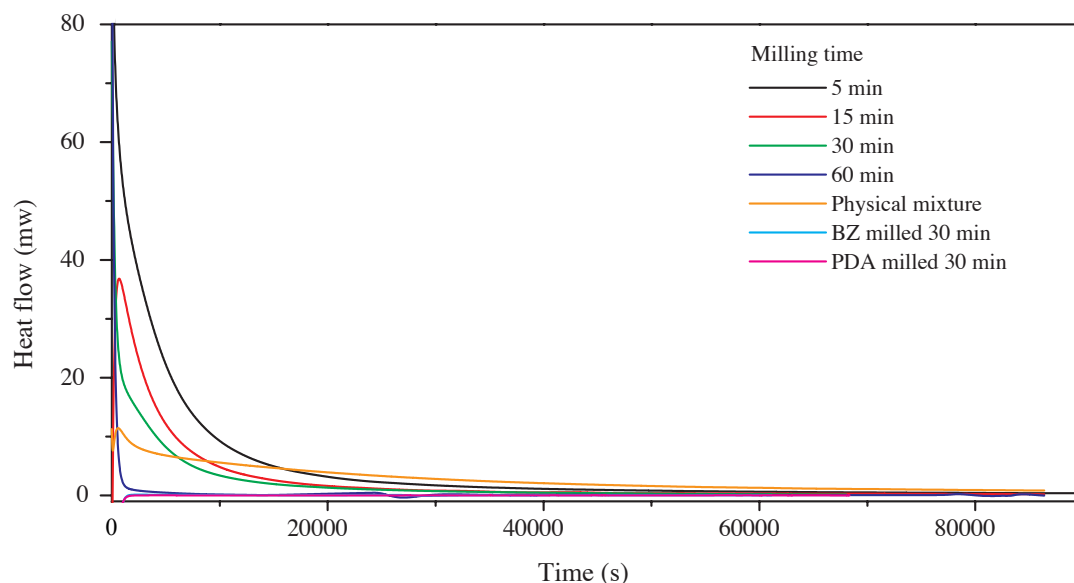


**Figure 3.17.** Heat release patterns for the reaction continuation after grinding for DPQ synthesis.

The heat released comes from events taking place in the reactant powder mixture because when the pure reactants were milled no heat flow was detected as it is shown **Figure 3.17**. The trend observed for the heat flow for the samples after 5, 15 or 30 min was the same. This is different from DBPZ synthesis in which for the short milling times two regions could be observed in the heat flow. For DPQ synthesis, the heat flow starts to decrease exponentially from the first instants of analysis and after 12 h it is very low, indicating that the transformations achieve the plateau. This trend was observed for DBPZ only after 60 min of grinding.

The physical mixture, i.e., when the reactants were milled separately for 30 min and then gently mixed, also released heat that constantly decreases. The pre-milling was necessary to homogenize the particle size as the PDA used is a fine powder and BZ is supplied with broad distribution containing crystals even bigger than 1 mm. The heat released by the physical mixture confirms that the powders react without continuous mechanical stress. However, such amount of heat released is directly associated to the huge surface area generated by the pre-milling treatment, and if no particle refinement was carried out, the reaction would progress very slowly. The reaction extension at the end of analysis reaches 42 % and further progress is hampered by diffusion limitations in the absence of mechanical action to clean off the surfaces.

The reaction extent for the milling time of 15 min was also followed. The result is presented in the **Figure 3.18** with the heat flow for this case.

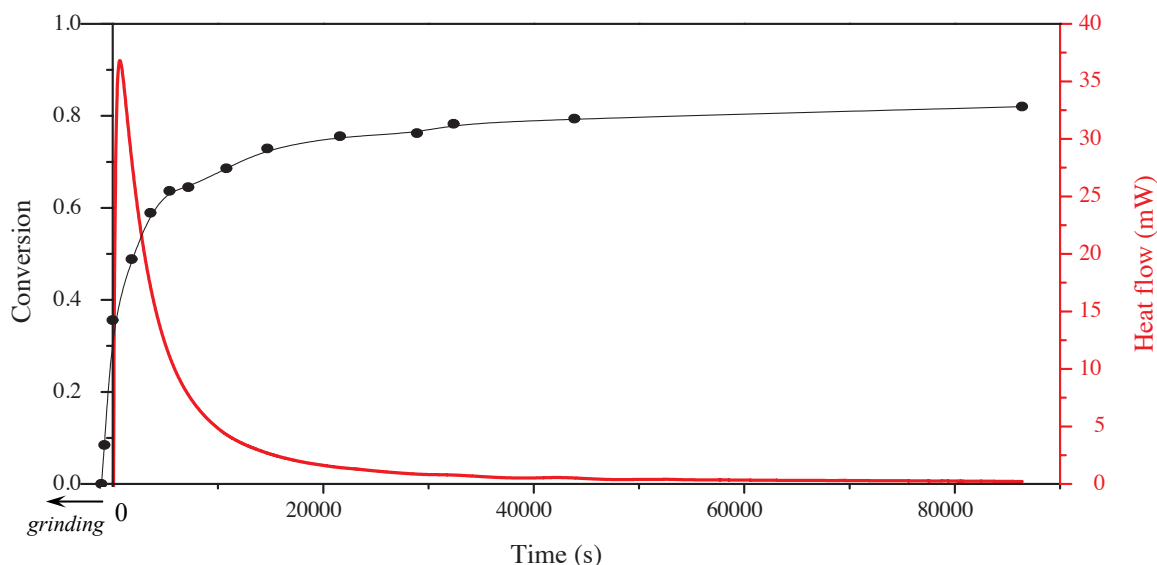


**Figure 3.18.** Heat flow and reaction extent after 15 min of grinding for DPQ synthesis.

The reaction progress observed in **Figure 3.18** follows the trend of the heat flow curve with the fast advancing on the reaction during the three first hours and the rapid decrease in the heat flow. The conversion is about 80 %, reached after 12 h in the static system, the same time where the heat flow is very low and continues to decrease slowly.

The amount of heat released is listed in **Table 3.2** in means of overall heat, the overall heat/gram of powder analyzed and also per mole of product generated.

**Table 3.2.** Heat released after grinding by the reactant powder mixture for DPQ synthesis.

<i>t</i> min	<i>Overall</i> $\Delta H$ J	$\Delta H$ J/g of sample	$\Delta H^a$ (kJ/ $\Delta$ mol <sub>BZ</sub> )	$\Delta H^b$ (kJ/ $\Delta$ mol <sub>DPQ</sub> )
5	-364.84 ± 31.95	-226.08 ± 18.50	-111.18 ± 9.74	-111.19 ± 9.74
15	-238.39 ± 26.64	-138.44 ± 15.47	-86.52 ± 9.67	-106.49 ± 11.90
30	-120.68 ± 9.11	-70.94 ± 5.36	-130.37 ± 9.93	-104.32 ± 7.88
60 <sup>c</sup>	-20.62	-12.71	-	-
PM <sup>d</sup>	-232.35 ± 9.24	-116.35 ± 4.63	-88.19 ± 3.55	-88.53 ± 3.56

<sup>a</sup>heat released per mole of benzil consumed during analysis, <sup>b</sup>heat released per mole of DPQ produced during analysis, <sup>c</sup>single determination, <sup>d</sup>PM=physical mixture.

As can be seen, the maximum overall value of heat released is obtained for 5 min of grinding and only 20 J was measured after 60 min. This is expected if the heat is associated to the reaction conversion during analysis. To confirm this, the overall values were related to the

amount of reactant consumed and to the product formation during analysis. In the contrary to DBPZ synthesis, the heats released per mole are very close and, regarding the standard deviation, they can be statistically considered as equivalents. Apart from the value of 130 kJ/mol (of BZ consumed) for the measure after 15 min of grinding, all the others, including the values for physical mixture, can be in their major part associated to the reaction, despite the exothermic effect of crystallization. The difficulty to work in such heterogeneous media for sampling and reproducibility must be considered when regarding the results.

The fact that the heat released might be related to reaction extent indicates that there was no accumulation of some active species, such as an intermediate is higher level of energy, during milling that could afford the product during analysis. When compared to DBPZ synthesis, this reinforces the assumption of a concerted addition forming an intermediate that accumulates during milling and can decay in energy towards the final product during calorimetric measurements.

Another important information that can be extracted from the calorimetric measurements (**Table 3.2**) is the physical mixture compared to 5 min of grinding. It can be seen that only 5 min of co-grinding of the raw materials, without pre-milling, is more efficient to induce reaction than the physical mixture with the very fine powder of reactants milled during 30min. It demonstrates that the mechanical energy has a role in addition to mix and surface renewal. The co-milling can activate the reaction mixture, which reacts faster than when the procedures are performed separately.

### 3.3.2.3 $^{13}\text{C}$ CP-MAS NMR investigations

$^{13}\text{C}$  CP-MAS NMR spectra were recorded immediately after grinding for different milling times (**Figure 3.19**). The samples of pure reactant BZ and the product DPQ did not generate spectra with good resolution and thus, they are not reported in **Figure 3.19**.

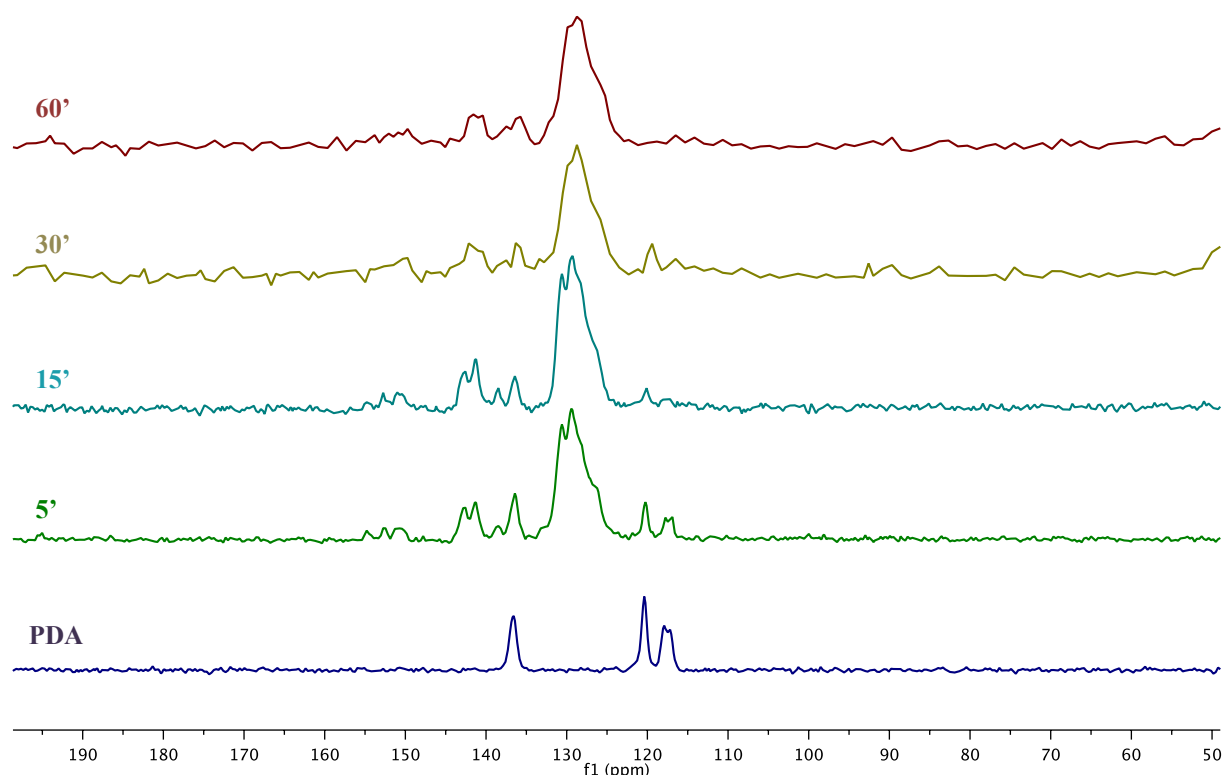


**Figure 3.19.**  $^{13}\text{C}$  CP-MAS NMR spectra for different milling times for DPQ synthesis. The acquisitions were performed immediately after the milling time.

As the reaction progresses the signal intensity of PDA decreases while the product is generated. However, in contrast to DBPZ synthesis,  $^{13}\text{C}$  NMR signals in the region of C-OH were not observed. It does not indicate that there is no intermediate, but the lifetime of the species are not long enough to be accumulated, which agrees with calorimetric measurements. It is unquestionable that at some instant an intermediate bearing at least one C-OH must exist, but it can be very unstable and under the mechanical action it goes fast towards product formation as shown by the kinetic monitoring. In addition, the accumulation of the C-OH in the form of intermediate AB, attributed to the concerted addition, is prevented by the positions of the C=O of BZ, which are not in the same plane as PQ.

The same trend is observed in the  $^{13}\text{C}$  CP-MAS NMR spectra recorded for the same sample milled 15 min during 24 h (**Figure 3.20**). The C-OH intermediate was not observed for the reaction continuation after grinding, but only the intensity decreasing of PDA signal such as C-NH<sub>2</sub> at 136 ppm and the appearance of the C=N between 150-155 ppm.

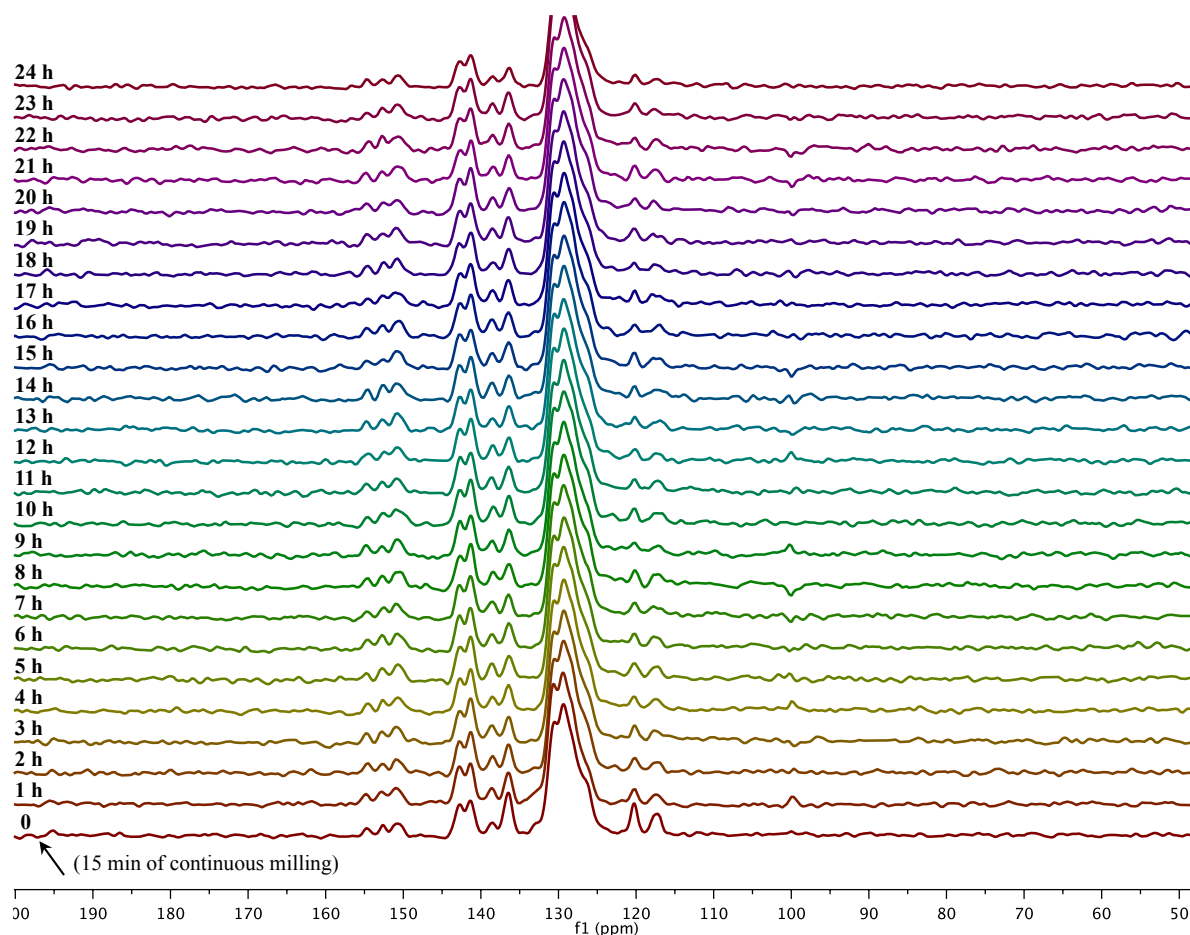


**Figure 3.20.**  $^{13}\text{C}$  CP-MAS NMR spectra after 15 min of grinding for DPQ synthesis. The acquisitions were performed each hour (20' of integration + 40' waiting) during 24 h.

#### 3.3.2.4 X-ray diffraction records

Following the same protocol as for DBPZ, XRD was used to monitor the solid form evolution during reaction. **Figure 3.21** shows the XRD patterns for the solid reactant mixture recorded at different milling times.

After only 5 min of grinding emerging peaks of the product are observed. The characteristic peaks of the reactants are visualized, but in low intensity as expected due to crystal size reduction, except at  $2\theta = 17.7^\circ$  that is a sum of Bragg peak of PDA and BZ. The XRD patterns at 35 and 65 min are very similar, despite the reaction extent be approximately 60 %.

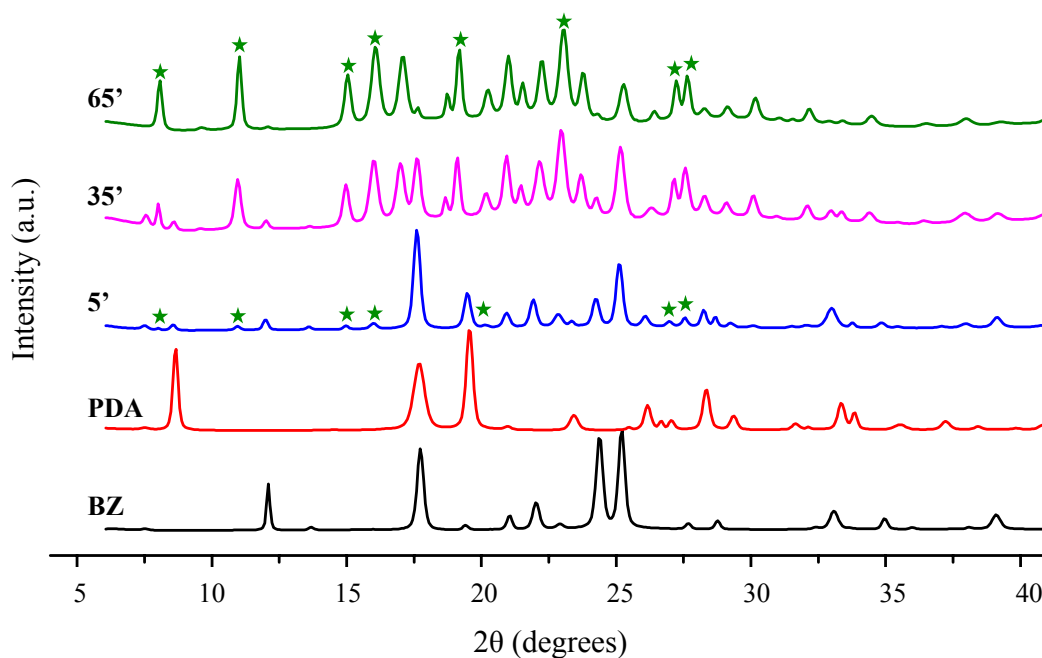


**Figure 3.21.** XRD patterns for solid-state qualitative monitoring of DPQ synthesis during continuous milling (BZ: black, PDA: red, DPQ: green). The acquisitions were taken *ex-situ* immediately after the milling times.

In the case of DPQ synthesis the presence of amorphous material is suggested. At 5 min the powder mixture is still composed by crystalline phases, but at 35 and 65 min a large diffuse scattering halo between  $2\theta = 15 - 30^\circ$  is seemingly superposed with the Bragg peaks of the crystalline phases. This suggests that the sample could be partly amorphous. Mechanochemical transformations are frequently mediated by amorphization during grinding. In fact, this is one of the main mechanisms associated to mechanochemical transformations (Frišćić and Jones, 2009; Jayasankar et al., 2006; Williard and Descamps, 2008). The XRD pattern of the final product obtained after 65 min of milling is composed by multiple peaks. In general, the number of the peaks is related to the symmetry of the unit cell and high symmetry often results in fewer peaks. In this manner, the final structure of DPQ after grinding could be composed by different crystalline arrangements and an amorphous part. However, the diffuse scattering halo is observed in a region of the diffractogram where a large number of Bragg peaks is present. It could also be the consequence - at least partly - of the superimposition of the wings of broadened Bragg peaks. The situation corresponds to a population of nanocrystals. Such a possibility is suggested by the evolution of the X-ray diffractogram upon aging (cf Figure 3.23). Aging induces a sharpening of the Bragg peaks, and a concomitant reduction of the diffuse halo intensity. Such an evolution could be related to crystallization from an amorphous part but also to a coarsening of the crystalline

microstructure. A detailed analysis of the Bragg peaks profiles and their evolution would be needed to quantitatively estimate the potential amount of an amorphous component. Such an analysis is difficult at this time since the crystal structure is not resolved. The outputs of this work and possible extensions will certainly help determining the exact role played by a transient amorphization in mechanochemically induced transformations.

In contrast to continuous milling, the amorphous phase is not observed for the sample milled for 15 min, for which XRD was recorded each hour during 24 h. This is shown in **Figure 3.22**.

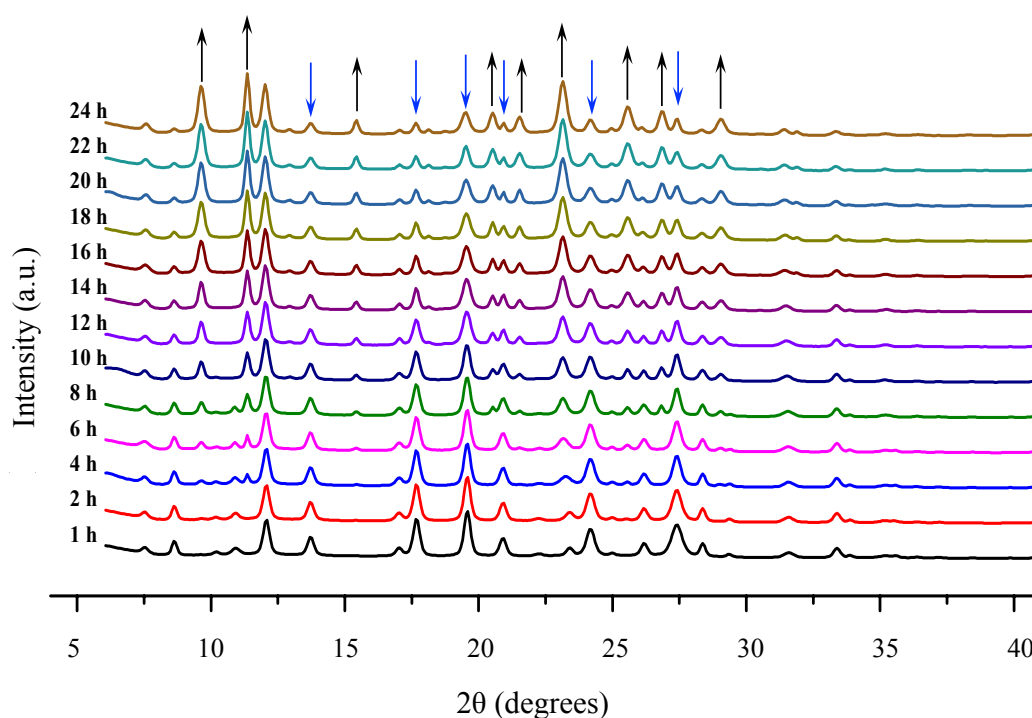


**Figure 3.22.** XRD patterns for solid-state qualitative monitoring of DPQ synthesis after 15 min of grinding. The acquisitions were taken each hour (26' of acquisition + 34 waiting) during 24 h.

The reaction progress is evidenced by the reduction of reactant peaks (e.g.  $2\theta = 8.6^\circ$ ,  $17.7^\circ$  and  $19.5^\circ$  for PDA and  $17.7^\circ$  and  $24.3^\circ$  for BZ) whereas others appear and increase in intensity ( $2\theta = 9.7^\circ$ ,  $11.3^\circ$ ,  $15.4^\circ$ ,  $20.5^\circ$ ,  $21.5^\circ$  and  $23.1^\circ$ ). As mentioned before, the broadness pattern observed for continuous milling is not present. The fact that the sample is left static, (without mechanical perturbation), allows the system to be arranged and the product starts forming directly in crystalline phases. As for DBPZ, the reaction is not completely finished after 24 h and the association between product and reactants through H-bonding is possible,

therefore, some of the peaks can be derived from this kind of configuration. It has also to bear in mind that some heating from the X-ray beam can also induce the reaction.

The product formed after grinding was stored for 2 months aiming to follow further evolution of the solid structure. The diffractogram of DPQ recrystallized from ethanol solution is also displayed in **Figure 3.23** with other samples that underwent some treatment such as exposition to moisture and heat.

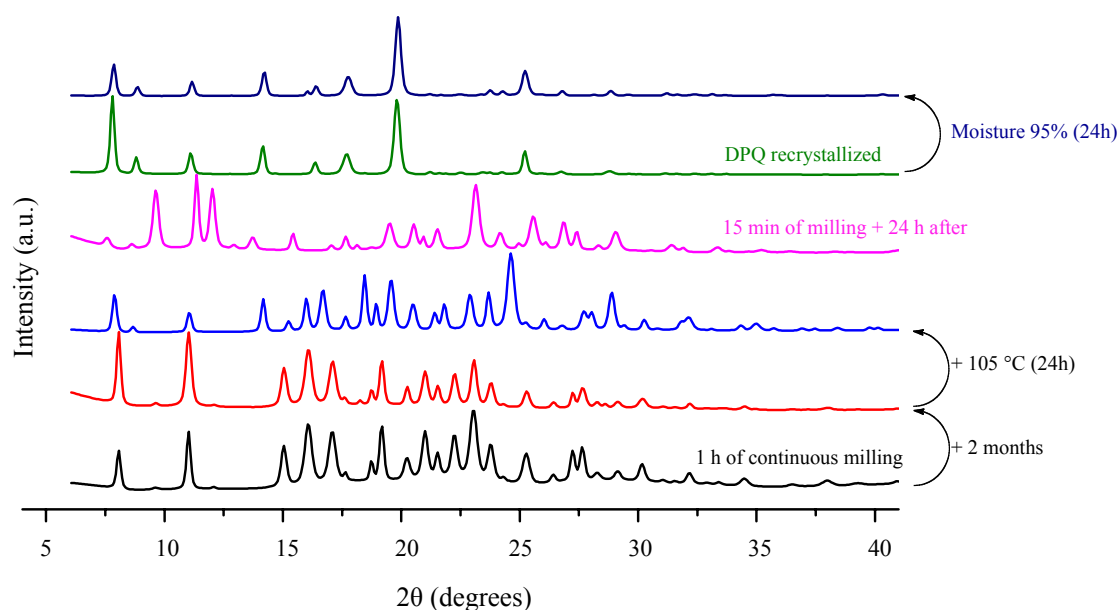


**Figure 3.23.** XRD patterns of DPQ obtained mechanochemically, from reaction continuation after grinding and recrystallized.

The sample prepared by continuous milling has an amorphous part. Two months later the XRD pattern of the same sample, storage at 21 °C in laboratory conditions, did not reveal any new polymorphism but further crystallization. The more intense peaks became sharper and still more intense when compared to the fresh product. Furthermore, the amorphous fraction is reduced. This sample was then, subject to heat treatment (24 h at 105 °C) and the diffractogram showed peak shifting, intensity changing and also new ones. As the crystal structure is not resolved, it is not possible to confirm which are the crystal-to-crystal transformations or if the water elimination upon heating is responsible for the different patterns. In any case, water within the molecules in the crystal lattice alter the planes and since it is eliminated the positions of the peaks change. This could be the case evidenced by the peak shifting at  $2\theta = 8.08^\circ$  to  $7.90^\circ$ , and the appearing peak from the sample after heating at  $2\theta = 14.3^\circ$ , which is characteristic of the solid form from classical recrystallization. In addition, when the recrystallized DPQ was exposed to moisture, the inverse was observed



with some peaks changing in intensity at  $2\theta = 7.8^\circ$  compared to the most intense peak, while new ones appear even if weak. These last at  $2\theta = 16.1^\circ$  and  $23.7^\circ$  can be found in the XRD pattern of the DPQ mechanochemically prepared.

As a matter of fact, characteristic peaks of the recrystallized form are found in the product obtained by continuous grinding, as well as for the reaction that was not completely finished after 24 h. This points to the presence of different crystalline forms.

On the other hand, other arrangements from crystal interconversion can also diffract in the same angle as another form, but it does not mean that they are the same, mainly because sometimes one or two Bragg's peak are found and not the entire characteristic set.

For XRD from both DBPZ and DPQ, further studies are necessary to elucidate all the phases and forms constituting the DPQ powder. For now, the technique was helpful indicating the differences in the crystal lattice as function of the way the DPQ was prepared and that crystal-to-crystal transformation is possible by heat or moisture exposition.

### 3.3.2.5 Remarks about the reaction continuation

DBPZ and DPQ are formed just by contact of the solid reactants as it was demonstrated by the calorimetric measurements of the physical mixture and the kinetic monitoring after milling. However, the same measurements showed that the mechanical action also has the function of activation of the reaction because even for short milling times, the reaction goes faster than when the pre-milled reactants are mixed. Therefore, these reactions can be considered at least as mechanically induced reactions.

The fact that the reaction continues after milling can be attributed to a diffusion process. It is expected that PDA be the species more easily detachable from the crystals due to the lower heat of sublimation among the reactants. **Table 3.3** lists some physical properties of those three compounds, BZ, PQ and PDA that could be relevant for the solid-solid reactions.

**Table 3.3.** Relevant solid phase data of the reactants used for DBPZ and DPQ mechanosynthesis.

Compound	<i>o</i> -phenylenediamine	9,10-phenanthrenequinone	benzil
	PDA	PQ	BZ
mp (°C)	100 – 102	209 – 212	94 – 95
$\Delta H_f$ (kJ/mol)	23.1	20.2	23.8
$\Delta H_{sub}$ (kJ/mol)	85.5	108.1	98.4
$\rho$ (g/cm <sup>3</sup> )	1.21	1.41	1.23

As it can be seen, all the three compounds possess high melting points and enthalpies of fusion. This is important because solid phase can be maintained, in exception of eutectic melts, during the mechanical treatment, even if some temperature increase occurs.

As mentioned, PDA has the lowest enthalpy of sublimation, requiring less energy for phase changing, and so, it is the more ready to sublimate. Additionally, PDA is the smallest molecule in the systems and can access some hindered spaces. These properties must be considered specially in static systems where diffusion might be the rate-limiting step.

The absolute density ( $\rho$ ) is also listed. Its role is not clear yet, but it was noticed that densities can play a role in molecular mobility associated with crystal packing, in molecular access to reactive sites and as a result, in the solid reactivity. But, in this moment it is possible to point out that in addition to the more electrophilic character of the carbonyl from benzil, the absolute density of this reactant is lower than 9,10-phenanthrenequinone one, which could contribute to the movement of the molecules of PDA with the crystals of the 1,2-dione. Furthermore, BZ can move more readily because it has a single bond enabling rotation, essential for the cyclisation forming the final DPQ. These aspects are better explored in chapter 5 for solid-state synthesis of phenol-hydrazones.

The reaction continuation was previously reported for solvent-free Knoevenagel condensation between malonitrile and arylaldehydes (Trotzki et al., 2008). High conversions could be achieved with some aldehydes when the solid mixture was left standing at room temperature after initial mechanochemical treatment. In addition to the chemical reactivity of the aldehydes, seeding the mixture of reactants with the target product could increase the yields. The case of DBPZ and DPQ can also be related to the formation of the product to enhance the reaction conversion.

### 3.4 CONCLUSIONS

The synthesis of two 1,4-diazines under mechanical action was investigated. The dibenzo[a,c]phenazine (DBPZ) synthesis was revisited and 2,3-diphenylquinoxaline (DPQ) synthesis was equally investigated. Both products could be obtained in the vibratory ball mill P0 in excellent conversion ratios.

The kinetic monitoring revealed different rate determining steps for the reactions. DBPZ follows an Avrami-Erofeev model for nucleation and growth and the reaction reaches completion after 240 min of continuous milling, whereas the DPQ is clearly zero-order

reaction type, which could be limited by the constant application of mechanical action and the reaction achieves completion in only 60 min of milling. The differences in reactivity come firstly from the chemical reactivity of the 1,2-diones, with BZ being more electrophilic than PQ. The nature of the solids such as density and molecular movements around  $\sigma$  single bonds contribute also to the differences in reactivity observed. This can also favor the faster reaction for DPQ synthesis because BZ is less dense than PQ and it can rotate around the  $\sigma$  bond between the two carbonyl groups, while PQ is a planar complete aromatic molecule.

The mechanisms of reaction were discussed, accounting the possibility of the mechanical energy to excite the PDA molecule to a  $C_s$  symmetry, which allows the concerted addition. This mechanism is possible for DBPZ synthesis due to the carbonyls configuration of PQ, and it is prevented in DPQ synthesis in which the carbonyls of 1,2-dione, BZ, is not in favored position. The  $^{13}\text{C}$  CP-MAS NMR and calorimetric measurements reinforced the assumption of formation of an intermediate under mechanical action for DBPZ, which was not evidenced for DPQ synthesis.  $^{13}\text{C}$  CP-MAS NMR detected an intermediate containing C-OH function for DBPZ and not for DPQ. In addition, the calorimetric measurements revealed that the heat release cannot be entirely attributed to the heat of reaction of DBPZ, but it seems to be very near for DPQ. The difference observed for the former was referred to the accumulation of an intermediate during grinding that when the calorimetric measurements is running it starts to be transformed in the final product and releases heat. In other words, larger amounts of this intermediate, that can correspond to the product of the concerted addition, is generated during milling and when the powder mixture is inserted in the calorimeter is as if the reaction starts from AB instead of A+B. The AB is the intermediate in the higher level of energy and to afford the product the energy released is higher than A+B. On the contrary, further reaction is possible only through stepwise mechanism.

The XRD showed different arrangements for the solid products as function of the preparation route. The products prepared mechanochemically are different from those obtained by recrystallization from solution. This was the case for both DPQ and DBPZ. Some differences in intensities and positions of Bragg's peak can be originated from water in the crystal lattice, but further investigations including the crystal structures definition are essential to elucidate the different XRD patterns. The DPQ showed changes in the XRD patterns when undergoing heat or moisture exposition, indicating crystal-to-crystal interconversion. The ball milling synthesis of this molecule also generates some amorphous phase that continues to crystallize after grinding. On the other hand, DBPZ crystalline forms seem to be stable and no significant change was observed after heat or moisture treatments.

In summary, the mechanical action showed to be able to induce transformations other than those for reaction in solution. This is the main subject for DBPZ synthesis with the intermediate formed under mechanical action. The comparison with DPQ synthesis was important to reinforce the hypothesis of an intermediate generated and accumulated upon application of mechanical stress. Several factors intervene on the mechanochemical reaction. The fact that no solvent was used avoiding the dissolution and solvation, renders possible upon mechanical action, reactions directly induced from excited states. In turn, these states generate intermediates with high energy levels, which would be unstable in solvated media, but that can accumulate while solids. The transformation towards the final product can be favored by the proximity of the molecules, increasing the tendency of crystallization after reaching a certain conversion ratio. Owing the susceptibility of evidencing very original mechanisms that appear within divided solids undergoing mechanical stresses, the understanding of the consequences of this mechanical action on molecular and orbital level is very important for further progress in this field of mechanochemistry, including molecular modeling such as DFT and vibronic coupling.

### 3.5 REFERENCES

- Branković, A. R.; Vidojković, V. M.; Milošević, S. D. Mechanochemical Activation of (SeO<sub>2</sub>+Na<sub>2</sub>CO<sub>3</sub>) Mixture and Sodium Selenite Synthesis in Vibrational Mill. *J. Solid State Chem.* **1998**, *135*, 256–259.
- Carlier, L.; Baron, M.; Chamayou, A.; Couarraze, G. Greener pharmacy using solvent-free synthesis: Investigation of the mechanism in the case of dibenzophenazine. *Powder Technol.* **2013**, *240*, 41–47.
- Carlier, L.; Baron, M.; Chamayou, A.; Couarraze, G. Use of co-grinding as a solvent-free solid state method to synthesize dibenzophenazines. *Tetrahedron Lett.* **2011**, *52*, 4686–4689.
- Cumbrera, F. L.; Sánchez-Bajo, F. The use of the JMAYK kinetic equation for the analysis of solid-state reactions: critical considerations and recent interpretations. *Thermochim. Acta* **1995**, *266*, 315–330.
- Declerck, V.; Nun, P.; Martinez, J.; Lamaty, F. Solvent-Free Synthesis of Peptides. *Angew. Chemie Int. Ed.* **2009**, *48*, 9318–9321.
- Dey, D.; Bose, A.; Bhattacharyya, D.; Basu, S.; Maity, S. S.; Ghosh, S. Dibenzo[a,c]phenazine: A Polarity-Insensitive Hydrogen-Bonding Probe. *J. Phys. Chem. A* **2007**, *111*, 10500–10506.
- Friščić, T.; Halasz, I.; Beldon, P. J.; Belenguer, A. M.; Adams, F.; Kimber, S. a J.; Honkimäki, V.; Dinnebier, R. E. Real-time and in situ monitoring of mechanochemical milling reactions. *Nat. Chem.* **2013**, *5*, 66–73.
- Friščić, T.; Jones, W. Recent advances in understanding the mechanism of cocrystal formation via grinding. *Crystal Growth and Design*, **2009**, *9*, 1621–1637.
- Gilman, J. J. Mechanochemistry. *Science*, **1996**, *274*, 65.

Hancock, J. D.; Sharp, J. H. Method of Comparing Solid-State Kinetic Data and Its Application to the Decomposition of Kaolinite, Brucite, and BaCO<sub>3</sub>. *J. Am. Ceram. Soc.* **1972**, *55*, 74–77.

Haruta, N.; Sato, T.; Tanaka, K.; Baron, M. Reaction mechanism in the mechanochemical synthesis of dibenzophenazine: application of vibronic coupling density analysis. *Tetrahedron Lett.* **2013**, *54*, 5920–5923.

Hickenboth, C. R.; Moore, J. S.; White, S. R.; Sottos, N. R.; Baudry, J.; Wilson, S. R. Biasing reaction pathways with mechanical force. *Nature* **2007**, *446*, 423–427.

Jayasankar, A.; Somwangthanaroj, A.; Shao, Z. J.; Rodríguez-Hornedo, N. Cocrystal formation during cogrinding and storage is mediated by amorphous phase. *Pharm. Res.* **2006**, *23*, 2381–2392.

Kaupp, G. Mechanochemistry: the varied applications of mechanical bond-breaking. *CrystEngComm* **2009**, *11*, 388–403.

Kaupp, G.; Naimi-Jamal, M. R. Quantitative Cascade Condensations between o-Phenylenediamines and 1,2-Dicarbonyl Compounds without Production of Wastes. *European J. Org. Chem.* **2002**, *2002*, 1368–1373.

Khawam, A.; Flanagan, D. R. Solid-state kinetic models: Basics and mathematical fundamentals. *J. Phys. Chem. B* **2006**, *110*, 17315–17328.

Laursen, J. B.; Nielsen, J. Phenazine Natural Products: Biosynthesis, Synthetic Analogues, and Biological Activity. *Chem. Rev.* **2004**, *104*, 1663–1686.

Lin, H.-L.; Lin, S.-Y.; Lin, C.-C.; Hsu, C.-H.; Wu, T.-K.; Huang, Y.-T. Mechanical grinding effect on thermodynamics and inclusion efficiency of loratadine–cyclodextrin inclusion complex formation. *Carbohydr. Polym.* **2012**, *87*, 512–517.

Muddasir, H.; Lu, P.; Gu, C.; Wang, Z.; Yang, S.; Yang, B.; Wang, C.; Ma, Y. Molecular properties of 9,10-phenanthrenequinone and benzil. *Chem. Res. Chinese Univ.* **2009**, *25*, 950–956.

Pereira, J. A.; Pessoa, A. M.; Cordeiro, M. N. D. S.; Fernandes, R.; Prudêncio, C.; Noronha, J. P.; Vieira, M. Quinoxaline, its derivatives and applications: A State of the Art review. *Eur. J. Med. Chem.* **2015**, *97*, 664–672.

Senna, M. Consequences of molecular strain on the solid state addition reaction. *J. Mater. Sci.* **2004**, *39*, 4995–5001.

Trotzki, R.; Hoffmann, M. M.; Ondruschka, B. The Knoevenagel condensation at room temperature. *Green Chem.* **2008**, *10*, 873–878.

Willart, J. F.; Descamps, M. Solid state amorphization of pharmaceuticals. *Mol. Pharm.* **2008**, *5*, 905–920.

---

**CHAPTER 4.**

**Kinetic studies of mechanically-induced  
2,3-diphenylquinoxaline synthesis**

---

## 4.1 INTRODUCTION

This chapter is addressed to parametric studies of 2,3-diphenylquinoxaline (DPQ) mechanosynthesis carried out in the vibratory ball mill Pulverisette 0 (P0) by reacting *o*-phenylenediamine (PDA) and benzil (BZ). This synthesis was chosen due to the rapid transformation as shown in the previous chapter as well as the analytical methodology for monitoring that allows identifying and quantifying the reactants and product. A brief discussion about the kinetic aspects of mechanochemical reaction is made in this first section, followed by the theoretical description of temperature dependence of the reaction rate constants.

Technical parameters adapted to P0, such as material of the milling bodies (bowl and ball), the size and weight of the ball were investigated. Experiments as function of milling temperature were performed aiming to determine kinetic parameters by using the classical approach of Arrhenius or Eyring plot. Finally, the grain size of the raw material, BZ, showed slight influence on the kinetics of transformation.

Concerning to the parameter varied, the milling temperature showed strong influence on the kinetics of transformation, as it is for the most chemical reactions. The Arrhenius and Eyring plots could be constructed in the range of milling temperature from 12 – 35 °C, which allowed the determination of an apparent activation energy ( $E_a$ ) or activation enthalpy ( $\Delta H^\ddagger$ ) for the former and the latter equations respectively. These values of energies were not found constants. They varied as function of temperature range, indicating a change in reaction mechanism such as eutectic contact melting as revealed by DSC – microscopy coupled techniques.

### 4.1.1 Kinetics investigation of mechanochemical reactions

The yields of reactions in classical routes vary in function of the concentration, solvents, catalysts, temperature and time as well the treatments after reaction. Likewise, the operational parameters of the ball milling devices, or mechanoreactors, may influence the kinetics of mechanochemical transformations. The effect of milling devices type, grinding material as well as the effect of weight and size of the milling bodies have been demonstrated not simply on the kinetics of transformation, but also on yields and selectivity. Stolle (2015) reviewed these technological and operational parameters of the milling devices that affects the reactions carried under the ball milling conditions.

On the other hand, concerning the kinetic studies for mechanochemical reactions, just a few examples explored the kinetic models in order to determine the rate laws and the apparent rate-limiting step (**Table 4.1**). That is because most of the researches are focused on quantitative transformations while kinetic aspects of such reactions are generally neglected.

As mentioned for the kinetics of DBPZ synthesis in the previous chapter, there is a lack of kinetic models for reactions under continuous milling. However, as the reactants for ball milling reactions are mainly solids, the classical kinetic models for solid-state reactions (Appendix I) have been used and can help in the mechanistic understanding. **Table 4.1** presents some kinetics of mechanochemical reactions with the respective rate law that better fits the experimental results.

**Table 4.1.** Mechanochemical systems that studied the kinetic aspects.

Reaction Type	Rate law	Ref.
<b><u>Cocrystal formation</u></b>		
Sulfadiimide and salicylic acid (SD•SA)	First-order – Nucleation ( $k = 0.11 \text{ min}^{-1}$ , for SD•SA, and $k = 0.08 \text{ min}^{-1}$ , SD•AA)	Caira et al. (1995)
Sulfadiimine and anthranilic acid (SD•AA)		
<b><u>Acid-base reaction</u></b>		
L-tartaric acid and sodium bicarbonate	Second-order/Diffusion-controlled (3D)	Liu et al. (2011)
<b><u>Metal-organic frameworks</u></b>		
ZnO and Methylimidazole (HMeIm)	LAG <sup>a</sup> – A2 model ( $k = 0.0212 \text{ s}^{-1}$ ) <sup>c</sup> ILAG <sup>b</sup> – D1 model ( $k = 0.00158 \text{ s}^{-1}$ ) <sup>c</sup>	Friščić et al. (2013)
ZnO and Imidazole (HIm)	First-order reaction kinetics LAG <sup>a</sup> – ( $t_{1/2} = 0.42 - 0.64 \text{ min}^{-1}$ ) ILAG <sup>b</sup> – ( $t_{1/2} = 1.59 - 2.35 \text{ min}^{-1}$ )	Halasz et al. (2014)
ZnO and Imidazole (HIm)	Second-order ( $k \propto f(\text{Hz}): 0.64 - 12.7 \text{ s}^{-1}$ )	Ma et al. (2014)

<sup>a</sup>Liquid Assisted Grinding (EtOH or DMF), <sup>b</sup>Ion- and Liquid Assited Grinding (EtOH or DMF with  $\text{NH}_4^+$  ( $\text{NO}_3^-$ ,  $\text{CH}_3\text{SO}_3^-$  or  $\text{SO}_4^{2-}$ )), <sup>c</sup>The rate constants were both obtained by fitting the data to a general Avrami-Erofeev model



The studies from **Table 4.1** represent the small number of publications that approached some kinetics of mechanochemical organic reactions. Caira et al. (1995) produced cocrystals of sulfadiimine (SD) by manually co-grinding with different acids, including anthranilic (AA) and salicylic (SA) acids. Analysis of the curves of extent of reaction *versus* time yielded a fit of the data to a first-order type. The behavior was not attributed to a reaction-order model, but to a random nucleation mechanism. They determined the rate constants at 25 °C of  $k = 0.11 \text{ min}^{-1}$  and  $0.08 \text{ min}^{-1}$  for SD•SA and SD•AA respectively. In the same sense, Liu et al. (2011) considerer the mechanochemical reaction between L-tartaric acid and sodium carbonate monohydrate as diffusion-determining step (Jander equation), despite the best fit correspond to a second-order reaction rate. This could be due to better physical interpretation of the mechanisms.

The mechanosyntheses of metal-organic frameworks utilizing ZnO – Imidazoles have been kinetically evaluated in liquid assisted grinding (LAG) and ion- and liquid assisted grinding (ILAG) systems. Frišćić and co-workers (2013, 2014) investigated the kinetic of transformation of these components. For ILAG of ZnO-Methylimidazole (HMeIm) the best fit corresponds to a D1 model indicating that nucleation is not the determining but diffusion. In contrast, for LAG experiments, the data were consistent with A2 kinetic model. The general Avrami-Erifeev model enabled the determination of the rate constants, much slower for LAG (Frišćić et al., 2013). More recently, they reproduced the apparatus for ZnO-Imidazole (HIm), where they found best fits to first-order reaction model for both LAG and ILAG (Halasz et al., 2014). Ma et al. (2014) also studied this last synthesis and the measurements revealed “pseud-fluid” behavior, in which a 2<sup>nd</sup>-order solution reaction was found for the disappearance of HIm. The difference between the same experiments from the two groups has to be carefully treated, first because the syntheses conditions were not the same (smaller amounts of liquid for LAG in Ma’s experiments), which can strongly influence the dynamic of amorphization, solubilization an then crystallization, and consequently favoring one or another step. Second, the analytical techniques were different, *in situ* X-ray diffraction and *ex situ* Raman spectroscopy for Frišćić’s and Ma’s works respectively.

The interests on the kinetics of reactions lie on the fact the through the rate law it possible to preview the conversion and also because it is essential for scaling up purposes and other aspects related to chemical reaction engineering. The kinetic investigation of mechanochemical reactions can help to explain the phenomena observed such as physical limitations and thus, enabling the development of strategies to solve these problems.

Nevertheless, the activation energy must also be determined. For this purpose, one of the ways is to obtain the reaction rate constant at different temperatures.

#### 4.1.2 The temperature dependence of rate constant and the activation energy

The mechanisms and barriers of mechanochemical reactions remains to be completely elucidate. The classical approach to calculate the apparent activation energy for chemical reactions is to use the equations such as Arrhenius and Eyring-Polanyi relating the reaction rate constant and the temperature.

##### 4.1.2.1 Arrhenius equation

The temperature influences reaction rate, and this dependence can be expressed by Arrhenius equation (4.1):

$$k = Ae^{-\frac{E_a}{RT}} \quad (4.1)$$

where,  $k$  is the rate constant at a certain temperature  $T$ ,  $A$  is the pre-exponential or frequency factor that is identified with the frequency of occurrence of the reaction configuration and, mathematically, it represents  $k_\infty$  at infinite temperature;  $R$  is the gas constant and,  $E_a$  is the activation energy, this is, the energy barrier which must be surmounted during transformation of reactants into products during the rate-limiting step.

Although Arrhenius equation has been extensively applied to countless chemical reaction of all possible types to give  $A$  and  $E_a$ , it finds some objections when used for solid-state reactions. The theoretical explanation of Arrhenius equation in homogeneous reaction starts with Maxwell-Boltzmann energy distribution function, which is not applicable for immobilized constituents of a solid. But, despite of it, Galwey and Brown (1995) showed that energy distribution functions, Fermi-Dirac and Bose-Einstein statistics for electrons and phonons respectively, approximate to the same form as that of Maxwell-Boltzmann distribution and hence are capable of explaining the fit of  $k - T$  to an Arrhenius-type equation for solid-state reactions (Galwey and Brown, 1995, 2002).

##### 4.1.2.2 Eyring-Polanyi equation

While Arrhenius equation derives from empirical observation and was firstly developed for gases and it is more related to collision theory, Eyring or Eyring-Polanyi equation is

theoretically based in transition state theory or absolute reaction rate theory. Transition state theory is the culmination of a series of investigations that are conveniently classified under three headings: (1) thermodynamic treatments, (2) kinetic theory treatments and (3) statistical-mechanical treatments. By focusing attention on the activated complexes which are assumed to be in “quasi-equilibrium” with reactants, the transition state theory provides a simple way of formulating reaction rates and gives a unique insight into how process occur (Laidler and King, 1983).

Two of the main principles of transition state theory are: (i) there is a thermodynamic equilibrium between the transition state and the state of the reactants at the top of the energy barrier, (ii) the rate of the chemical reaction is proportional to the concentration of the particles in the high-energy transition state. The Eyring equation (4.2) derives from all mentioned considerations and theories, and is presented as follows:

$$k = \frac{k_B T}{h} e^{-\frac{\Delta G^\ddagger}{RT}} \quad (4.2)$$

$k$  is the reaction rate constant,  $T$  the absolute temperature,  $k_B$  is the Boltzmann constant (gas constant  $R$ /Avogadro's number  $N_A$ ),  $h$  is the Planck constant, and  $\Delta G^\ddagger$  is the Gibbs free energy of activation. Nonetheless, as can be seen, Eyring equation is also an Arrhenius-like equation. The equation can be rearranged in terms of enthalpy ( $\Delta H^\ddagger$ ) and entropy ( $\Delta S^\ddagger$ ) of activation using the Gibbs-Helmholtz equation (4.3) to give equation (4.4):

$$\Delta G^\ddagger = \Delta H^\ddagger - T\Delta S^\ddagger \quad (4.3)$$

$$k = \frac{k_B T}{h} e^{\frac{\Delta S^\ddagger}{R}} e^{-\frac{\Delta H^\ddagger}{RT}} \quad (4.4)$$

Both, Arrhenius and Eyring-Polanyi equations are capable of giving values of activation energy and enthalpy respectively, from experimental data. The linear forms of these equations are:

$$\ln k = \ln A - \frac{Ea}{R} \frac{1}{T} \quad (4.5)$$

for Arrhenius equation, and

$$\ln\left(\frac{k}{T}\right) = -\frac{\Delta H^\ddagger}{R} \frac{1}{T} + \ln\left(\frac{k_B}{h}\right) + \frac{\Delta S^\ddagger}{R} \quad (4.6)$$

for Eyring-Polanyi equation. Plotting the data as  $\ln k \times 1/T$  or  $\ln(k/T) \times 1/T$  will allow the determination of the respective energies with the slope of curve, and frequency factor or entropy of activation from the interception.

One can see that  $Ea$  and  $\Delta H^\ddagger$  are parallel values as well as  $A$  and  $\Delta S^\ddagger$ , which makes possible to relate them. With no further demonstration the expressions are:

$$Ea = \Delta H^\ddagger + RT \quad (4.7)$$

and

$$A = \left(\frac{ek_B T}{h}\right) e^{\frac{\Delta S^\ddagger}{R}} \quad (4.8)$$

The Arrhenius and Eyring-Polanyi equations are suitable for applications in solid-state kinetics and they can be justified fundamentally and theoretically. However, owing the complexity in further understanding of the physical significance of the activation energy and the frequency factor, the Eyring-Polanyi could be useful as it gives thermodynamic parameters more readily interpretable, and that is why it will also be used.

On the other hand, Eyring equation does not distinguish the state of aggregation and, therefore, it can be applied for condensed phase (Wynne-Jones and Eyring, 1935). Although the activation parameters  $\Delta G^\ddagger$ ,  $\Delta H^\ddagger$  and  $\Delta S^\ddagger$  should be attributed to elementary reactions and not to an entire transformation, it has been successfully applied for organic transformations such as enzyme-catalyzed Co-C bond cleavage in Vitamin B<sub>12</sub> (Brown and Li, 1998) and the three-component synthesis of furanones in solution (Shahraki et al., 2015). Stearn and Eyring (1940) derived the Eyring equation for solid diffusion.

Finally, the interpretation of energy barriers must be studied carefully, because the values raise from experimental techniques that generally do not measure or isolate reaction rates of elementary steps but instead measure the overall rate of that process that usually involves several steps with different activation energies (Anslyn and Dougherty, 2005; Vyazovkin and Wight, 1997).

The Arrhenius and Eyring equation are used in order to estimate this overall or apparent activation energy for DPQ mechanosynthesis.

#### 4.1.2.3 The activation energy for mechanically-induced transformations

It is believed that one of the reasons why mechanically-induced transformations give excellent yields in shorter times and unexpected products through different pathways is a possible lowering of the activation barrier. Models in the sense of lowering activation barriers for transformations due to application of external force can be found for reversible bonds between cell surface molecules (Bell, 1978), dissociation of bimolecular complex (Lin et al., 2007), single-molecule pulling experiments (Dudko, 2006) and 1,3-cyclohexadiene ring-opening (Bailey and Mosey, 2012).

Propositions concerning grinding or milling systems were also reported. Zhurkov (1965) proposed a kinetic equation for strength solids, mainly applied to polymer degradation, in which the energy barrier determining the probability of breakage of bonds responsible for strength decreases linearly with the tensile stress applied. Baláž (2003, 2006) has discussed the work of Zelikman et al. (1975), in which the effect of breaking bonds in the ordered crystalline lattice brings about a decrease in the activation energy of leaching. Similarly, Takacs (2012, 2014) has presented a modified Arrhenius equation including the effect of mechanical tension applied to bond, primarily proposed by Zhurkov, to reduce the barrier for reaction. For these cases, the activation energy observed from ( $\Delta E$ ) is, in fact, a variation of the activation energy in absence of mechanical stress ( $E_0$ ) and the contribution that arises from this mechanical action ( $E^*$ ) (Eq. (4.9)). Kulczyki and Kajdas (2013) also presented a modified approach of Arrhenius equation for tribochemical reactions.

$$\Delta E = E_0 - E^* \quad (4.9)$$

Equation (4.9) shows that the activation energy for reaction decreases when the contribution of the mechanical energy increases. This reduction can be the result of thermal induction during milling or the mechanical energy itself for the same ground and excited states of the transformation. However, the equation does not consider the cases where different pathways can be induced by mechanical action that consequently would lead to an intrinsic reduction of  $E_0$ .

Owing to the above comments and the impossibility to further assess temperature due to experimental factors, for the purpose of the studies developed in this present work, the activation barriers from Arrhenius or Eyring equation will be considered in their overall values. In other words, the  $E_a$  or  $\Delta G^\ddagger$  ( $\Delta H^\ddagger$  and  $\Delta S$ ) coming from temperature or mechanical effects will be treated as overall apparent values without decomposition, contrarily as done in

Eq. (4.9). In any case, it is possible to compare the obtained values with frequent values of activation energy of organic reactions in solution as well as to compare the values between themselves. This will allow verifying the influences of the mechanical energy in lowering reaction barriers, if this effect is observed.

The kinetic studies presented in the following sections of this chapter aim to investigate the possible ability of the mechanical energy in reducing the activation barrier and also to complement the previous chapter in terms of the particularities of mechanochemical reactions.

## 4.2 EXPERIMENTAL SECTION

### 4.2.1 Materials

#### 4.2.1.1 Reagents

Benzil (BZ, 98 %, abcr GmbH) and *o*-phenylenediamine (PDA, 98%, Sigma-Aldrich) were used as received. All the solvents used for analyses, if necessary, have analytical degree. Milli-Q<sup>®</sup> water was used throughout the work.

#### 4.2.1.2 Milling device

The vibratory mill Pulverisette 0 – Fritsch (P0) was used as mechanochemical reactor. It is fully described in the experimental section of the previous chapter.

Different milling materials were used and are presented in **Table 4.2** with their specifications. The hollow balls made of stainless steel (SS2, SS3), copper (CU) and brass (BR) have 2.5 mm of shell thickness and were supplied by ball-tech Kugeltechnik GmbH. All the others and the bowls are from the P0 manufacturer (Fritsch). The weight of the hollow balls, when it was needed, was adjusted with fine sand.

### 4.2.2 General procedure for 2,3-diphenylquinoxaline (DPQ) synthesis

For a typical experiment, stoichiometric amounts of *o*-phenylenediamine (PDA, 0.66793 g) and benzil (BZ, 1.3207 g) totaling 2 g, without previous mechanical treatment, were placed in the bowl of the P0 with the ball at the equilibrium temperature, the milling was started and the amplitude adjusted at 2 mm. The grinding system, bowl + ball, was left to equilibrate at the

required temperature for at least 12 h before each run. The total weight of the powder of 2 g was maintained for all experiments. Other conditions for synthesis such as when the parameters vary are given in the respective section.

**Table 4.2.** Milling balls and bowls used for DPQ synthesis in the vibratory micro-mill Pulverisette 0 (P0).

<b>Milling Ball</b>	<b>Ball diameter (mm)</b>	<b>Weight (g)</b>	<b>Ball material</b>	<b>Bowl material</b>
SS1	50	507	Stainless steel, entirely solid	Stainless steel
SS2	50	171	Stainless steel, hollow	Stainless steel
SS3	40	109	Stainless steel, hollow	Stainless steel
SS4	30	109	Stainless steel, entirely solid	Stainless steel
CU	50	171	Copper, hollow	Stainless steel
BR	50	171	Brass, hollow	Stainless steel
AG	50	171	Agate, entirely solid	Agate

### 4.3 RESULTS AND DISCUSSION

The reaction between *o*-phenylenediamine (PDA) and benzil (BZ) to yield 2,3-diphenylquinoxaline (DPQ) was reported a few times by classical route, i.e., in solution medium. It was possible to pass from fair yields of 62 % in ethanol (Gazit, et al., 1996) to good and excellent yields, but the use of acidic media and/or catalysts has been required (Bhosale et al., 2005; Heravi et al., 2006; Darabi et al., 2008 ; Islami and Hassani, 2008). Although the yields have been increased and the reaction time reduced, wastes and, sometimes, not recommended solvents such as methanol were used, which do not fit the *Green Chemistry* principles. In comparison, Kaupp and Naimi-Jamal (2002) reported the mechanochemical reaction with the same reactants, BZ and PDA, yielding the pure DPQ after 1 h in a mixer-mill without further purification step.

The results present here do not intend to report a new synthesis procedure or a new molecule, but aim to study the kinetic aspects of DPQ synthesis. DPQ mechanosynthesis stands out owing the kinetic of reaction shown in chapter 1 and analytical method of quantification as well. The temperature of milling, the material, size and weight of the single ball, and finally the grain size of BZ reactant was investigated.

The reaction product was characterized by  $^1\text{H}$  NMR,  $^{13}\text{C}$  NMR and HRMS (Appendix II). Chromatographic analysis (HPLC) of reaction mixture demonstrated the absence of byproducts for all the experiments. An apparent zero-order reaction, from which the reaction rate constants could be determined, was observed for the experiments and it is discussed throughout the next sections.

### 4.3.1 Parameters assessment for DPQ synthesis in vibratory ball mill

The following experiments were used as preliminary studies on technological and processes parameters before further investigation of the effect of the milling temperature. Up to date, the parameters of milling of P0 were only studied by Chen (1992) for mechanical alloying and amorphization of  $\text{Ni}_x\text{Zr}_y$ . It was defined the specific milling intensity that is the momentum transferred per unit of time to the unit mass of powder. It was demonstrated that the stability of the phases are function of temperature, composition and this specific milling intensity. For this purpose, the P0 was equipped with a LVD transducer and a temperature controlling system. In the case of DPQ synthesis using the vibratory ball mill P0, the modification was only performed for temperature control.

#### 4.3.1.1 Effect of the ball material

The first assessment was performed for the material of milling balls and bowl. The milling material, the balls and vessels, could influence the reaction kinetics by different ways. Eventual catalytic effect for metals (Fulmer et al., 2009) or more acidic surfaces, as well as the magnitudes of mechanical stresses due to the mechanical properties of the materials (Young's modulus for example) can affect the reaction kinetics.

The following series of experiments were performed with four balls with 50 mm of diameter and 171g of different materials: stainless steel (SS2), copper (CU), brass (BR) and agate (AG). The weight of the hollow balls SS2, CU and BR were adjusted to the same of AG by filling them with fine sand. The results are presented **Figure 4.1**.



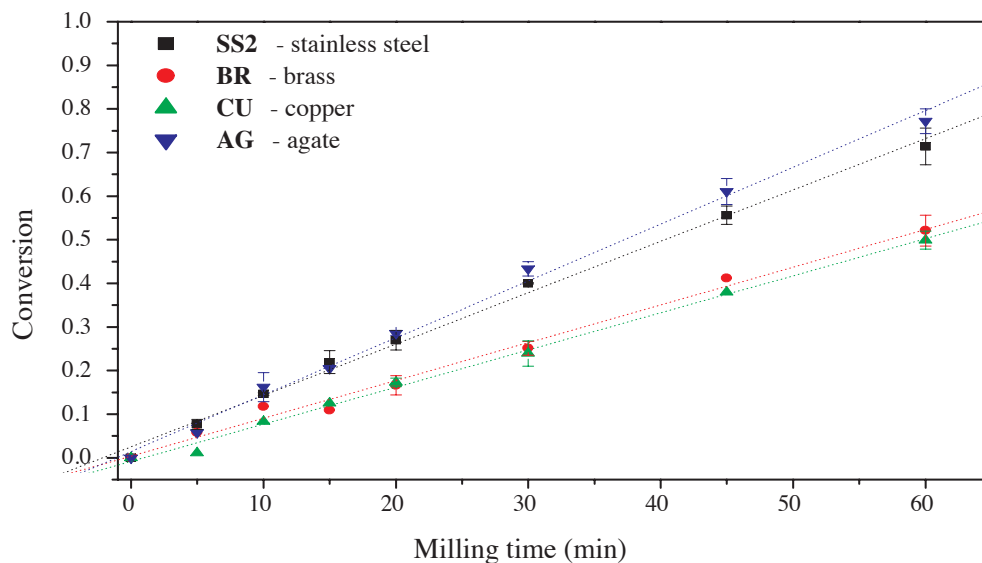


**Figure 4.1.** Effect of the milling ball material on the kinetics of transformation for DPQ synthesis.

The reaction rate seems to be affected by the properties of the grinding media. Brass and copper balls lead to lower reaction rates than stainless steel and agate balls. Further investigations are required to determine if these variations are due to chemical or mechanical features. Nevertheless, it is still possible to infer that when the ball and the bowl are made of the same material, cases of AG and SS2, the mechanical deformations will be directed most exclusively to the powder to be milled. On the other hand, when different materials are used for the ball and bowl, the cases of CU and BR balls, in which the bowl of stainless steel was employed, considerable stresses are transferred to deform the one with lowest Young's modulus ( $E$ ). For example, stainless steel ball and copper have the  $E$  around 200 and 110 GPa respectively (Callister, 2007). Remembering that brass is majorly constituted of copper, these values indicate that CU and BR are deformable upon impact against and stainless steel surface, contributing to decrease the reaction rate. **Figure 4.2** shows the copper ball (CU) and stainless steel ball (SS2) before and after 1 h of reaction. Note that CU is deformed after use.

The chemical composition of the milling balls are not excluded to induced side effects such as induced-surface oxidation of the reactive particles, anticatalytic effect or PDA-complex formation with copper (Khattar et al., 2015; Ghasemi et al., 2015).

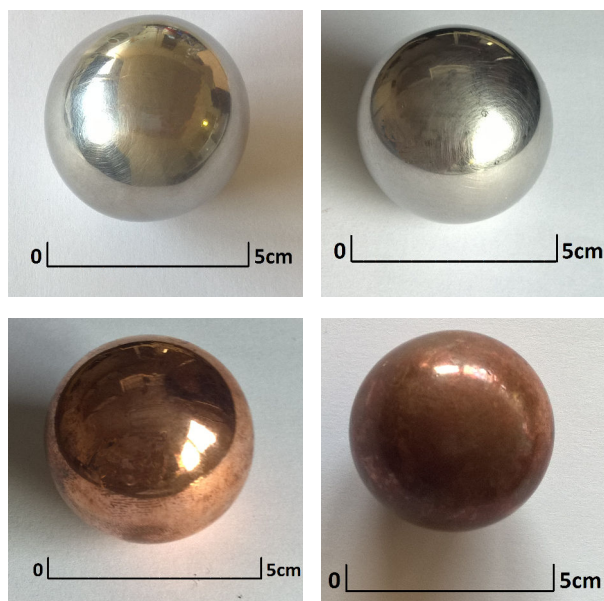


**Figure 4.2.** Pictures of stainless steel ball (SS2 - top) and copper ball (CU - bottom) before (left) and after (right) use.

#### 4.3.1.2 Effect of the ball weight

The ball-to-powder weight ratio (BPR) is an important parameter (Suryanarayana, 2001). In order to evaluate its influence, two stainless steel balls of 507 g (SS1, entirely solid) and 171 g (SS2, partially filled with sand), both with the same diameter, were used. As expected, **Figure 4.3** presents an increase of the rate constant with the mass of the milling ball for a constant mass of the reactive powder.

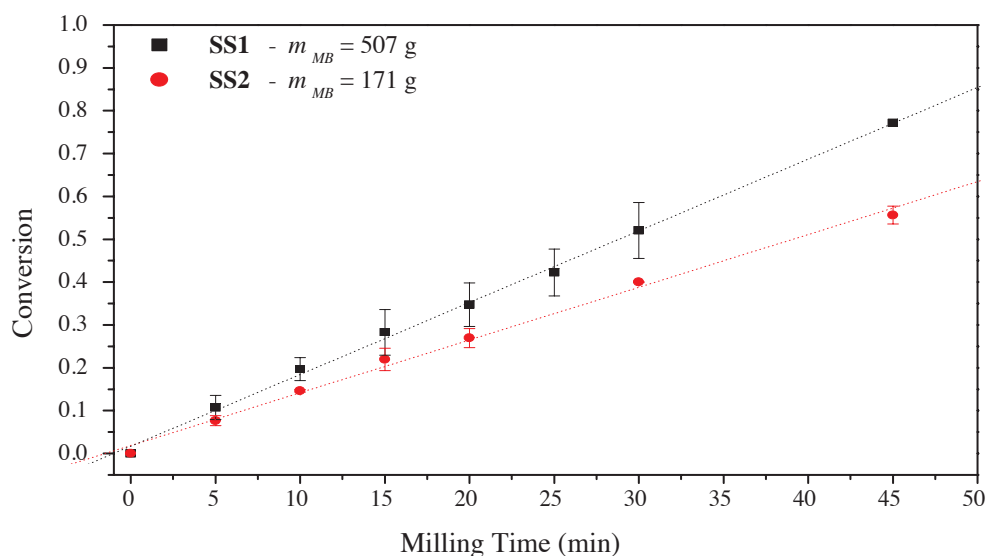


**Figure 4.3.** Effect of the weight of milling ball on the kinetics of transformation for DPQ synthesis.

In spite of the increasing tendency of the reaction rate when the weight of the ball is increased, no direct relation between BPR and the respective kinetic rate constant could be established. At a first moment, this could suggest that the energy is already too high for the ball of 171 g and, that any increment in the weight of the ball will increase the rate constant just slightly and not proportionally to the weight.

#### 4.3.1.3 Effect of the ball diameter

The influence of the diameter of the milling ball was also studied. For this purpose, two balls of 109 g in stainless steel with 40 mm, SS3 (entirely solid) and 30 mm, SS4 (hollow, partially filled with sand), of diameter were investigated. The influence of the ball diameter on the reaction rate is presented in **Figure 4.4**.

If the diameter influences the reaction rate for the balls with the same weight, intuitively, the ball with the small diameter will concentrate the energy for each impact, and therefore, increases the reaction rate. Contrarily, the kinetic curves from **Figure 4.4** shows that the rate constant for the ball of 40 mm is higher.

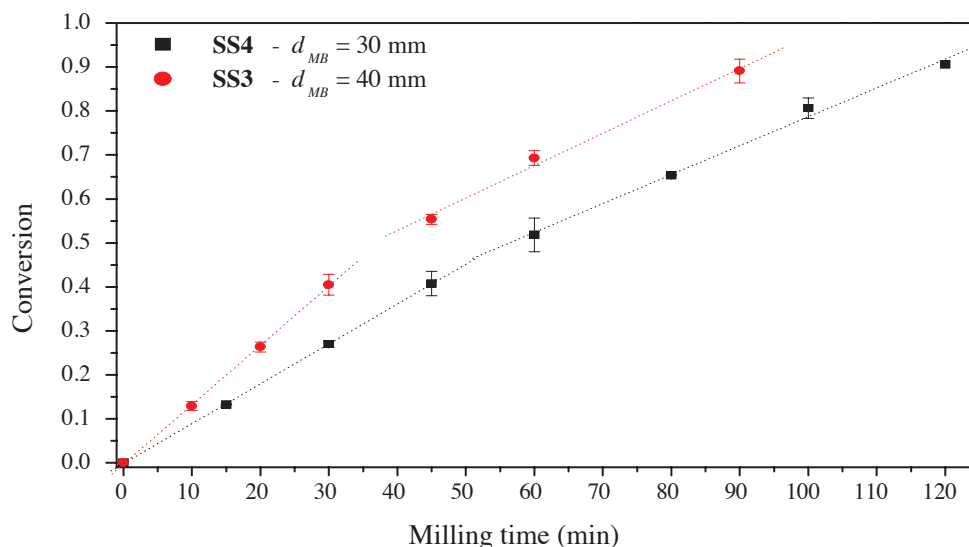


**Figure 4.4.** Effect of the milling ball diameter on the kinetics of transformation for DPQ synthesis.

A first hypothesis for this unexpected result (also according to the previous comment on BPR) could be the random movement of the small a ball that affects the presence of the grinding media itself in the efficient grinding zone, where the reactive powder is placed. Thereby, the increase of reaction rate when the diameter of the ball increases may be explained by the quantity of powder affected in each impact and as a consequence of the more constant efficient mechanical events. In addition, the amount of powder trapped in the ball-

bowl impact zone also depends on geometrical factors of the ball, bowl and powder, and mechanical properties according to Hertzian impact theory as well (Maurice and Courtney, 1990).

It is still appropriate to discuss the different zones of the kinetic curves. As for the other synthesis the reaction remains as zero-order type at the beginning, but, surprisingly, it suffers a change in the reaction rate to another zero-order. The reaction starts faster for  $d_{MB} = 40$  mm, but at a certain point the reaction rate changes and becomes closer to the one from  $d_{MB} = 30$  mm, that has also changed. An explanation to this, can also be attributed to the more stochastic movement of these small balls that fail in efficiency concerning in the occupation of the grinding zone, just in the bottom of the bowl. This is somehow related to the filling degree studied by Stolle and co-workers for planetary ball mills, in which an appropriate amount of balls (in means of their volume) must be used, neither more nor less, to obtain optimized results (Schmidt et al., 2015; Stolle, 2015; Burmeister et al., 2014; Stolle et al., 2014).

#### *4.3.1.4 Effect of the particle size*

The particle size of the raw material can influence the reaction rate. Some authors included this factor in the kinetics of the reaction for thermally induced inorganic reactions in solid state (Carter, 1961; Sasaki, 1964). Ramachandran et al. (1983) and Weng and Parrott (1984) also reported the effect of particle size but for static compacted systems.

In order to assess the effect of the reactant size on the initial reaction rate, raw BZ was sieved in three classes of size that were tested separately and the results compared to those of a global mix: BZ reactants coarser than 1 mm, BZ reactant size between 500  $\mu\text{m}$  and 1 mm, BZ reactant size smaller than 160  $\mu\text{m}$ . The experiments were performed with the ball SS2 ( $m_{MB} = 171$  g and  $d_{MB} = 50$  mm). The grain size of the raw reactant PDA was not evaluated because the powder was already too fine and not able to be sieved. The results presented in **Figure 4.5** show an increase of the reaction rate with the fineness of the reactants particles, even if slightly.

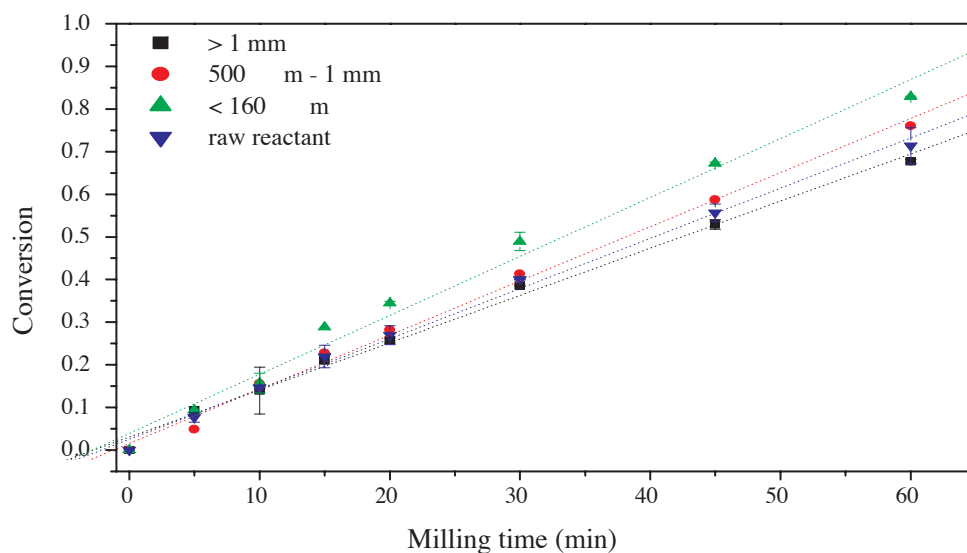


**Figure 4.5.** Effect of the particle size on the kinetics of transformation for DPQ synthesis.

The mechanical action for ball-milled reactions plays the role of particle refinement, constantly exposing new fresh surfaces to react, mixing, and to supply the energy necessary for reaction. Since the reaction starts with smaller particles, the fraction of energy necessary to break them can be transferred to another stage of the co-grinding such as the reaction itself. As result, the reaction rate increases. However, this increase does not impact pronouncedly because the biggest organic particles are quickly reduced independently from the distribution at the beginning of the ball milling. The DLS measurements for particle size distribution showed that after 10 min no further reduction is attained for raw BZ.

The mixture of BZ particle sizes is equivalent to the raw BZ without separation and classification (blue data in **Figure 4.5**). The kinetic curve for this case approaches the curve for particles coarser than 1 mm, which is expected because the particles of this size represent more than 50 % w/w of the raw BZ.

### 4.3.2 Temperature effect on the DPQ synthesis

The temperature can strongly influence the reaction rate of any chemical reaction. The aim of this series of experiments is to evaluate how the reaction rate changes as function of temperature and try to determine the rate-controlling step of the reaction, it means, diffusion-controlled, reaction-order as in solution and etc. Besides, the effect of the weight of ball was also evaluated at different temperatures.

This series of experiments was performed at six different temperatures of the milling system: 12, 16, 21, 27, 32 and 35 °C. The experiments were repeated at least twice (mostly in

triplicate) to confirm the curve trends. The stainless steel system (bowl and ball) was used and left to equilibrate 12 h before each run. In addition, two different weights of balls were investigated, 507 g and 130 g. **Figure 4.6** (a – f) shows the kinetic curves for those six temperatures and for the two weights of the balls in terms of mg of the reactant benzil per mg of the entire sample.

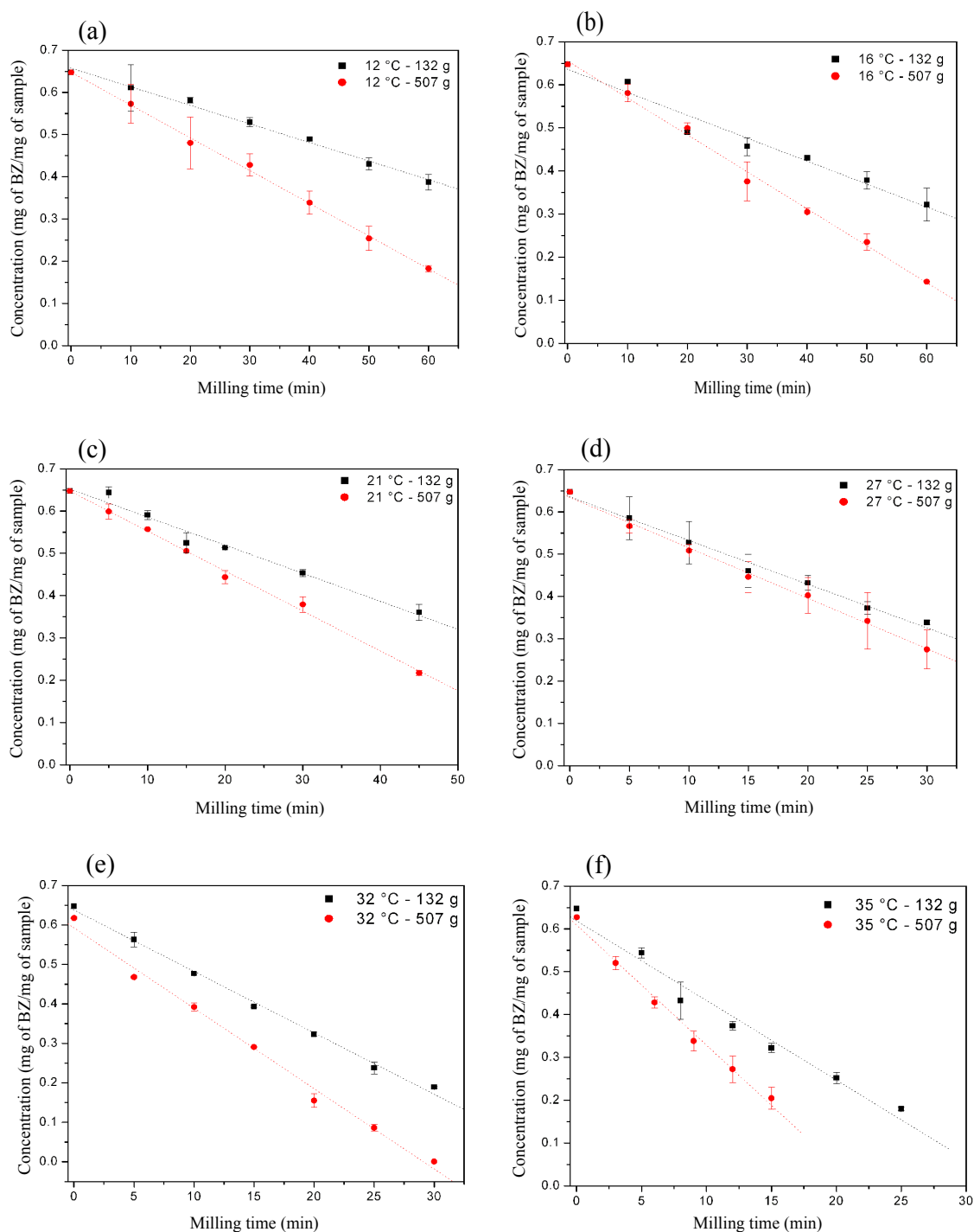


**Figure 4.6.** Kinetic curves of DPQ synthesis for different temperatures and weights of the balls: (a) 12 °C, (b) 16 °C, (c) 21 °C, (d) 27 °C, (e) 32 °C and (f) 35 °C.

The curves of kinetic monitoring for DPQ synthesis showed in **Figure 4.6**, for the studied temperature range and the different weights of the balls, are represented by straight lines. This linear behavior indicates a typical zero-order reaction for the DPQ synthesis performed under the described conditions. Just to compare to the others solid-state kinetic models, the data of conversion were tested with the models presented in Table 1, Part II of bibliographic introduction, and again, the best fit was for zero-order reaction model. It is very important to mention that several other factors, running at the same time as the reaction, are also occurring and this zero-order is, in fact, an apparent reaction order, which could be related to the constant mechanical energy supply for example. Branković et al. (1998) also found zero-order for sodium selenite ( $\text{Na}_2\text{SeO}_3$ ) mechanosynthesis by milling stoichiometric mixture of  $\text{SeO}_2$  and  $\text{Na}_2\text{CO}_3$  in vibrational mill with rings. Apparent zero-order kinetics was found for complex formation with loratadine drug being included into cyclodextrin cavity under grinding conditions (Lin et al., 2012). The kinetic results of DPQ mechanosynthesis also go along with Kaupp's discussion for some solid-state organic reactions presenting zero-order layout (Kaupp, 2003) and with solvent-free synthesis of peptides under ball-milling at different frequencies (Declerck, 2009).

Before going any further, it is essential to revisit the fact that this reaction can continue after grinding as it was showed in the previous chapter. Therefore, one can say that it is not a purely mechanochemical reaction, in which the reaction would occur only upon applying mechanical stress. Indeed, the solid mixture reacts when the solid reactants, previously grinded separately, are put in contact without further mechanical action after that. They react very slowly and after more than five days (125 h at  $25^\circ\text{C}$ ) the formation of DPQ did not exceed 50 % (See **Figure 4.7-a**). **Figure 4.7 (b)** shows that when the reactants are co-grinded during 15 min (conversion at 30 %), which implies in powder state of major particle size reduction and mixing, the reaction reaches 70 % of conversion after 12 h. The formation of fluid phase due to PDA sublimation could be one of the reasons for the reaction continuation, which can be enhanced by the milling process as demonstrated by Mikhalenko et al. (2004) for phthalic anhydride for phthalylsulphathiazole synthesis in ball mills. Furthermore, the conversion ration can be further increased since there is some product formed (seed effect) as it was described for the Knoevenagel condensation of malonitrile and arylaldehydes (Trotzki et al., 2008).

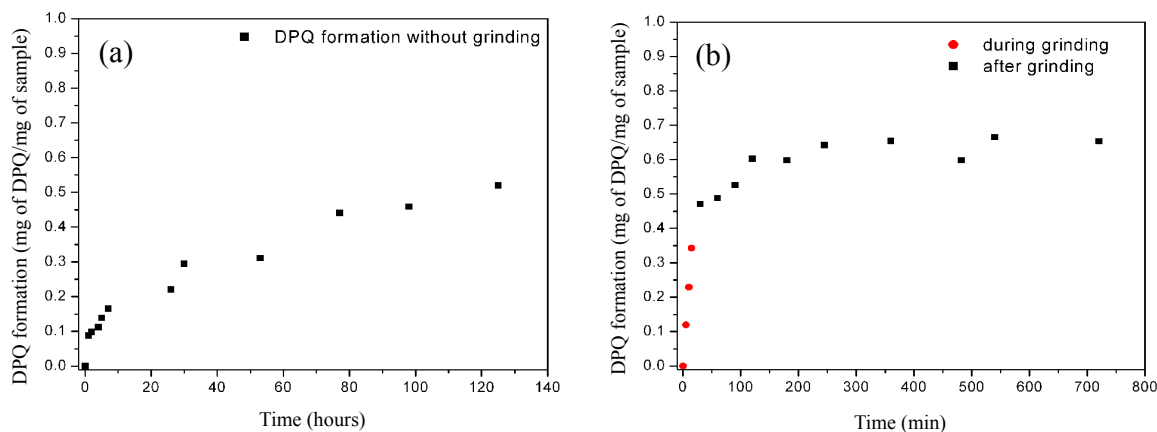


**Figure 4.7.** Kinetic curves for DPQ formation in no grinding state: (a) reactants mixture (they were milled separated before contact) and (b) co-milled during 15 min (red points) and left in static state. The temperature was maintained constant at 25 °C.

However, in addition to the TGA measurements that showed very slow mass loss rate at 25 °C or even at 45 °C (~1.5% after the whole measurement – 60 h, data not shown), the kinetic curves fit differently in continuous grinding or static kinetics presented in **Figure 4.6** and **Figure 4.7** respectively. Thus, the trends observed during the milling time are due to some other determining process that is a consequence of mechanical action. This is confirmed by the changes in reaction rate constants as function of the weight of milling ball. Furthermore, the adjustment of the kinetic curves to zero-order, or constant rate, demonstrates that the rate-determining step is not a physical phenomena such as diffusion taking place at the contact of solid reactive particles as mentioned before, when no classical kinetic models for solid-state reaction could represent the experimental data. Nevertheless, physical events such as size reduction, and more likely, the constant renewal of the particle surfaces to clean the product formed and generation of new fresh deformed surfaces, all results of mechanical action, are certainly embedded in the apparent kinetics.

The curves from **Figure 4.6** also show that the milling temperature ( $T_m$ ) influences the DPQ synthesis in the P0, such as it is expected for the majority of chemical reactions: increasing the temperature of milling, the rate constant also increases. The weight of the balls ( $m_{MB}$ ) also plays a role on the kinetics, which is a general characteristic of ball-milled mechanochemical reactions, because the higher the ball-to-powder weight ratio, the higher the conversion and shorter is the time for quantitative transformations. The slopes of the straight lines of the kinetic curves give the reaction rate constant ( $k$ ). **Table 4.3** summarizes  $k$  for each temperature and ball.



**Table 4.3.** Rate constants for zero-order kinetic model as function of milling temperature ( $T_m$ ) and weight of the ball ( $m_{MB}$ ).

Temperature (°C)	$k/s^{-1}$ ( $m_{MB} = 132$ g)	$k/s^{-1}$ ( $m_{MB} = 507$ g)
12	$(7.34 \pm 0.12) \times 10^{-5}$	$(1.29 \pm 0.05) \times 10^{-4}$
16	$(8.88 \pm 0.10) \times 10^{-5}$	$(1.41 \pm 0.08) \times 10^{-4}$
21	$(1.11 \pm 0.09) \times 10^{-4}$	$(1.57 \pm 0.04) \times 10^{-4}$
27	$(1.72 \pm 0.11) \times 10^{-4}$	$(1.81 \pm 0.31) \times 10^{-4}$
32	$(2.59 \pm 0.01) \times 10^{-4}$	$(3.39 \pm 0.21) \times 10^{-4}$
35	$(3.10 \pm 0.03) \times 10^{-4}$	$(4.68 \pm 0.44) \times 10^{-4}$

These values of  $k$  are graphically represented as function of  $T_m$  for the two different  $m_{MB}$  in **Figure 4.8**. Again, as expected, higher  $m_{MB}$  increases the reaction rate. Three different regions can be identified in **Figure 4.8**: (1) for low temperatures  $k$  changes progressively for both  $m_{MB}$ ; (2) then, at 27 °C the rate constants converge and have similar values of  $k=1.81(0.31) \times 10^{-4} \text{ s}^{-1}$  and  $k=1.72(0.11) \times 10^{-4} \text{ s}^{-1}$  for  $m_{MB} = 507$  g and 132 g respectively; and finally, (3) for high temperatures, above 27 °C,  $k$  increases differently for different weights of the balls, being more pronounced for the heavier ball.

In the first section between 12 °C and 27 °C, the use of a ball of 507 g instead of 132 g increases the reaction rate  $k$  for each temperature. This increase does not change  $k$  in the same ratio of the weights of milling balls, which is 3.84 (507 g/132 g), but it starts in the intercept with close value (0.92/0.23) and is reduced progressively converging to similar values at 27 °C (see **Table 4.3**). Nevertheless, this result is completely clear only after 12 °C because, unfortunately, no data are available below this temperature due to experimental limitations such as unavoidable condensation of water from the air, and then, any run was performed at  $T_m = 0$  °C to confirm the suggestion.

The second region, near to 27 °C, has the particularity of showing close values of the reaction rates for both  $m_{MB}$ . This could be a point of phase changing where the physical state is modified, which results it almost no effect of the milling balls at this point. To confirm this hypothesis, classical DSC measurements were carried out at 5 °C/min for a mixture of the solid reactants, PDA and BZ, where several events were detected, but they are not precisely distinguishable as can be seen in **Figure 4.9**.

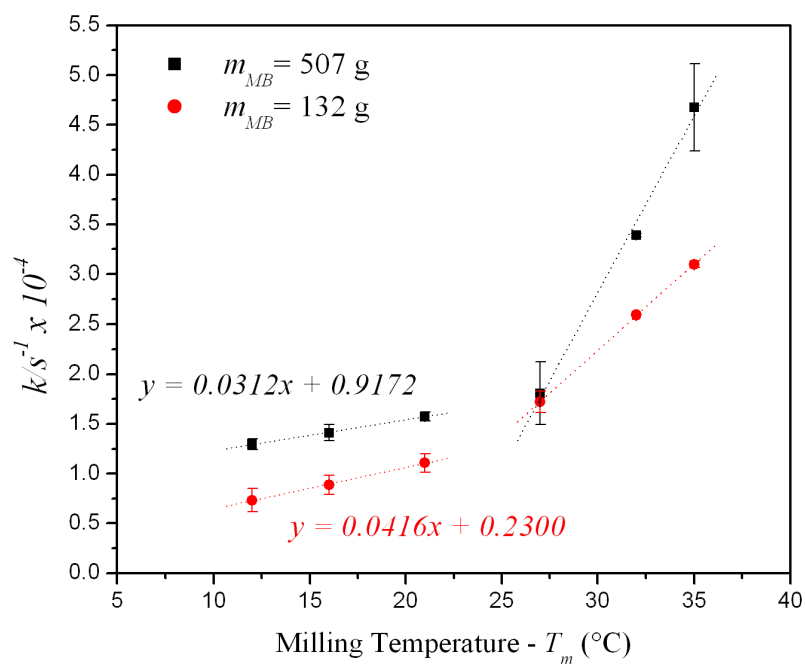


Figure 4.8. Rate constants as function of the milling temperature ( $T_m$ ).

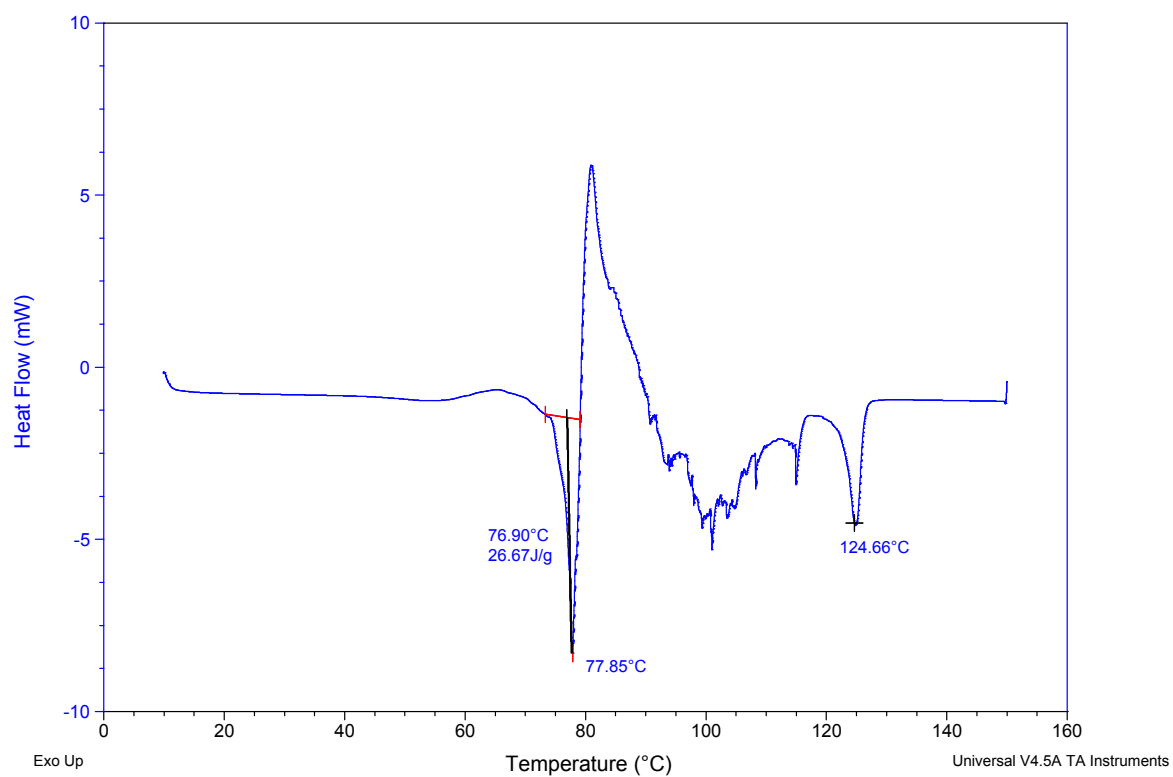
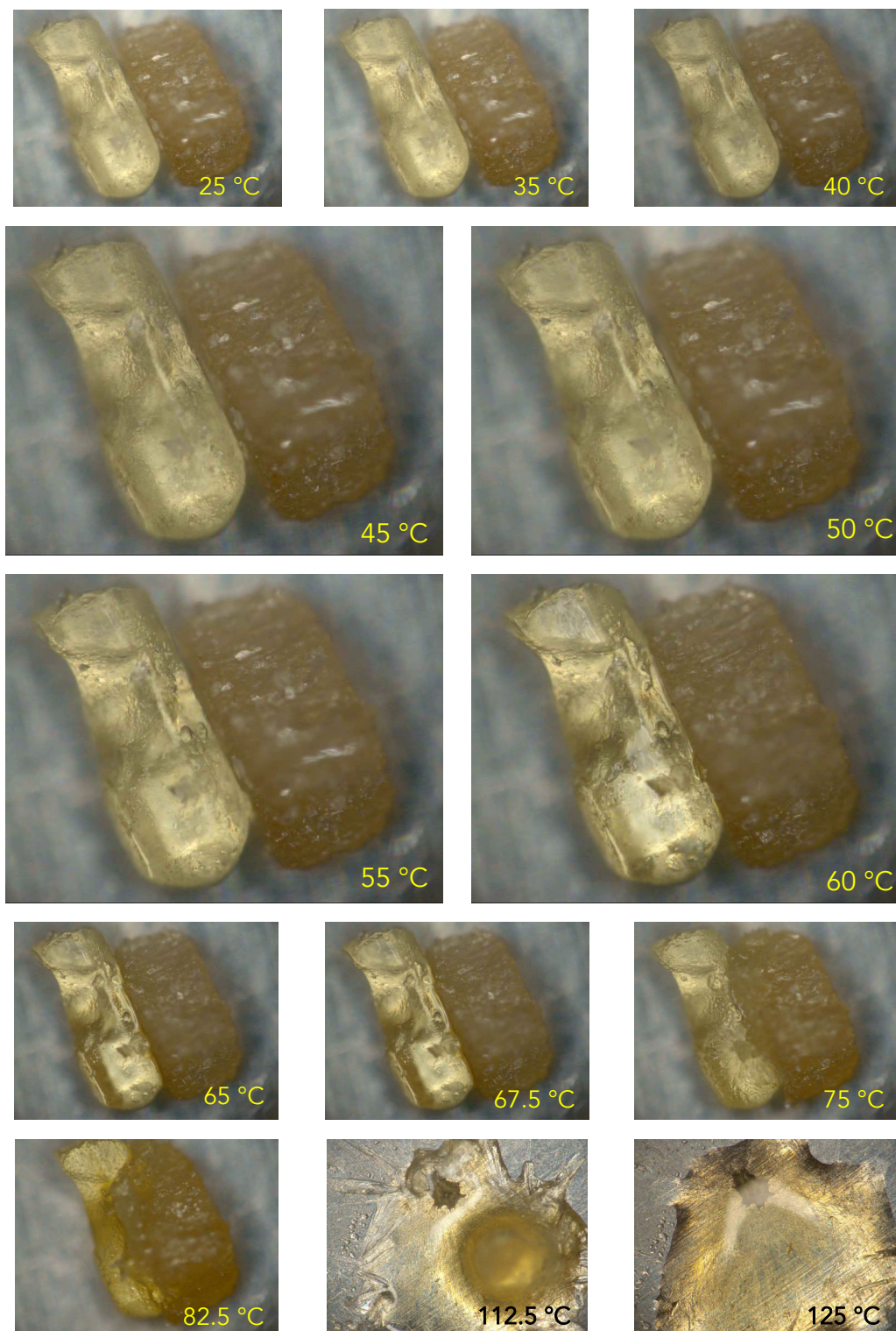


Figure 4.9. DSC thermogram for reactants mixture in equimolar amounts of PDA and BZ.

Reaction enthalpy, melting points and recrystallization can be proposed from the thermogram above, but the most interesting event is the endothermic one occurring at 76.9 °C before the melting points of the individual reactants, which are 94.7 °C for benzil and 100.8 °C for *o*-phenylenediamine. This indicates a possible contact eutectic melting formation, followed by an exothermic event between 78 °C – 90 °C composed by the heat of reaction in the new fluid phase and recrystallization of the product. Then, the remaining traces of reactants melt and water evaporates which appears as endothermic behavior from 95 °C to 120 °C, and finally, the product DPQ melt at 124.7 °C. The possibility to form eutectic melting started further investigation on the temperature in which it occurs. The DSC measurements suggest this melting, but a visual analysis could confirm if the event is in fact a melting of the reactant mixture. For this purpose, hot-stage microscopy apparatus was used. The details are described in the experimental section of present chapter. **Figure 4.10** presents a series of images of the contact between individual particles of the reactants at different temperatures.

The images confirm the eutectic melting of the solid particles that starts at the inter-particle contact interface between 40 °C and 60 °C and then, progresses to the bulk. However, this temperature is much lower than the one from classical DSC analysis. This can be a consequence of the optimized contact of the plane surface of solid reactants that could be assured for the microscopy, but not for classical DSC where the crucibles are closed, or even of geometrical particle effects (Sorescu and Xu, 2012; Yukimitu et al., 2005; Perlovich et al., 2001). But still, the temperature of melting is higher than 27 °C. Besides, the fact that none of the DSC measurements revealed phase change at the temperatures in the surroundings of 27 °C could indicate that the milling temperature is raised during the milling process. On the other hand, if this is valid, a change in the reaction rate should be observed during grinding, which is not the case. Therefore, the overall  $T_m$  is maintained, but the mechanical energy is suggested to induce the eutectic melting lowering the temperature in which it happens or the by the *hot spots* generated (Tokmakoff et al., 1993; Bowden and Yoffe, 1978; Fox, 1975). The latter was also suggested by Boldyreva and co-workers for  $\alpha$ -glycine –  $\beta$ -malonic acid system, in which the hot spots could induce volatilization or eutectic melting. The possibility of impact-induced detachment of molecules from the particles surfaces was also considered (Michalchuk, et al., 2014).



**Figure 4.10.** Images from the hot-stage cell with BZ (yellow) and PDA (brown-white) crystals under heat (10 °C/min) showing the different stages of the contact melting: 12 – 40°C solids, 45 – 60 °C the very beginning of liquid phase formation, 65 – 83 °C melting extending to the bulk, 112.5 some crystals of DPQ can be visualized and at 125 °C melting of DPQ.

Finally, to complete the discussion of the three stages of the  $k$  variation as function of milling temperature and weight of the ball (**Figure 4.8**), in the third part, after 27 °C, it is

observed that the  $k$  values diverge again. The fact that a phase change, more readily to react, is induced from 27 °C for both  $m_{MB}$ , or even owing to the fact the chemical kinetics are supposed to be fast at higher temperatures, the difference on the rate constants are consequence of the mechanical energy necessary to induce this phase changing that are supplied by the impacts. Consequently, the higher the  $m_{MB}$  more powder will be transformed, which is evidenced by adhesion of the powder onto the ball and bowl as the reaction progresses. In addition, the grindability of the powder, now more plastic, will change as a consequence of the pseudo-fluid formation during the ball-powder impact. Still, the  $m_{MB} = 507$  g can offer more energy to break this paraffin-like powder enabling the access of the non-reacted fractions, which is harder to be done by the ball of 132 g. To sum up, the kinetics after 27 °C are the result of induction-breakage of the physical phase, that does not take place in the whole bulk, but at punctual mechanical events. To avoid misunderstandings, it means that this paraffin-like is not macroscopic observed for the entire bulk, but it is detected when the reaction extends and the powder adheres in the bowl walls and balls as a consequence of the ball-powder contact during the mechanical stresses. This phase is also supported by the XRD presented for DPQ synthesis at 25 °C (near to the transition zone) in the previous chapter. It was discussed the presence of amorphous phase during continuous grinding that can correspond to this paraffin-like powder not crystallized yet.

#### *4.3.2.1 The temperature dependence of the reaction rate constant and estimation of activation energies*

The temperature dependence of the reaction rate constant is generally described by Arrhenius and Eyring equations as presented before in the section 4.1.2 of the introduction of this chapter. For the purpose of these studies, both equations were used, not with the aim to compare, but to be complementary in the discussions. Arrhenius equation is applied because it is the most used and could be justified even for solid-state reactions (Galway and Brown, 1995, 2002), and Eyring equation because the thermodynamic activation parameters,  $\Delta G^\ddagger$ ,  $\Delta H^\ddagger$ , and  $\Delta S^\ddagger$ , are useful to give some insight in the state or order of the system for DPQ synthesis. Even though a further complication arises from the fact that Eyring equation should be applied only to elementary reactions, which enables the interpretation of the absolute values of energies, nothing prevents its use to compare these energies for more complex reactions if they have the same molecularity.

In order to estimate the activation energy barriers for the experimental conditions of DPQ synthesis, the experimental data from **Table 4.3** with the rate constants as function of

temperature for the two different  $m_{MB}$  were plotted according to equations (4.5) and (4.6) and are displayed in **Figure 4.11** and **Figure 4.12** for Arrhenius and Eyring plot respectively.

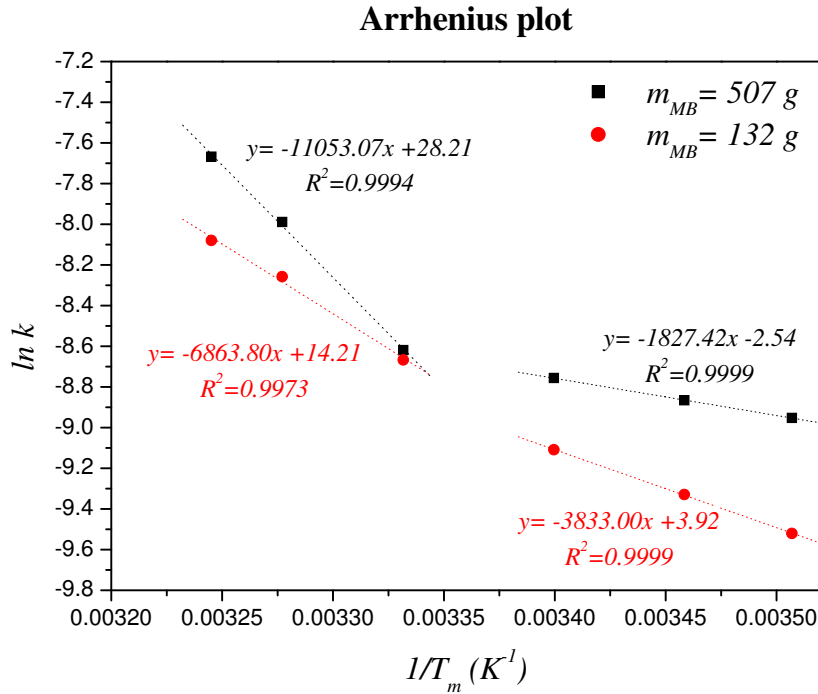


**Figure 4.11.** Arrhenius plot with the rate constants and the milling temperature ( $T_m$ ) for DPQ synthesis in P0 with different weights of the balls ( $m_{MB}$ ).

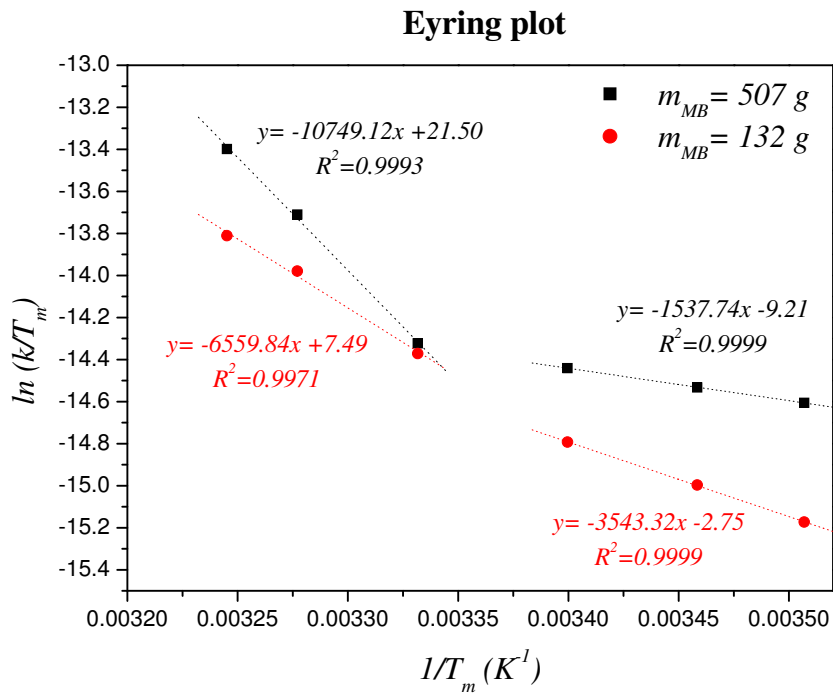


**Figure 4.12.** Eyring plot with the rate constants and the milling temperature ( $T_m$ ) for DPQ synthesis in P0 with different weights of the balls ( $m_{MB}$ ).

Straight lines are expected for Arrhenius and Eyring plots, from which the kinetic parameters, including the activation energies, can be determined. As can be seen, this is not the case for DPQ synthesis in the experimental conditions, where two linear regions are identified instead. Deviations from linearity implies in the variation of activation energy, fact that is not widely accepted, but that can be justified if changes in the reaction mechanism are considered. The experimental activation energy is not an absolute value for single step reaction, but, on the other hand, it represents an overall value of assembled of two or more single-reaction steps, each one with its own activation barrier. Therefore, the activation energy varies when one or another step becomes rate-determining. Vyazovkin (2000) discussed the variation of activation energy for condensed phases, specially solid reactions. Unlike the homogenous systems, the physical properties of solid reactants can evolve during the reaction, which directly affects the kinetics of such reaction, and besides, the activation energy may vary as well. In the case of DPQ synthesis under ball-milling conditions, the variation of activation energy as function of temperature is attributed to the mechanically-induced phase changing as discussed before.

Utilizing the linear fit from the **Figure 4.11** and **Figure 4.12** the equations 9 and 10, the kinetic parameters were estimated for each range of linearity for the two different  $m_{MB}$ . **Table 4.4** summarizes the calculated kinetic parameters  $E_a$  and  $\ln A$  for Arrhenius equation and,  $\Delta H^\ddagger$  and  $\Delta S^\ddagger$  for Eyring equation. The activation Gibbs free energy,  $\Delta G^\ddagger$ , was also evaluated from Gibbs–Helmholtz equation (4.3).

**Table 4.4.** Activation parameters using Arrhenius ( $E_a$  and  $\ln A$ ) and Eyring equations ( $\Delta H^\ddagger$ ,  $\Delta S^\ddagger$ ,  $\Delta G^\ddagger$ ) for DPQ synthesis in P0.

$T_m$ (°C)	$m_{MB}$ (g)	$E_a$ (kJ mol <sup>-1</sup> )	$\ln A$	$\Delta H^\ddagger$ (kJ mol <sup>-1</sup> )	$\Delta S^\ddagger$ (J mol <sup>-1</sup> K <sup>-1</sup> )	$\Delta G^\ddagger$ (kJ mol <sup>-1</sup> )
12 – 21	132	31.87	3.92	29.46	-220.37	92.14
	507	15.19	-2.54	12.78	-274.14	93.25
27 – 35	132	57.07	14.21	54.54	-135.24	95.10
	507	91.89	28.21	89.37	-18.82	95.72

In general, the activation parameters from Eyring equation,  $\Delta H^\ddagger$ ,  $\Delta S^\ddagger$ ,  $\Delta G^\ddagger$ , must be calculated for a certain temperature. But, if it is assumed that  $\Delta H^\ddagger$  and  $\Delta S^\ddagger$  do not vary with temperature, mainly for the narrow temperature range, they are valid average values for each range.  $\Delta G^\ddagger$  values from **Table 4.4** are calculated directly from Eyring equation for each rate

constant and the respective temperature or from Gibbs-Helmholtz equation, which gives the same values, and then, averaged for that range of  $T_m$ .  $\Delta G^\ddagger$  also has the similar values for each temperature in the range, it means, 12, 16 and 21 °C, and 27, 32 and 35 °C, they have the same Gibbs free energy, which confirms the consistence of the values.

The activation energy from Arrhenius equation,  $E_a$ , is different for different temperatures and milling balls. For lower temperatures, the  $E_a$  is 31.9 and 16.0 kJ/mol for  $m_{MB}$  of 132 and 507 g respectively. In general, these values do not correspond to energy barriers of typical organic reactions that have  $E_a$  of 40 – 200 kJ/mol. Then, one can say that the rate-limiting step is other than chemical reaction, such as diffusion or phase boundary formation. But, nevertheless, the experimental data do not have the pattern commonly found for thermal solid-state reactions and, in addition, at lower temperatures the chemical kinetics is supposed to be slower and then, determining the chemical reaction rate. Therefore, the kinetics observed at lower temperatures could be a result of the mechanical action accelerating the chemical kinetics and consequently lowering the activation energy of the transformation. The effect of  $m_{MB}$  is verified for the heaviest ball reducing the energy barrier more than the lightest one. Different authors have approached the role of mechanical action in lowering the activation barrier for transformation as presented in the bibliographic review. This may be the case for the DPQ synthesis at lower temperatures in the experimental conditions.

Above 27 °C, a second region is evidenced where the activation energy also changes as function of the weights of the milling balls, but differently than it was obtained for 12 – 21°C. For this temperature range between 27 and 35 °C an inverse effect is observed and the higher  $m_{MB}$  led to higher  $E_a$ , which is 57.1 kJ/mol for  $m_{MB} = 132$  g and 91.9 kJ/mol for  $m_{MB} = 507$  g. This inversed behavior can be explained by the mechanically-induced phase change from 27 °C. First, if the physical state is changed, the activation energy is affected possibly due to different mechanisms. Second, if that phase-changing is originally induced by the mechanical action, for higher energies of mechanical interaction more powder will suffer the transformation. Third, this induced phase, above called paraffin-like powder, behaves more like a fluid and, therefore, the activation energies should be characteristic of organic chemical reactions in solution. Indeed, the  $E_a$  increases for more intense mechanical treatment that is capable to generated larger amounts of this phase, attributed to eutectic contact melting formation, and consequently, more of reaction mixture reacts like in solution. This explain the fact that the ball of 132 g presents lower activation energy because, as it is lighter, less of the eutectic melting is induced and the reaction mixture has a smaller fraction reacting as in fluid



phases and more of solid-solid reaction, which presents lower activation barrier as in the case of the first temperature range of 12 – 21 °C. **Figure 4.13** illustrates and summarizes the stages of the discussion above as function of  $T_m$  and  $m_{BM}$ .

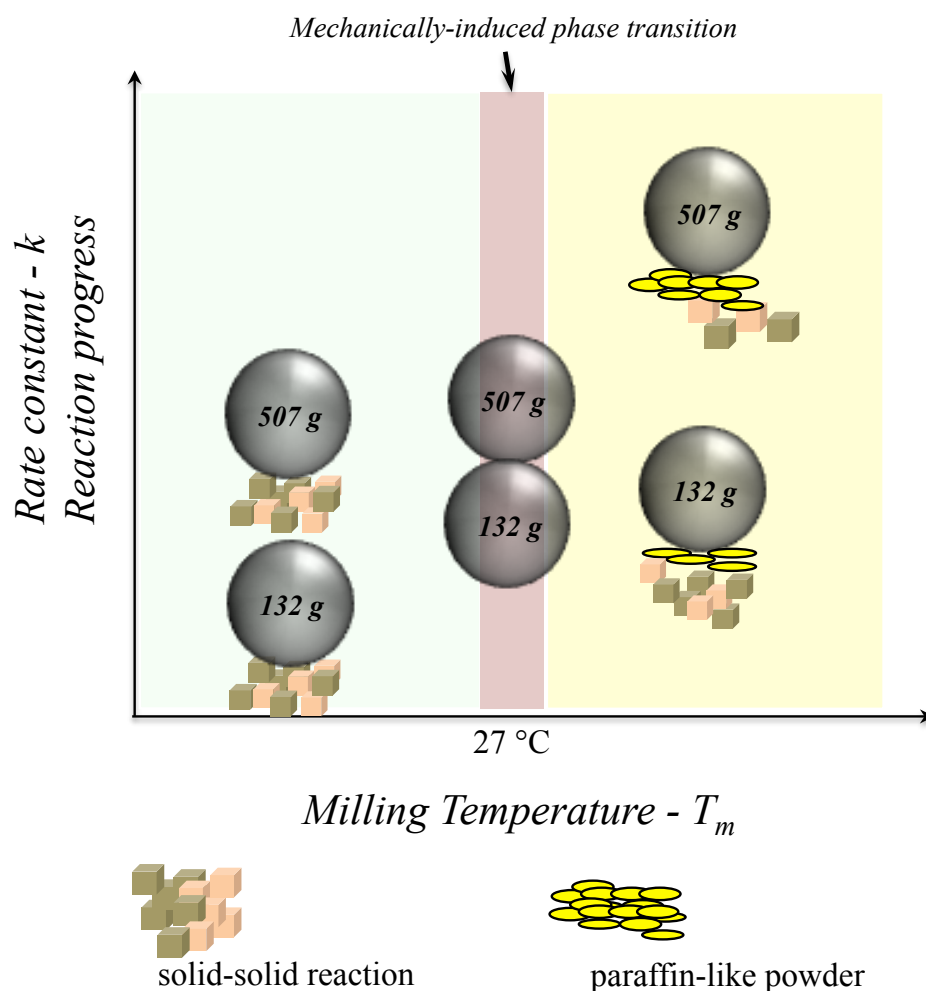


**Figure 4.13.** Proposed scheme of reaction rate for mechanically-induced DPQ synthesis as function of milling temperature and weigh of the milling ball in vibratory balm-mill P0. Below 27 °C solid-solid reaction predominates and above 27 °C phase-changing during mechanical stresses events.

Concerning the activation enthalpy  $\Delta H^\ddagger$  from Eyring equation, it is expected that the values be similar to  $E_a$ , which is confirmed in **Table 4.4**. Contrarily,  $\Delta G^\ddagger$  that generally also presents similar values to Arrhenius activation energy and  $\Delta H^\ddagger$ , is not comparable to them at lowest temperatures, probably due to high entropic contributions at lower temperatures, where the solid-solid reactions prevail.  $\Delta S^\ddagger$  values are more negative for  $T_m$  12 – 21 °C, in which the powder state is more crystalline and stable. The synergism of temperature increase and application of mechanical energy induce the transformation of the physical state to another less crystalline at the contact point for reaction, resulting in an increase of  $\Delta S^\ddagger$ . In turn, the

$\Delta G^\ddagger$  tends to values of  $E_a$  and  $\Delta H^\ddagger$ , culminating to be very close at 35 °C for  $m_{MB} = 507$  g. These similar values for higher temperatures, where the paraffin-like state is formed at the impact zone, represent more ideal systems that are common for gases and also liquids, and confirm somehow that at these  $T_m$  the reaction mixture react more likely in fluid phase.

In other words, regarding the Gibbs free energy, for the calculated values, which do not significantly vary for the whole array of experimental conditions, it seems to be the contrary of  $E_a$  that is reduced indicating lower activation barriers for lower temperatures. As mentioned before, the counterbalances between  $\Delta S^\ddagger$  and  $\Delta H^\ddagger$  might explain the close  $\Delta G^\ddagger$  values. In one side the reaction in solid-state is favored by the reduction of the activation barrier  $\Delta H^\ddagger$  due to mechanical stresses at lower temperatures, but in the other side, at this same temperature range the solid corresponds to a more crystalline form reflecting in more negative entropies. In the other temperature range (starting around 27 °C), less negative  $\Delta S^\ddagger$  are obtained, which would favor the reaction, but at the same time the activation barrier  $\Delta H^\ddagger$  increases due to the phase transition that behaves similarly to fluid systems with higher activation energies. Thus, enthalpy or entropy controlled regions can be identified, which results in the changes of curvature of the plots of **Figure 4.11** and **Figure 4.12** and indicates a change in the mechanism or pathways, but not in the structure of the transition state. Brown and Li (1998) verified this effect for enzyme conformational change, but in the other sense, i.e., the activation barriers were higher for lower temperatures.

#### 4.4 CONCLUSION

The DPQ synthesis under ball milling conditions was investigated. The overall kinetics revealed a zero-order reaction type. Technological parameters such as material, diameter and weight of the milling balls affect the reaction rate. When the ball and the bowl of the same material are employed, the reaction rate is not influenced. In the other side, the use of different materials can result in some deformation transferred to the milling body and not to induce the reaction, and then, the reaction is slower. The chemical nature of the ball could be another reason for lowering the reaction rate, but only further investigation on the chemistry of the balls of copper and brass will help to elucidate. The reaction rate increases for heavier balls as expected, but not proportionally to the increase in the weight. Smaller balls of 30 and 40 mm of diameter resulted in slower reactions and a change in the rate constant, but both of zero-order. These effects were attributed to the more random movement of these balls inside

the bowl, which affects directly the amount of the reactive solid mixture trapped in the grinding zone and reduces the number of effective impacts as well. The grain size of the raw material, BZ reactant, was also assessed and smaller particles led to higher conversion, but just slightly. Thereby, this factor was not considered for the next runs, specially because the grain size of these organic powders is quickly reduced during milling as showed by DLS measurements.

Studies of the milling temperature for two different weights of balls revealed unexpected changes in the reaction mechanism, which is supported by phase transition that was evidenced by an adapted hot-stage microscopy around 45-60°C. It was considered that this transition is anticipated by the mechanical action that reduces the temperature necessary to the contact melting and not a temperature increase during milling because the reaction rates did not change. As consequence of the phase change, two different apparent activation energies were estimated for each  $m_{MB}$  and as function of the milling temperature. Below 21 °C, the reaction is considered to be between solids, i.e., a mechanochemical reaction, and the mechanical energy acts to low the activation barriers ( $E_a$  and  $\Delta H^\ddagger$ ). When the heavier ball was used the activation barrier was the lowest one. As the temperature approaches 27 °C, the mechanical action could induce a phase transition that corresponds to a contact melting of the solid reactants, and above this temperature the reaction rates increases faster also for the heavier milling ball. But, in the contrary, the activation energy is higher for this one, approaching values expected for organic reactions in solution. This was attributed to the fact that as the melting of reactants is induced by mechanical stresses, the ball of 507 g supplies more energy at each mechanical event and then, the reaction goes faster in the media rich in that phase. Besides, this phase called paraffin-like powder requires higher energy to be milled because it impregnates and hampers the mixing. On the other hand, when the ball of 132 g was used, mainly solids should compose the reaction mixture and the mechanical action continues decreasing the activation energy. The values of activation entropies were more negative for lower temperatures (solid-solid), then increasing for the temperatures above 27 °C, when the reacting mixture is also constituted by some melting at impact zones.

The results indicated that the for further studies in mechanochemical reactions in ball mills, mild conditions (lower temperatures and lighter milling balls) must be used when the main objective is to evaluate the mechanical effects such as weight and diameter of the balls. It means that the preliminary assessments of the milling parameters that were performed at 26 °C, closer to the region of phase changing, would lead to more pronounced differences when modification of parameters is carried out at lower reaction temperatures. Similarly, the

temperature effects on the ball-milled DPQ synthesis are expected to be better evaluated with lighter balls. In spite of this, it was still possible to differentiate two regions: one, for lower temperatures, assigned as a solid-solid reaction, truly a mechanochemical reaction, in which the activation energy is very low, and, the other with a greater contribution of “pseudo-fluid” phase induced by the mechanical action at higher temperatures that reacts similar as in solution in means of activation energy. The DPQ synthesis in the vibratory ball mill with a single milling ball showed the solid-solid reactions and eutectic contact melting, both considered as possible mechanisms for mechanically-induced reactions can take place at particular conditions (Kaupp, 2003; Rothenberg et al., 2001). Deeper investigations could use DRX and Raman techniques to find some phases or intermediates other than crystals for temperatures higher than 27 °C (Hédoux et al., 2011; Willart and Descamps, 2008; Batzdorf et al., 2015).

It is interesting to notice that the main findings described in the chapter namely 1) the lowering of the the apparent activation energy at low temperature which the lowering of the apparent activation energy at low temperature which shows a greater effect of the mechanical action compared to a normal thermal activation and 2) the change of regime from "solid like" to "fluid like" at a temperature which is lower than that of the eutectic, find some analogy and are taken into account by the “driven material concept” developed by Martin and Bellon (1997) and further used for the milling of molecular materials by Willart and Descamps (2008). According to this model, the compound can be viewed as exploring its configuration space under the effect of two distinct mechanisms which act in parallel: the usual thermally activated molecular motions which operates in absence of the external mechanical forcing, and ballistic jumps which are generated by the external forcing. The behaviour of the compound results from a competition between the disorder induced by milling and on the other hand the diffusion effects which tend to restore the system to lower energy states.

In the frame of this model, the physical state of the system, which is ground at the real temperature  $T$  is that of the system in absence of milling at an effective temperature:

$$T_{\text{eff}} = T (1 + D_B / D)$$

where,  $D_B$  is the rate of ballistic jumps induced by milling, which is independent of temperature but depends on the milling intensity (depending on the mass and number of balls, frequency shocks...);  $D$  is the rate of thermal jumps which decreases when temperature decreases.

At high temperature thermal jumps are efficient enough to restore an equilibrium ( $T_{\text{eff}} \cong T$ ). However at low temperature  $T$ , thermal restoration becomes less efficient and  $T_{\text{eff}}$

eventually increases. At low enough milling temperature or (and) rather high milling intensity,  $T_{\text{eff}}$  overcomes the value of the melting temperature, and in the present case it is the value of the eutectic temperature. It looks as if, in our case, the critical temperature of 27°C, where the change of behaviour is observed, would be the eutectic temperature displaced according to the formula giving  $T_{\text{eff}}$ .

## 4.5 REFERENCES

Anslyn, E. V.; Dougherty, D. A. Chapter 7. Energy Surfaces and Kinetics Analysis. In *Modern Physical Organic Chemistry*; University Science Books, 2005; pp. 355–420.

Bailey, A.; Mosey, N. J. Prediction of reaction barriers and force-induced instabilities under mechanochemical conditions with an approximate model: A case study of the ring opening of 1,3-cyclohexadiene. *J. Chem. Phys.* **2012**, *136*, 044102-1 – 044102-11.

Baláž, P. Mechanical activation in hydrometallurgy. *Int. J. Miner. Process.* **2003**, *72*, 341–354.

Baláž, P.; Choi, W. S.; Fabián, M.; Godocikova, E. Mechanochemistry in the preparation of advanced materials. *Acta Montan. Slovaca* **2006**, *11*, 122–129.

Batzdorf, L.; Fischer, F.; Wilke, M.; Wenzel, K.-J.; Emmerling, F. Direct In Situ Investigation of Milling Reactions Using Combined X-ray Diffraction and Raman Spectroscopy. *Angew. Chemie Int. Ed.* **2015**, *54*, 1799–1802.

Bhosale, R. S.; Sarda, S. R.; Ardhapure, S. S.; Jadhav, W. N.; Bhusare, S. R.; Pawar, R. P. An efficient protocol for the synthesis of quinoxaline derivatives at room temperature using molecular iodine as the catalyst. *Tetrahedron Lett.* **2005**, *46*, 7183–7186.

Bowden, F. P.; Yoffe, A. D. Fast reactions in solids, Butterworth Scientific Publication: London, 1958.

Branković, A. R.; Vidojković, V. M.; Milošević, S. D. Mechanochemical Activation of (SeO<sub>2</sub>+Na<sub>2</sub>CO<sub>3</sub>) Mixture and Sodium Selenite Synthesis in Vibrational Mill. *J. Solid State Chem.* **1998**, *135*, 256–259.

Brown, K. L.; Li, J. Activation Parameters for the Carbon–Cobalt Bond Homolysis of Coenzyme B 12 Induced by the B 12 -Dependent Ribonucleotide Reductase from *Lactobacillus leichmannii*. *J. Am. Chem. Soc.* **1998**, *120*, 9466–9474.

Burmeister, C. F.; Stolle, A.; Schmidt, R.; Jacob, K.; Breitung-Faes, S.; Kwade, A. Experimental and Computational Investigation of Knoevenagel Condensation in Planetary Ball Mills. *Chem. Eng. Technol.* **2014**, *37*, 857–864.

Caira, M. R.; Nassimbeni, L. R.; Wildervanck, A. F. Selective formation of hydrogen bonded cocrystals between a sulfonamide and aromatic carboxylic acids in the solid state. *J. Chem. Soc. Perkin Trans. 2* **1995**, 2213–2216.

Callister, W. D. *Materials science and engineering: An introduction*; 7th ed.; John Wiley & Sons, Inc., 2007.

Carter, R. E. Kinetic Model for Solid-State Reactions. *J. Chem. Phys.* **1961**, *34*, 2010.

Chen, Y.; Bibole, M.; Le Hazif, R.; Martin, G. Ball-milling-induced amorphization in NixZry compounds: A parametric study. *Phys. Rev. B* **1993**, *48*, 14–21.

Darabi, H. R.; Tahoori, F.; Aghapoor, K.; Taala, F.; Mohsenzadeh, F. NH<sub>4</sub>Cl-CH<sub>3</sub>OH: an efficient, acid- and metal-free catalyst system for the synthesis of quinoxalines. *J. Braz. Chem. Soc.* **2008**, *19*, 1646–1652.

- Declerck, V.; Nun, P.; Martinez, J.; Lamaty, F. Solvent-Free Synthesis of Peptides. *Angew. Chemie Int. Ed.* **2009**, *48*, 9318–9321.
- Dudko, O. K.; Hummer, G.; Szabo, A. Intrinsic rates and activation free energies from single-molecule pulling experiments. *Phys. Rev. Lett.* **2006**, *96*, 108101-1 – 1081101-4.
- Friščić, T.; Halasz, I.; Beldon, P. J.; Belenguer, A. M.; Adams, F.; Kimber, S. a J.; Honkimäki, V.; Dinnebier, R. E. Real-time and in situ monitoring of mechanochemical milling reactions. *Nat. Chem.* **2013**, *5*, 66–73.
- Fox, P. G. Mechanically initiated chemical reactions in solids. *J. Mater. Sci.* **1975**, *10*, 340–360.
- Fulmer, D. a.; Shearouse, W. C.; Medonza, S. T.; Mack, J. Solvent-free Sonogashira coupling reaction via high speed ball milling. *Green Chem.* **2009**, *11*, 1821.
- Galway, A. K.; Brown, M. E. A Theoretical Justification for the Application of the Arrhenius Equation to Kinetics of Solid State Reactions (Mainly Ionic Crystals). *Proc. R. Soc. A Math. Phys. Eng. Sci.* **1995**, *450*, 501–512.
- Galway, A. K.; Brown, M. E. Application of the Arrhenius equation to solid state kinetics: can this be justified? *Thermochim. Acta* **2002**, *386*, 91–98.
- Gazit, A.; App, H.; McMahon, G.; Chen, J.; Levitzki, A.; Bohmer, F. D. Tyrphostins. 5. Potent Inhibitors of Platelet-Derived Growth Factor Receptor Tyrosine Kinase: Structure–Activity Relationships in Quinoxalines, Quinolines, and Indole Tyrphostins. *J. Med. Chem.* **1996**, *39*, 2170–2177.
- Ghasemi, K.; Rezvani, A. R.; Shokrollahi, A.; Razak, I. A.; Refahi, M.; Moghimi, A.; Rosli, M. M.; *J. Mol. Struct.* **2015**, *1096*, 102–109.
- Halasz, I.; Friščić, T.; Kimber, S. a J.; Užarević, K.; Puškarić, A.; Mottillo, C.; Julien, P.; Strukil, V.; Honkimaki, V.; Dinnebier, R. E. Quantitative in situ and real-time monitoring of mechanochemical reactions. *Faraday Discuss.* **2014**, 203–221.
- Hédoux, A.; Guinet, Y.; Descamps, M. The contribution of Raman spectroscopy to the analysis of phase transformations in pharmaceutical compounds. *Int. J. Pharm.* **2011**, *417*, 17–31.
- Heravi, M. M.; Bakhtiari, K.; Tehrani, M. H.; Javadi, N. M.; Oskooie, H. A. Facile synthesis of quinoxaline derivatives using o-iodoxybenzoic acid (IBX) at room temperature. *Arkivoc* **2006**, *2006*, 16–22.
- Islami, M. R.; Hassani, Z. One-pot and efficient protocol for synthesis of quinoxaline derivatives. *Arkivoc* **2008**, *2008*, 280–287.
- Kaupp, G. Solid-state molecular syntheses: complete reactions without auxiliaries based on the new solid-state mechanism. *CrystEngComm*, **2003**, *5*, 117-133.
- Kaupp, G.; Naimi-Jamal, M. R. Quantitative Cascade Condensations betweeno-Phenylenediamines and 1,2-Dicarbonyl Compounds without Production of Wastes. *European J. Org. Chem.* **2002**, *2002*, 1368–1373.
- Khattar, R.; Yadav, A.; Mathur, P. *Spectrochim. Acta Part A Mol. Biomol. Spectrosc.* **2015**, *142*, 375–381.
- Kulczycki, A.; Kajdas, C. A New Attempt to Better Understand Arrhenius Equation and Its Activation Energy. In *Tribology in Engineering*; Pihtili, H., Ed.; InTech, 2013; pp. 47–62.
- Laidler, K. J.; King, M. C. Development of transition-state theory. *J. Phys. Chem.* **1983**, *87*, 2657–2664.
- Lin, H.; Chen, H.; Sheng, Y.; Tsao, H. Bell's expression and the generalized Garg form for forced dissociation of a biomolecular complex. *Phys. Rev. Lett.* **2007**, *98*, 088304-1 – 088304-4.
- Lin, H.-L.; Lin, S.-Y.; Lin, C.-C.; Hsu, C.-H.; Wu, T.-K.; Huang, Y.-T. Mechanical grinding effect on thermodynamics and inclusion efficiency of loratadine–cyclodextrin inclusion complex formation. *Carbohydr. Polym.* **2012**, *87*, 512–517.

Liu, X.; Liu, G.; Zhao, H.; Zhang, Z.; Wei, Y.; Liu, M.; Wen, W.; Zhou, X. The quantitative monitoring of mechanochemical reaction between solid l-tartaric acid and sodium carbonate monohydrate by terahertz spectroscopy. *J. Phys. Chem. Solids* **2011**, *72*, 1245–1250.

Ma, X.; Yuan, W.; Bell, S. E. J.; James, S. L. Better understanding of mechanochemical reactions: Raman monitoring reveals surprisingly simple “pseudo-fluid” model for a ball milling reaction. *Chem. Commun.* **2014**, *50*, 1585–1587.

Martin, G.; Bellon, P. Driven alloys. *Solid State Phys.* 1997,50,189-331.

Maurice, D. R.; Courtney, T. H. The physics of mechanical alloying: A first report. *Metall. Trans. A* **1990**, *21*, 289–303.

Michalchuk, A. A. L.; Tumanov, I. A.; Drebushchak, V. A.; Boldyreva, E. V. Advances in elucidating mechanochemical complexities via implementation of a simple organic system. *Faraday Discuss.* **2014**, *170*, 311–335.

Mikhailenko, M. a.; Shakhtshneider, T. P.; Boldyrev, V. V. On the mechanism of mechanochemical synthesis of phthalylsulphthiazole. In *Journal of Materials Science*; **2004**; Vol. 39, pp. 5435–5439.

Perlovich, G. L.; Hansen, L. K.; Bauer-Brandl, A. The Polymorphism of Glycine. Thermochemical and structural aspects. *J. Therm. Anal. Calorim.* **2001**, *66*, 699–715.

Ramachandran, S.; Baradarajan, A.; Satyanarayana, M. Diffusion and reaction in solids. *Powder Technol.* **1983**, *34*, 143–149.

Rothenberg, G.; Downie, a. P.; Raston, C. L.; Scott, J. L. Understanding solid/solid organic reactions. *J. Am. Chem. Soc.* **2001**, *123*, 8701–8708.

Sasaki, H. Introduction of Particle-Size Distribution into Kinetics of Solid-State Reaction. *J. Am. Ceram. Soc.* **1964**, *47*, 512–516.

Schmidt, R.; Burmeister, C. F.; Baláž, M.; Kwade, A.; Stolle, A. Effect of Reaction Parameters on the Synthesis of 5-Arylidene Barbituric Acid Derivatives in Ball Mills. *Org. Process Res. Dev.* **2015**, *19*, 427–436.

Shahraki, M.; Habibi-Khorassani, S. M.; Dehdab, M. Effect of different substituents on the one-pot formation of 3,4,5-substituted furan-2(5H)-ones: a kinetics and mechanism study. *RSC Adv.* **2015**, *5*, 52508–52515.

Sorescu, M.; Xu, T. Particle size effects on the thermal behavior of hematite. *J. Therm. Anal. Calorim.* **2012**, *107*, 463–469.

Stearn, A. E.; Eyring, H. Absolute Rates of Solid Reactions: Diffusion. *J. Phys. Chem.* **1940**, *44*, 955–980.

Stolle, A. CHAPTER 10. Technical Implications of Organic Syntheses in Ball Mills. In *Ball Milling Towards Green Synthesis*; Stolle, A.; Ranu, B., Eds.; Royal Society of Chemistry: Cambridge, 2015; pp. 241–276.

Stolle, A.; Schmidt, R.; Jacob, K. Scale-up of organic reactions in ball mills: process intensification with regard to energy efficiency and economy of scale. *Faraday Discuss.* **2014**, *170*, 267–286.

Takacs, L. Mechanochemistry and the other branches of chemistry: Similarities and differences. *Acta Phys. Pol. A* **2012**, *121*, 711–714.

Takacs, L. What Is Unique About Mechanochemical Reactions? *Acta Phys. Pol. A* **2014**, *126*, 1040–1043.

Tokmakoff, A.; Fayer, M. D.; Dlott, D. D. Chemical reaction initiation and hot-spot formation in shocked energetic molecular materials. *J. Phys. Chem.* **1993**, *97*, 1901–1913.

Trotzki, R.; Hoffmann, M. M.; Ondruschka, B. The Knoevenagel condensation at room temperature. *Green Chem.* **2008**, *10*, 873–878.

Vyazovkin, S.; Wight, C. a. Kinetics in solids. *Annu. Rev. Phys. Chem.* **1997**, *48*, 125–149.

Vyazovkin, S. On the phenomenon of variable activation energy for condensed phase reactions. *New J. Chem.* **2000**, *24*, 913–917.

Weng, H.; Parrott, E. L. Solid-solid reaction between sulfacetamide and phthalic anhydride. *J. Pharm. Sci.* **1984**, *73*, 1059–1063.

Willart, J. F.; Descamps, M. Solid state amorphization of pharmaceuticals. *Mol. Pharm.* **2008**, *5*, 905–920.

Wynne-Jones, W. F. K.; Eyring, H. The Absolute Rate of Reactions in Condensed Phases. *J. Chem. Phys.* **1935**, *3*, 492-502.

Yukimitu, K.; Oliveira, R. C.; Araújo, E. B.; Moraes, J. C. S.; Avanci, L. H. DSC studies on crystallization mechanisms of tellurite glasses. *Thermochim. Acta* **2005**, *426*, 157–161.

Zelikman, A. N.; Voldman, G. M.; Beljajevskaja, L. V. Theory of hydrometallurgical processes. *Metallurgija, Moscow (in Russian)*, **1975**.

Zhurkov, S. N. Kinetic concept of the strength of solids. *Int. J. Fract.* **1984**, *26*, 295–307.





---

## **CHAPTER 5.**

**The application of mechanochemistry as  
a greener route for synthesis of  
pharmaceutically attractive molecules:  
hydrazones mechanosynthesis and their  
antituberculosis activity**

---



## 5.1 INTRODUCTION

This chapter explores the application of mechanochemical route to synthesize pharmaceutically interesting hydrazones. After the discussions in Chapter 3 and 4 about fundamental and processing understanding of mechanochemistry, it is now applied as a greener protocol for synthesis of potentially active molecules with excellent yields and time-reduced preparation. Firstly, phenolic hydrazones were successfully synthesized by the reaction of solid reactants, a phenolic aldehyde and a hydrazine. Some discussion is carried out about the reactivity of the solid hydrazines in terms of electronic, chemical reactivity, and the contribution of the solid form to increase or reduce the conversion ratio. The second series of hydrazones was prepared using exclusively the hydrazine isoniazid with aldehydes containing imidazole, indazole or indole structures. In this case, the use of *p*-toluene sulfonic acid (*p*-TSA) was necessary to reach complete conversions, allowing the time of reaction to be reduced to one or two hours, due to catalytic effects and to a melting when the three reagents (isoniazid + indole/indazole aldehyde + *p*-TSA) were mixed. The hydrazones are mostly present in DMSO solution as a mixture of conformers originated from amide bond rotation. DFT calculations, dynamic NMR studies as well as the simulated and experimental  $^1\text{H}$  and  $^{13}\text{C}$  NMR spectra were used For the case of isoniazid derivatives to identify and confirm the conformers. The hydrazones were subject of biological tests against *Mycobacterium tuberculosis* that revealed good to excellent activities for the molecules bearing the isoniazid moiety, compared to the isoniazid itself, a frontline drug. The stability in solution of the main compounds was evaluated and no hydrolysis was observed for a prolonged time in solution.

### 5.1.1 The pharmaceutical interest for mechanochemistry

In the pharmaceutical area, the milling devices have mostly been used to enhance some physical or physicochemical properties such as tableting and bioavailability by inducing phase transition between polymorphic forms as well as amorphization and also through molecular associations as the case of cocrystal formation and solid-dispersions (Frišćić, 2012; Delori et al., 2012). However, the use of mechanochemistry is not limited to supramolecular organizations and some examples can be found concerning the synthesis of drugs already known (Tan et al., 2014; Boldyrev, 2004) and others that are very important intermediates or

structures for medicinal chemistry such as nitrogen-containing molecules (Claramunt, et al., 2014).

The pharmaceutical researches are also concerned to *Green Chemistry* principles. It is the pharmaceutical industry that presents the highest values of waste generation (Sheldon, 2007). The high purity required for the active pharmaceutical ingredient (API) results in several steps of treatment such as separation and recrystallization and, large amounts of organic solvents are often needed. In this context the mechanochemistry can offer an alternative to thermal methods to synthesize APIs at least at the early stages of drug discovery, for example, for high-screening synthesis of target molecules to find the lead candidate.

Regarding drug discovery and development, the lead molecule comes from different trials, in which a plethora of candidates are previously prepared and tested. This requires a great effort from academic and industrial researchers that must be able to prepare, including synthesis and characterization, all those molecules in reasonable time and cost.

The advantages of mechanochemical routes for synthesis cover not only the waste reduction but, if well controlled, the mechanochemical preparation of molecules can lead to pure molecules also in terms of selectivity. In addition, concerning the capacity to produce sets of candidate molecules, the milling devices for laboratory scale are able to run until eight syntheses at once (the case of planetary ball mill PM 400 - Retsch).

### 5.1.2 Hydrazones

Hydrazones are a class of organic compounds that possesses the following structure:

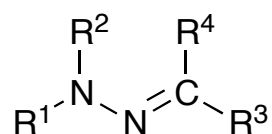


**Figure 5.1.** Hydrazone structure

They can be found in nature in plants, microorganisms and in marine organisms (Le Goff and Ouazzani, 2014). Natural and synthetic hydrazones have a wide array of biological activities such as for anticonvulsant, antidepressant, analgesic, anti-inflammatory, hypertension, antimicrobial, antitubercular, antiviral and antitumoral treatments (Rollas and Küçükgükel, 2007; Narang et al., 2012; Verma et al., 2014). In particular, acyl hydrazones with an azomethine proton –  $\text{NHN}=\text{CH}$  – represent relevant candidates for drug discovery,

and therefore, a number of hydrazones have been synthesized and biologically evaluated as target structures (Rollas and Küçükgükel, 2007).

The main procedure to synthesized hydrazones is the reaction between a hydrazine and a carbonyl compound such as aldehydes and ketones in alcoholic and/or acidic solutions as well as in toluene under reflux. The use of heat and diluted media generates some drawbacks, for example, separation, purification and, sometimes, lower yields due to chemical equilibrium establishment. Alternative synthetic protocols include solvent-free conditions using microwave irradiation yielding the hydrazones in short times with high yield, but sometimes the use of small amounts of solvent are required and the amount of reagents used are often around 0.5-5 mmols (Bandgar et al., 2011; Ješelnik et al., 2002; Li et al., 2006; Hajipour et al., 2009).

The mechanochemical route has also been utilized for hydrazone synthesis. For now, hydrazones and semicarbazone derivatives were prepared by Hajipour et al. (2009) from the corresponding hydrazine and semicarbazide with aldehydes or ketones. The procedure presented quantitative yields by milling in mortar with sodium hydroxide and silica gel as solid support that acts as facilitator. Kaupp et al. (2000) obtained benzoylhydrazone by milling a benzhydrazine with solid aldehyde or ketone. High yields at room temperature and in stoichiometric conditions were observed as well as spectroscopic purity. For the ketone, due to its low reactivity including the solid-state effects, the obtained yields were lower (around 75%). Similarly, the kneading method was able to produce phenylhydrazones in a melt system (Mokhtari et al., 2009). More recently, Nun et al. (2011) carried out the synthesis of hydrazones. A large variety of Boc- (*tert*-butyloxycarbonyl), Bz- (benzoyl), Ts- (tosyl) and Fmoc- (9-fluorenylmethyloxycarbonyl) protected hydrazines were milled with equimolar amount of carbonyl compound to produce the corresponding hydrazones in quantitative yields. They also reported the subsequent N-alkylation.

In this chapter the mechanochemical route was applied to hydrazones synthesis. The examples reported here originate from hydrazines structurally known for being biologically relevant, such as the case of isoniazid targeting *Mycobacterium tuberculosis* (*Mtb*), and therefore, the hydrazones were prepared with the intention to be tested concerning their therapeutic activity.

### 5.1.3 Targeting tuberculosis disease

Tuberculosis (TB) remains a major global health problem, responsible for ill health among millions of people each year. TB is a leading cause of worldwide mortality, ranking as the second cause of death due to a single infection agent worldwide, after the human immunodeficiency virus (HIV). The latest estimates included in the *Global tuberculosis report 2014* from the World Health Organization (WHO) are that there were 9.0 million new TB cases in 2013 and 1.5 million TB deaths. There is a correlation of the registered number of new cases of TB worldwide with economic conditions: over 95% of TB deaths occur in low- and middle-income countries. However, it has become an urgent health problem in the developed countries as well, due in part to HIV co-infection (WHO TB report 2014, Chin et al., 1996). Moreover, several issues can complicate the treatment of TB in patients with HIV: spectrum of replication states of *M. tuberculosis* bacilli (Johnson et al., 2009), pharmacokinetic drug–drug interactions, particularly with antiretroviral therapy (ART) drugs; and patient adherence given the lengthy treatment duration necessary to achieve non-relapsing cure. In HIV-infected individuals pharmacokinetic interactions with HIV drugs result in intolerance, loss of efficacy and toxicities.

Tuberculosis is caused by *Mycobacterium tuberculosis*, and current chemotherapeutic treatments are based on the use of antibiotics, the most important being isoniazid (INH), rifampicin, pyrazinamide, ethambutol and streptomycin. These were developed in the 1940s and 1950s, and all of these have since given rise to a drug-resistant clinical isolates when singly-administered during pharmacotherapy (Crofton, 1997). Despite the current global situation, anti-tubercular drugs have remained largely unchanged over the last four decades. The absence of concerted drug development has paradoxically paved the way for the introduction of fixed-dose combinations of two (isoniazid and rifampicin), three (isoniazid, rifampicin and pyrazinamide) and four (isoniazid, rifampicin, pyrazinamide and ethambutol) drugs (Lienhardt et al., 2011). The widespread use of these agents, and the time needed to remove infection, has promoted the emergence of resistant *Mycobacterium tuberculosis* strains.

The cell envelope of *Mycobacterium tuberculosis* (*Mtb*) consists of three structural components: the inner membrane, the cell wall, and a polysaccharide-rich capsule. The cell wall and outer capsule are unique and are tightly associated with its pathogenicity (Takayama et al., 2005; Brennan, 2003). Outside the membrane, *Mtb*'s peptidoglycan (PG) layer is covalently linked to arabinogalactan (AG), which is in turn attached to the mycolic acids. This

mycolate-arabinogalactan-peptidoglycan (mAGP) complex, a very hydrophobic barrier with very poor permeability, is critical to the survival of *M. tuberculosis* in macrophages and contributes significantly to the resistance against many chemotherapies (Brennan, 2003). Therefore, the enzyme involved in the bacterial fatty acid biosynthetic pathway are between the most attractive targets.

Mycolic acids are the major building blocks of the protective layer in the *Mtb* cell envelope. Mycolic acids are  $\beta$ -hydroxy fatty acids with a long  $\alpha$ -alkyl side chain (Asselineau and Lederer, 1950). There are five general forms of mycolic acids in *M. tuberculosis*:  $\alpha$ -mycolic acid, *cis*- / *trans*-methoxy mycolic acids, *cis*- / *trans*-ketomycolic acids (**Figure 5.2**). Among them, the  $\alpha$ -mycolic acid is the dominant species, accounting for more than 70 %, whereas other forms are less than 30% (Takayama et al., 2005).

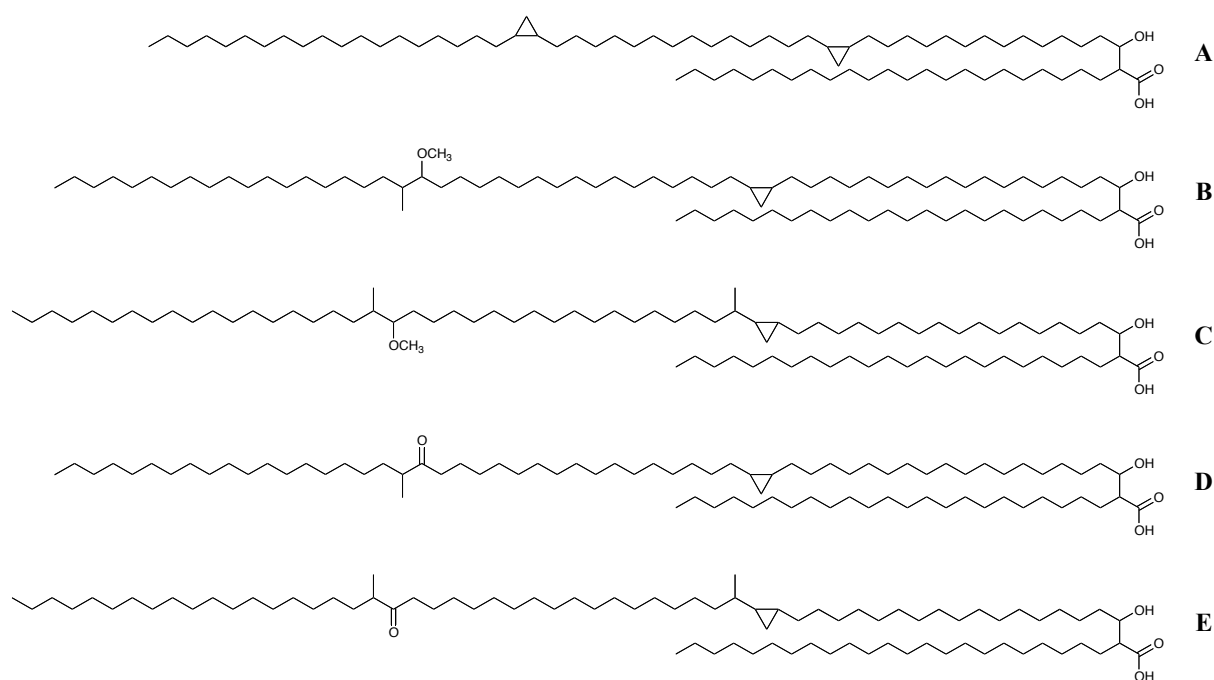


**Figure 5.2.** Structures of mycolic acids: A –  $\alpha$ -mycolic acid; B – *cis*-methoxy mycolic acid; C – *trans*-methoxy mycolic acid; D – *cis*-ketomycolic acid; E – *trans*-ketomycolic acid.

The synthesis of mycolic acid achieves by enzymes called fatty acid synthases (FAS). *M. tuberculosis* has both FAS-I and FAS-II systems. Its FAS-I, a multienzyme complex is in charge of synthesis of short chain fatty acids, and type II fatty acid synthetase (FAS-II), a discrete synthetase system continues to elongate the short chain fatty acids ( $C_{16}$ - to  $C_{18}$ -CoA products) to long chain fatty acids ( $C_{26}$  and  $C_{56}$ ) (Takayama et al., 2005) (**Figure 5.3**).



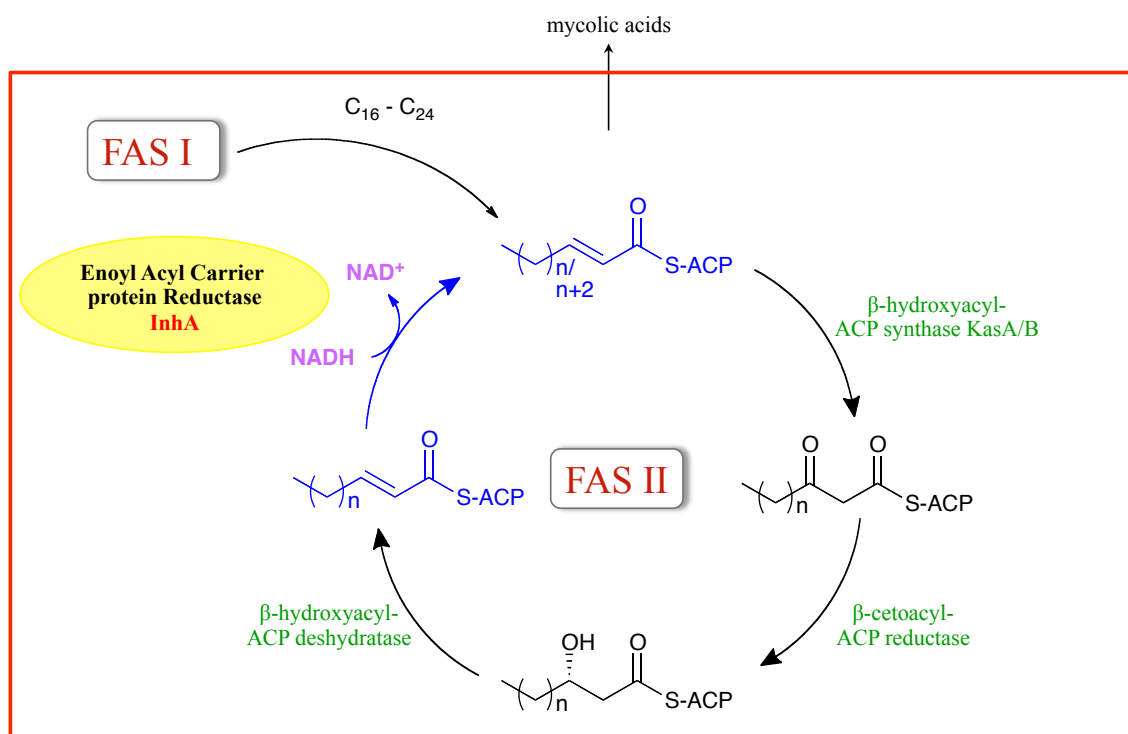


**Figure 5.3.** Synthesis of mycolic acids in *M. tuberculosis*.

Fatty acid biosynthesis in bacteria is catalyzed by a set of distinct, monofunctional enzymes collectively known as the type II FAS. It is important to note that mammals do not synthesize mycolic acids and thus the FAS-II pathway must play an essential role in mycobacteria (Pan and Tonge, 2012). This belief is supported by the knowledge that old and still effective frontline drugs isoniazid and ethionamide target InhA, the enoyl-ACP reductase in the *M. tuberculosis* FAS-II pathway (Banerjee et al., 1994; Dessen et al., 1995; Quémard et al., 1995; Rozwarski et al., 1998; Rawat and al., 2003).

The InhA protein (ENR, EC number: 1.3.1.9) is part of FAS-II and shows an NADH-dependent enoyl-ACP reductase activity. InhA that is an essential enzyme of *M. tuberculosis* specifically catalyzes the reduction of the double bond of the ethylenic thioester substrate (**Figure 5.4**) (Quémard et al., 1995).

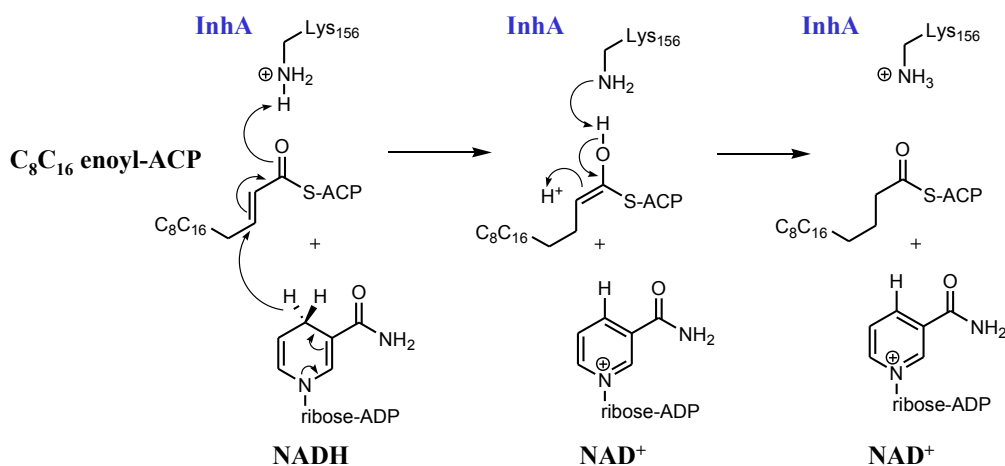


**Figure 5.4.** Substrate reduction mechanism catalyzed by NADH-dependent enoyl-ACP reductase (InhA).

### 5.1.3.1 Treatment and antituberculosis drugs

The treatment of tuberculosis must act against the extra and intracellular bacillus. Nowadays, it consists of an association of diverse antibiotics aiming to prevent any selection of the resistant strains. In general, the antibiotic treatments are effective and performed in two phases with the called first and second-line antibiotic drugs.

The first-line antituberculosis drugs (**Figure 5.5**) are considered the most active and currently encompass the isoniazid (INH), rifampicin (RIF), pyrazinamide (PZA) and ethambutol (EMB) that are administered daily or three times per week. The RIF and PZA drugs reduced the treatment from 12-18 to 6-9 months. Recently, bedaquiline, a new drug was approved to fight *Mtb* in the front-line treatment (Andries et al., 2005; Palomino and Martin, 2013).

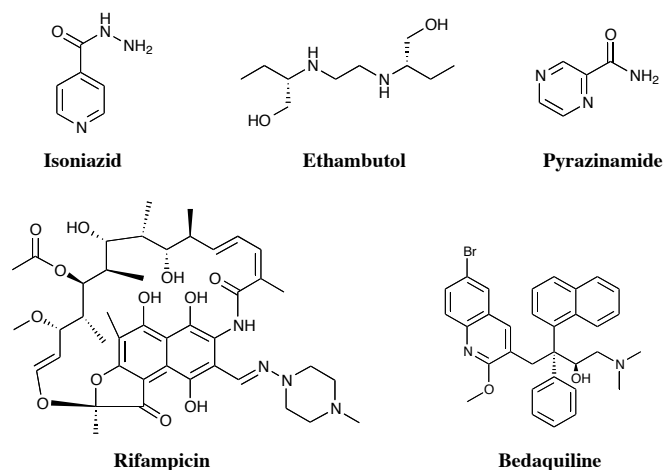


**Figure 5.5.** First-line antitubercular drugs structures.

One can mention some of the second-line antibiotic drugs, which are associated in the treatment together with those of first-line. Amikacin, capreomycin, streptomycin, kanamycin, *D*-cycloserine, ethionamide (ETH), *p*-aminosalicylic acid (PSA) and levofloxacin are some examples (**Figure 5.6**). These antituberculosis drugs may present side effects, making the treatment very difficult.

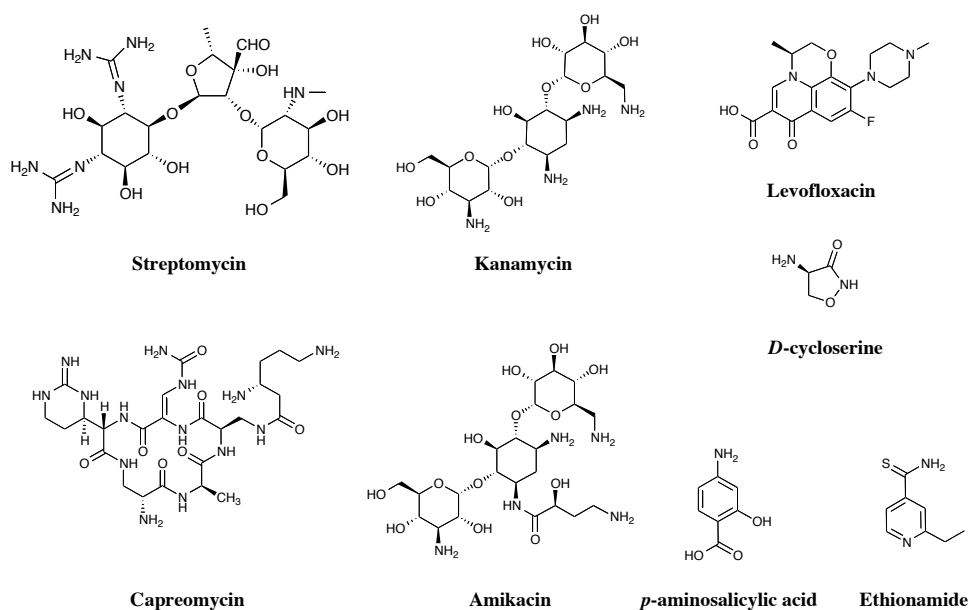


**Figure 5.6.** Second-line antitubercular drug structures.

As mentioned before, these second-line drugs are used to treat the infections caused by strains that resist to the first-line antibiotics.

### 5.1.3.2 Antituberculosis drugs targeting the cell wall biosynthesis – Isoniazid (INH)

Isoniazid has a minimum inhibitory concentration (MIC) ranging from 0.02 to 0.2  $\mu\text{g/mL}$  and, since its discovery, it has been the subject of numerous studies to determine its mechanism of action. Although it is not completely elucidated, it is widely accepted that INH acts mainly through a process involving two intracellular stages, each of them involving an enzyme of the *M. tuberculosis* (**Figure 5.7**):

- the first is an activation step (oxidation) of INH by the catalase-peroxidase *katG*, which has the primary function of cellular detoxification (e.g. resulting oxygen species) (Ghiladi et al., 2005);
- the second stage concerns the cell inhibition by interference of the active form of INH with the production of mycolic acids. One of the targets that would be preferred is the enoyl-ACP reductase (InhA) (Quemard et al., 1995).

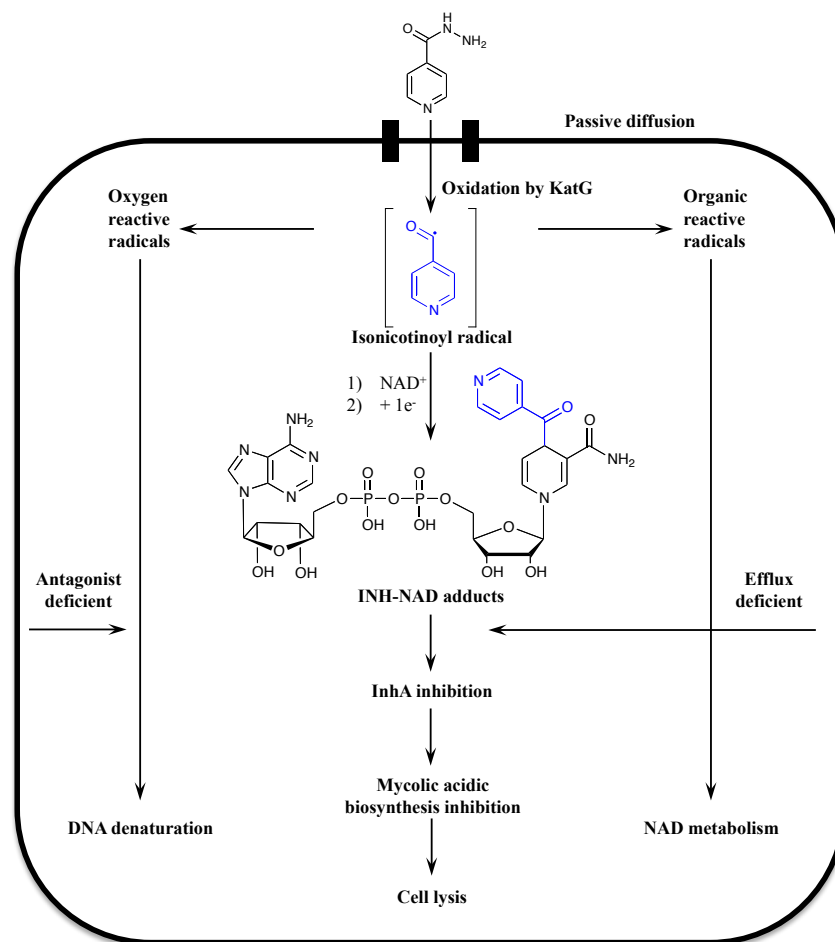


**Figure 5.7.** Mechanism of action of isoniazid (INH).

The mechanism of oxidation of INH by the enzyme *katG* gives activated species of the bioprecursor (most likely the isonicotinic acyl radical), which binds covalently to a form of NADH (oxidized form NAD<sup>+</sup> or a radical one NAD<sup>•</sup>). This yields the INH-NAD adducts (**Figure 5.7**) that are the potential inhibitors of the cell wall lipid and nucleic acid biosynthetic enzymes (Rozwarski et al., 1998; Rawat et al., 2003; Timmins and Deretic, 2006; Wiming and Johnsson, 1999). Bernadou and Meunier have also contributed to elucidate the mechanism of action of isoniazid (Nguyen et al., 2001; Stigliani et al., 2008).

#### 5.1.4 Hydrazine- Hydrazone derivatives targeting *M. tuberculosis*

Recent researches seek to find lead compounds to fight against the multi-drug resistant strains. Several groups have worked on the elaboration of hydrazine- hydrazones derivatives inspired- bearing antitubercular activities, and, frontline drugs such as isoniazid are commonly chosen as coupling partners to develop new derivatives. **Table 5.1** brings the some works dedicated to the synthesis and/or biological evaluation of new compounds designed to

act against *M. tuberculosis* and its drug resistant strains. In this instance, Maccari et al. (2002, 2005) reported the synthesis and biological activities of isoniazid-related hydrazones, hydrazides and cyanoboranes, among them, some with similar or better efficiency as the INH. Kumar et al. (2014), Sriram et al. (2005) and Coelho et al. (2012) have also carried out the synthesis and evaluation of isonicotinoyl hydrazone derivatives with prominent biological results. In this same sense, Baltas and co-workers reported the synthesis of cinnamic derivatives, strategically designed, within their research program on the topics of tuberculosis. Among the new compounds, cinnamic acids were coupled with isoniazid to afford the respective (*E*)-*N'*-[3-(4-alkoxyphenyl) propenoyl] isonicotinohydrazide derivatives (**Table 5.1, entry L**) in good yields (61-81%). Excellent values of MIC were obtained, specially, for the methyl-substituent (**Table 5.1, entry L, R=CH<sub>3</sub>**) (De et al., 2011). Nevertheless, it must be pointed out that most of the compounds evaluated containing all these types of frames, possess to the best the same antitubercular activity as the first line isoniazid, and in most cases the biological target, if not InhA, is not determined.

Differently from isonicotinoyl derivatives, Vavříková et al. (2011) prepared fluorine-containing hydrazones by coupling ethyl benzoylhydrazonoformate with ciprofloxacin (CPX), an antibiotic drug. In addition, the evaluating against multi-drug resistant tuberculosis showed that the hydrazones were more active than the CPX itself, and that they were also active against two strains of *M. kansasii*, while the MIC of ethambutol (3.12 µg/mL) and rifampicin (2.0 µg/mL) was comparable to those of three 7-chloro-4-quinolinylhydrazones (2.5 µg/mL) obtained by Candéa et al. (2009).

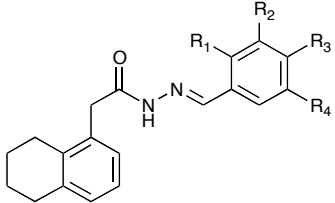
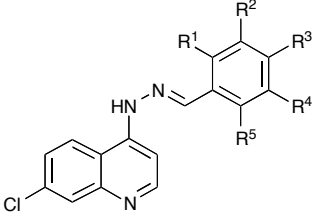
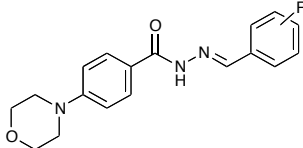
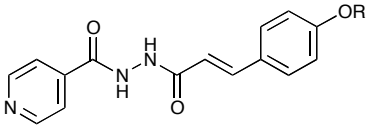
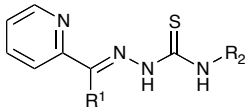
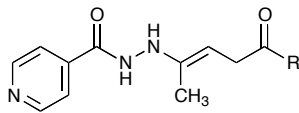
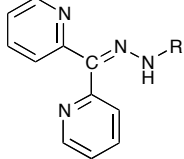
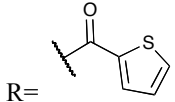
The recent synthesis of N-acylhydrazones containing a thiophene nucleus can also be mentioned (Cardoso et al., 2014). These authors studied the anti tuberculosis activity and also investigated the existence of conformers as for the parent acylhydrazones.

Concerning the hydrazine- hydrazones as antitubercular agents showed in **Table 5.1**, other examples are the elaboration of sulfonyl-hydrazones as potent inhibitors of the *M. tuberculosis* protein tyrosine phosphatase B (Oliveira et al., 2011), L-proline based hydrazones tested against *M. smegmatis* (Reddy et al., 2014), the syntheses of the thiosemicarbazones, semicarbazones, dithiocarbazates and hydrazide/hydrazones developed by Pavan et al. (2010) and morpholin-based benzohydrazides that reduced the *H<sub>37Rv</sub>* by up to 97 % with doses of 0.05 µg/mL (Raparti et al., 2009). Özdemir et al. (2010) synthesized tetrahydronaphtalen acetic acid benzylidene hydrazides but the biological results demonstrated low activity of the molecules, excepted for one hydroxy- and nitro-substituted hydrazone.

**Table 5.1.** Reported examples of relevant biologically active hydrazones/hydrazides against *M. tuberculosis*.

Entry	Structure	Most relevant compounds	Biological activity	Ref
<b>Isonicotinoyl hydrazones</b>				
<i>H<sub>37</sub>Rv</i> MIC				
A		R= 2-OEt	0.59 μM	Kumar et al., 2014
		R= 2-F	0.65 μM	
B		R=	0.56 μM	Sriram et al., 2005
C		R= H, R'= CF <sub>3</sub>	0.05 μg/mL	Maccari et al., 2002, 2005
		R= H, R'= CH <sub>3</sub>	0.025 μg/mL	
		R= CH <sub>3</sub> , R'= CF <sub>3</sub>	0.05 μg/mL	
		R= H, R'= 4-CF <sub>3</sub> -Ph	0.05 μg/mL	
		R= H, R'= 2-F-Ph	0.05 μg/mL	
D		R= 2-OMe	RG500 <sup>a</sup> MIC	Coelho et al., 2012
			0.98 μM	
<b>Thiophene-containing N-acylhydrazones</b>				
<i>H<sub>37</sub>Rv</i> MIC				
E		Aryl= 5-NO <sub>2</sub> -furan-2-yl	9.0 μM	Cardoso et al., 2014
		Aryl= 5-NO <sub>2</sub> -thien-2-yl	8.5 μM	
<b>L-proline derived hydrazones</b>				
IC <sub>50</sub> <sup>b</sup>				
F		R <sub>1</sub> =OMe, R <sub>2</sub> = H, R <sub>3</sub> = Ph	527 μg/mL	Reddy et al., 2014
<b>Fluorine-containing hydrazones</b>				
<i>H<sub>37</sub>Rv</i> MIC				
G		R =4-CF <sub>3</sub>	1.83 μM	Vavříková et al., 2011
		R =3-CF <sub>3</sub>	3.67 μM	
		R =4-F	2.02 μM	
<b>Sulfonyl-hydrazones</b>				
PtpB IC <sub>50</sub> <sup>c</sup>				
H		R'=H, R''=NO <sub>2</sub>	41 μM	Oliveira et al., 2011
		R'=CH <sub>3</sub> , R''=H	18 μM	
		R'=CH <sub>3</sub> , R''=4-Cl	21 μM	
		R'=CH <sub>3</sub> , R''=4-Br	39 μM	

Table 5.1. cont.

Tetrahydronaphthalen acetic acid benzylidene hydrazone		$H_{37}Rv$ IC <sub>50</sub>
I		$R_1 = R_2 = H, R_3 = OH, R_4 = NO_2$ 3.072 $\mu\text{g/mL}$
Özdemir et al., 2010		
7-chloro-4-quinolinylhydrazones		$H_{37}Rv$ MIC
J		$R^3 = Br, R^1 = R^2 = R^4 = R^5 = H$ 2.50 $\mu\text{g/mL}$
Candéa et al., 2009		
		$R^3 = OMe, R^1 = R^2 = R^4 = R^5 = H$ 2.50 $\mu\text{g/mL}$
4-(morpholin-4-yl)-N'-(arylidene)benzohydrazides		$H_{37}Rv$ % RLU <sup>d</sup> (0.05 $\mu\text{g/mL}$ )
K		$R = 4\text{-Cl}$ 78.09 %
Raparti et al., 2009		
		$R = 4\text{-F}$ 96.78 %
4-alkoxycinnamic hydrazides		$H_{37}Rv$ MIC
L		$R = CH_3$ 0.3 $\mu\text{M}$ $R = CF_3$ 1.1 $\mu\text{M}$ $R = \text{ethyl}$ 1.3 $\mu\text{M}$ $R = CH_2CF_3$ 2.2 $\mu\text{M}$ $R = \text{isopentenyl}$ 2.3 $\mu\text{M}$ $R = \text{geranyl}$ 1.9 $\mu\text{M}$
De et al., 2011		
Thiosemicarbazones		$H_{37}Rv$ MIC
M		$R^1 = CH_3, R^2 = \text{ethyl}$ 14.08 $\mu\text{M}$ $R^1 = CH_3, R^2 = \text{cyclohexyl}$ 2.82 $\mu\text{M}$ $R^1 = \text{pyridyl}, R^2 = \text{Ph}$ 2.34 $\mu\text{M}$
Hydrazides		
N		$R = \text{Ph}$ 11.13 $\mu\text{M}$ $R = \text{Me}$ 28.51 $\mu\text{M}$
Pavan et al., 2010		
Hydrazones		
O		$R = \text{isonicotinoyl}$ 10.32 $\mu\text{M}$
		5.06 $\mu\text{M}$
<sup>a</sup> RG 500 (pan-susceptible resistant strain), <sup>b</sup> determined against <i>M. smegmatis</i> mc <sup>2</sup> 155 cells, <sup>c</sup> determined for a protein tyrosine phosphate from <i>M. tuberculosis</i> PtpB, <sup>d</sup> Percentage of reduction in relative light units (RLU) calculated using luciferase reporter phages (LRP).		

The biological results shown in **Table 5.1** are just an excerpt of the most relevant hydrazide and hydrazones synthesized among several that have been screened. Regardless of the different techniques to assess the biological activities and how the results are indicated (i.e., MIC, IC<sub>50</sub> or % of reduction,  $\mu\text{M}$  or  $\mu\text{g/mL}$ ) it is clear that the most prominent compounds have isonicotinoyl moiety.

## 5.2 EXPERIMENTAL SECTION

### 5.2.1 Chemistry

#### 5.2.1.1 Materials for synthesis

All the chemicals for used throughout this part were purchased in purity required for synthesis and used as received (Maybridge, TCI, Aldrich or Alfa Aesar, 97-99%).

#### 5.2.1.2 General procedure for phenolic hydrazones synthesis

The syntheses were carried out in a vibratory ball mill Pulverisette 0 (P0, Fritsch, Germany) equipped with a single stainless steel ball of 50 mm of diameter and 500 g, in a semi-spherical vessel of 9.5 cm of diameter. The plate vibrates with a frequency of 50 Hz and amplitude of 2.0 mm. A mixture of hydrazine (1 equivalent) and a phenolic aldehyde (1 equivalent), both solids, in a total amount of 2 g, was placed in the equipment at room temperature (25 – 28 °C) and the grinding was performed during times varying from 2 to 8 h. The transformations were followed by TLC. After the grinding time the powder was recovered to be analyzed without any purification, except when triethylamine was used with hydralazine hydrochloride. In this case, the powder was washed with water to eliminate the triethylamine salt, and then dried under vacuum. The system ball/powder/vessel never exceeded 32 °C.

#### 5.2.1.3 General procedure for isoniazid nitrogen-containing heterocycles derivatives

The second series is related to the hydrazones derived from isoniazid and indolic, indazolic or imidazolic aldehydes. A mixture the solid reactants, hydrazine isoniazid (1 equivalent), the aldehyde (1 equivalent) and the catalyst when necessary ( $\text{AlCl}_3$  or *p*-toluenesulfonic acid (*p*-TSA), 0.1-0.5 mol/mol) was placed in milling device and the reaction proceeded between 1h – 8 h, depending on the catalyst. The Cryomill (Restch) was used for the screening of catalysts (milling started at the room temperature) at 25 Hz during 1 h. After the choice of the



catalyst (*p*-TSA), all the reactions were carried out in the P0 in larger amounts of reactant powder (stoichiometric conditions for reactants totalizing 1 g + the amount of catalyst). The transformation was monitored by TLC. After the reaction time, the powder mixture was washed with a NaHCO<sub>3</sub> solution to eliminate the catalyst and the powder was dried under vacuum.

## 5.2.2 Biological assays

The biological tests concerning anti-TB activity were carried out at University of Pavia, by the team of Maria Rosalia Pasca (PhD), Department of Biology and Biotechnology “Lazzaro Spallanzani”.

### 5.2.2.1 Growth conditions of *M. tuberculosis* H<sub>37</sub>Rv

*M. tuberculosis* H<sub>37</sub>Rv strain was grown either in Middlebrook 7H9 broth (Difco) supplemented with 0.05% Tween 80, or on Middlebrook 7H11 agar (Difco) supplemented with 0.5% glycerol, both supplemented with 10% (vol/vol) OADC. All compounds were dissolved in dimethyl sulfoxide (DMSO). Mycobacterial cultures were usually grown at 37°C without shaking.

### 5.2.2.2 MIC determinations

A single colony of *M. tuberculosis* strain was used to inoculate complete Middlebrook 7H9. The cultures were incubated at 37°C until exponential growth phase (~10<sup>8</sup> CFU/mL) was reached, corresponding to an OD<sub>600nm</sub> ranging from 0.8 and 1.0. Cultures were diluted to the final concentration of about 10<sup>7</sup> CFU/mL; 1 µl of the diluted cultures was then streaked onto plates containing two-fold serial dilutions of appropriate compound. MIC values were scored as the lowest drug concentrations inhibiting bacterial growth. All assays were repeated three times.

### 5.2.2.3 *M. tuberculosis* clinical isolate and drug susceptibility testing

The *M. tuberculosis* MDR isolate was collected at the Sondalo Division of the Valtellina and Valchiavenna, Italy, hospital authority in the 2012. The clinical isolate was grown in BACTEC™ MGIT™ 960 and Lowenstein–Jensen slants. Drug susceptibility testing for all first-line antitubercular drugs was performed with the BACTEC™ MGIT™ 960 System (Becton-Dickinson Diagnostic Systems, Sparks, Maryland). MIC determination to second-line drugs was also performed by the MGIT™ 960 System.

#### 5.2.2.4 *InhA* expression and purification

The production and purification of the InhA-6xHis protein from a protease-deficient strain of *E. coli* BL21(DE3) transformed with the pHAT5/*inhA* plasmid were performed as followed. 1 mL of the bacteria was grown in 100 mL of LB medium containing ampicillin (100mg/mL) at 37°C. After 4 h, the solution was rediluted in 1 L of the same medium and re-grown at 37°C. When the proper concentration ( $OD_{595} = 0.6-0.8$ ) was reached, protein expression was induced for overnight incubation with 1 mM isopropyl-b-D-galactopyranoside (IPTG) at 20°C. Cells were harvested by centrifugation at 6,000 g for 30 min at 4°C. The dry pellet was kept at -80°C for several months. Thawed cells (1.5 g) were sonicated in 20 mL lysis buffer (300 mM NaCl, 10 mM imidazole, 50 mM sodium phosphate buffer, pH 8.0). After centrifugation at 10,000 g for 45 min at 4 °C, the supernatant was applied onto a nickel-chelated His-Trap HP 1 mL column (GE Healthcare) previously equilibrated with the binding buffer (50 mM NaCl, 10 mM imidazole, 50 mM sodium phosphate buffer, pH 8.0). First, the unbound proteins were washed out with 10 column volume of binding buffer, and then a higher imidazole concentration (25 mM) allows the elution of non-specifically bound proteins. The His<sub>6</sub>-tagged InhA protein was eluted with an imidazole gradient from 25 mM to 300 mM over a range of 20 column volume. Fractions containing the target protein were pooled, concentrated to 2.0 mL and loaded on a HiLoad 16/60 Superdex 200 column (GE Healthcare) equilibrated with 150 mM NaCl, 30 mM PIPES, pH 6.8. Samples were analyzed using SDS-PAGE and Coomassie blue staining and then stored at 4°C for short term storage or 80°C with 20% glycerin for long-term storage.

#### 5.2.2.5 *InhA* activity inhibition

Isoniazide and NADH were obtained from Sigma-Aldrich. Stock solutions of all compounds were prepared in DMSO such that the final concentration of this co-solvent was constant at 5% v/v in a final volume of 1 mL for all kinetic reactions. Kinetic assays were performed using *trans*-2-dodecenoyl-coenzyme A (DDCoA) and wild type InhA. The reactions were performed at 25°C in an aqueous buffer (30 mM PIPES and 150 mM NaCl pH 6.8) containing additionally 250 μM cofactor (NADH), 50 μM substrate (DDCoA) and the tested compound (at 50 μM or 10 μM). Reactions were initiated by addition of InhA (100 nM final) and NADH oxidation was followed at 340 nm. The inhibitory activity of each derivative was expressed as the percentage inhibition of InhA activity (initial velocity of the reaction) with respect to the control reaction without inhibitor. Triclosan was used as a positive control. All activity assays

were performed in triplicate. For the most potent compounds,  $IC_{50}$  values were determined using the 4-parameter curve-fitting software XLFit (IDBS) with at least six points.

## 5.3 RESULTS AND DISCUSSION

### 5.3.1 Mechanochemical synthesis of phenolic hydrazones<sup>9</sup>

As mentioned, the classical solvated methods to synthesize hydrazones are generally carried out at low concentration, and require times from 3 to 24 or even 48 hours in reflux of toluene or ethanol in order to obtain good yields. In this framework we employed the vibratory mill P0 to synthesize the hydrazones mechanochemically. Aiming to compare the respective reactivities of reactants under mechanochemical conditions, 24 examples of hydrazones were synthesized (**Table 5.2**), including some that were already described by the group using classical methods (Belkheri et al., 2010; Vanucci-Bacqué et al., 2014). **Figure 5.8** displays the general solid-state mechanochemical reaction between a hydrazine and an aldehyde to produce the respective hydrazones.

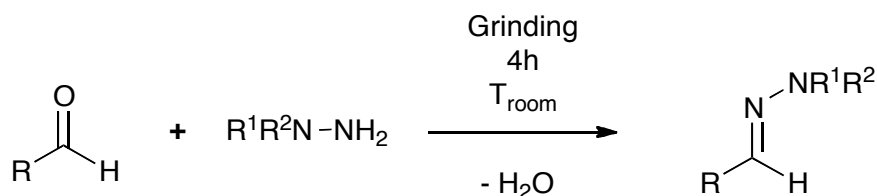


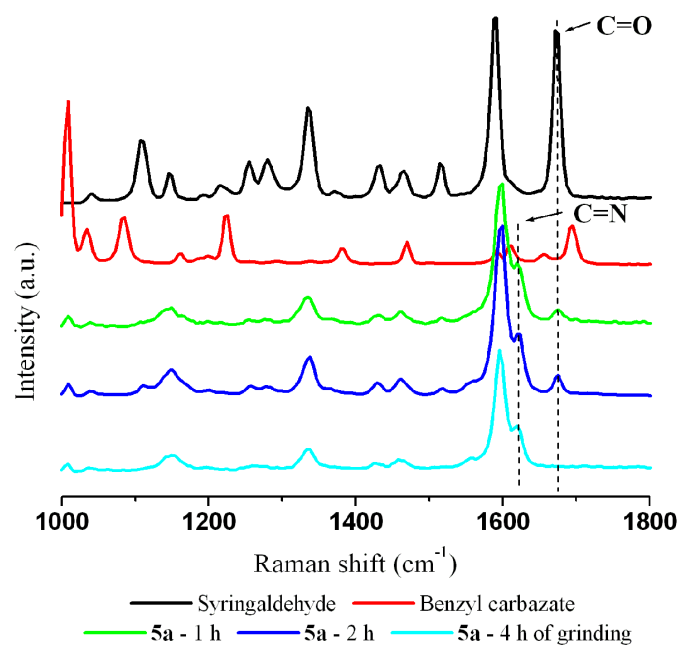
**Figure 5.8.** General synthesis of hydrazones in solid-state by co-grinding of a hydrazine and an aldehyde.

Once the objective was to investigate the production of hydrazones in solid-state, the mandatory conditions of choice of reagents was the melting point above the temperature of synthesis. As the reactions were carried out at room temperature all the reagents presented in **Table 5.2** fulfill the requirement. The syntheses with hydralazine hydrochloride were performed in the presence of 1 equivalent of triethylamine (TEA) in order to liberate the base from its respective salt. **Table 5.2** also summarizes the time of grinding and the conversion obtained by analysis of <sup>1</sup>H NMR spectra for each synthesis. TLC showed the consumption of the reagents and the consequent appearance of the hydrazone, which was confirmed by <sup>1</sup>H

<sup>9</sup> The entire section 5.3.1 was reproduced from Oliveira et al., *RSC Adv.*, **2014**, *4*, 56736-56742. Reproduced by permission of The Royal Society of Chemistry. Available in [dx.doi.org/10.1039/C4RA10489G](https://doi.org/10.1039/C4RA10489G).

and  $^{13}\text{C}$  NMR analysis demonstrating final conversions of up to 99% (and thus yields) depending on the aldehyde-hydrazine couple and no byproducts were detected. In addition, the progress of the reactions can be followed by Raman analysis. This technique could be a rapid way to monitor mechanochemical reactions without using solvents as reported elsewhere (Ma et al., 2014). For illustrative purposes, **Figure 5.9** displays the example of the reaction between syringaldehyde and benzyl carbazate, in which the peak of the C=O of the aldehyde at  $1671\text{ cm}^{-1}$  can be easily followed until disappearance, while at  $1623\text{ cm}^{-1}$  the imine bond C=N appears indicating the hydrazone formation.

The hydrazones listed in **Table 5.2** were obtained with a high transformation ratio in grinding times of 4h.  $^1\text{H}$  NMR spectra revealed conversions with respect to the aldehydes and hydrazines over 90% in almost all the explored syntheses and no byproducts were found. In **Table 5.2** we have also introduced conversions (if quantitative) and yields (where purification was needed) for a series of hydrazones obtained under classical conditions (1 mmol of each reagent/30ml of solvent under reflux for 6-24h) (Belkheri et al., 2010; Vanucci-Bacqué et al., 2014). For hydralazine hydrochloride reagent the classical reaction was performed in the absence of base (triethylamine) and the hydrazone hydrochloride was isolated.

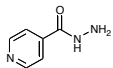
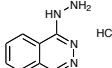
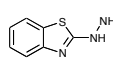
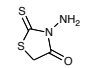
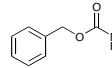
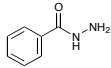
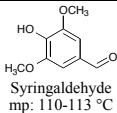
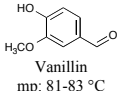
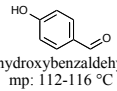
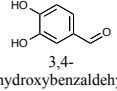


**Figure 5.9.** Raman spectra of hydrazone formation (**5a**) after 1, 2 and 4 hours of grinding.

The mechanochemical route, maybe due to its original mechanism and the intimate contact of the reactive species, seems to be more efficient when comparing the results with

the classical ones under reflux and heat. With regard to the couplings with isoniazid, hydrazones are obtained through analogous conversions and yields between the classical and mechanochemical method. The same is true for benzyl carbazate where the conversions and yields are almost quantitative in both cases. The hydrazones derivatives have shown some particularity related to conformational isomerism that it is discussed in the section 4.3.3. For the 2-hydrazinobenzothiazole, reactions appear better under classical conditions, while for hydralazine hydrochloride and 3-aminorhodanine the mechanochemical route appears much more optimal. It is worth pointing out that with regard to the hydrazones formation with 3-aminorhodanine, conversion and yields can be greatly improved in favor of the mechanochemical process but also by performing the later reaction for 8 h (tested as an example with this hydrazine); almost quantitative conversions and yields (no further purification needed) were obtained. This example is a clear illustration of the potential of mechanochemistry as a green route to synthesize potentially active pharmaceutical ingredients. The reactivity of the hydrazines observed by mechanochemical route could be explained as a result of electronic effects and the solid form influences.

**Table 5.2.** Solids aldehydes (column) and hydrazines (line) used for the synthesis of hydrazones and degree of conversion<sup>a</sup> for corresponding hydrazones for 4 hours of grinding as well as the yields<sup>b</sup> from classical method in parentheses.

		Hydrazines (R <sup>1</sup> R <sup>2</sup> N-NH <sub>2</sub> )						
		1	2	3	4	5	6	
								
		Isoniazid mp: 171-173 °C	Hydralazine hydrochloride <sup>c</sup> mp: 273 °C	2-hydrazinobenzothiazole mp: 198-202 °C	3-aminorhodanine mp: 100-103 °C	Benzyl carbazate mp: 65-68 °C	Benzhydrazine mp: 112-114 °C	
Aldehydes (RCHO)								
<b>a</b>		<b>1a</b> 90 % (97 %)	<b>2a</b> 99 % (75 %)	<b>3a</b> 92 % (97 %)	<b>4a</b> 88 % ≥ 99 % <sup>d</sup> (70 %)	<b>5a</b> ≥ 99 % (90 %)	<b>6a</b> ≥ 99 %	
	<b>b</b>		<b>1b</b> 90 % (90 %)	<b>2b</b> 99 % (90 %)	<b>3b</b> 94 % (99 %)	<b>4b</b> 84 % ≥ 99 % <sup>d</sup> (37 %)	<b>5b</b> ≥ 99 % (99 %)	<b>6b</b> ≥ 99 %
	<b>c</b>		<b>1c</b> 95 %	<b>2c</b> 99 %	<b>3c</b> 95 %	<b>4c</b> 93 % ≥ 99 % <sup>d</sup>	<b>5c</b> ≥ 99 %	<b>6c</b> ≥ 99 %
	<b>d</b>		<b>1d</b> 88 % (81 %)	<b>2d</b> 99 % (81 %)	<b>3d</b> 98 % (74 %)	<b>4d</b> 86 % ≥ 99 % <sup>d</sup>	<b>5d</b> ≥ 99 % (99 %)	<b>6d</b> ≥ 99 %

<sup>a</sup>Determined by <sup>1</sup>H NMR. In reactions where <sup>1</sup>H NMR indicated a conversion lower than quantitative, the degree of conversion was calculated from the corresponding NMR intensities of the product and the unreacted aldehyde or hydrazine.

<sup>b</sup>Yields obtained by the classical method with 1mmol/30 mL under reflux in times from 8 to 24 h (See Ref. 38 and 46).

<sup>c</sup>These syntheses with hydralazine hydrochloride were performed in presence of 1 equivalent of triethylamine (TEA) and the hydrazone was obtained after washing with water to eliminate the TEA salt. <sup>d</sup>Conversion after 8 hours of grinding.

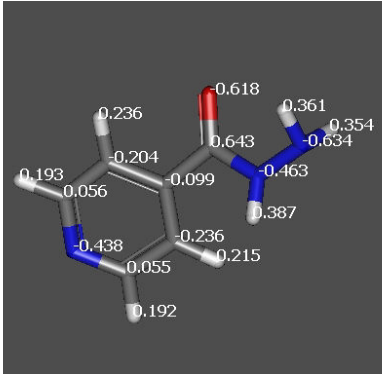
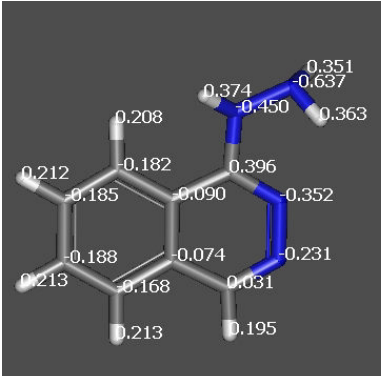
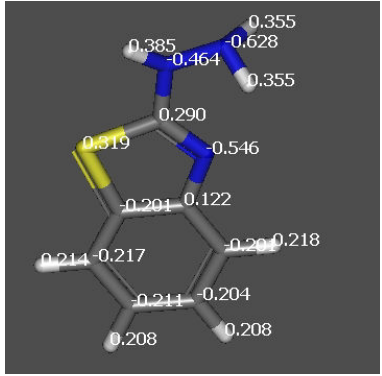
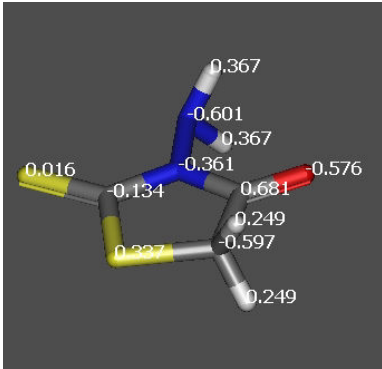
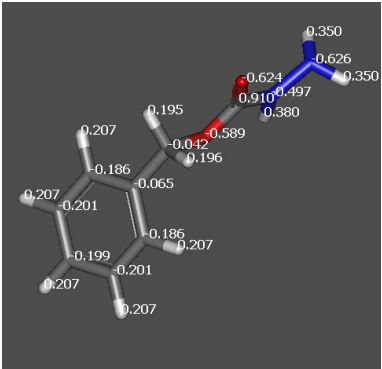
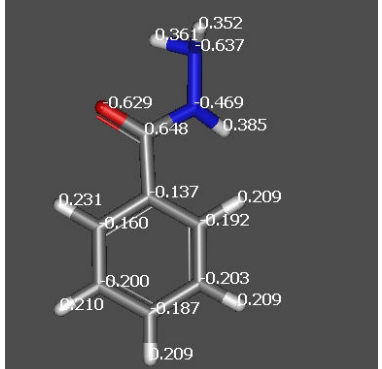
### 5.3.1.1 Electronic effects

Substitution patterns on hydrazines ( $R^1$ ,  $R^2$ ) may influence the electronic effects and distribution at the terminal  $NH_2$  functionality thus modifying its reactivity. In order to get an insight into the reactivity of the different hydrazines the electronic density was evaluated. **Table 5.3** shows the results of natural bond orbital (NBO) (Reed, et al., 1988) analysis to access the partial atomic charges of the hydrazines, which was performed in the B3LYP/6-311+G(d,p) (Becke, 1993; Lee et al., 1988) level of theory for the structures of hydrazines obtained by density functional theory (DFT) calculated with Gaussian 09 software. In a preliminary approach, these simulations were used to attribute values to the pure chemical reactivity, making the following comparison possible: the more negative the charge, the more nucleophilic or basic the atom. The charge density on the reactive part of the aldehydes used was also determined. The values obtained under the same level of theory do not indicate any strong preference in favor of one of them (all values are between 0.0413 and 0.0414). We can thus assume that the conversion/yields of the hydrazones obtained under classical conditions reflect the  $NH_2$  reactivity.

The most striking difference is observed for 3-aminorhodanine where the charge density on the terminal  $NH_2$  group of the hydrazine appears much less than for all other compounds. It is reasonable to assume in this case that this effect might explain the lack of reactivity and the low yields specially obtained under classical conditions (70% and 37%). The effect is more pronounced in solution than under mechanochemical conditions, where total conversion could be achieved after a more prolonged time. For the other hydrazines used, the charge density differences are small, in accordance with analogous yields obtained under solution conditions.

Despite the fact that the calculations of partial atomic charges represent a great panoramic for the prevision of the nucleophile sites for the explored cases herein, the hydrazines do not follow the expected results in some cases, when mechanochemical conditions are used. This is specially the case for isoniazid that should be the one with highest conversions comparable to those of benzhydrazide, and benzyl carbazate, which in turn showed to be the more reactive. Based on this outlook, it is believed that these solid-state mechanosynthesis are not only guided by electronic aspects but for the solid characteristics such as the crystal packing, the solid form, the density, and finally, in summary, the accessibility of reactive sites in organic solids

**Table 5.3.** Minimum geometry (B3LYP/6-311+G(d,p)) and charge density of the  $-NH_2$  group (NBO<sup>a</sup>, in brackets) of hydrazines

Isoniazid (-0.634)	Hydralazine <sup>b</sup> (-0.637)	2-hydrazinobenzothiazole (-0.628)
		
3-aminorhodanine (-0.601)	Benzyl carbazate (-0.626)	Benzhydrazide (-0.637)
		

<sup>a</sup>Natural bond orbital (NBO) analysis performed in the B3LYP/6-311+G(d,p) level of theory for the structures of hydrazines obtained by density functional theory (DFT) calculated with Gaussian 09 software. <sup>b</sup>NBO was performed for hydralazine base.

### 5.3.1.2 The solid-state role

The mechanisms of solid-state transformations during grinding were generally attributed to a formation of eutectic melts (Rothenberg et al., 2001), molecular transport through surfaces due to sublimation (Mikhailenko et al., 2004; Kuroda et al., 2004) or in the bulk of material (Kaupp et al., 2001; Kaupp, 2003) and to a reaction mediated by amorphous or metastable crystalline phases (Jayasankar et al., 2006; Descamps et al., 2007). This part is focused in the nature of raw materials that could facilitate the reaction or make it harder. In solid crystals, molecules are not free as in gas or in solution, but trapped in the lattice trying to form the most stable arrangement. All the other surrounding molecules interact mainly by van der Waals' forces and/or H-bonding, which govern the crystal packing. In this section some

properties of the solid hydrazines were used to discuss the role of the solid-state in the conversion and reactivity. Crystal properties of some hydrazines, such as crystallographic data, the intermolecular interactions resumed here by hydrogen bonds and the absolute density, were employed to postulate a balance between the electronic properties, previously discussed and the steric effects originated from the solid form. Melting points and heat of fusion ( $\Delta H_{fus}$ ) were also evaluated in order to find some relation with the reactivity of the reactant solids.

First, the thermal behavior of the starting hydrazines was investigated aiming to reveal some relation with the reactivity of the solids. It means, lower melting points associated to lower enthalpy of fusion would lead to higher conversion due to a fluid phase locally formed upon application of mechanical energy. However, DSC measurements were performed, but the melting point and the molar  $\Delta H_{fus}$  obtained for the reactants do not explain their reactivity in this study (see **Table 5.4**). As example, 3-aminorhodanine has the lower  $\Delta H_{fus}$  and the second lower melting point in the series, which suggests it could melt easily during grinding and increase the reaction rate. However, 3-aminorhodanine still remains the less reactive.

Intermolecular hydrogen bondings are responsible for the stabilization of the crystal structure. Therefore, in order to perform a reaction in solid state it is necessary to dissociate the H-bonding, and, consequently, the stronger the H-bonds, the higher the energy required to dissociate them. As an approximation, FTIR spectrometry was used to investigate the hydrogen bond strength of the starting hydrazines both by dilution method and temperature variation in the solid state. The stretching vibrations associated with the  $\text{NH}_2$  group of hydrazines were studied depending on the concentration ( $A = f(\text{concentration})$  in solution) or  $\nu = f(\text{temperature in solid state})$ , but the results were generally inconclusive, except for 3-aminorhodanine (the lowest reactive hydrazine by mechanical route). For this hydrazine, in accordance with literature data (Jabeen et al., 2010), the  $\nu_s(\text{NH}_2)$  and  $\nu_{as}(\text{NH}_2)$  modes were observed at 3295 and 3325  $\text{cm}^{-1}$  in the IR spectrum, respectively. Two additional bands were present at 3149 and 3233  $\text{cm}^{-1}$ , which have been assigned to combination band of the CO stretching and  $\text{NH}_2$  bending modes and an overtone of the 1536  $\text{cm}^{-1}$  band, respectively (Miyazawa, 1960). In addition, a linear variation of the wavenumber at  $\nu$  3149 was observed as the temperature increased (from 25 to 85°C), demonstrating for this hydrazine the existence of intermolecular interactions in the solid that varies when energy is applied (Figure 1S, Appendix III). On the other hand, the calculated FTIR spectra (in the gas phase at 298° K) do not reveal any intramolecular H-bonds (Table 1S, Appendix III). Some data from literature also support this discussion. Recent studies have shown that the crystal packing of 3-



aminorhodanine is governed by H bonding (Jabeen et al., 2009). The molecules are linked by N—H...O, N—H...N and N—H...S hydrogen bonds, forming a three-dimensional network that probably reduces the nitrogen reactivity. Similarly, a recent investigation of the crystal structure of isoniazid showed that predominantly C-H...N, C-H...O and N-H...N types of intermolecular hydrogen-bonding interactions are responsible for the molecular packing of the crystal (Rajalaksmi et al., 2014). These interactions form an infinite spiral type structure in the crystal (Jensen, 1954). Molecules also form  $\pi$ — $\pi$  interactions in the crystal at a distance of 3.760 Å. These intermolecular hydrogen-bonds, not always present in the benzhydrazide, could help explain the lower reactivity of isoniazid than expected and reducing still more that of 3-aminorhodanine. The crystal arrangements of the other hydrazines are probably guided by hydrogen bonds as well, but no study is described in the literature.

In addition to the hydrogen bonding and stacking, the proximity of the molecules must also influence the accessibility of the reactive nitrogen. The density of the hydrazines was used as a first approach to represent the proximity of the molecules. The values of density were obtained with a helium pycnometer through the real volume, which does not take the empty spaces into consideration, and are given in **Table 5.4** in  $\text{g cm}^{-3}$ .

**Table 5.4.** Absolute density ( $\text{g cm}^{-3}$ ) of the solid hydrazines

Hydrazines	mp (°C)	$\Delta H_{fus}$ (kJ/mol)	$\rho$ ( $\text{g cm}^{-3}$ )
Isoniazid	170.9	31.86	1.4318
Hydralazine hydrochloride	273 (dec.)	-	1.4799
2-hydrazinobenzothiazole	198.6	29.86	1.4525
3-aminorhodanine	98.3	19.04	1.6603
Benzyl carbazate	67.8	21.64	1.2559
Benzhydrazide	112.7	24.97	1.3006

The density of benzyl carbazate is the smallest at  $1.2559 \text{ g cm}^{-3}$ , followed by benzhydrazide, isoniazid, 2-hydrazinobenzothiazole, hydralazine and 3-aminorhodanine with  $1.6603 \text{ g cm}^{-3}$ . Intuitively, a small density could express farther molecules and more freedom to move. Seen in this way, 3-aminorhodanine has the tighter form and the benzyl carbazate the looser one, with its reactivity in solid state affected by this factor. For the 3-aminorhodanine, the higher density further hampers the access to the reaction site. Isoniazid also has a higher density than the benzyl carbazate and benzhydrazide and is less available in

the lattice to react. In the same way that in density charge calculations, hydrazinobenzothiazole occupies a midterm in the series of density and the same is found for the conversions always at about 95%.

One can discuss the influence of the mobility of the reactive site of the hydrazine. The chain bearing the reactive  $\text{-NH}_2$  can move more readily as the chain is longer, which most likely facilitates its accessibility toward the carbonyl group of the aldehyde. For example, benzyl carbazate presents the longer one and complementary experiments, not presented in the **Table 5.2**, for the synthesis of **5a** showed conversions around 88%, 95% for 1 and 2h grinding, respectively, confirming the ability of benzyl carbazate to react quickly under these conditions. The Raman spectra of these runs and the starting materials in solid state were already present in **Figure 5.9**. The presence of hydrazone bond  $\text{C}=\text{N}$  at  $1600\text{ cm}^{-1}$  and a notable decrease of  $\text{C}=\text{O}$  at  $1670\text{ cm}^{-1}$  of the aldehyde when compared with the syringaldehyde shows that after only one hour the major part is the product. On the contrary, the partial intracyclic inclusion of the hydrazino group of 3-aminorhodanine acts by reducing the freedom of the reactive site of the hydrazine and the grinding time is extended to 8h to attain transformations of around 99%.

Finally, **Figure 5.10** summarizes the importance of different characteristics of hydrazines acting potentially in these solid-state mechanosyntheses of hydrazones.

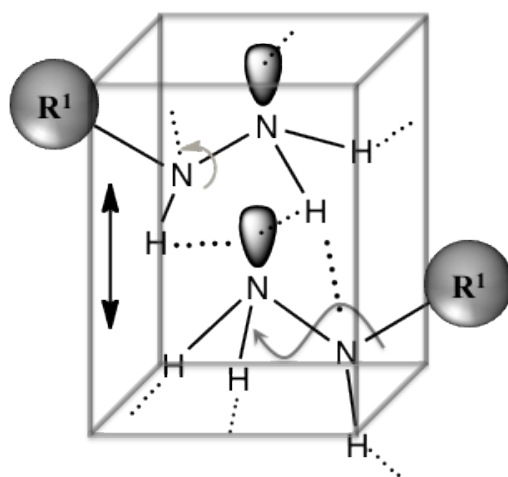


**Figure 5.10.** The electronic and solid-state balance in reactivity of hydrazines. Orbitals are represented only for  $\text{-NH}_2$ , hydrogen bonds are represented by dotted lines, density by vertical arrows and degree of freedom by curved arrows (from Oliveira et al., 2014. Reproduced by permission of The Royal Society of Chemistry).

Other papers have discussed the electronic effects and the crystal packing for solid-state reactivity. It was observed that the products and kinetics are guided by the crystal packing (subject of topochemistry) (Singh et al., 1994). Through detailed studies and computer calculations, Gavezzotti had already concluded that a prerequisite for crystal reactivity is the availability of free space around the reaction site (Gavezzotti, 1983, 1987). Years later, Sarma *et al.* (2000) discussed the role of free volume of some aldehydes for solid-state bromination and found differences in selectivity from solution. More recently, it has been demonstrated that the amount and form of energy and how the mechanical energy is applied concerning the mechanochemical systems, strongly influence the products and kinetics (McKissic et al., 2014; Michalchuk et al., 2013; Tumanov et al., 2011). The difference in selectivity of the products from solution and solid syntheses has shown that mechanical energy is capable of surpassing some classical rules in chemistry leading to the comprehension of the same molecule in its different states of aggregation and under different perturbations (Collom et al., 2013; Konda et al., 2013; Hickenboth et al., 2007; Haruta et al., 2013). With regard to the synthesis of hydrazones the results point to a balance between the electronic contributions (orbitals), the strength of hydrogen bonds (dotted lines), the proximity of the molecules, expressed by absolute density (vertical arrow) and the degree of freedom or movement (curved arrows) as suggested in Figure 2. What is not mentioned is that the mechanical energy can essentially favor the reaction by breaking and destabilizing the solid, which increases Gibbs free enthalpy (Descamps et al., 2007) and by activating on a macro and molecular level.

### 5.3.2 Mechanochemistry of isoniazid hydrazone derivatives

The prominent results obtained for the hydrazones in the previous section prepared with phenolic aldehydes in terms of good to excellent conversion ratios and time of reaction, constituting an example of greener protocol, induced further syntheses of this class. A new series of hydrazones derived from isoniazid as hydrazine and various heterocyclic indole-, indazole or imidazole-containing the aldehyde function C=O was prepared. **Figure 5.11** shows the structures of the non-substituted rings of indole, indazole and imidazole.

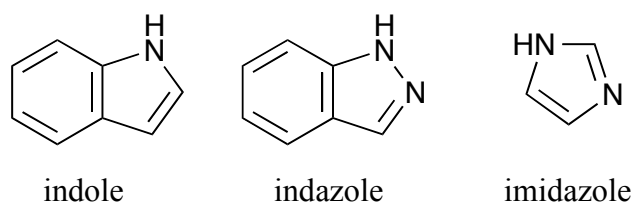


**Figure 5.11.** Indole, indazole and imidazole ring structures.

The isoniazid was kept for this series of molecules due to the noticeable biological results obtained for the phenolic hydrazones, which are presented in the section 5.3.4. Similarly, indolic, indazolic and imidazolic aldehydes were chosen because their derivatives are also of pharmaceutical relevance. These nitrogen-containing heterocycles are very important in organic chemistry and are found in large number of natural or synthetic biological active molecules. Indeed, some of these are active pharmaceutical ingredients exhibiting antibacterial, anticancer, antioxidants, anti-inflammatory, antidiabetic, antiviral, antiproliferative, antituberculosis, antispermatogenic, antipsychotic activity (Shalini et al., 2010; Verma et al., 2013; Thangadurai et al., 2012; De Luca, 2006; Sharma et al., 2010).

Contrary to the mechanosynthesis of phenolic hydrazones, the procedure adopted to synthesize the isoniazid derivatives showed to be more complicated. Firstly, the same protocol described for phenolic compounds was used with the 4-methylimidazolecarboxaldehyde as model of heterocyclic aldehyde. It means that the reactive powders (isoniazid + aldehyde) were placed in the bowl of P0 at 25 °C and the milling carried out by up to eight hours and the transformation was qualitatively followed by TLC. However, TLC and NMR showed incomplete conversion of the reactants, probably due to the lower reactivity of this aldehyde in comparison with the phenolic ones used before for the first series. For this reason, the use of substances with catalytic effects was evaluated in order to increase the conversion ratio and reduce the time of grinding. The green chemistry principles also approaches the catalysts as a solution for selectivity and time- energy saving. For this purpose, the reactions were performed with  $\text{AlCl}_3$  and the *p*-toluenesulfonic acid (*p*-TSA) in 0.3 mol/mol. In this case, another milling device, Cryomill (Retsch), was employed but at room temperature. It can hold up to four vials of 5 mL running in parallel, and thus, a fast screening of catalysts. The screening was again performed with 4-imidazolecarboxaldehyde and the *p*-TSA showed to be the better candidate. Then, the same procedure was followed for that imidazole and other nine aldehydes in the P0 to give ten hydrazones derived from isoniazid (**Table 5.5, 7a-j**) in 1 – 2 h, adjusting the amount of *p*-TSA to 0.5 mol/mol for

further enhancement of conversions. **Figure 5.12** shows the general scheme for isoniazid derivatives synthesis

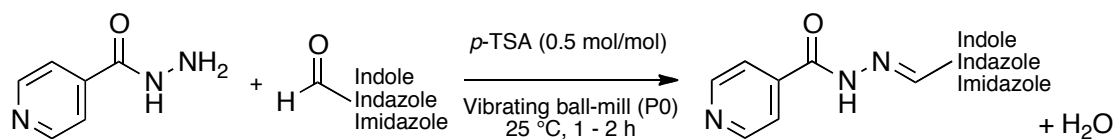


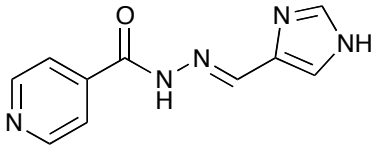
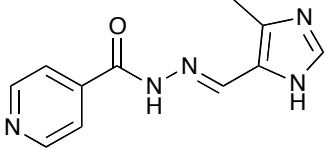
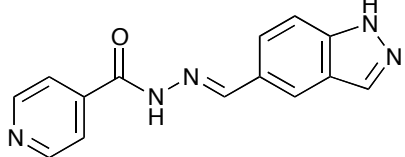
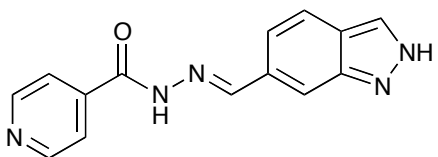
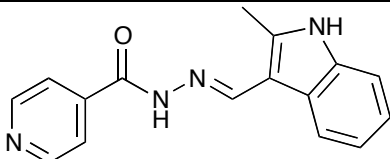
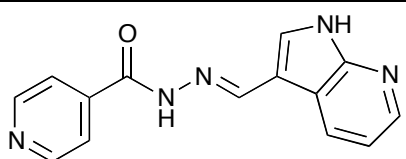
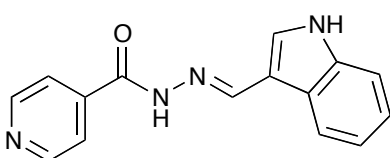
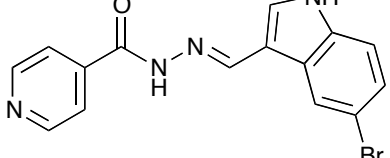
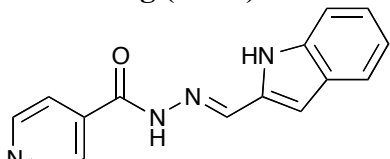
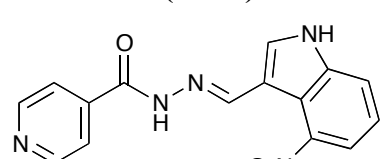
**Figure 5.12.** General scheme of isoniazid derivative mechanochemical synthesis using *p*-TSA.

After the milling procedure, the *p*-TSA was eliminated by washing with NaHCO<sub>3</sub> aqueous solution (1.1 eq. in respect to *p*-TSA used for each run) and the powder dried under vacuum before further analysis (yields after washing are presented in **Table 5.5**). After this procedure, TLC plates indicated quantitative conversions, this is, it did not reveal impurities, which was confirmed by mass spectroscopy (MS) and high-resolution mass spectroscopy (HRMS) that identified only one pure product for the whole series. Instead, <sup>1</sup>H NMR spectra of this crude material indicated some minor peaks that could be remaining reactants or byproducts. Then, further purification step would be necessary to afford the pure product. Methanol, ethanol, water and their mixtures were used to recrystallize depending on the hydrazone, and after drying, new <sup>1</sup>H NMR spectra were recorded, which revealed the same minor peaks.

This fact led to an investigation about the possibility of isomerism that is fully discussed in the next subsection. Actually, the hydrazones were obtained quantitatively from the beginning and that, in fact, the recrystallization was not necessary.

It is still important to mention that, differently from the phenolic hydrazones, a melting was produced when the *p*-TSA was added into the medium, and therefore, the reaction is not fully in solid-state. The formation of a fluid phase is vastly found for solid mixtures (eutectic melting, e.g. Rothenberg et al., 2001) and surely contributed to reach high conversions in short times of grinding for these hydrazones. As a matter of fact, the melting formed a sticky mixture, and some intervention had to be made to take off the mass ensuring the grinding and the progress of the reaction. But, still, the mechanical energy is mandatory to induce the reaction to completion, through the mixing, generation and exposition of fresh surfaces and also contributing for the reaction itself

**Table 5.5.** The hydrazones produced by reacting isonicotinic aldehyde as hydrazine and imidazole, indazole or indolic aldehydes.

Aldehyde	Hydrazones derived from isonicotinic aldehyde	
Imidazole derivatives	 <b>7a (80 %) <sup>a</sup></b>	 <b>7b (98 %) <sup>a</sup></b>
	 <b>7c (98 %) <sup>a</sup></b>	 <b>7d (99 %) <sup>a</sup></b>
Indole derivatives	 <b>7e (99 %) <sup>a</sup></b>	 <b>7f (94%) <sup>a</sup></b>
	 <b>7g (99 %) <sup>a</sup></b>	 <b>7h (99 %) <sup>a</sup></b>
	 <b>7i (91 %) <sup>a</sup></b>	 <b>7j (99%) <sup>a</sup></b>

<sup>a</sup>Yields after washing to eliminate *p*-TSA. According to TLC, <sup>1</sup>H NMR and MS, the conversions were quantitative.

### 5.3.3 The structural analysis of isonicotinoyl hydrazones by DFT and NMR

The structures of all the hydrazones were identified and characterized by <sup>1</sup>H NMR and <sup>13</sup>C NMR, MS and HRMS, FTIR and UV-vis. The characterization data for each of them is attached in Appendix II. The <sup>1</sup>H and <sup>13</sup>C NMR spectra in DMSO solution indicated pure products and the shifts were attributed without ambiguity, except for the isonicotinic derivatives. The NMR spectra for the whole **7a-j** series and the isonicotinic **1a-d** showed small signals in addition to the major peaks, which could lead to misleading interpretations. On the other hand, the MS and HRMS spectra displayed quasimolecular ion peaks for the expected

hydrazones, confirming their molecular weights. These results indicate that the isonitonic hydrazones are present in different forms in DMSO solution.

NMR spectral and theoretical studies previously reported demonstrated that acylhydrazones generally exist predominantly or solely as a mixture of isomers (Palla et al., 1986; Syakaev et al., 2006; Ünsal-Tan et al., 2010). In theory, it may exist four possible arrangements of *N*-acylhydrazones in respect to (*E/Z*)-configurational isomers relative to the C=N bond and rotamers caused by the inversion of amide bonds C(O)NH. In the absence of a formal nomenclature for this rotamers, herein it was adopted the *cis/trans* amide conformers according to Palla et al. (1986) and Patorski et al. (2013) (**Figure 5.13**).

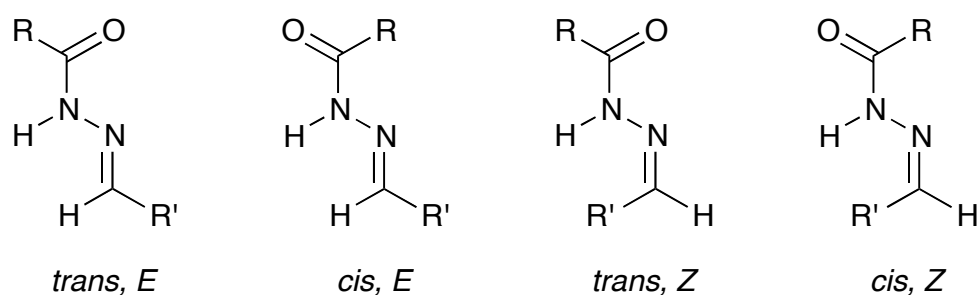


**Figure 5.13.** Possible forms of *N*-acylhydrazones.

Although the four forms being considered, *E/Z* isomerization is generally not observed and the *Z* geometric isomers are absent or present only in poor portions as a consequence of steric hindrance (Palla et al., 1986; Ünsal-Tan et al., 2010). An exception is for R'=pyridyl, in which strong intramolecular hydrogen bonds are present in the (*Z*)-form (Syakaev et al., 2006), mainly in less polar solvents.

For study purposes of the hydrazones mechanochemically synthesized, two isoniazid derivatives were chosen to be further investigated, one phenolic hydrazone (**1c**) and one indazolic hydrazone (**7d**).

#### 5.3.3.1 (*E*)-*N'*-(4-hydroxybenzylidene)isonicotinohydrazide (**1c**)

The  $^1\text{H}$  NMR spectra of **1c** in DMSO showed two sets of signals indicating the possibility of equilibrium between rotamers in solution. Theoretical assessment of the existence of the isomers was carried out. The four structures of *E/Z* geometrical isomers and *cis/trans* amide conformers of **1c** were modeled by DFT, using Gaussian 09, at first at HF/STO-3G level. As expected, the (*Z*)-conformers were found higher in energy than the *E* ones (Ünsal-Tan et al., 2010). Therefore, only the *cis* and *trans E*-isomers were modeled at

the high level of theory (B3LYP/6-31+G(d,p)) and frequencies calculations were performed on the optimized geometries at 298K (**Figure 5.14**), showing all positive frequencies and allowing evaluation of the Gibbs free energy. Table 6 displays the relative energies of minima and transition state for the possible rotamers of **1c**.

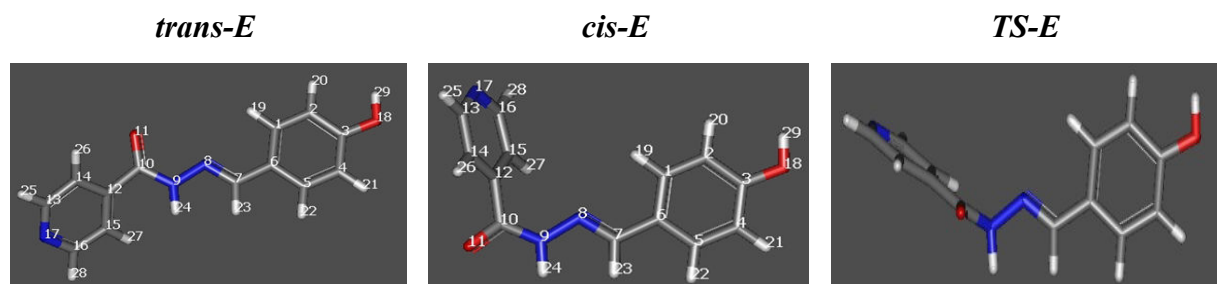


**Figure 5.14.** Optimized geometry for **1c** *E*-rotamers and the transition state (TS)

According to the calculated values, following Boltzmann distribution, ( $P_i/P_j = \exp((G_j - G_i)/k_B T)$ ), in gas phase, *cis-E*-isomer was present at 92.3% and *trans-E* at 7.7%, whereas in DMSO, using the polarizable solvent continuum model (SMD), the ratio *cis/trans* was inverted for *cis/trans* : 5.6/94.4 (**Table 5.6**). This indicates that the minor and major peaks in  $^1\text{H}$  NMR would be from the *cis-E* and *trans-E* respectively.

**Table 5.6.** Energies of minima and transition state for *cis/trans-E* isomers of **1c** obtained at B3LYP/6-31+G(d,p) level in the gas phase and using DMSO polarizable continuum model (SMD).

Isomer	Gas phase				DMSO continuum			
	E (au)	G (au)	$\Delta G$ (kcal/mol)	%p	E (au)	G (au)	$\Delta G$ (kcal/mol)	%p
<i>trans-E</i>	- 816.730569	-816.553707	1.47	7.7	-816.763427	-816.585816	-1.68	94.4
<i>cis-E</i>	- 816.733307	-816.730569	0	92.3	-816.761415	-816.583145	0	5.6
<i>TS-E</i>	-	-	-	-	-816.765271	-816.557724	17.63	-

In confirmation that conformers of **1c** were present in solution, variable-temperature (298 K – 388 K)  $^1\text{H}$  NMR experiments were performed in DMSO solution and the spectra are shown in **Figure 5.15**.

A complete coalescence is observed for entire set of small signals at different temperatures. The reversibility of these changes was verified when the experimental temperature decreased from 388 to 298 K again, and by the same ratio of the conformers at 298 K before and after the experiment. These results confirm the hypothesis of the conformers as well as that *cis-trans* amide conformers is the only process of isomerization, by



circumvention of the energy barrier to interconvert when the temperature rises. And, in addition, at lower temperature they only exist as a mixture. Others authors obtained the same results, but for the case of acylhydrazones (Lopes et al., 2013; Patorski et al., 2013).

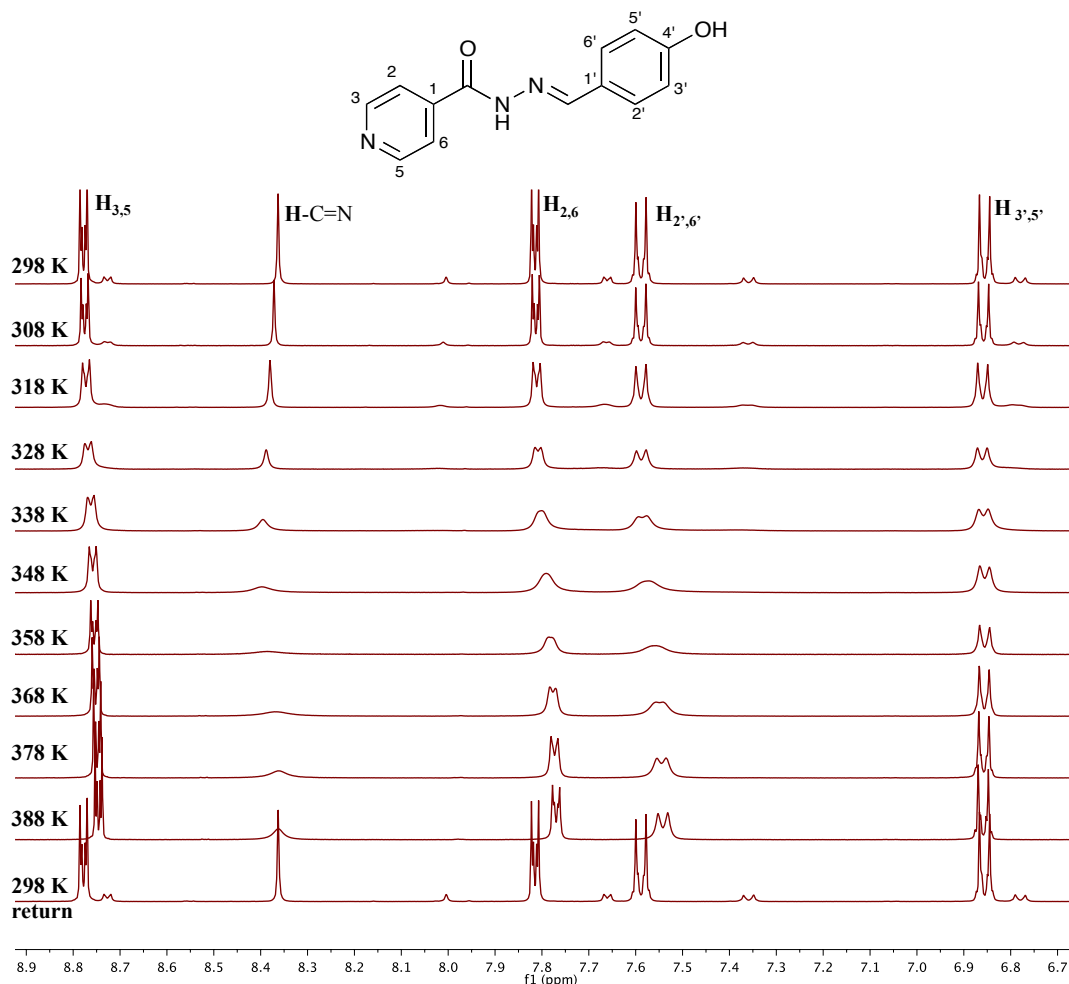


**Figure 5.15.**  $^1\text{H}$  NMR spectra of **1c** recorded at different temperatures showing the coalescent of the small signals.

Furthermore, this  $^1\text{H}$  NMR study at increasing temperatures allowed calculating the activation barrier of *cis/trans* interconversion. Correlation of the coalescence temperatures ( $T_c$ ) with the difference in chemical shift of the signals led to  $\Delta G^\ddagger$  following the equations (5.1) and (5.2). At the  $T_c$ :

$$k_{\text{exch}} = \frac{\pi(\Delta\nu)}{\sqrt{2}} = 2.22(\Delta\nu) \quad (5.1)$$

and according to Eyring equation for the transition state, with the Boltzmann ( $k_B$ ) and Planck ( $h$ ) constants;

$$k_{exch} = \frac{k_B T}{h} e^{-\frac{\Delta G^\ddagger}{RT}} \quad (5.2)$$

Values of  $\Delta G^\ddagger$  are consigned in **Table 5.7**. The mean value obtained on several signals gives  $\Delta G^\ddagger = 17.58 \text{ kcal.mol}^{-1}$ . This experimental value is in good agreement with the calculated one at B3LYP/6-31+G(d,p) displayed in **Table 5.6** ( $\Delta G^\ddagger = 17.63 \text{ kcal.mol}^{-1}$ ) that correspond to the difference of energies between the transition state and the ground of the *cis-E*–isomer.

**Table 5.7.** Determination of activation energy ( $\Delta G^\ddagger$ ) from coalescence temperatures  $T_c$  and rate exchange  $k_{exch}$  at different chemical shifts for **1c** conformers.

Nuclei	$T_c$ (K)	$k_{exch}$ (Hz)	$\Delta G^\ddagger$ (kcal/mol)
H <sub>3,5</sub>	338	33.97	17.52
H-C=N	368	239.1	17.71
H <sub>2,6</sub>	352	102.6	17.50
H <sub>2',6'</sub>	362	153.2	17.73
H <sub>3',5'</sub>	342	51.28	17.45

To assist the attribution of the minor and major signals to the correct conformational isomers, NMR chemical shift calculations were then performed using B3LYP/6-311+(2d,p) and the chloroform polarizable continuum model (PCM) for both conformers. Isotropic shielding constants ( $\sigma$ ) for  $^1\text{H}$  and  $^{13}\text{C}$  nuclei were transformed in chemical shift ( $\delta$ ) using linear regression procedure proposed by Tantillo (2012). These calculations were used to compare with the experimental chemical shifts from  $^1\text{H}$  and  $^{13}\text{C}$  NMR spectra. Calculated values are consigned in the **Table 5.8** ( $^1\text{H}$  NMR) and **Table 5.9** ( $^{13}\text{C}$  NMR) alongside with the experimental ones. The atom numbering is displayed in **Figure 5.15**.

**Table 5.8.** Calculated and experimental  $^1\text{H}$  chemical shifts for the *cis-E* and *trans-E* conformers of **1c** in DMSO, and the ratio from integration of the minor (*cis-E*) and major (*trans-E*) signals.

Nuclei	Calculated $\delta$ (ppm)		Experimental $\delta$ (ppm)		Ratio
	<i>trans-E</i>	<i>cis-E</i>	major	minor	
$^1\text{H}$					
H <sub>3',5'</sub>	6.87	6.78	6.86	6.78	0.11
H <sub>2',6'</sub>	7.73	7.66	7.59	7.36	0.11
H <sub>2,6</sub>	7.57	7.55	7.84	7.66	0.11

<b>H-C=N</b>	7.82	7.44	8.36	8.00	0.11
H <sub>3,5</sub>	8.72	8.74	8.77	8.73	0.11

**Table 5.9.** Calculated and experimental <sup>13</sup>C chemical shifts for the *cis-E* and *trans-E* conformers of **1c** in DMSO.

Nuclei <sup>13</sup> C	Calculated $\delta$ (ppm)		Experimental $\delta$ (ppm)	
	<i>trans-E</i>	<i>cis-E</i>	Major	minor
C <sub>3',5'</sub>	113.60	113.48	116.23	116.09
C <sub>2,6</sub>	119.86	122.50	121.93	123.58
C <sub>1'</sub>	125.16	125.14	125.56	125.35
C <sub>2',6'</sub>	129.35	128.94	129.54	129.07
C <sub>1</sub>	140.67	141.31	141.15	142.34
C=N	146.08	143.45	149.82	145.59
C <sub>3,5</sub>	150.06	148.92	150.73	149.95
C <sub>4'</sub>	158.28	157.87	160.16	159.78
C=O	160.15	166.16	161.73	167.84

The <sup>1</sup>H NMR signal of N-H would be helpful because more or less shielding could indicate some interaction with C=O for the *cis*-isomer, but, unfortunately, the signal was broad making the interpretation difficult. The O-H signal was also broad, and, in addition it resonates far from the C(O)NH region, and thus not followed by the hydrogen atoms. All the other signals were well defined. Comparing the other peaks, the <sup>1</sup>H NMR chemical shifts from **Table 5.8** of the minors are shifted upfield in relation to the major ones. The differences between them,  $\Delta\delta$ , are expected to be more pronounced for the protons near to the concerning moiety C(O)NHN=C-H. Indeed, the H-C=N was the most affected with  $\Delta\delta= 0.36$  ppm, followed by the protons in the *ortho* position from both isonicotinic ( $\Delta\delta= 0.18$  ppm) and phenolic rings ( $\Delta\delta= 0.23$  ppm). The upfield shifting of the H-C=N agrees with the results by Palla et al. (1986), suggesting the *cis-E* as the minor conformer. Another information from **Figure 5.8** is the constant ratio of isomers that is 89/11 % for major/minor or *trans-E*/*cis-E* respectively. The ratio is reasonably in accordance with the calculated ratio (94/6 %, *trans/cis*), mainly in terms of major and minor conformer.

In <sup>13</sup>C NMR spectra of **1c**, another set of signals, in addition to the higher, was also observed. Regarding the main concerned <sup>13</sup>C NMR shifts, C=O and C=N, the carbon

chemical shifts differ greatly in *cis* and *trans* conformers, compared to  $^1\text{H}$  NMR. The chemical shift of C=O of the small signal is deshielded to  $\delta = 167.84$  ppm in comparison to the major signal at  $\delta = 161.73$  ppm. Syrakaev et al. (2006) attributed this behavior to the reduced contribution of the conjugative form  $\text{N}^+=\text{C}-\text{O}^-$  of steric hindered amides. The difference in the shifts of  $\Delta\delta = 6.11$  ppm, also corresponds to Syrakaev's work and with the calculated values from **Table 5.9**. The opposite is found for the C=N, for which the  $^{13}\text{C}$  assignment is shifted downfield for the major conformer ( $\delta = 149.82$  ppm) and is more shielded for the minor ( $\delta = 145.59$  ppm). The same examination, for both C=N and C=O was made by Palla et al. (1986), who attributed the downfield shifting of C=N and the upfield shifting of C=O to the *trans*-isomer, corresponding very well with the spectra of **1c** and the calculated values, in which it is expected the major fraction for the *trans-E* conformer.

In summary, DFT calculation indicated the possibility of two arrangements for the hydrazone **1c**. The dynamic NMR experiments confirmed the presence of two forms that could interconvert. The calculated and the experimental values of the energy barrier to interconvert ( $\Delta G^\ddagger \approx 17$  kcal.mol $^{-1}$ ) match, and it is attributed to energy of the *cis-E* conformer in respect to the transition state. The calculated and the experimental  $^1\text{H}$  and  $^{13}\text{C}$  NMR chemical shifts also correspond well, indicating that *trans-E* isomer is, thus, present in higher amounts. The up- and downfield shifting of the main concerned nuclei, it means those in the C(O)NHC=N region, agrees with the previously reported works by Palla et al. (1986), Syakaev et al. (2006), Patorski et al. (2013) and Lopes et al. (2013), all in respect to acylhydrazones or derivatives. This leads unambiguously to the conclusion that the *trans-E* conformer of the hydrazone **1c** is the major one.

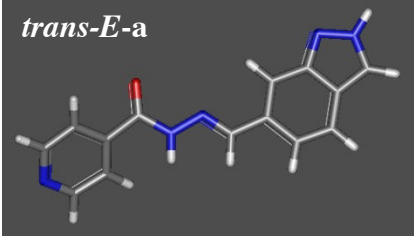
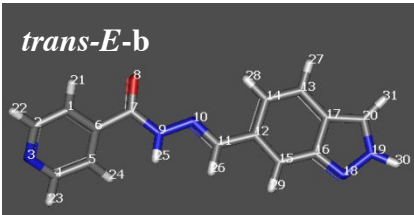
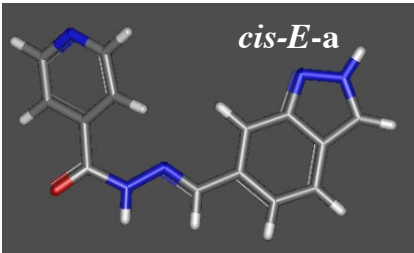
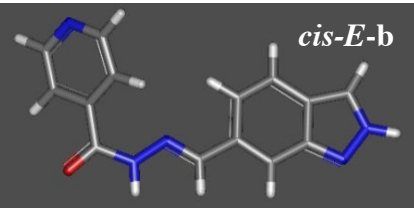
#### 5.3.3.2 (*E*)-*N'*-((2*H*-indazol-6-yl)methylene)isonicotinohydrazide (**7d**)

The compound **7d** was subjected to same studies performed for **1c**. In addition to the four possible forms *E/Z* geometrical isomers and the *cis/trans* rotamers around the C(O)NH, other two rotamers are possible in respect to the N=C — **indazole** bond, due to the non symmetric moieties, resulting in eight possibilities of arrangements. But, as previously, the (*Z*) isomers were found higher in energy using at HF/STO-3G level in DFT calculations, and, therefore, only the (*E*) isomers were considered.

DFT calculations were carried on at the B3LYP/6-31+G(d,p) level on the four isomers: *cis/trans* (C(O)NH) *E*-isomers and the two rotamers (N=C — **indazole**), in the gas phase and in the DMSO modeled by the SMD polarizable continuum model. Boltzmann analysis was used to determine the relative distribution of each conformer both in the gas

phase and in the DMSO continuum model. In the gas phase *cis* compounds are majorities, whereas in the DMSO continuum, *trans* conformation prevails; *trans-E* = 79.7%, *cis-E* = 20.3%. **Table 5.10** displays the optimized geometries as well as the Gibbs free energy and Boltzmann distribution for the four conformations of **7d**. Despite the possibility of the rotamers due to the indazole rotation the *trans-E* (a,b) and *cis-E* (a-b) isomers were treated together.

**Table 5.10.** Geometries, Gibbs free energies and Boltzmann distribution the (*E*) conformers of **7d** at B3LYP/6-31+G(d,p) level in the gas phase and in the DMSO continuum solvent model (PCM).

Isomer - Geometry	Gas phase		DMSO continuum	
	G (au)	%	G (au)	%
<i>trans-E-a</i> 	-888.907360	0.34	-888.944712	28.22
<i>trans-E-b</i> 	-888.909926	5.09	-888.945280	51.50
<i>cis-E-a</i> 	-888.910465	9.00	-888.941968	1.54
<i>cis-E-b</i> 	-888.912591	85.57	-888.944326	18.72

Dynamic NMR experiments were also performed for **7d** in DMSO solution in order to verify the existence of different forms of this hydrazone and to determine the energy barrier for *cis* => *trans* conversion. <sup>1</sup>H NMR spectra were recorded as function of temperature (298 –

358 K) allowing establishing whether the coalescence of the duplicated signals would be observed.

From **Figure 5.16**, the complete coalescence can be observed for the minor signals. Furthermore, these changes were reversible when the temperature was back to 298 K, fact that indicate more than one conformer, which can interconvert upon reaching the energy required for C-N amide bond rotation, and that at lower temperatures **7d** conformers co-exist in DMSO solution. The proportion of the isomers before and after dynamic NMR experiments were the same, indicating that amide the amide bond conformational transformation is the main process of isomerization. Similarly for the results previously reported and just alike for **1c**, the activation barrier to interconvert obtained according to equations (5.1) and (5.2) with the  $T_c$  of different chemical shifts was about  $\Delta G^\ddagger=17.28$  kcal/mol (**Table 5.11**).

**Table 5.11.** Determination of activation energy ( $\Delta G^\ddagger$ ) from coalescence temperatures  $T_c$  and rate exchange  $k_{exch}$  at different chemical shifts for **7d** conformers.

Nuclei	$T_c$ (K)	$k_{exch}$ (Hz)	$\Delta G^\ddagger$ (kcal/mol)
H <sub>3,5</sub>	328	26.64	17.14
H-C=N	358	239.76	17.20
H <sub>5'</sub>	338	35.30	17.49
H <sub>2',6' / H<sub>2,6</sub></sub>	348	108.56	17.25
H <sub>7'</sub>	358	199.80	17.33

In order to confirm which conformer is in majority,  $^1\text{H}$  and  $^{13}\text{C}$  NMR chemical shifts were calculated at the B3LYP/6-311+G(2d,p) using DMSO continuum model (PCM), taking into account the Boltzmann distribution of the two conformers for each isomer, that means *trans-E-a/trans-E-b*, 35.4/64.6 %, and *cis-E-a/ cis-E-b*, 7.6/92.4 %. Comparing calculated and experimental chemical shifts from  $^1\text{H}$  and  $^{13}\text{C}$  NMR, **Table 5.12** and **Table 5.13** show that, likewise for **1c**, *trans-E* isomer is the major form in the DMSO.

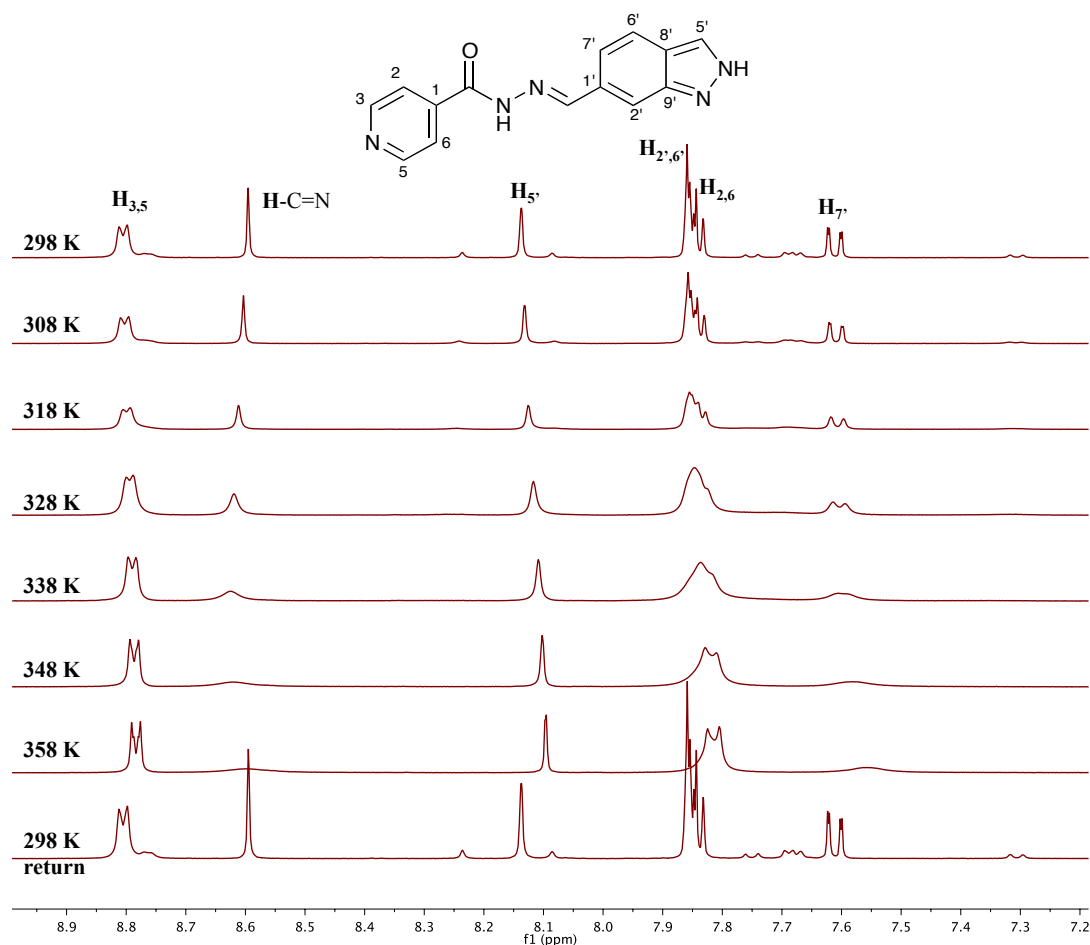


**Figure 5.16.**  $^1\text{H}$  NMR spectra of **7d** recorded at different temperatures showing the coalescent of the small signals.

**Table 5.12.** Calculated and experimental  $^1\text{H}$  chemical shifts for the *cis-E* and *trans-E* conformers of **7d** in DMSO, and the ratio from integration of the minor (*cis-E*) and major (*trans-E*) signals.

Nuclei	Calculated $\delta$ (ppm)		Experimental $\delta$ (ppm)		Ratio
	<i>trans-E</i>	<i>cis-E</i>	major	minor	minor/major
$\text{H}_{7'}$	7.71	7.49	7.61	7.31	0.12
$\text{H}_{2'}$	8.15	7.81	7.84	7.67	0.12
$\text{H}_{6'}$	7.91	7.76	7.82	7.75	0.14
$\text{H}_{2,6}$	7.63	7.59	7.86	7.69	0.13
$\text{H}_{5'}$	8.08	8.02	8.14	8.09	0.12
<b>H-C=N</b>	8.08	7.82	8.60	8.24	0.12
$\text{H}_{3,5}$	8.76	8.55	8.80	8.77	0.13

**Table 5.13.** Calculated and experimental  $^{13}\text{C}$  chemical shifts for the *cis-E* and *trans-E* conformers of **7d** in DMSO.

Nuclei $^{13}\text{C}$	Calculated $\delta$ (ppm)		Experimental $\delta$ (ppm)	
	<i>trans-E</i>	<i>cis-E</i>	Major	minor
C <sub>2</sub>	118.96	120.81	110.75	110.42
C <sub>7</sub>	119.16	117.15	119.02	118.57
C <sub>2,6</sub>	119.5	122.39	121.51	121.51
C <sub>6</sub>	121.33	121.29	122.01	122.01
C <sub>8</sub>	121.80	121.36	124.39	124.10
C <sub>1</sub>	131.44	131.72	132.43	132.27
C <sub>5</sub>	121.76	121.73	134.21	134.21
C <sub>9</sub>	147.50	147.45	140.33	140.33
C <sub>1</sub>	140.43	141.46	140.95	140.95
C=N	147.40	144.73	150.03	145.80
C <sub>3,5</sub>	150.15	148.99	150.77	150.77
C=O	160.20	166.75	162.08	168.4

In respect to the chemical shifts from  $^1\text{H}$  and  $^{13}\text{C}$  NMR of the most concerned moiety,  $-\text{C}(\text{O})\text{NH}-\text{N}=\text{CH}-$ , the results are very similar to **1c**. The  $^1\text{H}$  NMR chemical shifts of the minor signals are shielded compared to the major signals and can be attributed to the *cis-E* conformer based on the Palla's (1986) and Syrakaev's (2006) works, as well as on the DFT calculations.  $\text{H}-\text{C}=\text{N}$  shifts from 8.60 ppm to 8.24 ppm ( $\Delta\delta = 0.36$  ppm) for the minor conformer, which is the same variation found between **1c** rotamers. The isomer ratios are very similar and can be considered as 88/12 % in relation to major/minor forms, for the best resolved signals. The calculated fraction for the *trans-E/cis-E* conformers in DMSO continuum (**Table 5.10**) is 79.7/20.3 %. Despite the difference, these values correspond in terms of major/minor conformers, it means minor/*cis-E* and major/*trans-E*, specially taking into account that in the experimental DMSO solutions, aggregates, hydrogen bonding and dimers can be formed, which could favor the *trans-E* conformation.

In  $^{13}\text{C}$  NMR, the C=N appears upfielded for the minor signal ( $\delta = 145.80$  ppm) in relation to the major at  $\delta = 150.03$  ppm. The contrary is expected for the C=O, in which the minor signal is more deshielded, corresponding to the *cis-E* amide rotamer (168.4) and shielded for the majority conformer, *trans-E* (162.08).



In the same manner for **1c**, based on the DFT calculations for the relative energies of the isomers, the activation energy for amide bond rotation as well as the predicted and experimental  $^1\text{H}$  and  $^{13}\text{C}$  chemical shifts for NMR led to attribute the *cis-E* and *trans-E* isomers as minority and majority conformers of the hydrazone **7d** in DMSO solution. In addition, the dynamic NMR experiments revealed two conformers that can interconvert reversibly around the C-N amide bond. As mentioned before, previous authors reported that hydrazones derived from substituted hydrazides are present mainly as (*E*) isomer, and that *cis/trans* amide rotamers are in equilibrium in solution, with the *trans-E* in majority proportion (Palla et al., 1986; Syakaev et al., 2006; Patorski et al., 2013; Lopes et al., 2013).

It is still worth to mention the role of the solvent. As it could be seen from DFT calculations, the ratio between *cis/trans* rotamers was inverted from gas phase to DMSO continuum. This shows the strong influence of the medium, which can enhance or hamper intra and intermolecular interactions between molecules, favoring the stabilization of determined specie. Furthermore, the ratio of *E/Z* isomers, when possible, is also affected by the polarity of the solvents. Syakaev et al. (2006) and Palla et al. (1986) demonstrated the effect of DMSO or  $\text{CDCl}_3$  in the fractions of the isomers of aryl- and acylhydrazones.

### **5.3.4 Biological activities of mechanochemically synthesized hydrazones against *M. tuberculosis***

#### *5.3.4.1 Biological evaluation of phenolic hydrazones (1-5a-d)*

Apart from the hydrazones derived from benzhydrazide, the others synthesized hydrazones were evaluated by determining the minimal inhibitory concentration (MIC) necessary to inhibit the growth of *M. tuberculosis* H<sub>37</sub>Rv strain. Isoniazid, a frontline drug and a coupling partner used to produce some of these hydrazones, was used for comparison.

In **Table 5.14** summarizes the biological results obtained for the hydrazones possessing a phenolic moiety in the aldehydic partner of the Schiff base formation (**1-5a-d**). In that series the hydrazine and aldehydic partners were varied.

**Table 5.14.** Phenolic hydrazones tested as inhibitory agents against *M. tuberculosis* growth (H<sub>37</sub>Rv strain)

Cpd	MW (g mol <sup>-1</sup> )	MIC (µg mL <sup>-1</sup> ) (µM)	LogP	Cpd	MW (g mol <sup>-1</sup> )	MIC (µg mL <sup>-1</sup> ) (µM)	LogP
<b>1a</b>	301.30	0.125 (0.41)	1.38	<b>1c</b>	241.25	0.0125 (0.05)	1.64
<b>2a</b>	324.33	> 10 (> 30.8)	2.76	<b>2c</b>	264.28	> 10 (> 37.8)	3.01
<b>3a</b>	329.97	> 10 (> 30.4)	3.73	<b>3c</b>	269.32	> 10 (> 37.1)	3.98
<b>4a</b>	312.36	> 10 (> 32.0)	2.04	<b>4c</b>	252.31	> 10 (> 39.7)	2.29
<b>5a</b>	330.34	> 10 (> 30.3)	3.14	<b>5c</b>	270.28	> 10 (> 37)	3.40
<b>1b</b>	271.27	0.125 (0.46)	1.51	<b>1d</b>	257.24	0.125 (0.49)	1.25
<b>2b</b>	294.31	> 10 (> 34.0)	2.88	<b>2d</b>	280.28	> 10 (> 35.7)	2.62
<b>3b</b>	299.35	> 10 (> 33.4)	3.85	<b>3d</b>	285.32	> 10 (> 35.0)	3.59
<b>4b</b>	282.34	> 10 (> 35.4)	2.17	<b>4d</b>	268.31	> 10 (> 37.3)	1.90
<b>5b</b>	300.31	> 10 (> 33.3)	3.27	<b>5d</b>	286.28	> 10 (> 34.93)	3.01
<b>INH</b>	137.14	0.025 (0.18)	-0.64				

Considering the different hydrazine frames it is clear that only the isonicotinoyl derivatives behave well, i.e., the hydrazones, in which, the isoniazid moiety is coupled (compounds **1a-d**). On the contrary, the compounds possessing either the benzothiophene (**3a-d**) or the carbazate (**5a-d**) moieties are much less potent as well as for the aminorhodanine derivatives (**4a-d**) with MIC values higher than 10 µg/ml. This is also the case for the hydralazine derivatives (**2a-d**), in accordance with previous results on cinnamoyl hydrazinamides (De et al., 2011). Among the four isoniazid derivatives prepared in this series, those bearing two or more substituents *ortho* to the phenolic function present potent activities with MIC value of 0.125 µg/ml, which is five times higher than that of INH. The compound **1c**, produced from *p*-hydroxybenzaldehyde and isoniazid, is the most potent derivative synthesized with a MIC value of 0.0125 µg/mL (0.05 µM), which is 2-4 times lower in comparison to INH (0.025 µg/ml - 0.18 µM). The MIC values of the hydrazones, other than isoniazid derivatives, were higher than 10 µg/mL, which means out of the interesting range of concentration for these studies. The limits of concentration were not established and no relation between the hydrazone structures and antimycobacterial activity was identified.

The resistance to the current drugs (first and second lines) remains a very serious problem, mostly resulting from *InhA* and *katG* mutations (Campbell et al., 2011), and culminates in the occurrence of multidrug-resistant (MDR) strains, including resistances

against INH and RIF. Owing the good results obtained for the phenolic hydrazones derived from isoniazid, compounds **1a-d** were then tested against the clinical isolate IC2 that is a multidrug-resistant *M. tuberculosis* strain (**Table 5.15**). The compounds **1a** and **1b** exhibited a 20 fold less efficiency as for the H<sub>37</sub>Rv strain and at the same level as isoniazid, while the compound **1d** was the most efficient against IC2 strain with MIC of 1 µg/mL (3.89 µM). In turn, the MIC of the compound **1c**, the better one concerning the H<sub>37</sub>Rv strain, was determined as 10.36 µM.

**Table 5.15.** MIC of phenolic hydrazones isoniazid derivatives for MDR clinical isolate IC2.

Compound	IC2* MIC (µg/mL)	IC2* MIC (µM)
<b>1a</b>	> 2.5	> 8.30
<b>1b</b>	> 2.5	> 9.22
<b>1c</b>	2.5	10.36
<b>1d</b>	1	3.89
<b>INH</b>	> 1	> 7.29

\* *Mtb* clinical isolate, IC2: drug resistance profile: resistant to streptomycin, isoniazid, rifampicin, ethambutol, pyrazinamide, ethionamide, capreomicin

#### 5.3.4.2 Biological activity evaluation of isoniazid-nitrogen heterocyclic hydrazones (**7a-j**)

The H<sub>37</sub>Rv MIC values obtained for second family of hydrazones bearing the isoniazid moiety coupled with different N-heterocyclic aldehydes (imidazole, indazole and indole derivatives) are listed in **Table 5.16**.

**Table 5.16.** Isoniazid-nitrogen heterocyclic hydrazones tested as inhibitory agents of *M. tuberculosis* growth (H<sub>37</sub>Rv strain).

Cpd	MW (g mol <sup>-1</sup> )	MIC (µg mL <sup>-1</sup> ) (µM)	LogP	Cpd	MW (g mol <sup>-1</sup> )	MIC (µg mL <sup>-1</sup> ) (µM)	LogP
<b>7a</b>	215.21	0.03 (0.14)	-1.00	<b>7f</b>	265.27	0.015 (0.056)	0.24
<b>7b</b>	229.24	0.03 (0.13)	-1.37	<b>7g</b>	264.28	0.06 (0.23)	0.86
<b>7c</b>	265.27	0.06 (0.23)	1.38	<b>7h</b>	343.18	0.125 (0.36)	1.69
<b>7d</b>	265.27	0.03 (0.11)	-0.52	<b>7i</b>	264.28	0.06 (0.23)	0.52
<b>7e</b>	278.31	0.25 (0.90)	0.49	<b>7j</b>	309.28	0.25 (0.81)	1.39
<b>INH</b>	137.14	0.05 (0.36)	-0.64				

In general, most of these compounds present similar or better activities when compared to INH. On the contrary, the compounds **7e** and **7j**, both are indole derivatives, conducted to the highest MIC values; while the azaindole derivative **7f** is as much active as the phenolic compound **1c** with a MIC value of 0.015  $\mu\text{g/mL}$  (0.056  $\mu\text{M}$ ).

After the compound **7f**, the compound **7d** with an indazole moiety also presented good MIC of 0.11  $\mu\text{M}$ , followed by the imidazole derivatives (**7a-b**) that also resulted in small concentrations to inhibit the H<sub>37</sub>Rv (MIC = 0.13-0.14  $\mu\text{M}$ ). It is noted that these molecules have poor lipophilicity (LogP < 0.4).

#### 5.3.4.3 *InhA* inhibition assay

After activation by *katG*, INH forms a covalent adduct with NAD<sup>+</sup> (INH-NAD), and it is this adduct that inhibits *InhA*, the NADH-dependent fatty acid biosynthesis (FAS-II) enoyl reductase from *M. tuberculosis* (see **Figure 5.7**). Therefore, the evaluation of the inhibition ratio of the enzyme *InhA* gives some insight about the target for the tested compounds.

Recombinant *M.tb* *InhA* was expressed in *E. coli* and subsequently purified. The selected synthetic compounds, corresponding to the phenolic hydrazones bearing the isoniazid unit and the entire **7a-j** series, were evaluated *in vitro* for inhibition of *InhA* from *Mycobacterium tuberculosis* at 50  $\mu\text{M}$  by applying a commonly used method described in the experimental section. The results are shown in **Table 5.17**.

**Table 5.17.** Percentage of *InhA* enzyme inhibition values for the isoniazid derivatives.

Compound	% Inhibition at 50 $\mu\text{M}$	Compound	% Inhibition at 50 $\mu\text{M}$
<b>1a</b>	63.9	<b>7d</b>	19.3
<b>1b</b>	47.8	<b>7e</b>	43.2
<b>1c</b>	44.9	<b>7f</b>	39.19
<b>1d</b>	54.05	<b>7g</b>	41.91
<b>7a</b>	54.4	<b>7h</b>	32.35
<b>7b</b>	2.94	<b>7i</b>	78.67
<b>7c</b>	32.8	<b>7j</b>	precipitation
<b>INH</b>	> 99		

Considering the four phenolic derivatives, the trisubstituted one (**1a**) presents the better *InhA* activity with a value of 64% inhibition at 50 $\mu\text{M}$ . The other compounds bearing he

catecholic function or the disubstituted and monosubstituted derivatives **1d** and **1c** are less potent with 54%, 48% and 45% InhA inhibition at 50  $\mu\text{M}$ , respectively. Under these conditions isoniazid itself inhibits 99%.

Concerning the isoniazid hydrazones bearing the heteroaromatic frames, compounds **7a-b** and **7j** were difficult to evaluate due to solubility issues. Compound **7d** is a very poor inhibitor of InhA exhibiting value of 19% while the compounds **7c**, **7e** and **7f** may be considered as poor inhibitors with values 32%, 43% and 39%, respectively. Finally, the compound **7i** is the only derivative exhibiting 78% of InhA inhibition, which is a very interesting result.

#### 5.3.4.4 Cytotoxicity and Selectivity Index determination

Cytotoxicity of all compounds bearing the isoniazid moiety was also evaluated on MRC5 human fibroblast cells. Almost all compounds tested present toxicities above 80  $\mu\text{M}$  (**Table 5.18**), except for **1d** ( $\text{LD}_{50} = 36.3 \mu\text{M}$ ). The ascertainment of  $\text{LD}_{50}$  is essential to determine the selectivity index (SI), which indicates the best candidates in terms of high biological activity against the target and low cytotoxicity. The SI presented in **Table 5.18** is the ratio between  $\text{LD}_{50}$  and the *in vitro* MIC value against *M.tb.* H<sub>37</sub>Rv previously obtained.

**Table 5.18.** Cytotoxicity ( $\text{LD}_{50}$ ) and selectivity index (SI) for the most active hydrazones against H<sub>37</sub>Rv *Mtb.*

Compound	$\text{LD}_{50}$ ( $\mu\text{M}$ )	SI	Compound	$\text{LD}_{50}$ ( $\mu\text{M}$ )	SI
<b>1a</b>	> 80	> 195	<b>7d</b>	> 80	> 727
<b>1b</b>	> 80	> 173	<b>7e</b>	129	143
<b>1c</b>	> 80	> 1600	<b>7f</b>	> 80	> 1429
<b>1d</b>	36.3	74	<b>7g</b>	> 80	> 364
<b>7a</b>	> 80	> 571	<b>7h</b>	> 80	> 222
<b>7b</b>	> 80	> 615	<b>7i</b>	71.4	310
<b>7c</b>	> 80	> 364	<b>7j</b>	156	193
<b>INH</b>	-	-			

Apart from the compound **1d**, due to its high toxicity, the phenolic hydrazones presented good selectivities higher than 170. A great result was obtained for **1c**, the hydrazone resulting from isoniazid and *p*-hydroxybenzaldehyde reaction. This molecule has the lowest

H<sub>37</sub>Rv MIC value (0.0125 µg/mL) and good cell toleration (LD<sub>50</sub> > 80 µM) as well. As a result, this compound has the highest SI (> 1600).

The *N*-heterocyclic isoniazid derivatives present good SI values, except for **7e** and **7j**, which possess the highest H<sub>37</sub>Rv MIC values within this family of compounds. The compound **7h** has a SI higher than 222, while this value is raised for **7c** and **7g**, both with SI > 364. At the same level (MIC= 0.06 µg/mL, LD<sub>50</sub> = 71.4 µM and SI = 310), the **7i** must be considered, mainly due to its InhA inhibition of 78 %. After them, great SI values closer to 600 are found for **7a-b**, but, nonetheless, some reservation must be taken due to the poor solubility of these molecules. Finally, the SI of compound **7d** is higher than 727 and an excellent value is obtained for **7f**. With an SI higher than 1469, **7f** is highlighted with MIC = 0.015 µg/mL.

### 5.3.5 Hydrolytic stability and *pK<sub>a</sub>* determination of most active hydrazones

The biological assays with the synthesized hydrazones revealed excellent activities against *M. tuberculosis*. The most prominent results were obtained for the hydrazones bearing the isoniazid moiety. This is the case of the phenolic hydrazones **1a-d**, as well as the **7d**, despite its low InhA inhibition and **7f**.

In order to confirm that the biological activities evidenced for these hydrazones originate from the complete chemical structure itself, and not from hydrolysis of the imine bond, stability studies were carried out. UV-*vis* spectrophotometry was used to monitor the stability of some compounds. **Table 5.19** summarizes the storage conditions of the hydrazones and the respective results observed.

**Table 5.19.** Stability monitoring of hydrazones.

Compound	Solution	Conc. (mol/L)	pH	t (h)	Stability
<b>1a</b>	28% EtOH/H <sub>2</sub> O	5.9 x 10 <sup>-5</sup>	6.2	21	stable
<b>1b</b>		6.9 x 10 <sup>-5</sup>	6.3	15	stable
<b>1c</b>		6.0 x 10 <sup>-5</sup>	6.1	22	stable
<b>1d</b>		6.3 x 10 <sup>-5</sup>	6.5	22	stable
<b>7d</b>	5% EtOH/ PIPES	4.1 x 10 <sup>-5</sup>	6.8	20	3% Abs. reduction
<b>7f</b>	buffer (50 mM)	3.1 x 10 <sup>-5</sup>	6.8	20	stable
				7 days	5% Abs. reduction

As expected, the hydrazone solutions monitored by UV-*vis* spectroscopy at the  $\lambda_{\max}$  of the related molecules in those conditions, demonstrated that all the compounds are stable for a prolonged time and no significant decomposition was observed. Hence, the biological results are, indeed, from the hydrazones. Only **7d** had a very small reduction (3 %) in the absorbance. It is known that hydrazones possess greater intrinsic hydrolytic stability compared to imines. In addition to the contribution of the NH-N=C in electron delocalization, the resonance forms in acylhydrazones increases the negative-charge on the C=N and thus, reduces its electrophilicity and the affinity to the nucleophile attack from water (Kalia and Raines, 2008). Furthermore, the repulsion of the lone pairs of the NH-N can be relieved in the conjugates (Wiberg and Glaser, 1992).

### 5.3.5.1 pKa determination

The acid dissociation constant ( $K_a$ , or more commonly expressed by  $pK_a$ ) is a very important physicochemical parameter in a wide range of research areas, including the development of active molecules due to solubility issues. The  $pK_a$  of the same molecules studied for stability could be also determined using UV-*vis* spectrometry based on the variation of the absorbance as function of the pH due to the presence of chromophores close to the ionization site of the molecules. The molar absorptivity varies according to the conjugation forms that dynamically change when and where the molecule is charged by the effect of pH of medium and protonation/dissociation. **Figure 5.17** proposes the different protonation states for the hydrazone **1a**.

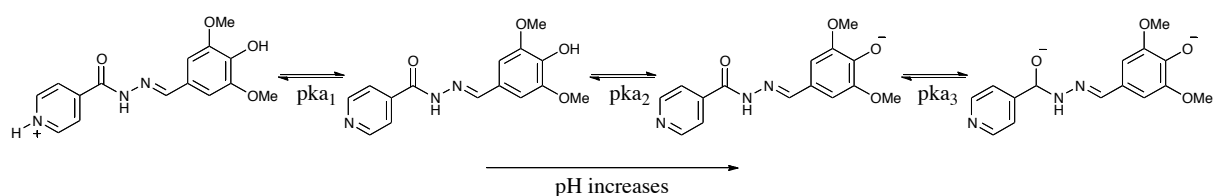


**Figure 5.17.** Charges of the hydrazone **1a** as function of pH.

For experimental  $pK_a$  determination, the molecules were solubilized in hydroalcoholic solutions at 28 % of ethanol and the ionic strength was maintained by the addition of KCl (0.1 M). The pH was adjusted with concentrated solutions of KOH and HCl. The UV spectra were recorded at each variation on the pH, and, at least three wavelengths were monitored and the

absorbance variation was traced as function of the pH. Figure 5.18 shows the variations on the UV-*vis* **1a** spectra, and **Figure 5.19**, the resulting plot for specific wavelengths.

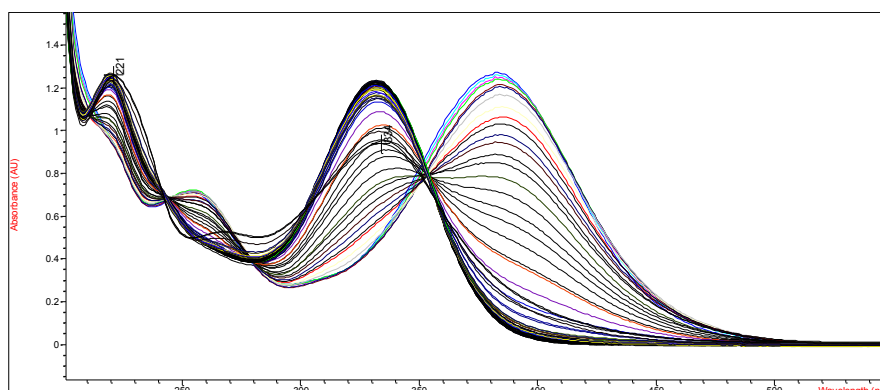
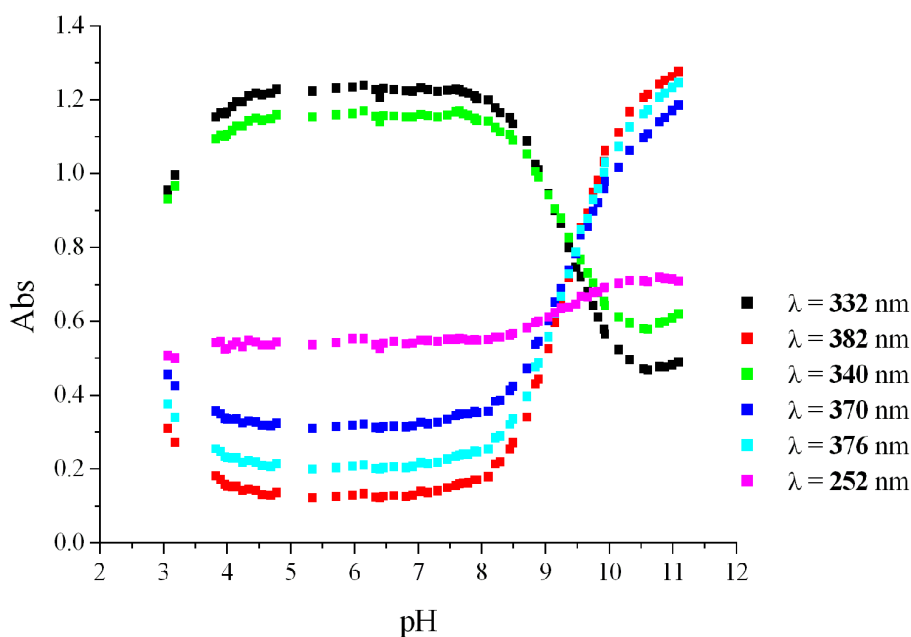


Figure 5.18. Changes on the UV-*vis* **1a** spectra as function of pH variation.



**Figure 5.19.** Plots of absorbance at specific wavelengths ( $\lambda/\text{nm}$ ) as function of pH.

The protonation/dissociation of the molecule is accompanied by a variation in the absorbance, which can be seen in Figure 5.18 and it is graphically represented in **Figure 5.19**. The inflection points of the curves correspond to the change in that protonate/dissociated state of the molecule, and therefore, the pH at that point amounts to the pKa. If the curves have more than one inflection points, it can indicate more than one pKa. This is the case of **1a** as proposed is **Figure 5.17**. Thus, using this method, the pKa's of **1a** were determined. The same



protocol was applied for the other molecules and the resulted pKa is presented in Table 5.20, as an average value from three different  $\lambda$ .

Table 5.20. Determine pKa of isonicotinoyl hydrazones

Compound	1a	1b	1c	1d	7d	7f
pKa <sub>1</sub>	3.0	-	-	-	-	-
pKa <sub>2</sub>	9.5 ± 0.0	9.1 ± 0.1	9.2 ± 0.1	7.7 ± 0.1	10.4 ± 0.1	11
pKa <sub>3</sub>	> 11	-	-	8.9 ± 0.0	-	-

There is always some inflection close to pH 3 related with the protonation of 4-pyridinic nitrogen of isoniazid moiety (pKa<sub>2</sub> of isoniazid = 3.5), and it corresponds to pKa<sub>1</sub> of the molecules. The pKa<sub>2</sub> of the molecules ranges from 7.7 to 11. It means that they are in dissociated form from milder (**1d**) to stronger basic conditions for case of **7f**.

## 5.4 CONCLUSIONS

The mechanochemical route was successfully applied to synthesize various examples of pharmaceutically attractive hydrazones from solid materials. The greenness of the procedure is reflected in excellent conversions and atom economy as well as the use of compounds with catalytic effects that reduce the reaction time and increases conversion, and finally no use of organic solvents for synthesis, reducing the waste generation whereas the process becomes safer.

The phenol hydrazones presented differences on the conversion ratio, which was investigated from the electronic and solid matter effects of the solid hydrazines. Obviously, it is mandatory that the reactants be reactive or become reactive such as for the case of reactions in solution, but additional effects intrinsic of the solid state also plays a role in reactions involving solids. It was observed that even when the nucleophilicity of the reactive site of the hydrazine is higher, this does not ensure higher conversions. This is the example of isoniazid that has higher electronic density on the reactive nitrogen, but reacts slower in comparison to benzyl carbazate, which is slightly less nucleophile, but reacts very well (> 99%). The proximity of the molecules in the crystal (steric hindrance from the solid), the density, the H-bonding interactions can favor the freedom of the molecule towards the reaction. Benzyl carbazate has the lowest density among the hydrazines while benzhydrazine, different from

the isoniazid in the cyclic nitrogen, has less H-bonds and is less hindered in the crystal, giving better results as well. Nevertheless, it was demonstrated the electronic and the solid effects working in the sense of reduction of the product formation, the case of 3-aminorhodanine (lower charge density, higher density, strong intermolecular interactions), can be circumvented by constant mechanical action for more prolonged time, resulting in complete conversion.

The use of *p*-TSA for the reaction between isoniazid and nitrogen-containing heterocyclic aldehydes, allowed producing hydrazones in shorter times with excellent yields, also due to the formation of a fluid phase upon contact of *p*-TSA with the reactant solids. This is characteristic for systems pronouncing eutectic behavior. It was observed for this series as well as for the phenolic hydrazones an equilibrium between two conformers about the amide bond rotation in DMSO solution. DFT calculations and dynamic NMR were essential to elucidate the structure and proportion of the species and indicated the majority of the *trans-E* conformers. The energy barrier for conformers to interconvert was determined experimentally and agrees with the calculated values ( $\Delta G^\ddagger=17$  kcal/mol). Moreover, it is fundamental to know the complete structure, including possible conformational arrangements, for lead optimization in drug discovery.

The hydrazones, from both phenolic and nitrogen-containing heterocyclic aldehydes, were evaluated concerning their biological activity against H<sub>37</sub>Rv *M. tuberculosis*. Many of the synthesized molecules, those bearing isoniazid moiety, present encouraging anti-TB activities. The four phenolic hydrazones possessing isonicotinoyl frame (**1a-d**) presented good results of H<sub>37</sub>Rv MIC (0.41 – 0.05 μM), but the high cytotoxicity of **1d**, and consequently low SI, makes it less favorable for further screening. The excellent MIC and LD<sub>50</sub> values obtained for the compound (*E*)-*N*'-(4-hydroxybenzylidene)isonicotinohydrazide (**1c**) led to the highest SI value, higher than 1600, while a moderate InhA inhibition was determined. Another compound that showed to be good candidate for further studies is the (*E*)-*N*'-((1*H*-pyrrolo[2,3-*b*]pyridin-3-yl)methylene)isonicotinohydrazide (**7f**). This molecule have good anti-TB with MIC similar to **1c** (0.056 μM) and high selectivity. Apart from **7e** and **7j**, most of the molecules from family **7a-j** have significant anti-TB activity, with highlight for **7i** that could inhibit by up to 80 % of the enzyme InhA activity, showing that this protein is probably the target of the compound. In addition, the main compounds were stable for several hours, or days, when evaluated at hydroalcoholic solutions, in which the pKa was also determined.

Overall, the mechanochemistry can be used as a methodology to synthesize molecules in high purities and in shorter times, enabling the fast production of molecules to be tested concerning the biological activities and, therefore, helping in the stage of molecules screening that aims to find lead compounds in the drug discovery course.

### 5.5 REFERENCES

Andries, K.; Verhasselt, P.; Guillemont, J.; Gohlmann, H.; Neefs, J.-M.; Winkler, H.; Van Gestel, J.; Timmerman, P.; Zhu, M.; Lee, E.; et al. A Diarylquinoline Drug Acrive on the ATP Synthase of Mycobacterium tuberculosis. *Science*, **2005**, *307*, 223–227.

Asselineau, J.; Lederer, E. Structure of the Mycolic Acids of Mycobacteria. *Nature* **1950**, *166*, 782–783.

Banerjee, A.; Dubnau, E.; Quemard, A.; Balasubramanian, V.; Um, K.; Wilson, T.; Collins, D.; de Lisle, G.; Jacobs, W. inhA, a gene encoding a target for isoniazid and ethionamide in Mycobacterium tuberculosis. *Science*. **1994**, *263*, 227–230.

Becke, A. D. Density-functional thermochemistry. III. The role of exact exchange. *J. Chem. Phys.* **1993**, *98*, 5648–5652.

Belkheiri, N.; Bouguerne, B.; Bedos-Belval, F.; Duran, H.; Bernis, C.; Salvayre, R.; Nègre-Salvayre, A.; Baltas, M. Synthesis and antioxidant activity evaluation of a syringic hydrazones family. *Eur. J. Med. Chem.* **2010**, *45*, 3019–3026.

Boldyrev, V. V. Mechanochemical modification and synthesis of drugs. *J. Mater. Sci.* **2004**, *39*, 5117–5120.

Brennan, P. Structure, function, and biogenesis of the cell wall of Mycobacterium tuberculosis. *Tuberculosis* **2003**, *83*, 91–97.

Campbell, P. J.; Morlock, G. P.; Sikes, R. D.; Dalton, T. L.; Metchock, B.; Starks, A. M.; Hooks, D. P.; Cowan, L. S.; Plikaytis, B. B.; Posey, J. E. Molecular Detection of Mutations Associated with First- and Second-Line Drug Resistance Compared with Conventional Drug Susceptibility Testing of Mycobacterium tuberculosis. *Antimicrob. Agents Chemother.* **2011**, *55*, 2032–2041.

Candéa, A. L. P.; Ferreira, M. D. L.; Pais, K. C.; Cardoso, L. N. d. F.; Kaiser, C. R.; Henriques, M. das G. M. d. O.; Lourenço, M. C. S.; Bezerra, F. A. F. M.; de Souza, M. V. N. Synthesis and antitubercular activity of 7-chloro-4-quinolinylhydrazones derivatives. *Bioorg. Med. Chem. Lett.* **2009**, *19*, 6272–6274.

Cardoso, L. N. F.; Bispo, M. L. F.; Kaiser, C. R.; Wardell, J. L.; Wardell, S. M. S. V.; Lourenço, M. C. S.; Bezerra, F. a. F. M.; Soares, R. P. P.; Rocha, M. N.; de Souza, M. V. N. Anti-Tuberculosis Evaluation and Conformational Study of N -Acylhydrazones Containing the Thiophene Nucleus. *Arch. Pharm. (Weinheim)*. **2014**, *347*, 432–448.

Chin, D. P.; Osmond, D.; Page-Shafer, K.; Glassroth, J.; Rosen, M. J.; Reichman, L. B.; Kvale, P. A.; Wallace, J. M.; Poole, W. K.; Hopewell, P. C. Reliability of anergy skin testing in persons with HIV infection. The pulmonary Complications of HIV Infection Study Group. *Am. J. Respir. Crit. Care Med.* **1996**, *153*, 1982–1984.

Claramunt, R. M.; López, C.; Sanz, D.; Elguero, J. Chap 3: Mechano Heterocyclic Chemistry: Grinding and Ball Mills. In *Advances in Heterocyclic Chemistry*; Elsevier, 2014; Vol. 112, pp. 117–143.

Coelho, T. S.; Cantos, J. B.; Bispo, M. L. F.; Gonçalves, R. S. B.; Lima, C. H. S.; Da Silva, P. E. A.; De Souza, M. In vitro anti-mycobacterial activity of (E)-N'-(monosubstituted-benzylidene) isonicotinohydrazide derivatives against isoniazid-resistant strains. *Infect. Dis. Rep.* **2012**, *4*, 49-51.

Collom, S. L.; Anastas, P. T.; Beach, E. S.; Crabtree, R. H.; Hazari, N.; Sommer, T. J. Differing selectivities in mechanochemical versus conventional solution oxidation using Oxone. *Tetrahedron Lett.* **2013**, *54*, 2344–2347.

De Luca, L. Naturally occurring and synthetic imidazoles: their chemistry and their biological activities. *Curr. Med. Chem.* **2006**, *13*, 1–23.

De, P.; Koumba Yoya, G.; Constant, P.; Bedos-Belval, F.; Duran, H.; Saffon, N.; Daffé, M.; Baltas, M. Design, Synthesis, and Biological Evaluation of New Cinnamic Derivatives as Antituberculosis Agents. *J. Med. Chem.* **2011**, *54*, 1449–1461.

Delori, A.; Friščić, T.; Jones, W. The role of mechanochemistry and supramolecular design in the development of pharmaceutical materials. *CrystEngComm* **2012**, *14*, 2350-2362.

Descamps, M.; Willart, J. F.; Dudognon, E.; Caron, V. Transformation of pharmaceutical compounds upon milling and comilling: The role of Tg. *J. Pharm. Sci.* **2007**, *96*, 1398–1407.

Dessen, A.; Quemard, A.; Blanchard, J.; Jacobs, W.; Sacchetti, J. Crystal structure and function of the isoniazid target of Mycobacterium tuberculosis. *Science*, **1995**, *267*, 1638–1641.

Friščić, T. Supramolecular concepts and new techniques in mechanochemistry: cocrystals, cages, rotaxanes, open metal–organic frameworks. *Chem. Soc. Rev.* **2012**, *41*, 3493-3510.

Gavezzotti, A. Packing analysis in reactive crystals: the decomposition of bis(3,3,3-triphenylpropanoyl)peroxide in the solid state. *Tetrahedron* **1987**, *43*, 1241–1251.

Gavezzotti, a. The calculation of molecular volumes and the use of volume analysis in the investigation of structured media and of solid-state organic reactivity. *J. Am. Chem. Soc.* **1983**, *105*, 5220–5225.

Ghiladi, R. a.; Medzihradzky, K. F.; Rusnak, F. M.; Ortiz de Montellano, P. R. Correlation between Isoniazid Resistance and Superoxide Reactivity in Mycobacterium tuberculosis KatG. *J. Am. Chem. Soc.* **2005**, *127*, 13428–13442.

Hajipour, A. R.; Mohammadpoor-Baltork, I.; Bigdeli, M. A Convenient and Mild Procedure for the Synthesis of Hydrazones and Semicarbazones from Aldehydes or Ketones under Solvent-free Conditions. *J. Chem. Res.* **1999**, *55*, 570–571.

Haruta, N.; Sato, T.; Tanaka, K.; Baron, M. Reaction mechanism in the mechanochemical synthesis of dibenzophenazine: application of vibronic coupling density analysis. *Tetrahedron Lett.* **2013**, *54*, 5920–5923.

Hickenboth, C. R.; Moore, J. S.; White, S. R.; Sottos, N. R.; Baudry, J.; Wilson, S. R. Biasing reaction pathways with mechanical force. *Nature* **2007**, *446*, 423–427.

Jabeen, S.; Dines, T. J.; Leharne, S. a.; Withnall, R.; Chowdhry, B. Z. A vibrational spectroscopic investigation of rhodanine and its derivatives in the solid state. *J. Raman Spectrosc.* **2010**, *41*, 1306–1317.

Jabeen, S.; Palmer, R. a.; Potter, B. S.; Helliwell, M.; Dines, T. J.; Chowdhry, B. Z. Low Temperature Crystal Structures of Two Rhodanine Derivatives, 3-Amino Rhodanine and 3-Methyl Rhodanine: Geometry of the Rhodanine Ring. *J. Chem. Crystallogr.* **2009**, *39*, 151–156.

Jayasankar, A.; Somwangthanaroj, A.; Shao, Z. J.; Rodríguez-Hornedo, N. Cocrystal formation during cogrinding and storage is mediated by amorphous phase. *Pharm. Res.* **2006**, *23*, 2381–2392.

Jensen, L. H. The Crystal Structure of Isonicotinic Acid Hydrazide I. *J. Am. Chem. Soc.* **1954**, *76*, 4663–4667.

Ješelnik, M.; Varma, R. S.; Polanc, S.; Kočevar, M. Solid-state synthesis of heterocyclic hydrazones using microwaves under catalyst-free conditions. *Green Chem.* **2002**, *4*, 35–38.

Johnson, J. L.; Hadad, D. J.; Dietze, R.; Noia Maciel, E. L.; Sewali, B.; Gitta, P.; Okwera, A.; Mugerwa, R. D.; Alcaneses, M. R.; Quelapio, M. I.; et al. Shortening Treatment in Adults with Noncavitary Tuberculosis and 2-Month Culture Conversion. *Am. J. Respir. Crit. Care Med.* **2009**, *180*, 558–563 DOI: 10.1164/rccm.200904-0536OC.

Kalia, J.; Raines, R. T. Hydrolytic Stability of Hydrazones and Oximes. *Angew. Chemie Int. Ed.* **2008**, *47*, 7523–7526.

Kaupp, G. Solid-state molecular syntheses: complete reactions without auxiliaries based on the new solid-state mechanism. *CrystEngComm*, **2003**, *5*, 117-133.

Kaupp, G.; Schmeyers, J.; Boy, J. Iminium Salts in Solid-State Syntheses Giving 100% Yield. *J. für Prakt. Chemie* **2000**, *342*, 269–280.

Kaupp, G.; Schmeyers, J.; Boy, J. Waste-free solid-state syntheses with quantitative yield. *Chemosphere* **2001**, *43*, 55–61.

Konda, S. S. M.; Brantley, J. N.; Varghese, B. T.; Wiggins, K. M.; Bielawski, C. W.; Makarov, D. E. Molecular Catch Bonds and the Anti-Hammond Effect in Polymer Mechanochemistry. *J. Am. Chem. Soc.* **2013**, *135*, 12722–12729.

Kumar, H. S. N.; Parumasivam, T.; Jumaat, F.; Ibrahim, P.; Asmawi, M. Z.; Sadikun, A. Synthesis and evaluation of isonicotinoyl hydrazone derivatives as antimycobacterial and anticancer agents. *Med. Chem. Res.* **2014**, *23*, 269–279.

Kuroda, R.; Higashiguchi, K.; Hasebe, S.; Imai, Y. Crystal to crystal transformation in the solid state. *CrystEngComm*, **2004**, *6*, 463-468.

Le Goff, G.; Ouazzani, J. Natural hydrazine-containing compounds: Biosynthesis, isolation, biological activities and synthesis. *Bioorg. Med. Chem.* **2014**, *22*, 6529–6544.

Lee, C.; Yang, W.; Parr, R. G. Development of the Colle-Salvetti correlation-energy formula into a functional of the electron density. *Phys. Rev. B* **1988**, *37*, 785–789.

Li, J. P.; Zheng, P. Z.; Zhu, J. G.; Liu, R. J.; Qu, G. R. an Expedient Method for the Synthesis of Bis (Acyldiazones ) Under Microwave Irradiation in Solvent-Free Medium. *South African J. Chem.* **2006**, *59*, 90–92.

Lienhardt, C.; Cook, S. V; Burgos, M.; Yorke-Edwards, V.; Rigouts, L.; Anyo, G.; Kim, S.-J.; Jindani, A.; Enarson, D. A.; Nunn, A. J. Efficacy and Safety of a 4-Drug Fixed-Dose Combination Regimen Compared With Separate Drugs for Treatment of Pulmonary Tuberculosis. *JAMA* **2011**, *305*, 1415–1423.

Lodewyk, M. W.; Siebert, M. R.; Tantillo, D. J. Computational Prediction of <sup>1</sup>H and <sup>13</sup>C Chemical Shifts: A Useful Tool for Natural Product, Mechanistic, and Synthetic Organic Chemistry. *Chem. Rev.* **2012**, *112*, 1839–1862.

Lopes, A.; Miguez, E.; Kümmerle, A.; Rumjanek, V.; Fraga, C.; Barreiro, E. Characterization of Amide Bond Conformers for a Novel Heterocyclic Template of N-acylhydrazone Derivatives. *Molecules* **2013**, *18*, 11683–11704.

Ma, X.; Yuan, W.; Bell, S. E. J.; James, S. L. Better understanding of mechanochemical reactions: Raman monitoring reveals surprisingly simple “pseudo-fluid” model for a ball milling reaction. *Chem. Commun.* **2014**, *50*, 1585–1587.

Maccari, R.; Ottana, R.; Monforte, F.; Vigorita, M. G. In Vitro Antimycobacterial Activities of 2'-Monosubstituted Isonicotinohydrazides and Their Cyanoborane Adducts. *Antimicrob. Agents Chemother.* **2002**, *46*, 294–299.

Maccari, R.; Ottanà, R.; Vigorita, M. G. In vitro advanced antimycobacterial screening of isoniazid-related hydrazones, hydrazides and cyanoboranes: Part 14. *Bioorg. Med. Chem. Lett.* **2005**, *15*, 2509–2513.

- McKissic, K. S.; Caruso, J. T.; Blair, R. G.; Mack, J. Comparison of shaking versus baking: further understanding the energetics of a mechanochemical reaction. *Green Chem.* **2014**, *16*, 1628.
- Michalchuk, A. A. L.; Tumanov, I. A.; Boldyreva, E. V. Complexities of mechanochemistry: elucidation of processes occurring in mechanical activators via implementation of a simple organic system. *CrystEngComm* **2013**, *15*, 6403–6412.
- Mikhailenko, M. a.; Shakhtshneider, T. P.; Boldyrev, V. V. On the mechanism of mechanochemical synthesis of phthalylsulphthiazole. *J Mater. Sci.*, **2004**; Vol. 39, pp. 5435–5439.
- Miyazawa, T. Normal vibrations of monosubstituted amides in the *cis* configuration and infrared spectra of diketopiperazine. *J. Mol. Spectrosc.* **1960**, *4*, 155–167.
- Mokhtari, J.; Naimi-Jamal, M. R.; Hamzeali, H.; Dekamin, M. G.; Kaupp, G. Kneading Ball-Milling and Stoichiometric Melts for the Quantitative Derivatization of Carbonyl Compounds with Gas-Solid Recovery. *ChemSusChem* **2009**, *2*, 248–254.
- Narang, R.; Narasimhan, B.; Sharma, S. A Review on Biological Activities and Chemical Synthesis of Hydrazide Derivatives. *Curr. Med. Chem.* **2012**, *19*, 569–612.
- Nguyen, M.; Claparols, C.; Bernadou, J.; Meunier, B. A fast and efficient metal-mediated oxidation of isoniazid and identification of isoniazid-NAD(H) adducts. *Chembiochem* **2001**, *2*, 877–883.
- Nun, P.; Martin, C.; Martinez, J.; Lamaty, F. Solvent-free synthesis of hydrazones and their subsequent N-alkylation in a Ball-mill. *Tetrahedron* **2011**, *67*, 8187–8194.
- Oliveira, K. N.; Chiaradia, L. D.; Martins, P. G. A.; Mascarello, A.; Cordeiro, M. N. S.; Guido, R. V. C.; Andricopulo, A. D.; Yunes, R. A.; Nunes, R. J.; Vernal, J.; et al. Sulfonyl-hydrazones of cyclic imides derivatives as potent inhibitors of the Mycobacterium tuberculosis protein tyrosine phosphatase B (PtpB). *Medchemcomm* **2011**, *2*, 500–504.
- Özdemir, A.; Kaplancıklı, Z. A.; Turan-Zitouni, G.; Revial, G. Synthesis of some novel hydrazone derivatives and evaluation of their antituberculosis activity. *MARMARA Pharm. J.* **2010**, *2*, 79–83.
- Palla, G.; Predieri, G.; Domiano, P.; Vignali, C.; Turner, W. Conformational behaviour and / isomerization of -acyl and -aroylhydrazones. *Tetrahedron* **1986**, *42*, 3649–3654.
- Palomino, J. C.; Martin, A. TMC207 becomes bedaquiline, a new anti-TB drug. *Future Microbiol.* **2013**, *8*, 1071–1080.
- Pan, P.; J. Tonge, P. Targeting InhA, the FASII Enoyl-ACP Reductase: SAR Studies on Novel Inhibitor Scaffolds. *Curr. Top. Med. Chem.* **2012**, *12*, 672–693.
- Patorski, P.; Wyrzykiewicz, E.; Bartkowiak, G. Synthesis and Conformational Assignment of N-(E)-Stilbenyloxymethylenecarbonyl-Substituted Hydrazones of Acetone and o-(m- and p-) Chloro- (nitro-) benzaldehydes by Means of and NMR Spectroscopy. *J. Spectrosc.* **2013**, *2013*, 1–12.
- Pavan, F. R.; Maia, P. I. d. S.; Leite, S. R. A.; Deflon, V. M.; Batista, A. a.; Sato, D. N.; Franzblau, S. G.; Leite, C. Q. F. Thiosemicarbazones, semicarbazones, dithiocarbazates and hydrazide/hydrazones: Anti – Mycobacterium tuberculosis activity and cytotoxicity. *Eur. J. Med. Chem.* **2010**, *45*, 1898–1905.
- Quemard, A.; Sacchettini, J. C.; Dessen, A.; Vilcheze, C.; Bittman, R.; Jacobs, W. R.; Blanchard, J. S. Enzymic Characterization of the Target for Isoniazid in Mycobacterium tuberculosis. *Biochemistry* **1995**, *34*, 8235–8241.
- Rajalakshmi, G.; Hathwar, V. R.; Kumaradhas, P. Topological analysis of electron density and the electrostatic properties of isoniazid: An experimental and theoretical study. *Acta Crystallogr. Sect. B Struct. Sci. Cryst. Eng. Mater.* **2014**, *70*, 331–341.

Raparti, V.; Chitre, T.; Bothara, K.; Kumar, V.; Dangre, S.; Khachane, C.; Gore, S.; Deshmane, B. Novel 4-(morpholin-4-yl)-N'-(arylidene)benzohydrazides: Synthesis, antimycobacterial activity and QSAR investigations. *Eur. J. Med. Chem.* **2009**, *44*, 3954–3960.

Rawat, R.; Whitty, A.; Tonge, P. J. The isoniazid-NAD adduct is a slow, tight-binding inhibitor of InhA, the Mycobacterium tuberculosis enoyl reductase: Adduct affinity and drug resistance. *Proc. Natl. Acad. Sci.* **2003**, *100*, 13881–13886.

Reddy, K. S.; Ramesh, M.; Srimai, V.; Chandra, K. S.; Satyender, A. Synthesis, antimycobacterial activity and docking studies of L-proline derived hydrazones. *Der Pharma Chemica*, **2014**, *6*, 267–271.

Reed, A. E.; Curtiss, L. a; Weinhold, F. Intermolecular interactions from a natural bond orbital, donor-acceptor viewpoint. *Chem. Rev.* **1988**, *88*, 899–926.

Rollas, S.; Küçükgülzel, S. G. Biological Activities of Hydrazone Derivatives. *Molecules* **2007**, *12*, 1910–1939.

Rothenberg, G.; Downie, a. P.; Raston, C. L.; Scott, J. L. Understanding solid/solid organic reactions. *J. Am. Chem. Soc.* **2001**, *123*, 8701–8708.

Rozwarski, D. a. Modification of the NADH of the Isoniazid Target (InhA) from Mycobacterium tuberculosis. *Science*, **1998**, *279*, 98–102.

Sarma, J. a. R. P.; Nagaraju, A.; Majumdar, K. K.; Samuel, P. M.; Das, I.; Roy, S.; McGhie, A. J. Solid state nuclear bromination with N-bromosuccinimide. Part 2. Experimental and theoretical studies of reactions with some substituted benzaldehydes. *J. Chem. Soc. Perkin Trans. 2* **2000**, 1119–1123.

Shalini, K.; Sharma, P.; Kumar, N. Imidazole and its biological activities: A review. *Chem. Sin.* **2010**, *1*, 36–47.

Sharma, V.; Kumar, P.; Pathak, D. Biological importance of the indole nucleus in recent years: A comprehensive review. *J. Heterocycl. Chem.* **2010**, *47*, 491–502.

Sheldon, R. A. The E Factor: fifteen years on. *Green Chem.* **2007**, *9*, 1273–1283.

Singh, N. B.; Singh, R. J.; Singh, N. P. Organic solid state reactivity. *Tetrahedron* **1994**, *50*, 6441–6493.

Sriram, D.; Yogeewari, P.; Madhu, K. Synthesis and in vitro and in vivo antimycobacterial activity of isonicotinoyl hydrazones. *Bioorg. Med. Chem. Lett.* **2005**, *15*, 4502–4505.

Stigliani, J. L.; Arnaud, P.; Delaine, T.; Bernardes-Génisson, V.; Meunier, B.; Bernadou, J. Binding of the tautomeric forms of isoniazid-NAD adducts to the active site of the Mycobacterium tuberculosis enoyl-ACP reductase (InhA): A theoretical approach. *J. Mol. Graph. Model.* **2008**, *27*, 536–545.

Syakaev, V. V.; Podyachev, S. N.; Buzykin, B. I.; Latypov, S. K.; Habicher, W. D.; Konovalov, A. I. NMR study of conformation and isomerization of aryl- and heteroarylaldehyde 4-tert-butylphenoxyacetylhydrazones. *J. Mol. Struct.* **2006**, *788*, 55–62.

Takayama, K.; Wang, C.; Besra, G. S. Pathway to Synthesis and Processing of Mycolic Acids in Mycobacterium tuberculosis. *Clin. Microbiol. Rev.* **2005**, *18*, 81–101.

Tan, D.; Štrukil, V.; Mottillo, C.; Friščić, T. Mechanochemical synthesis of pharmaceutically relevant sulfonyl-(thio)ureas. *Chem. Commun.* **2014**, *50*, 5248–5250.

Thangadurai, A.; Minu, M.; Wakode, S.; Agrawal, S.; Narasimhan, B. Indazole: A medicinally important heterocyclic moiety. *Med. Chem. Res.* **2012**, *21*, 1509–1523.

Timmins, G. S.; Deretic, V. Mechanisms of action of isoniazid. *Mol. Microbiol.* **2006**, *62*, 1220–1227.

Tumanov, I. a.; Achkasov, A. F.; Boldyreva, E. V.; Boldyrev, V. V. Following the products of mechanochemical synthesis step by step. *CrystEngComm* **2011**, *13*, 2213–2216.

Ünsal-Tan, O.; Özden, K.; Rauk, A.; Balkan, A. Synthesis and cyclooxygenase inhibitory activities of some N-acylhydrazone derivatives of isoxazolo[4,5-d]pyridazin-4(5H)-ones. *Eur. J. Med. Chem.* **2010**, *45*, 2345–2352.

Vanucci-Bacqué, C.; Carayon, C.; Bernis, C.; Camare, C.; Nègre-Salvayre, A.; Bedos-Belval, F.; Baltas, M. Synthesis, antioxidant and cytoprotective evaluation of potential antiatherogenic phenolic hydrazones. A structure–activity relationship insight. *Bioorg. Med. Chem.* **2014**, *22*, 4269–4276.

Vavříková, E.; Polanc, S.; Kočevár, M.; Horváti, K.; Bösze, S.; Stolaříková, J.; Vávrová, K.; Vinšová, J. New fluorine-containing hydrazones active against MDR-tuberculosis. *Eur. J. Med. Chem.* **2011**, *46*, 4937–4945.

Verma, A.; Joshi, S.; Singh, D. Imidazole: Having versatile biological activities. *J. Chem.* **2013**, *2013*, 1-12

Verma, G.; Marella, A.; Shaquiquzzaman, M.; Akhtar, M.; Ali, M. R.; Alam, M. M. A review exploring biological activities of hydrazones. *J. Pharm. Bioallied Sci.* **2014**, *6*, 69-80.

Wiberg, K. B.; Glaser, R. Resonance interactions in acyclic systems. 4. Stereochemistry, energetics, and electron distributions in 3-center-four- $\pi$ -electron systems A:BC. *J. Am. Chem. Soc.* **1992**, *114*, 841–850.

Wilming, M.; Johnsson, K. Spontaneous Formation of the Bioactive Form of the Tuberculosis Drug Isoniazid. *Angew. Chemie Int. Ed.* **1999**, *38*, 2588–2590.

World Health Organization – Global tuberculosis report 2014. Available in [http://www.who.int/tb/publications/global\\_report/en/](http://www.who.int/tb/publications/global_report/en/), consulted in 6<sup>th</sup> August, 2015.





---

# **GENERAL CONCLUSIONS AND PERSPECTIVES**

---



## GENERAL CONCLUSIONS

Mechanochemistry is clearly a defined domain in chemical and physicochemical sciences. The possibilities of transforming the raw materials upon application of mechanical energy, mostly in ball milling devices, has opened the field for a vast applications, other than for minerals and comminution. In organic systems, physicochemical transformations, intermolecular interactions, catalysis and chemical reactions with covalent bond formation, exemplify the versatility of this route, without mentioning its role among greener techniques for a sustainable chemistry development, including pharmaceuticals.

In this present research, the mechanochemical studies were carried out in three distinct levels: the electronic mechanistic interpretation of mechanically induced reactions, the powder processing and kinetics studies, and finally, the application toward the synthesis of pharmaceutically attractive compounds inserted in a atom-economical environmentally friendly framework. It was possible to scan from the electronic level, even if indirectly, the processing, up to the application of mechanochemistry with medicinal chemistry purposes.

In terms of reaction mechanisms, the condensed 1,4-diazines synthesis was investigated. Dibenzo[a,c]phenazine jointly with 2,3 diphenylquinoxaline mechanosynthesis were performed and analyzed in solid state. This fact allowed detecting by  $^{13}\text{C}$  CP-MAS NMR a chemical intermediate for DBPZ synthesis, not possible or not stable in solution. The values of calorimetric measurements indicated that the heat released did not correspond to the heat of formation from the starting reactants, but that might be originated from a different state of high energy, probably the intermediate detected in NMR, which continues to react after grinding and releases more heat. Again, these intermediate can be a result of a concerted addition as anticipated by DFT and vibronic coupling density calculations. The kinetics of DBPZ reaction could be represented by a mathematical model of nucleation and growth, which could also be detected in XRD patterns. It is important to say that the comparison of DBPZ and DPQ synthesis was essential for the conclusions.

The kinetic studies of DPQ synthesis showed that for physicochemical mechanism investigations, such as amorphization and eutectic melting, lower temperature and energy input (light milling balls), i.e., milder conditions, are preferred in order to emerge the events occurring during continuous milling. Likewise, the temperature effects on the kinetics of transformation were evaluated enabling the construction of Arrhenius and Eyring plots for estimation of the apparent activation barriers. This study revealed a mechanism changing from a certain temperature that was attributed to a phase transition, induced by milling,

resulting in a eutectic melting at the impact zone. The values of the apparent activation energies are lower for the region below the transition zone where the reaction media is constituted by solids, and thus, the mechanical energy has an effect more pronounced by lowering the barrier for reaction. In the other hand, for higher temperatures and under continuous milling the induction of a fluid phase formation, the system responds as reactions in solutions with higher activation energies. The  $\Delta G^\ddagger$  does not vary significantly for the entire range of the temperatures studied, however, the two distinct parts can be considered as enthalpy- or entropy-controlled.

Finally, this thesis is closed by the successful application of the mechanochemical route to synthesize a series of hydrazones. The compounds were tested against *M. tuberculosis* and the isoniazid derivatives have shown great activity, even superior to isoniazid itself. It was demonstrated that excellent to quantitative conversions could be obtained by adjusting the milling time or by addition a catalyst. Electronic reactivity of the hydrazines plays a very important role on the conversion ratio, but it must be associated to the solid-state aspects that can favor or prevent further reaction. When in DMSO solution, most of these hydrazones exist as a mixture of conformers that can interconvert when enough energy is supplied.

Recapitulating one of the ambitions of this thesis was to identify the frequent features present in all the studied systems, for the DBPZ and DPQ synthesis, and also for the hydrazones. These observations involve the transformations experienced by the powder as well as the aspects that can influence the reactions in solids under ball milling conditions.

- The continuous milling can lead to the generation of an amorphous phase that continues to crystallize afterwards as well as induce eutectic melting, but, in addition the reaction can also occur between crystalline species;
- The mechanical energy can, indeed, decrease the overall activation barrier for solid state reactions;
- The electronic reactivity of the chemical entity surely plays an important role on the reaction conversion, however, it cannot be considered singly;
- The proximity of the molecules, the space to move, in the crystals can be approximated by the absolute density of crystals, and for the lower densities the conversion ratio of a reaction is enhanced because the molecules can move more readily;

- The mobility of the molecules in rigid structures, such as in solids, can be further increased by increasing the number of single  $\sigma$  bonds, in the region of the reactive group, that represent certain degrees of freedom, making the reaction easier. The contrary is observed when the reactive site is closer to big groups or do not have single bonds to rotate. This hampers and retard the reaction;
- The continuous mechanical energy applied on solids can be capable to generated excited structures that allow reaction pathways different from solution-based media, and, thereby, intermediates can form and accumulated in the solid mixture.

The macroscopic events and the electronic levels were discussed articulately, which enabled deeper understanding of the mechanochemical reactions. Additionally elucidations may arise from other investigations. But these findings may contribute for the choice of the reactant partners for optimization in conversions as well as for obtaining designed structures in a sustainable way.



## PERSPECTIVES

This thesis aims to contribute to organic mechanochemistry understanding and development. The results obtained can be used as the base for further investigations, including issues observed for the cases reported here:

- The role of water eliminated in these syntheses is an interesting point. The water could play the role of catalyst, plasticizer, etc;
- The crystallization process during the synthesis is also a point to be clarified, mainly how the presence of the target product, i.e. acting as template, could influence the reaction kinetics;
- In relation to mechanistic understanding, the use of molecular modeling (molecular mechanics and quantum chemical calculations) is essential to be associated with experimental results. For this purpose, the use of other model reactions, such as Diels-Alder could be a starting point to study the ability and limitation of the mechanical energy to induce reactions.

These three subjects above could help on the elaboration of general guidelines for mechanochemical reactions.

In terms of chemical reaction engineering, there are highlighting aspects to be developed:

- Particle modeling, in means of discrete element methods (DEM) for the vibratory ball mill could be interesting since there are sorts of these ball mills for industrial applications;
- Scaling-up purposes are also intended with a direct link with the previous item. However, the energetics of the milling treatment, in relation to the conversions obtained in the device, must be associated;

It was demonstrated that the mechanochemical routes could be used to synthesize pharmaceutically interesting molecules within the *Green Chemistry* framework. Therefore, other molecules with potential therapeutic activity may be designed, considering the aspects already addressed for the hydrazones mechanosynthesis.

- For example, the synthesis of triazole derivatives as candidates to treat tuberculosis disease has already been studied at LSPCMIB.





---

# **RÉSUMÉ LONG EN FRANÇAIS**

---



## Contexte et intérêt

Les thématiques de recherche privilégiées par les universitaires et les industriels ces dernières années, sont souvent liées aux questions environnementales. On observe en effet une mobilisation générale en faveur du développement durable et de la préservation des ressources naturelles. Les industries chimiques et pharmaceutiques sont directement concernées car elles ont des impacts potentiels sur l'environnement à court et long termes, ce qui fait qu'elles s'orientent vers le développement de procédés non polluants. L'éco-conception des produits chimiques est formalisée dans les douze principes de la *Chimie Verte*<sup>1</sup> qui incitent à la conception de produits et de procédés chimiques plus respectueux de l'environnement, en mettant l'accent sur la prévention de la pollution. Ils doivent être bénins ou non dangereux depuis leur conception et leur développement, jusqu'à leur fabrication et leurs applications. Dans ce contexte, de multiples technologies ont été appliquées et développées afin de réduire l'utilisation de solvants dans la production chimique, car ils représentent la source principale de la production de déchets. Les protocoles sans solvant sont ainsi des voies primordiales pour le développement durable.

La mécanochemie est présentée comme une alternative aux méthodes classiques pour transformer les produits chimiques sans utiliser de solvants ou, si nécessaire, en utilisant seulement de très petites quantités.

L'utilisation de l'énergie mécanique, à la place de l'énergie thermique en milieu solvaté, a été appliquée avec succès et a donné lieu à une intense production scientifique et d'intérêt industriel dans les quinze dernières années pour ce qui concerne la mécanochemie organique.

Dans le domaine pharmaceutique, où le concept de pharmacie verte est plus que jamais d'actualité,<sup>2</sup> la mécanochemie est appliquée pour l'amélioration des propriétés physico-chimiques des principes actifs telles que la compressibilité pour la fabrication de comprimés et la solubilité par l'utilisation d'interactions intermoléculaires. En plus de cette application visant l'amélioration des propriétés physicochimiques, la mécanochemie fait également l'objet d'études pour la synthèse de principes actifs de médicaments déjà sur le marché ou pour de futures molécules candidates.

---

<sup>1</sup> Anastas, P. T., Warner, J. C., *Green Chemistry : Theory and Practice*, Oxford University Press, New York, 1998.

<sup>2</sup> Baron, M. Towards a greener pharmacy by more eco design. *Waste Biomass Valor* **2012**, *3*, 395–407.

*Mécanochimie pharmaceutique : une voie de chimie durable*, est le thème central de la présente étude. Celle-ci est motivée par le besoin de protocoles de production de produits chimiques plus respectueux de l'environnement, et par la recherche, la découverte et le développement de nouveaux médicaments.

Les études de mécanochimie reportées dans cette thèse ne sont pas limitées à la synthèse de molécules d'intérêt thérapeutique, mais portent également sur la meilleure compréhension des phénomènes qui se produisent lorsque la matière est perturbée par une action mécanique induisant des réactions chimiques.

Le potentiel de la mécanochimie présente un caractère particulièrement innovant, comme cela a été démontré par l'observation de mécanismes de réactions inattendues lors de l'application de contraintes mécaniques. Dans le cas de la manipulation d'une seule molécule, le stress mécanique permet de contourner des barrières énergétiques de manière spécifique, parfois différente des activations thermiques et photochimiques.<sup>3</sup> D'autre part, l'utilisation de broyage à billes, permet d'effectuer des réactions organiques sur des réactifs solides avec d'excellents rendements.

De véritables progrès ont donc été accomplis pour la manipulation d'une seule molécule et pour les réactions obtenues par broyage ou co-broyage, mais malheureusement peu d'études traitent de ces deux aspects conjointement, ce qui est susceptible de retarder de nouvelles avancées et l'enrichissement du domaine de la mécanochimie. Car d'un côté les investigations sont dédiées à des manipulations contrôlées de liaisons covalentes. Et de l'autre, l'objectif est d'obtenir des produits et des architectures de formes solides. Beaucoup a été fait concernant les interactions intermoléculaires et les transformations physico-chimiques de la poudre, mais les états électroniques doivent encore être étudiés. Par exemple, on ne trouve guère plus dans la littérature que les discussions de Gilman<sup>4</sup> et celles de Senna<sup>5</sup> au sujet du rapprochement des niveaux HOMO-LUMO pour des molécules stressées mécaniquement. Les investigations du mécanisme de la réaction mécaniquement induite pour la synthèse de la dibenzo[a,c]phénazine initiées et développées par Baron et ses collaborateurs,<sup>6,7</sup> ont aussi démontré quelques particularités de ces systèmes mécaniquement

---

<sup>3</sup> Hickenboth, C. R.; Moore, J. S.; White, S. R.; Sottos, N. R.; Baudry, J.; Wilson, S. R. Biasing reaction pathways with mechanical force. *Nature* **2007**, *446*, 423–427.

<sup>4</sup> Gilman, J. J. Mechanochemistry. *Science*, **1996**, *274*, 65.

<sup>5</sup> Senna, M. Consequences of molecular strain on the solid state addition reaction. *J. Mater. Sci.* **2004**, *39*, 4995–5001.

<sup>6</sup> Carlier, L.; Baron, M.; Chamayou, A.; Couarraze, G. Use of co-grinding as a solvent-free solid state method to synthesize dibenzophenazines. *Tetrahedron Lett.* **2011**, *52*, 4686–4689.

activés. Un travail préliminaire complémentaire également mené par Baron avec l'Université de Kyoto<sup>8</sup> a également permis d'initier un projet de recherche conjoint avec cette Université,<sup>9</sup> qui est en partie intégré dans la présente thèse.

Cette thèse de doctorat a été dirigée et réalisée au Centre RAPSODEE, en codirection avec le Laboratoire de Synthèse et Physico-Chimie des Molécules d'Intérêt Biologique (LSPCMIB) de l'Université Paul Sabatier, Toulouse III. Cette collaboration a été essentielle pour associer les compétences de ces deux laboratoires. La technologie des poudres, des procédés et la mécano-chimie pour le premier, et pour le deuxième l'expérience pour le développement et la synthèse des molécules présentant de potentiels intérêts biologiques. Ces deux laboratoires sont membres de la Plateforme Gala en galénique avancée, laquelle a été l'entité fédératrice qui a permis d'établir cette collaboration.

### Objectif général de la recherche

L'objectif de cette thèse est l'utilisation de la mécano-chimie en tant que voie durable pour la production de molécules d'intérêt pharmaceutique, en même temps qu'elle vise à contribuer à la connaissance de ce domaine, en utilisant les réactions dans un broyeur comme moyens de compréhension des états pouvant être atteints par activation mécanique. La thèse se propose de rapprocher les études de différentes voies réactionnelles et la transformation globale obtenue dans les mécanoréacteurs.

#### *Objectifs spécifiques*

- Synthèse de molécules obtenues directement par réaction entre solides, en accord avec les principes de la *Chimie Verte* ;
- Conception de composés possédant des structures connues pour leur action thérapeutique ;
- Identification des espèces intermédiaires (de nature physique ou chimique différente) qui sont potentiellement générées durant les procédés de broyage ;

---

<sup>7</sup> Carlier, L.; Baron, M.; Chamayou, A.; Couarraze, G. Greener pharmacy using solvent-free synthesis: Investigation of the mechanism in the case of dibenzophenazine. *Powder Technol.* **2013**, *240*, 41–47.

<sup>8</sup> Haruta, N.; Sato, T.; Tanaka, K.; Baron, M. Reaction mechanism in the mechanochemical synthesis of dibenzophenazine: application of vibronic coupling density analysis. *Tetrahedron Lett.* **2013**, *54*, 5920–5923.

<sup>9</sup> CNRS/JSPS France-Japan joint research project (n° PRC0709, 2013-2014).

- Investigation des paramètres de fonctionnement du dispositif de broyage et estimation de l'énergie d'activation de la réaction mécano-chimique ;
- Identification des similarités dans les différentes transformations observées lors des réactions mécano-chimiques afin de déterminer quels aspects influencent et orientent principalement ces systèmes solides.

### **CHAPITRE 1. Bibliographie générale**

Les fondamentaux de la mécano-chimie et les recherches pertinentes relatives à cette thèse sont présentés dans cette revue de la littérature. La raison pour laquelle ce domaine a attiré l'attention vient d'une approche plus respectueuse de l'environnement qui permet la synthèse sans solvant avec des rendements quantitatifs, ainsi que du caractère unique de certaines transformations qui ne sont possibles que par cette voie. Le cadre vert dans lequel s'inscrit la mécano-chimie est évoqué, mais l'accent est mis sur les aspects mécanistiques. Les transitions subies par la poudre lors de l'application de l'action mécanique sont discutées, ainsi que les résultats les plus importants contribuant à la mécano-chimie. L'objectif de cette brève revue est de donner un panorama des phénomènes susceptibles de se produire lors d'un stress mécanique ou aussitôt après son application, et qui sont la conséquence de l'action mécanique. En outre, elle vise à poser un regard critique sur les points non encore élucidés.

### **CHAPITRE 2. Procédures expérimentales et techniques de caractérisation**

Les réacteurs généralement utilisés en mécano-chimie sont des dispositifs de broyage à billes ou à boulets et des machines permettant d'atteindre des pressions élevées. Dans le cas présent, l'appareil expérimental utilisé tout au long des études est le broyeur à bille vibrant Pulverisette 0 (Fritsch). Il est décrit dans ce chapitre dans lequel se trouvent également les principales techniques utilisées pour l'analyse et la caractérisation. Par contre pour le cas des hydrazones, les caractéristiques de chaque méthode de synthèse et des évaluations biologiques sont incluses dans le chapitre concerné.

### **CHAPITRE 3. Investigation des mécanismes de la mécanosynthèse des 1,4-diazines**

Cette première partie des résultats est dédiée à la compréhension fondamentale des réactions mécano-chimiques pour la synthèse de 1,4-diazines. Les synthèses de la dibenzo[a,c]phénazine (DBPZ) et de la 2,3-diphénylquinoxaline (DPQ), qui sont des structures chimiques basiques intéressantes pour des molécules thérapeutiques, sont étudiées ici. Ces réactions ont été choisies en fonction des résultats précédemment obtenus et des

mécanismes proposés pour la mécanosynthèse de la DBPZ<sup>7,8</sup>, et pour la similarité de la structure et de la synthèse de la DPQ avec celle de la DBPZ. Les produits ont pu être obtenus dans le broyeur vibrant P0, avec des conversions quantitatives.

Le suivi cinétique a montré que l'étape déterminante est différente pour les deux réactions. Pour la synthèse de la DBPZ, elle suit un modèle du type Avrami-Erofeev de nucléation et croissance et la réaction atteint sa conversion maximale après 240 min de broyage en continu. Dans le cas de la DPQ, la réaction se termine après 60 min de broyage et la cinétique est du type ordre zéro, ce qui peut être expliqué par l'application constante de l'action mécanique. Les différences de réactivité viennent dans un premier temps de la réactivité chimique des 1,2-diones aromatiques, le benzil (BZ) étant plus électrophile que la 9,10-phenanthrenequinone. La nature des solides et leurs propriétés intrinsèques, avec par exemple la densité et le mouvement moléculaire autour des liaisons simples  $\sigma$ , peuvent aussi contribuer aux différences de réactivité observées. Ces effets peuvent également favoriser une réaction plus rapide pour la synthèse de la DPQ parce le BZ est moins dense que la PQ et une rotation est possible autour de la liaison  $\sigma$  entre les deux groupes carbonyles, tandis que la PQ est une molécule constituée uniquement de noyaux aromatiques condensés inscrits dans un plan.

Les mécanismes réactionnels ont été discutés en considérant la possibilité que procure l'énergie mécanique d'exciter la molécule d'*o*-phenylenediamine dans une symétrie  $C_s$ , ce qui permet une addition concertée. Ce mécanisme est possible pour la synthèse de DBPZ en raison de la configuration de carbonyles de la PQ, et n'est pas favorisé dans le cas de la synthèse de la DPQ pour laquelle la conformation *cis* des carbonyles de la 1,2-dione de départ, BZ, n'est pas privilégiée. La RMN <sup>13</sup>C CP-MAS et les mesures calorimétriques ont renforcé l'hypothèse de la formation d'un intermédiaire sous l'action mécanique pour la DBPZ, qui n'a pas été mis en évidence pour la synthèse de la DPQ. La RMN <sup>13</sup>C CP-MAS a détecté un intermédiaire contenant une fonction C-OH pour la DBPZ, non observé dans le cas de la DPQ. En outre, les mesures calorimétriques ont révélé que le dégagement de chaleur ne peut être entièrement attribué à la chaleur de réaction de la DBPZ, alors qu'il semble être très proche dans le cas de la DPQ. La différence observée pour la première a été associée à l'accumulation d'un intermédiaire AB au cours du broyage, lequel commence à se transformer en produit final, ce qui dégage plus de la chaleur, lorsque les mesures calorimétriques sont en cours. En d'autres termes, de plus grandes quantités de ce produit intermédiaire, qui peut correspondre au produit de l'addition concertée, sont générées pendant le broyage et lorsque le mélange de poudres est introduit dans le calorimètre, tout se passe comme si la réaction



commençait à partir de AB au lieu de A+B. L'intermédiaire AB étant à un niveau d'énergie élevé la quantité d'énergie libérée lors de cette transformation est supérieure à celle de A+B. Par contre cette réaction n'est possible seulement qu'à travers un mécanisme pas à pas.

La DRX a montré des arrangements différents pour les produits solides en fonction de la voie de préparation. Les produits préparés mécano-chimiquement sont différents de ceux obtenus par recristallisation à partir d'une solution. Ce fut le cas pour les deux : la DPQ et la DBPZ. Des différences dans les intensités et les positions des pics de Bragg peuvent provenir de la présence de molécules d'eau dans le réseau cristallin, mais d'autres investigations, y compris la définition des structures cristallines sont essentielles pour élucider les différents diagrammes de la XRD. Les diffractogrammes de la DPQ ont montré des changements en fonction de la chaleur ou de l'humidité, indiquant une interconversion de cristal à cristal. La synthèse de cette molécule par broyage génère aussi une certaine phase amorphe qui continue à cristalliser après broyage. D'autre part, les formes cristallines de la DBPZ semblent stables et aucun changement significatif n'a été observé après les traitements thermiques ou à l'humidité.

En résumé, l'action mécanique est capable d'induire des transformations autres que celles obtenues pour les réactions en solution, ce qu'illustre la synthèse de DBPZ avec leur intermédiaire formé sous action mécanique. La comparaison avec la synthèse de la DPQ était importante pour renforcer l'hypothèse d'un intermédiaire généré et accumulé lors de l'application d'une contrainte mécanique. Plusieurs facteurs interviennent sur la réaction mécano-chimique. Le fait qu'aucun solvant ne soit utilisé, évitant la dissolution et la solvation, rend les réactions possibles à partir des états excités directement induits par l'action mécanique. D'un autre côté, ces états intermédiaires génèrent des niveaux élevés d'énergie, qui seraient instables en milieux solvatés, mais qui peuvent s'accumuler ici en phase solide. La transformation vers le produit final peut être favorisée par la proximité des molécules, ce qui augmente la tendance à la cristallisation après avoir atteint un certain taux de conversion. La compréhension des conséquences de cette action mécanique au niveau moléculaire et des orbitales est très importante en raison de la possibilité de mettre en évidence des mécanismes très originaux qui apparaissent au sein de solides divisés subissant des stress mécaniques. Cette compréhension va permettre de poursuivre les progrès dans ce domaine de la mécano-chimie, y compris utilisation de la modélisation moléculaire comme la DFT ou du couplage vibronique.

#### **CHAPITRE 4. Études cinétiques de la synthèse mécaniquement induite de la 2,3-diphénylquinoxaline**

Ce chapitre concerne les études paramétriques pour la mécanosynthèse de la DPQ dans le broyeur vibrant Pulverisette 0 (P0) à partir de la réaction entre l'*o*-phenylenediamine (PDA) et le benzil (BZ). Cette synthèse a été choisie parce que sa transformation est rapide comme cela a été démontré dans le chapitre précédent et également parce que la méthodologie analytique pour le suivi cinétique permet l'identification et la quantification des réactifs et du produit.

Les paramètres techniques adaptés à la P0, tel que le matériel de broyage (bol et billes), la taille et le poids des billes ont été étudiés. Des expériences en fonction de la température de broyage ont été réalisées pour déterminer les paramètres cinétiques en utilisant l'approche classique de Arrhenius ou Eyring. Enfin, la granulométrie de la matière première, le réactif BZ, a montré une légère influence sur la cinétique de transformation.

Parmi les paramètres étudiés, la température de broyage a montré une forte influence sur la cinétique de transformation, comme pour la majorité des réactions chimiques. Les graphiques à partir des équations d'Arrhenius et d'Eyring ont pu être construits pour une gamme de température de broyage située entre 12 et 35 °C, ce qui a permis la détermination d'une énergie d'activation apparente ( $E_a$ ) ou d'une enthalpie d'activation ( $\Delta H^\ddagger$ ) pour la première et la dernière équation respectivement. Ces énergies ont varié en fonction de la plage de température, ce qui indique un changement dans le mécanisme de réaction : une fusion eutectique à partir d'un contact entre les solides telle que l'ont révélée les techniques couplées de DSC et microscopie.

#### **CHAPITRE 5. L'application de la mécano-chimie en tant que voie verte pour la synthèse de molécules d'intérêt pharmaceutique : la mécanosynthèse des hydrazones et leur activité contre *Mycobacterium tuberculosis***

Dans ce chapitre on a exploré l'application de la voie mécano-chimique pour la synthèse des hydrazones à potentiel pharmaceutique. Après les discussions des chapitres 3 et 4 concernant la compréhension de certains aspects fondamentaux et du procédé de mécano-chimie, cette voie est donc appliquée en tant que protocole pour des synthèses de molécules potentiellement actives avec un temps de réaction réduit et d'excellents rendements.

Premièrement, nous avons synthétisé des hydrazones phénoliques à partir des réactifs solides (aldéhydes et hydrazines). Les résultats ont permis une discussion par rapport aux hydrazines solides en termes de réactivité électronique, et donc de réactivité chimique, et de la

contribution de la forme solide pour augmenter ou réduire le taux de conversion pour un même temps de broyage.

La deuxième série d'hydrazones a été préparée en utilisant seulement l'hydrazine isoniazide et différents aldéhydes qui contiennent des motifs imidazole, indazole ou indole. Pour ces cas-là, l'utilisation de l'acide *p*-toluène sulfonique (*p*-TSA) s'est révélée nécessaire, en raison des réactivités réduites des aldéhydes. En conséquence de l'ajout de *p*-TSA au milieu, des conversions maximales ont pu être obtenues en une ou deux heures de réaction. Cette augmentation des taux de conversion est due aux effets catalytiques du *p*-TSA et également à l'apparition de fusions eutectiques lorsqu'il a été introduit dans le mélange des réactifs solides (isoniazide + indole/indazole aldehyde + *p*-TSA).

Les hydrazones sont principalement présentes en tant que mélange de conformères dans une solution de DMSO, en raison d'une possible rotation autour de la liaison amide. Les calculs DFT, les études de RMN dynamiques ainsi que les spectres de  $^1\text{H}$  RMN et  $^{13}\text{C}$  RMN simulés et expérimentaux ont été utilisés dans le cas des dérivés de l'isoniazide pour identifier et confirmer ces conformères.

Les hydrazones ont fait l'objet d'essais biologiques contre *Mycobacterium tuberculosis*, lesquelles ont révélé de bonnes à excellentes activités pour les molécules portant le fragment isoniazide, par rapport à l'isoniazide lui-même, qui est un médicament de première ligne. La stabilité en solution des composés principaux a été évaluée et aucune hydrolyse n'a été observée pendant une période prolongée en solution.

### Conclusions Générales

La mécanochemie est clairement définie comme un domaine des sciences chimiques et physico-chimiques. Les possibilités de transformation des matières premières lors de l'application de l'énergie mécanique, principalement dans les appareils de broyage à billes, ont ouvert le champ à de vastes applications, au delà du domaine des minéraux et du simple broyage pour la réduction de taille. Les transformations physico-chimiques, les interactions intermoléculaires, la catalyse et les réactions chimiques avec formation de liaisons covalentes, illustrent la polyvalence de cette voie dans le cas des systèmes organiques. Elle est également considérée comme une technique écologique pour le développement d'une chimie plus durable, y compris pour les produits pharmaceutiques.

Dans la présente thèse, les études mécanochemiques ont été réalisées à trois niveaux distincts : l'interprétation mécanistique électronique de réactions induites mécaniquement, la transformation de la poudre et les études cinétiques associées, et enfin, l'application vers la

synthèse de composés pharmaceutiquement attractifs, dans le cadre des économies d'atomes selon les principes de la chimie verte. Il a été possible d'étudier le niveau électronique, même de façon indirecte, en passant par le procédé de broyage, jusqu'à l'application de la mécanochimie à des fins de chimie médicinale.

En récapitulant, l'une des ambitions de cette thèse était d'identifier les caractéristiques souvent présentes dans l'ensemble des systèmes étudiés, pour la synthèse de DBPZ et DPQ, et également pour la synthèse des hydrazones. Ces observations impliquent les transformations subies par la poudre ainsi que les aspects pouvant influencer les réactions solides dans des conditions de broyage.

- Le broyage continu peut conduire à la génération des phases amorphes qui poursuivent leur cristallisation après broyage. Cela peut induire une fusion eutectique, et la réaction peut également se produire entre espèces cristallines ;
- L'énergie mécanique peut diminuer la barrière d'activation globale pour les réactions à l'état solide ;
- La réactivité électronique de l'entité chimique joue sans aucun doute un rôle important sur le taux de conversion de la réaction, cependant, elle ne peut pas être considérée de manière isolée ;
- La proximité des molécules dans les cristaux, et l'espace permettant leur mobilité, peut être estimé par la densité absolue des cristaux, avec pour les densités plus faibles un taux de conversion de la réaction amélioré parce que les molécules peuvent se déplacer plus facilement ;
- La mobilité des molécules dans les structures rigides, tels que dans les solides, peut encore être augmentée en augmentant le nombre de liaisons simples  $\sigma$ , dans la région du groupe réactif. Ces liaisons  $\sigma$  apportent certains degrés de liberté, ce qui rend la réaction plus facile. Le contraire est observé lorsque le site réactif est plus proche de structures à fort encombrement stérique ou lorsqu'il n'y a pas de liaisons simples susceptibles d'entrer en rotation. Cela retarde et empêche la réaction ;
- L'énergie mécanique appliquée de façon continue à la matière solide est capable de générer des structures excitées qui ouvrent des voies de réactions différentes de celles réalisées dans des milieux solvants. Des intermédiaires peuvent se former et s'accumuler dans le mélange solide.

Les événements se produisant au niveau macroscopique ainsi qu'au niveau électronique ont été discutés de façon concertée, ce qui a permis de mieux comprendre les

réactions mécano-chimiques. L'approfondissement des investigations permettra d'apporter davantage d'explications. Mais les résultats présentés peuvent d'ores et déjà contribuer au choix de couples réactifs pour l'optimisation des conversions ainsi que pour l'obtention de structures conçues d'une manière durable.

---

# APPENDIX

---



## APPENDIX I – KINETIC MODELS FOR SOLID-STATE REACTIONS

The mechanisms of reactions may be revealed from chemical dynamics during the reactions. The chemical kinetics studies the reaction rates and the trends can indicate one or another limiting step, which enables some deduction of the reaction pathway. This is widely used for gas phase and reactions in solution, i.e., homogenous reactions. For solid-state reactions, the most of the kinetic concepts come originally from homogeneous systems but the kinetic models have been developed or modified to include the specificities of heterogeneous media. Khawan and Flanagan (2006<sup>a,b</sup>)<sup>1</sup> reviewed the basics and mathematical fundamentals of solid-state reaction models. Further and more complete development of those models can be found in Brown et al. (1980),<sup>2</sup> Galwey and Brown (1999)<sup>3</sup> and House (2007).<sup>4</sup> These latter are books or book chapters dedicated to chemical kinetics, essentially for solid-state reactions of inorganics. Indeed, the kinetic models for solid-state reactions are successfully applied to inorganic thermal decompositions, majorly, and dehydrations.

**Table** summarizes rate laws in the integral form as function of the extent of the reaction or conversion fraction ( $\alpha$ ) for the most used kinetic models for solids.  $\alpha$  can be determined by several analytical methods, each one the most adapted for the respective case. For gravimetric measurement,  $\alpha$  is defined by

$$\alpha = \frac{m_0 - m_t}{m_0 - m_\infty} \quad (3)$$

where,  $m_0$  is the initial weight,  $m_t$  is the weight at time  $t$ , and  $m_\infty$  is the final weight.

Then, the rate of the reaction can be generally described by

$$\frac{d\alpha}{dt} = A e^{-\left(\frac{E_a}{RT}\right)} f(\alpha) \quad (4)$$

where,  $A$  is the preexponential (frequency) factor,  $E_a$  is the activation energy,  $T$  is absolute temperature,  $R$  is the gas constant,  $f(\alpha)$  is the reaction model (differential form).

<sup>1</sup> Khawam, A.; Flanagan, D. R. Basics and applications of solid-state kinetics: A pharmaceutical perspective. *J. Pharm. Sci.* **2006**, *95*, 472–498. bKhawam, A.; Flanagan, D. R. Solid-state kinetic models: Basics and mathematical fundamentals. *J. Phys. Chem. B* **2006**, *110*, 17315–17328.

<sup>2</sup> Brown, M. E.; Dollimore, D.; Galwey, A. K. Theory of Solid State Reaction Kinetics. In *Reactions in the Solid State*; Bamford, C. H.; Tipper, C. F. H., Eds.; Comprehensive Chemical Kinetics; Elsevier, 1980; Vol. 22, pp. 41–113.

<sup>3</sup> Galwey, A. K.; Brown, M. E. Kinetic Models for solid state reactions. In *Thermal Decomposition of Ionic Solids: chemical properties and reactivities of ionic crystalline phases*; Galwey, A. K.; Brown, M. E., Eds.; Studies in Physical and Theoretical Chemistry; Elsevier, 1999; Vol. 86, pp. 75–115.

<sup>4</sup> House, J. E. Kinetics of Reactions in Solid State. In *Principles of Chemical Kinetics*; Elsevier, 2007; pp. 229–265.



**Table A.I** Rate laws for reactions in solids.

<b>Model</b>		<b>Integral form <math>g(\alpha) = kt</math></b>
<b><i>Nucleation models</i></b>		
<b>Pn</b>	Power Law	$\alpha^{1/n}$
<b>A2</b>	Avrami-Erofeev (two-dimensional growth of nuclei)	$[-\ln(1 - \alpha)]^{1/2}$
<b>A3</b>	Avrami-Erofeev (three-dimensional growth of nuclei)	$[-\ln(1 - \alpha)]^{1/3}$
<b>A4</b>	Avrami-Erofeev	$[-\ln(1 - \alpha)]^{1/4}$
<b>B1</b>	Prout-Tompkins	$\ln[\alpha / (1 - \alpha)]$
<b><i>Geometrical contracting models</i></b>		
<b>R2</b>	Contracting area	$1 - (1 - \alpha)^{1/2}$
<b>R3</b>	Contracting volume	$1 - (1 - \alpha)^{1/3}$
<b><i>Diffusion models</i></b>		
<b>D1</b>	One-dimensional diffusion	$\alpha^2$
<b>D2</b>	Two-dimensional diffusion	$((1 - \alpha)\ln(1 - \alpha)) + \alpha$
<b>D3</b>	Three-dimensional diffusion (Jander equation)	$(1 - (1 - \alpha)^{1/3})^2$
<b>D4</b>	Ginstling-Brounstein	$1 - (2/3)\alpha - (1 - \alpha)^{2/3}$
<b><i>Reaction-order models</i></b>		
<b>F0</b>	Zero-order	$\alpha$
<b>F1</b>	First-order	$-\ln(1 - \alpha)$
<b>F2</b>	Second-order	$[1/(1 - \alpha)] - 1$
<b>F3</b>	Third-order	$(1/2)[(1 - \alpha)^{-2} - 1]$

Most of kinetic models are based on mechanistic grounds. Some of them have physicochemical meaning, but others are purely mathematical representations. According to the mechanistic basis, the models presented in **Table** are classified as nucleation, geometrical contraction, diffusion and reaction order models. Khawam and Flanagan (2006<sup>a</sup>)<sup>1</sup> summed them up as follows:

*Nucleation models.* The rate-limiting step is assumed to be the formation and growth of nuclei, which is a finite quantity of product in the reactant lattice. After formation, a nucleus grows and the nucleation rate is different from that of nuclei growth.

- Power law (P) models: The rate of nucleation follows the power law and nuclei growth is assumed constant;
- Avrami-Erofeev equation (A2, A3, A4): It considers a random nuclei that grow and ingest other;

- The Prout-Tompkins equation (B1): It concerns autocatalytic model and the rate of a solid-state reaction is assumed to be controlled by linearly growing nuclei that branch into chains.

Nucleation models have described many solid-state reactions including crystallization, crystallographic transition, decomposition, adsorption, hydration and desolvation.

*Geometrical contraction models (Phase boundary models).* Nucleation is assumed to be instantaneous throughout the surface and the rate-limiting step is the progress of the product layer from the surface (phase boundaries) of the crystal inward. Depending on crystal shape, different mathematical models may be derived, such as moving surface (R2) as a cross-section of a cylinder, or contracting volume (R3) as happens for a sphere or a cube.

*Diffusion models (D).* The rate-limiting step is the diffusion of reactants into reaction sites or products away from the reaction sites.

The mobility of constituents in the system is the major difference between homogeneous and heterogeneous kinetics. While reactant molecules are usually readily available to one another in homogeneous systems, solid-state reactions often occur between crystal lattices or with molecules that must permeate into lattices where motion is restricted and may depend on lattice defects. In diffusion-limited reaction, the movement of one reactant species to, or a product from, a reaction interface determines the overall rate. This is less usual for solid decomposition reactions, but in contrast, a diffusion process plays an important role and can be the rate-controlling step for interactions between two solids, where reactants are originally retained in separate lattices.

There is a number of ancient works that were dedicated to investigate solid-state reactions between two organic solids. They concerned in face two cylindrical pellets of the reactants with the interface marked and put this system in the certain condition. Ramachandran et al. (1983)<sup>5</sup> performed these experiments and studied the effect of compaction pressure, the particle size, porosity and temperature for the case of phthalic anhydride and *p*-nitroaniline. The same group also studied a mixed system for succinic anhydride and found that the

---

<sup>5</sup> Ramachandran, S.; Baradarajan, A.; Satyanarayana, M. Diffusion and reaction in solids. *Powder Technol.* **1983**, *34*, 143–149.

reaction was phase boundary controlled (Narayan et al., 1982).<sup>6</sup> Tamhankar and Doraiswamy (1978)<sup>7</sup> developed a model for coupled diffusion and reaction in solid-solid systems in form of pellets. Arrowsmith and Smith (1966)<sup>8</sup> also produced pellets to investigate diffusion for phthalic anhydride-sulphathiazole systems, while Rastogi et al. (1962)<sup>9</sup> used capillaries and could observe that the diffusion was the rate-limiting step for naphthalene and picric acid reaction because the phase-boundary process occurred rapidly and the equilibrium is quickly established.

The issue of using a diffusion-controlled model is highly adapted for static systems as the above-mentioned, where the product is generated at the contact zone between two reactant particles and, if immobile, remains there. However, these models have to be carefully treated for mechanochemical reactions as they consist of dynamic moving systems.

*Order-based reaction models.* The rate law is based on the reaction order, similar to the same rate expressions in homogeneous kinetics.

In these models, the reaction rate is generally proportional to concentration, amount or fraction remaining of reactant(s) raised to a particular power (integral or fractional) which is the reaction order. As concentration is difficult to conceptualize for solids and so, it is not usually a meaningful term in solid-state reactions, and so, the order-based models are derived from the following general equation in terms of conversion fraction ( $\alpha$ ).

$$\frac{d\alpha}{dt} = k(1 - \alpha)^n \quad (5)$$

where  $da/dt$  is the rate of reaction,  $k$  is the rate constant, and  $n$  is the reaction order.

For zero-order ( $n = 0$ ), the model becomes

$$\frac{d\alpha}{dt} = k \quad (6)$$

that after separating variables and integrating is

$$\alpha = kt, \quad (7)$$

which corresponds to the F0 model in **Table**. The same mathematical manipulation for any other  $n$  is possible leading to F $n$  order-based reaction model.

---

<sup>6</sup> Narayan, R. A.; Baradarajan, A.; Satyanarayana, M.; Ramachandran, S. Solid state reaction of mixed powder compacts of succinic anhydride and paranitraniline. *Powder Technol.* **1982**, *33*, 187–193.

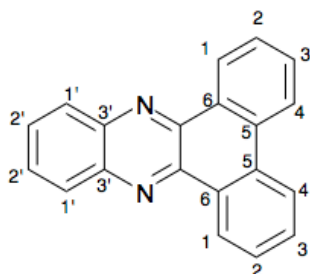
<sup>7</sup> Tamhankar, S. S.; Doraiswamy, L. K. Solid-Solid Reactions. Diffusion and Reaction in Pellet-Pellet Systems. *Ind. Eng. Chem. Fundam.* **1978**, *17*, 84–89.

<sup>8</sup> Arrowsmith, R. J.; Smith, J. M. Diffusion and Reaction in Solids. *Ind. Eng. Chem. Fundam.* **1966**, *5*, 327–335.

<sup>9</sup> Rastogi, R. P.; Bassi, P. S.; Chadha, S. L. Kinetics of reaction between naphthalene and picric acid in the solid state. *J. Phys. Chem.* **1962**, *66*, 2707–2708.

## APPENDIX II – CHARACTERIZATION DATA

The characterization data for all hydrazones are summarized as follows. The chemical shift  $\delta$  (ppm) is attributed for the major conformer in the case of hydrazones. For DBPZ and DPQ, only  $^1\text{H}$  NMR,  $^{13}\text{C}$  NMR and HRMS/MS are shown.



Chemical formula:  $\text{C}_{20}\text{H}_{12}\text{N}_2$   
Molecular Weight: 280.32

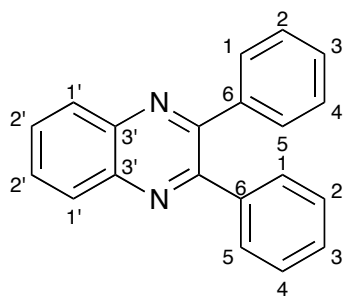
**Dibenzo[a,c]phenazine (DBPZ).** mp: 224 °C

$^1\text{H}$  NMR (300 MHz, Chloroform-*d*)  $\delta$  ppm: 7.68 – 7.83 (m, 4H,  $\text{H}_{2,3}$ ), 7.87 (dd,  $J = 6.6, 3.4$  Hz, 2H,  $\text{H}_{2'}$ ), 8.36 (dd,  $J = 6.5, 3.4$  Hz, 2H,  $\text{H}_{1'}$ ), 8.54 (dd,  $J = 7.7, 1.7$  Hz, 2H,  $\text{H}_1$ ), 9.41 (dd,  $J = 7.9, 1.7$  Hz, 2H,  $\text{H}_4$ ).

$^{13}\text{C}$  NMR (75 MHz, Chloroform-*d*)  $\delta$  ppm: 122.89 (s, 2C,  $\text{C}_1$ ), 126.32 (s, 2C,  $\text{C}_4$ ), 127.94 (s, 2C,  $\text{C}_2$ ), 129.30 (s, 2C,  $\text{C}_{1'}$ ), 129.86 (s, 2C,  $\text{C}_{2'}$ ), 129.99 (s, 2C,  $\text{C}_6$ ), 130.39 (s, 2C,  $\text{C}_1$ ), 132.03 (s, 2C,  $\text{C}_5$ ), 141.94 (s, 2C, C=N), 142.27 (s, 2C,  $\text{C}_1, \text{C}_{3'}$ ).

MS (ES, TOF,  $\text{CH}_2\text{Cl}_2$ ) m/z: 281.1081 [ $\text{M}+\text{H}^+$ ]

HRMS (ES, TOF) m/z:  $\text{C}_{20}\text{H}_{13}\text{N}_2$  (calc./found) 281.1079/281.1081 [ $\text{M}+\text{H}^+$ ].



Chemical formula:  $\text{C}_{20}\text{H}_{14}\text{N}_2$   
Molecular Weight: 282.34

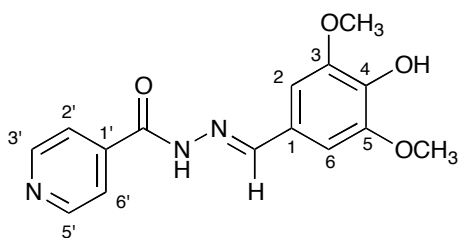
**2,3-diphenylquinoxaline (DPQ).** mp: 125 °C

$^1\text{H}$  NMR (300 MHz, Chloroform-*d*)  $\delta$  ppm: 7.30 – 7.46 (m, 6H,  $\text{H}_{2,3,4}$ ), 7.47 – 7.62 (m, 4H,  $\text{H}_{1,5}$ ), 7.80 (dd,  $J = 6.4, 3.4$  Hz, 2H,  $\text{H}_{2'}$ ), 8.21 (dd,  $J = 6.4, 3.4$  Hz, 2H,  $\text{H}_{1'}$ ).

$^{13}\text{C}$  NMR (75 MHz, Chloroform-*d*)  $\delta$  ppm: 128.27 (s, 4C,  $\text{C}_{1,5}$ ), 128.81 (s, 2C,  $\text{C}_3$ ), 129.20 (s, 4C,  $\text{C}_{2,4}$ ), 129.85 (s, 2C,  $\text{C}_{1'}$ ), 129.97 (s, 2C,  $\text{C}_{2'}$ ), 139.07 (s, 2C,  $\text{C}_6$ ), 141.22 (s, 2C,  $\text{C}_{3'}$ ), 153.47 (s, 2C, C=N).

MS (ES, TOF, MeOH) m/z: 283.1237 [ $\text{M}+\text{H}^+$ ]

HRMS (ES, TOF) m/z:  $\text{C}_{20}\text{H}_{15}\text{N}_2$  (calc./found) 283.1235/283.1237 [ $\text{M}+\text{H}^+$ ].



Chemical formula:  $C_{15}H_{15}N_3O_4$   
 Molecular Weight: 301.30  
 Rf: 0.14 (EtAc/PE 1:1 v/v)

**(E)-N'-(4-hydroxy-3,5-dimethoxybenzylidene)isonicotinohydrazide (1a).** mp: 228 °C.

$^1\text{H NMR}$  (300 MHz,  $\text{DMSO-}d_6$ )  $\delta$  ppm: 3.83 (s, 6H,  $\text{OCH}_3$ ), 7.01 (s, 2H,  $\text{H}_{2,6}$ ), 7.81 (dd,  $J = 4.5, 1.7$  Hz, 2H,  $\text{H}_{2',6'}$ ), 8.35 (s, 1H,  $\text{H-C=N}$ ), 8.76 (dd,  $J = 4.5, 1.7$  Hz, 2H,  $\text{H}_{3',5'}$ ), 8.98 (s, 1H, OH), 11.94 (s, 1H, NH).

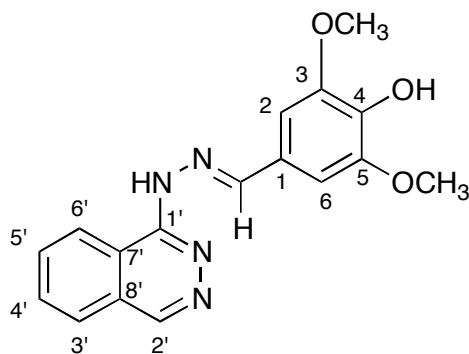
$^{13}\text{C NMR}$  (101 MHz,  $\text{DMSO-}d_6$ )  $\delta$  ppm: 56.54 (s, 2C,  $\text{OCH}_3$ ), 105.35 (s, 2C,  $\text{C}_{2,6}$ ), 121.96 (s, 2C,  $\text{C}_{2',6'}$ ), 124.70 (s, 1C,  $\text{C}_1$ ), 138.77 (s, 1C,  $\text{C}_4$ ), 141.16 (s, 1C,  $\text{C}_{1'}$ ), 148.63 (s, 2C,  $\text{C}_{3',5'}$ ), 150.16 (s, 1C,  $\text{C=N}$ ), 150.74 (s, 1C,  $\text{C}_{3,5}$ ), 161.85 (s, 1C,  $\text{C=O}$ ).

**FTIR (KBr)**  $\nu$   $\text{cm}^{-1}$ : 3403 (O–H), 3195 (H–C=N), 2997 (C– $\text{H}_{\text{ar}}$ ), 2946 – 2846 (C–H, O– $\text{CH}_3$ ), 1648 (C=N), 1586 (C=C ar), 1550 (C $_{\text{ar}}$   $\rightleftharpoons$  N), 1515 (C=C ar), 1219 (C–O), 1119 (CO).

**UV (EtOH, 39.83  $\mu\text{M}$ , 25°C):**  $\lambda = 336$  nm,  $\epsilon = 24116$   $\text{mol}^{-1} \cdot \text{L} \cdot \text{cm}^{-1}$

**MS (ES, TOF, MeOH) m/z:** 302.1142 [ $\text{M}+\text{H}^+$ ]

**HRMS (ES, TOF) m/z:**  $C_{15}H_{15}N_3O_4$  (calc./found) 302.1141/302.1142 [ $\text{M}+\text{H}^+$ ].



Chemical formula:  $C_{15}H_{16}N_4O_3$   
 Molecular Weight: 324.33  
 Rf: 0.49 (EtAc/PE 1:1 v/v)

**(E)-4-hydroxy-3,5-dimethoxybenzaldehyde phthalazin-1-ylhydrazone (2a).** mp: 179 °C;

$^1\text{H NMR}$  (300 MHz,  $\text{DMSO-}d_6$ )  $\delta$  ppm: 3.86 (s, 6H,  $\text{OCH}_3$ ), 7.33 (s, 2H,  $\text{H}_{2,6}$ ), 7.60 – 7.99 (m, 3H,  $\text{H}_{3',4',5'}$ ), 8.24 (s, 1H,  $\text{H}_{2'}$ ), 8.46 (s, 1H,  $\text{H}_{6'}$ ), 8.84 (s, 1H,  $\text{HC=N}$ ), 10.50 (s, 1H, OH).

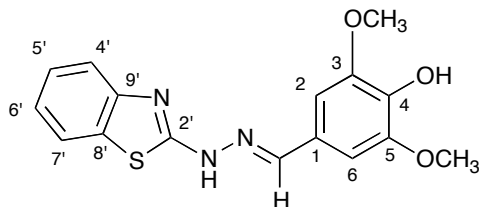
$^{13}\text{C NMR}$  (75 MHz,  $\text{DMSO-}d_6$ )  $\delta$  ppm: 56.66 (s, 2C,  $\text{OCH}_3$ ), 106.30 (s, 2C,  $\text{C}_{2,6}$ ), 124.37, 125.81, 127.15, 127.58, 132.47, 133.24, 138.40, 148.07, 148.48, 154.15 (C=N).

**FTIR (KBr)**  $\nu/\text{cm}^{-1}$ : 3372 (O–H), 1607 (C=N), 1592 (C=C ar), 1515 (C=C ar), 1219 (C–O), 1117 (C–O).

UV (EtOH, 37 $\mu$ M, 21°C):  $\lambda=378$  nm,  $\epsilon=26450$  mol<sup>-1</sup>.L.cm<sup>-1</sup>;  $\lambda=304$  nm,  $\epsilon=16739$  mol<sup>-1</sup>.L.cm<sup>-1</sup>.

MS (ES, TOF, MeOH) m/z: 325.1295 [M+H<sup>+</sup>]

HRMS (ES, TOF) m/z: C<sub>17</sub>H<sub>17</sub>N<sub>4</sub>O<sub>3</sub> (calc./found) 325.1301/325.1295 [M+H<sup>+</sup>].



Chemical formula: C<sub>16</sub>H<sub>15</sub>N<sub>3</sub>O<sub>3</sub>S

Molecular Weight: 324.33

Rf: 0.49 (EtAc/PE 1:1 v/v)

**(E)-4-Hydroxy-3,5-dimethoxybenzaldehyde-1,3-benzothiazol-2-ylhydrazone (3a).** mp: 248 °C.

<sup>1</sup>H NMR (300 MHz, DMSO-*d*<sub>6</sub>)  $\delta$  ppm: 3.83 (s, 6H, OCH<sub>3</sub>), 6.99 (s, 2H, H<sub>2,6</sub>), 7.09 (t, *J* = 7.8 Hz, 1H, H<sub>5'</sub>), 7.28 (t, *J* = 8.2 Hz, 1H, H<sub>6'</sub>), 7.41 (d, *J* = 7.9 Hz, 1H, H<sub>4'</sub>), 7.76 (d, *J* = 7.8 Hz, 1H, H<sub>7'</sub>), 8.02 (s, 1H, HC=N), 8.85 (s, 1H, OH), 12.13 (s, 1H, NH).

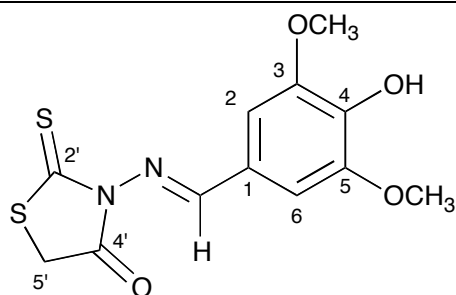
<sup>13</sup>C NMR (101 MHz, DMSO-*d*<sub>6</sub>)  $\delta$  ppm: 56.43 (s, 2C, OCH<sub>3</sub>) 104.64 (s, 2C, C<sub>2,6</sub>) 121.81 (s, 1C, C<sub>6'</sub>), 121.94 (s, 1C, C<sub>5'</sub>), 125.12 (s, 1C, C<sub>1</sub>), 126.33 (s, 2C, C<sub>4',7'</sub>), 138.04 (s, 1C, C<sub>4</sub>), 148.64, 167.28 (s, 1C, C<sub>2</sub>).

FTIR (KBr)  $\nu$  cm<sup>-1</sup>: 3542 (N-H), 3500 (O-H), 3200 (H-C=N), 2956 (C-H<sub>ar</sub>), 2840 (C-H, O-CH<sub>3</sub>), 1612 (C=N), 1574 (C=C ar), 1517 (C=C ar), 1323 (C-N), 1249 (O-C<sub>ar</sub>), 1222 (O-C), 1114 (O-C).

UV (EtOH, 27.32  $\mu$ M, 25°C):  $\lambda=346$ ,  $\epsilon=31920$  mol<sup>-1</sup>.L.cm<sup>-1</sup>

MS (ES, TOF, MeOH) m/z: 330.0915 [M+H<sup>+</sup>]

HRMS (ES, TOF) m/z: C<sub>16</sub>H<sub>15</sub>N<sub>3</sub>O<sub>3</sub>S (calc./found) 330.0912/330.0915 [M+H<sup>+</sup>].



Chemical Formula: C<sub>12</sub>H<sub>12</sub>N<sub>2</sub>O<sub>4</sub>S<sub>2</sub>

Molecular Weight: 312.36

Rf: 0.14 (PE/EtAc 4:1)

**(E)-3-((4-hydroxy-3,5-dimethoxybenzylidene)amino)-2-thioxothiazolidin-4-one (4a).** mp: 201.5 °C.

<sup>1</sup>H NMR (400 MHz, DMSO-*d*<sub>6</sub>)  $\delta$  ppm: 3.83 (s, 6H, OCH<sub>3</sub>), 4.36 (s, 2H, CH<sub>2</sub>/H<sub>5'</sub>), 7.20 (s, 2H, H<sub>2,6</sub>), 8.49 (s, 1H, HC=N), 9.44 (s, 1H, OH).

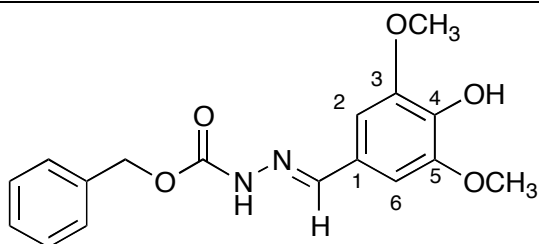
**<sup>13</sup>C NMR (101 MHz, DMSO-*d*<sub>6</sub>) δ ppm:** 35.06 (s, 1C, CH<sub>2</sub>/C<sub>5'</sub>), 56.55 (s, 2C, OCH<sub>3</sub>), 107.07 (s, 2C, C<sub>2,6</sub>), 122.25 (s, 1C, C<sub>1</sub>), 141.24 (s, 1C, C<sub>4</sub>), 148.61 (s, 2C, C<sub>3</sub>), 170.25 (s, 1C, C=O/C<sub>4'</sub>), 171.38 (s, 1C, C=N), 197.15 (s, 1C, C=S/C<sub>5'</sub>).

**FTIR (KBr) ν cm<sup>-1</sup>:** 3470 (N-H), 3473 (O-H), 30118 (H-C=N), 2977 (CH<sub>2</sub>), 2924 (C-H<sub>ar</sub>), 2843 (C-H, -OCH<sub>3</sub>), 1738 (>C=O), 1618 (C=N), 1580 (C=C ar), 1513 (C=C ar), 1323 (C-N), 1222 (O-C<sub>ar</sub>), 1162 (C-O), 1116 (C-O), 1031 (C=S).

**UV (EtOH, 35.21 μM, 25°C):** λ=296, ε=28064 mol<sup>-1</sup>.L.cm<sup>-1</sup>

**MS (ES, TOF, MeOH) m/z:** 313.0318 [M+H<sup>+</sup>]

**HRMS (ES, TOF) m/z:** C<sub>12</sub>H<sub>12</sub>N<sub>2</sub>O<sub>4</sub>S<sub>2</sub> (calc./found) 313.0317/313.0318 [M+H<sup>+</sup>].



Chemical Formula: C<sub>17</sub>H<sub>18</sub>N<sub>2</sub>O<sub>5</sub>  
Molecular Weight: 330.34  
Rf: 0.48 (EtAc/PE 1:1 v/v)

**(E)-benzyl 2-(4-hydroxy-3,5-dimethoxybenzylidene)hydrazinecarboxylate (5a). Mp:** 165 °C.

**<sup>1</sup>H NMR (300 MHz, DMSO-*d*<sub>6</sub>) δ ppm:** 3.79 (s, 6H, OCH<sub>3</sub>), 5.17 (s, 2H, CH<sub>2</sub>), 6.89 (s, 2H, H<sub>2,6</sub>), 7.29 – 7.47 (m, 5H, H<sub>ar</sub>), 7.91 (s, 1H, HC=N), 8.80 (s, 1H, OH), 11.12 (s, 1H, NH).

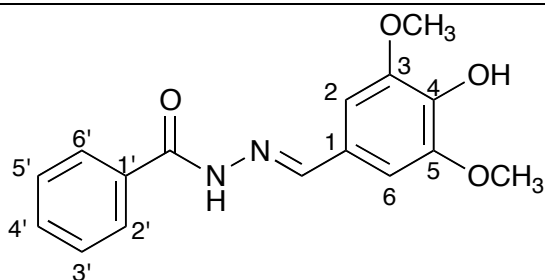
**<sup>13</sup>C NMR (75 MHz, DMSO-*d*<sub>6</sub>) δ ppm:** 56.42 (s, 2C, OCH<sub>3</sub>), 66.25 (s, 2C, CH<sub>2</sub>), 104.61 (s, 2C, C<sub>2,6</sub>), 125.07 (s, 1C, C<sub>1</sub>), 128.48 (s, 1C, C<sub>ar</sub>), 128.46 (s, 2C, C<sub>ar</sub>), 128.88 (s, 2C, C<sub>ar</sub>), 137.12 (s, 1C, C<sub>4</sub>), 137.89 (s, C<sub>hypso</sub>), 145.38 (s, 1C, C=N), 148.53 (s, 2C, C<sub>3,5</sub>), 153.81 (s, 1C, C=O).

**IR (KBr) ν cm<sup>-1</sup>:** 3501 (N-H), 3403 (O-H), 3237 (H-C=N), 3060 (C-H<sub>ar</sub>), 2942 (>C-H<sub>2</sub>), 2842 (C-H, -OCH<sub>3</sub>), 1713 (C=O), 1618 (C=N), 1591 (C=C ar), 1551 (C-N), 1514 (C=C ar), 1247 (C-O-C), 1218 (C-O), 1114 (C-O).

**UV (EtOH, 42.38 μM, 25°C):** λ=234, ε=24752 mol<sup>-1</sup>.L.cm<sup>-1</sup>; λ=310, ε= 24117 mol<sup>-1</sup>.L.cm<sup>-1</sup>.

**MS (ES, TOF, MeOH) m/z:** 331.1293 [M+H<sup>+</sup>]

**HRMS (ES, TOF) m/z:** C<sub>17</sub>H<sub>19</sub>N<sub>2</sub>O<sub>5</sub> (calc./found) 331.1294/331.1293 [M+H<sup>+</sup>].



Chemical Formula: C<sub>16</sub>H<sub>16</sub>N<sub>2</sub>O<sub>4</sub>  
 Molecular Weight: 300.31  
 Rf: 0.18 EtAc/PE (70/30 v/v)

**(E)-N'-(4-hydroxy-3,5-dimethoxybenzylidene)benzhydrazide (6a).** mp: 229 °C.

**<sup>1</sup>H NMR (300 MHz, DMSO-*d*<sub>6</sub>) δ ppm:** 3.83 (s, 6H, OCH<sub>3</sub>), 7.00 (s, 2H, H<sub>2,6</sub>), 7.38 – 7.69 (m, 3H, H<sub>3',4',5'</sub>), 7.91 (dd, *J* = 7.0, 1.7 Hz, 2H, H<sub>2',6'</sub>), 8.35 (s, 1H, HC=N), 8.92 (s, 1H, OH), 11.73 (s, 1H, NH).

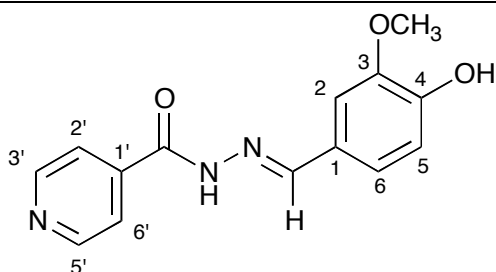
**<sup>13</sup>C NMR (75 MHz, DMSO-*d*<sub>6</sub>) δ ppm:** 56.49 (s, 2C, OCH<sub>3</sub>), 105.10 (s, 2C, C<sub>2,6</sub>), 125.03 (s, 1C, C<sub>1</sub>), 128.01 (s, 2C, C<sub>2',6'</sub>), 128.90 (s, 2C, C<sub>3',5'</sub>), 132.04 (s, 1C, C<sub>4'</sub>), 134.12 (s, 1C, C<sub>1'</sub>), 138.43 (s, 1C, C<sub>4</sub>), 148.60 (s, 2C, C<sub>3,5</sub>), 148.94 (s, 1C, C=N), 163.43 (s, 1C, C=O).

**FTIR (KBr) ν cm<sup>-1</sup>:** 3536 (O–H), 3229 (N–H), 3050-2839 (C–H), 1644 (C=O), 1604 (C=N), 1516 (C=C ar).

**UV (EtOH, 40.07 μM, 20°C):** λ=330 nm, ε=26541 mol<sup>-1</sup>.L.cm<sup>-1</sup>

**MS (ES, TOF, MeOH) m/z:** 301.1188 [M+H<sup>+</sup>]

**HRMS (ES, TOF) m/z:** C<sub>16</sub>H<sub>17</sub>N<sub>2</sub>O<sub>4</sub> (calc./found) 301.1188/301.1188 [M+H<sup>+</sup>].



Chemical Formula: C<sub>14</sub>H<sub>13</sub>N<sub>3</sub>O<sub>3</sub>  
 Molecular Weight: 271.27  
 Rf: 0.17 (EtAc/PE 1:1 v/v)

**(E)-N'-(4-hydroxy-3-methoxybenzylidene)isonicotinohydrazide (1b).** mp: 229 °C.

**<sup>1</sup>H NMR (300 MHz, DMSO-*d*<sub>6</sub>) δ ppm:** 3.84 (s, 3H, OCH<sub>3</sub>), 6.86 (d, *J* = 8.1 Hz, 1H, H<sub>5</sub>), 7.12 (dd, *J* = 8.1, 1.8 Hz, 1H, H<sub>6</sub>), 7.33 (d, *J* = 1.8 Hz, 1H, H<sub>2</sub>), 7.81 (dd, *J* = 4.4, 1.7 Hz, 2H, H<sub>2',6'</sub>), 8.35 (s, 1H, HC=N), 8.78 (dd, *J* = 4.4, 1.7 Hz, 2H, H<sub>3',5'</sub>), 9.62 (s, 1H, OH), 11.89 (s, 1H, NH).

**<sup>13</sup>C NMR (101 MHz, DMSO-*d*<sub>6</sub>) δ ppm:** 56.01 (s, 1C, OCH<sub>3</sub>), 109.46 (s, 1C, C<sub>2</sub>), 115.91 (s, 1C, C<sub>5</sub>), 121.95 (s, 2C, C<sub>2',6'</sub>), 122.91 (s, 1C, C<sub>6</sub>), 125.82 (s, 1C, C<sub>1</sub>), 141.13 (s, 1C, C<sub>1'</sub>), 148.51 (s, 1C, C<sub>3</sub>), 149.74 (s, 1C, C<sub>4</sub>), 150.00 (s, 1C, C=N), 150.75 (s, 2C, C<sub>3',5'</sub>), 161.77 (s, 1C, C=O).

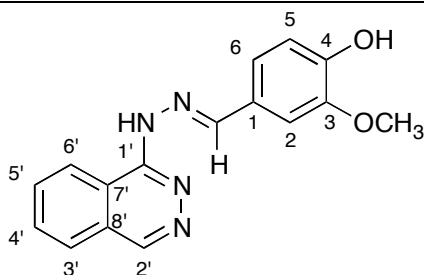


**FTIR (KBr)  $\nu$   $\text{cm}^{-1}$ :** 3516 (O-H), 3448 (N-H), 3070 (C-H<sub>ar</sub>), 3002 (C-H<sub>ar</sub>), 2850 (C-H, O-CH<sub>3</sub>), 1666 (C=N), 1595 (C=C ar.), 1552 (C≡N), 1513 (C=C ar.), 1190 (C-O).

**UV (EtOH, 44.23 $\mu$ M, 25°C):**  $\lambda$ =334 nm,  $\epsilon$ =21255 mol<sup>-1</sup>.L.cm<sup>-1</sup>;  $\lambda$ =216 nm,  $\epsilon$ =19409 mol<sup>-1</sup>.L.cm<sup>-1</sup>.

**MS (ES, TOF, MeOH) m/z:** 272.1036 [M+H<sup>+</sup>]

**HRMS (ES, TOF) m/z:** C<sub>14</sub>H<sub>13</sub>N<sub>3</sub>O<sub>3</sub> (calc./found) 272.1035/272.1036 [M+H<sup>+</sup>].



Chemical Formula: C<sub>16</sub>H<sub>14</sub>N<sub>4</sub>O<sub>2</sub>

Molecular Weight: 294.11

Rf: 0.50 (EtAc/PE 1:1 v/v)

**(E)-4-hydroxy-3-methoxybenzaldehyde phthalazin-1-ylhydrazone (2b). mp:** 162 °C.

**<sup>1</sup>H NMR (300 MHz, DMSO-*d*<sub>6</sub>)  $\delta$  ppm:** 3.90 (s, 3H, OCH<sub>3</sub>), 6.82 (d, *J*=8.1 Hz, 1H, H<sub>5</sub>), 7.21 (dd, *J*= 8.1, 1.8 Hz, 1H, H<sub>6</sub>), 7.70 – 7.80 (m, 3H, H<sub>3',4',5'</sub>), 7.82 (d, *J*=1.8 Hz, 1H, H<sub>2</sub>), 8.18 (s, 1H, H<sub>2'</sub>), 8.34 (d, 1H, H<sub>6'</sub>), 8.38 (s, 1H, HC=N), 9.47 (s, 1H, OH), 12.35 (br s, 1H, OH).

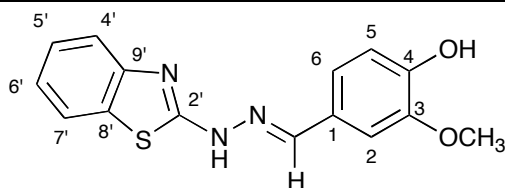
**<sup>13</sup>C NMR (101 MHz, DMSO-*d*<sub>6</sub>)  $\delta$  ppm:** 56.46 (s, 1C, OCH<sub>3</sub>), 110.64 (s, 1C, C<sub>2</sub>), 115.79 (s, 1C, C<sub>5</sub>), 119.45 (s, 1C, C<sub>1</sub>), 124.73 (s, 1C, C<sub>1</sub>), 125.16 (s, 1C, C<sub>6</sub>), 125.98 (s, 1C, C<sub>6'</sub>), 128.28 (s, 1C, C<sub>3'</sub>), 128.66 (s, 1C, C<sub>8'</sub>), 134.16 (s, 1C, C<sub>5'</sub>), 136.33 (s, 1C, C<sub>4'</sub>), 145.04 (s, 1C, C<sub>2'</sub>), 147.87 (s, 1C, C<sub>3</sub>), 148.77 (s, 1C, C<sub>4</sub>), 151.14 (s, 1C, C<sub>1'</sub>), 153.85 (C=N).

**FTIR (KBr)  $\nu$   $\text{cm}^{-1}$ :** 3533 (N-H), 3350 (O-H), 1617 (C=N), 1596 (C=C ar), 1511 (C=C ar), 1228 (C-O).

**UV (EtOH, 47.6 $\mu$ M, 25°C):**  $\lambda$ =374 nm,  $\epsilon$ =22712 mol<sup>-1</sup>.L.cm<sup>-1</sup>;  $\lambda$ =292 nm,  $\epsilon$ =16480 mol<sup>-1</sup>.L.cm<sup>-1</sup>.

**MS (ES, TOF, MeOH) m/z:** 295.1198 [M+H<sup>+</sup>]

**HRMS (ES, TOF) m/z:** calcd for C<sub>16</sub>H<sub>15</sub>N<sub>4</sub>O<sub>2</sub> [M+H<sup>+</sup>] 295.1195, found 295.1198.



Chemical Formula: C<sub>15</sub>H<sub>13</sub>N<sub>3</sub>O<sub>2</sub>S

Molecular Weight: 299.35

Rf: 0.42 (EtAc/PE 1:1 v/v)

**(E)-4-Hydroxy-3-methoxybenzaldehyde-1,3-benzothiazol-2-ylhydrazone (3b).** mp: 200.5 °C.

**<sup>1</sup>H NMR (300 MHz, DMSO-*d*<sub>6</sub>) δ ppm:** 3.84 (s, 3H, OCH<sub>3</sub>), 6.84 (d, *J* = 8.1 Hz, 1H, H<sub>5</sub>), 7.06-7.12 (m, 2H, H<sub>2,5'</sub>), 7.22-7.35 (m, 2H, H<sub>6,6'</sub>), 7.41 (d, *J* = 8.1 Hz, 1H, H<sub>7</sub>), 7.75 (dd, *J* = 7.2, 1.0 Hz, 1H, H<sub>4'</sub>), 8.03 (s, 1H, HC=N), 9.48 (s, 1H, OH), 12.04 (br s, 1H, NH);

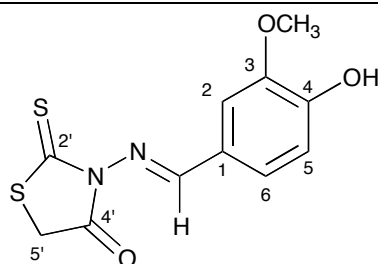
**<sup>13</sup>C NMR (101 MHz, DMSO-*d*<sub>6</sub>) δ ppm:** 56.49 (s, 1C, OCH<sub>3</sub>), 109.71 (s, 1C, C<sub>2</sub>), 116.07 (s, 1C, C<sub>5</sub>), 121.39 (s, 1C, C<sub>6</sub>), 121.78 (s, 1C, C<sub>6'</sub>), 121.92 (s, 1C, C<sub>7'</sub>), 126.27 (s, 1C, C<sub>1</sub>), 126.32 (s, 2C, C<sub>5'</sub>), 148.43, 149.01, 167.27 (s, 1C, C<sub>2'</sub>).

**FTIR (KBr) ν cm<sup>-1</sup>:** 3495 (O-H), 3187 (H-C=N), 3067 (C-H<sub>ar</sub>), 2964 (C-H<sub>ar</sub>), 2887 (C-H, O-CH<sub>3</sub>), 2826 (C-H, O-CH<sub>3</sub>), 1626 (C=N), 1576 (C=C ar.), 1559 (C=N), 1508 (C=C ar.), 1245 (O-C<sub>ar</sub>), 1213 (C-O), 1125 (C-O);

**UV (EtOH, 33.41 μM, 25°C):** λ=344 nm ε=30012 mol<sup>-1</sup>.L.cm<sup>-1</sup>.

**MS (ES, TOF, MeOH) m/z:** 300.0807 [M+H<sup>+</sup>]

**HRMS (ES, TOF) m/z:** C<sub>15</sub>H<sub>13</sub>N<sub>3</sub>O<sub>4</sub>S (calc./found) 300.0807/300.0807 [M+H<sup>+</sup>].



Chemical Formula: C<sub>11</sub>H<sub>10</sub>N<sub>2</sub>O<sub>3</sub>S<sub>2</sub>  
Molecular Weight: 282.3  
Rf: 0.25 (PE/EtAc 4:1 v/v)

**(E)-3-((4-hydroxy-3-methoxybenzylidene)amino)-2-thioxothiazolidin-4-one (4b).** mp: 185 °C.

**<sup>1</sup>H NMR (300 MHz, DMSO-*d*<sub>6</sub>) δ ppm:** 3.84 (s, 3H, OCH<sub>3</sub>), 4.34 (s, 2H, CH<sub>2</sub>/H<sub>5'</sub>), 6.93 (d, *J* = 8.2 Hz, 1H, H<sub>5</sub>), 7.32 (dd, *J* = 8.2, 1.7 Hz, 1H, H<sub>6</sub>), 7.46 (d, *J* = 1.7 Hz, 1H, H<sub>2</sub>), 8.48 (s, 1H, HC=N), 10.09 (s, 1H, OH).

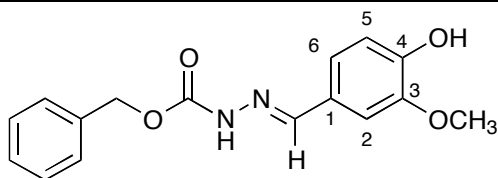
**<sup>13</sup>C NMR (75 MHz, DMSO-*d*<sub>6</sub>) δ ppm:** 35.07 (s, 1C, CH<sub>2</sub>/C<sub>5'</sub>), 56.07 (s, 1C, OCH<sub>3</sub>), 110.89 (s, 1C, C<sub>2</sub>), 116.07 (s, 1C, C<sub>5</sub>), 123.51 (s, 1C, C<sub>1</sub>), 125.37 (s, 1C, C<sub>6</sub>), 148.56 (s, 1C, C<sub>3</sub>), 152.24 (s, 1C, C<sub>4</sub>), 170.26 (s, 1C, C=O), 171.29 (s, 1C, C=N), 197.17 (s, 1C, C=S).

**FTIR (KBr) ν cm<sup>-1</sup>:** 3526 (O-H), 3448 (N-H), 2970 (-CH<sub>2</sub>-), 2919 (C-H), 1726 (C=O), 1615 (C=N), 1599 (C=C ar.), 1513 (C=C ar.), 1236 (C-O), 1176,5 (C-O), 1031 (C=S).

**UV (EtOH, 53.18 μM, 25°C):** λ= 292 nm, ε=23610 mol<sup>-1</sup>.L.cm<sup>-1</sup>; λ= 324 nm, ε=16328 mol<sup>-1</sup>.L.cm<sup>-1</sup>.

**MS (ES, TOF, MeOH) m/z:** 283.0212 [M+H<sup>+</sup>]

**HRMS (ES, TOF) m/z:** C<sub>11</sub>H<sub>11</sub>N<sub>2</sub>O<sub>3</sub>S<sub>2</sub> (calc./found) 283.0211/283.0212 [M+H<sup>+</sup>].



Chemical Formula: C<sub>16</sub>H<sub>16</sub>N<sub>2</sub>O<sub>4</sub>  
 Molecular Weight: 300.31  
 Rf: 0.53 (EtAc/PE 1:1 v/v)

**(E)-benzyl 2-(4-hydroxy-3-methoxybenzylidene)hydrazinecarboxylate (5b). mp:**

152.2 °C.

**<sup>1</sup>H NMR (300 MHz, DMSO-*d*<sub>6</sub>) δ ppm:** 3.80 (s, 3H, OCH<sub>3</sub>), 5.16 (s, 2H, CH<sub>2</sub>), 6.80 (d, *J* = 8.1 Hz, 1H, H<sub>5</sub>), 7.00 (dd, *J* = 8.1, 1.9 Hz, 1H, H<sub>6</sub>), 7.20 (d, *J* = 1.9 Hz, 1H, H<sub>2</sub>), 7.28 – 7.46 (m, 5H, H<sub>ar</sub>), 7.92 (s, 1H, HC=N), 9.44 (br s, 1H, OH), 11.06 (br s, 1H, NH).

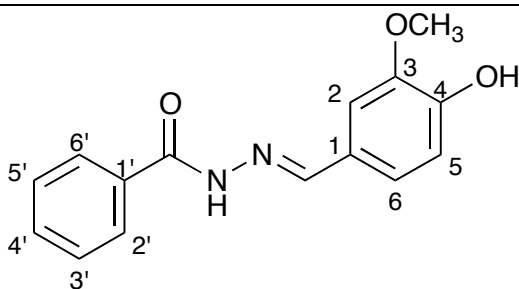
**<sup>13</sup>C NMR (75 MHz, DMSO-*d*<sub>6</sub>) δ ppm:** 55.96 (s, 1C, OCH<sub>3</sub>), 66.22 (s, 1C, CH<sub>2</sub>), 109.42 (s, 1C, C<sub>2</sub>), 115.87 (s, 1C, C<sub>5</sub>), 121.64 (s, 1C, C<sub>6</sub>), 126.22 (s, 1C, C<sub>1</sub>), 128.41 (s, 1C, C<sub>ar</sub>), 128.46 (s, 2C, C<sub>ar</sub>), 128.88 (s, 2C, C<sub>ar</sub>), 137.15 (s, 1C, C<sub>hyppo</sub>), 145.22 (s, 1C, C=N), 148.37 (s, 1C, C<sub>4</sub>), 148.94 (s, 1C, C<sub>3</sub>), 153.79 (s, 1C, C=O).

**FTIR (KBr) ν cm<sup>-1</sup>:** 3400 (N-H), 3238 (O-H), 3041 (C-H<sub>ar</sub>), 2979 (-CH<sub>2</sub>-), 2952-2930 (-CH, O-CH<sub>3</sub>), 1711 (C=O), 1601 (C=N), 1545 (C-N), 1509 (C=C ar.), 1264 (C-O-C), 1243 (O-C), 1063 (O-C).

**UV (EtOH, 46.62 μM, 25°C):** λ=312 nm, ε=21128 mol<sup>-1</sup>.L.cm<sup>-1</sup>; λ=288 nm, ε=20471 mol<sup>-1</sup>.L.cm<sup>-1</sup>.

**MS (ES, TOF, MeOH) m/z:** 301.1190 [M+H<sup>+</sup>]

**HRMS (ES, TOF) m/z:** C<sub>16</sub>H<sub>17</sub>N<sub>2</sub>O<sub>4</sub> (calc./found) 301.1188/301.1190 [M+H<sup>+</sup>].



Chemical Formula: C<sub>15</sub>H<sub>14</sub>N<sub>2</sub>O<sub>3</sub>  
 Molecular Weight: 270.28  
 Rf: 0.37 EtAc/PE (70/30 v/v)

**(E)-N'-(4-hydroxy-3-methoxybenzylidene)benzhydrazide (6b). mp:** 110 °C (car.).

**<sup>1</sup>H NMR (300 MHz, DMSO-*d*<sub>6</sub>) δ ppm:** 3.84 (s, 3H, OCH<sub>3</sub>), 6.85 (d, *J* = 8.1 Hz, 1H, H<sub>5</sub>), 7.09 (dd, *J* = 8.1, 1.9 Hz, 1H, H<sub>6</sub>), 7.33 (d, *J* = 1.9 Hz, 1H, H<sub>2</sub>), 7.44 – 7.65 (m, 3H, H<sub>3',4',5'</sub>), 7.91 (dd, *J* = 6.9, 1.5 Hz, 2H, H<sub>2',6'</sub>), 8.35 (s, 1H, HC=N), 9.55 (s, 1H, OH), 11.68 (s, 1H, NH).

**<sup>13</sup>C NMR (75 MHz, DMSO-*d*<sub>6</sub>) δ ppm:** 56.02 (s, 1C, OCH<sub>3</sub>), 109.42 (s, 1C, C<sub>2</sub>), 115.90 (s, 1C, C<sub>5</sub>), 122.61 (s, 1C, C<sub>6</sub>), 126.18 (s, 1C, C<sub>1</sub>), 127.99 (s, 2C, C<sub>2',6'</sub>), 128.89 (s, 2C, C<sub>3',5'</sub>),

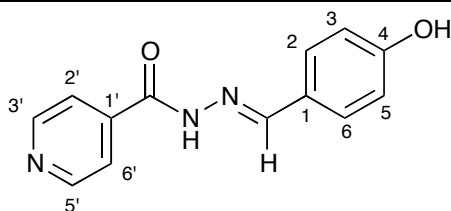
132.02 (s, 1C, C<sub>4'</sub>), 134.11 (s, 1C, C<sub>1'</sub>), 148.50 (s, 1C, C<sub>3</sub>), 148.82 (s, 1C, C=N), 149.46 (s, 1C, C<sub>4</sub>), 163.35 (s, 1C, C=O).

**FTIR (KBr)  $\nu$  cm<sup>-1</sup>:** 3486 (O–H), 3242 (N–H), 3062 (C–H), 1635 (C=O), 1605 (C=CN), 1513 (C=C ar).

**UV (EtOH, 66.74  $\mu$ M, 20°C):**  $\lambda$ =328 nm,  $\epsilon$ =26117 mol<sup>-1</sup>.L.cm<sup>-1</sup>

**MS (ES, TOF, MeOH) m/z:** 271.1083 [M+H<sup>+</sup>], 293.0902 [M+Na<sup>+</sup>].

**HRMS (ES, TOF) m/z:** C<sub>15</sub>H<sub>15</sub>N<sub>2</sub>O<sub>3</sub> (calc./found) 271.1083, 271.1079 [M+H<sup>+</sup>].



Chemical Formula: C<sub>13</sub>H<sub>11</sub>N<sub>3</sub>O<sub>2</sub>  
Molecular Weight: 241.25  
Rf: 0.23 (EtAc/PE 1:1 v/v)

**(E)-N'-(4-hydroxybenzylidene)isonicotinohydrazide (1c). Mp:** >260 °C (not determined)

**<sup>1</sup>H NMR (400 MHz, DMSO-*d*<sub>6</sub>)  $\delta$  ppm:** 6.86 (dt,  $J$  = 8.7, 2.8, 2.0 Hz, 2H, H<sub>3,5</sub>), 7.59 (dt,  $J$  = 8.7, 2.8, 1.9 Hz, 2H, H<sub>2,6</sub>), 7.82 (dd,  $J$  = 4.4, 1.6 Hz, 2H, H<sub>2',6'</sub>), 8.37 (s, 1H, HC=N), 8.78 (dd,  $J$  = 4.4, 1.7 Hz, 2H, H<sub>3',5'</sub>), 9.98 (s, 1H, OH), 11.86 (s, 1H, NH).

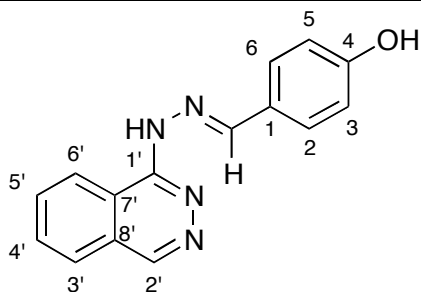
**<sup>13</sup>C NMR (101 MHz, DMSO-*d*<sub>6</sub>)  $\delta$  ppm:** 116.23 (s, 2C, C<sub>3,5</sub>), 121.93 (s, 2C, C<sub>2',6'</sub>), 125.46 (s, 1C, C<sub>1</sub>), 129.54 (s, 2C, C<sub>2,6</sub>), 141.15 (s, 1C, C<sub>1'</sub>), 149.82 (s, 2C, C<sub>3',5'</sub>), 150.73 (s, 1C, C=N), 160.16 (s, 1C, C<sub>4</sub>), 161.73 (s, 1C, C=O).

**FTIR (KBr)  $\nu$  cm<sup>-1</sup>:** 3426 (O-H), 3021(C-H<sub>ar</sub>), 1639 (C=N), 1582 (C=C ar.), 1551 (C=N), 1512 (C=C ar.), 1168 (O-C).

**UV (EtOH, 62.17 $\mu$ M, 25°C):**  $\lambda$ =322 nm,  $\epsilon$ =22677 mol<sup>-1</sup>.L.cm<sup>-1</sup>.

**MS (ES, TOF, MeOH) m/z:** 242.0930 [M+H<sup>+</sup>]

**HRMS (ES, TOF) m/z:** C<sub>13</sub>H<sub>12</sub>N<sub>3</sub>O<sub>2</sub> (calc./found) 294.0930/294.0930 [M+H<sup>+</sup>].



Chemical Formula: C<sub>15</sub>H<sub>12</sub>N<sub>4</sub>O  
Molecular Weight: 264.28  
Rf: 0.63 (EtAc/PE 1:1 v/v)

**(E)-4-hydroxybenzaldehyde phthalazin-1-ylhydrazone (2c). mp:** 207.3 °C.

**<sup>1</sup>H NMR (300 MHz, DMSO-*d*<sub>6</sub>) δ ppm:** 6.82 (dt, *J* = 8.6, 2.7, 1.9 Hz, 2H, H<sub>3,5</sub>), 7.65 – 7.80 (m, 3H, H<sub>3', 4', 5'</sub>), 7.86 (dt, *J* = 8.6, 2.7, 1.9 Hz, 2H, H<sub>2,6</sub>), 8.07 (s, 1H, H<sub>2'</sub>), 8.28 (d, *J* = 8.2 Hz, 2H, H<sub>6'</sub>), 8.36 (s, 1H, HC=N), 9.85 (s, 1H, OH), 12.03 (br s, 1H, NH).

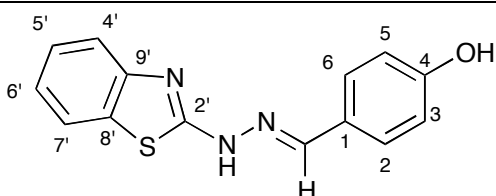
**<sup>13</sup>C NMR (75 MHz, DMSO-*d*<sub>6</sub>) δ ppm:** 115.81 (s, 2C, C<sub>3,5</sub>), 123.97 (s, 1C, C<sub>6'</sub>), 126.52 (s, C<sub>7'</sub>), 126.86 (s, 1C, C<sub>3'</sub>), 127.01 (s, 1C, C<sub>1</sub>), 127.43 (s, 1C, C<sub>8'</sub>), 130.31 (s, 2C, C<sub>8'</sub>), 132.14 (s, 1C, C<sub>5'</sub>), 132.63 (s, 1C, C<sub>4'</sub>), 137.92 (s, 1C, C<sub>2'</sub>), 148.06 (s, 1C, C<sub>1'</sub>), 153.73 (s, 1C, C=N), 159.68 (s, 1C, C<sub>4</sub>).

**FTIR (KBr) ν cm<sup>-1</sup>:** 3300 (O-H), 2968 (C-H<sub>ar</sub>), 1607 (C=N), 1598 (C=C ar.), 1583 (C≡N), 1514 (C=C ar.), 1282 (O-C).

**UV (EtOH, 42.9 μM, 21°C):** λ=372 nm, ε=23923 mol<sup>-1</sup>.L.cm<sup>-1</sup>; λ=296 nm, ε=22601 mol<sup>-1</sup>.L.cm<sup>-1</sup>.

**MS (ES, TOF, MeOH) m/z:** 265.1090 [M+H<sup>+</sup>]

**HRMS (ES, TOF) m/z:** C<sub>15</sub>H<sub>13</sub>N<sub>4</sub>O (calc./found) 265.1089/265.1090 [M+H<sup>+</sup>].



Chemical Formula: C<sub>14</sub>H<sub>11</sub>N<sub>3</sub>OS  
Molecular Weight: 269.3  
Rf: 0.37 (EtAc /PE 1:1 v/v)

**(E)-4-hydroxybenzaldehyde-1,3b-benzothiazol-2-ylhydrazone (3c). mp:** 256 °C.

**<sup>1</sup>H NMR (400 MHz, DMSO-*d*<sub>6</sub>) δ ppm:** 6.85 (dt, *J* = 8.6, 2.6, 2.0 Hz, 2H, H<sub>3,5</sub>), 7.08 (td, *J* = 7.8, 1.2 Hz, 1H, H<sub>4'</sub>), 7.28 (td, *J* = 7.6, 1.3 Hz, 1H, H<sub>7'</sub>), 7.41 (d, *J* = 7.9 Hz, 1H, H<sub>7'</sub>), 7.54 (dt, *J* = 8.6, 2.6, 2.0 Hz, 2H, H<sub>2,6</sub>), 7.74 (d, *J* = 7.4 Hz, 1H, H<sub>4'</sub>), 8.05 (s, 1H, HC=N), 9.86 (s, 1H, OH), 12.00 (s, 1H, NH).

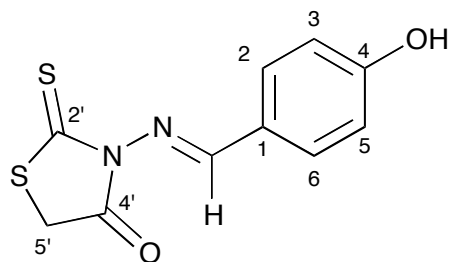
**<sup>13</sup>C NMR (101 MHz, DMSO-*d*<sub>6</sub>) δ ppm:** 116.20 (s, 2C, C<sub>2,6</sub>), 121.76 (s, 1C, C<sub>6'</sub>), 121.89 (s, 1C, C<sub>7'</sub>), 125.84 (s, 2C, C<sub>1</sub>), 126.32 (s, 1C, C<sub>5'</sub>), 128.72 (s, 2C, C<sub>3,5</sub>), 159.49 (s, 1C, C=N), 167.28 (s, 1C, C<sub>2'</sub>).

**FTIR (KBr) ν cm<sup>-1</sup>:** 3300 (O-H), 3196 (H-C=N), 2987 (C-H<sub>ar</sub>), 2877 (C-H), 1610 (C=N), 1598 (C=C ar.), 1560 (C-N), 1512 (C=C), 1445 (N-H bend), 1119 (C-O), 1168 (O-C).

**UV (EtOH, 37.13 μM, 25°C):** λ=340 nm, ε=36625 mol<sup>-1</sup>.L.cm<sup>-1</sup>.

**MS (ES, TOF, MeOH) m/z:** 270.0706 [M+H<sup>+</sup>]

**HRMS (ES, TOF) m/z:** C<sub>14</sub>H<sub>12</sub>N<sub>3</sub>OS (calc./found) 270.0701/270.0706 [M+H<sup>+</sup>].



Chemical Formula: C<sub>10</sub>H<sub>8</sub>N<sub>2</sub>O<sub>2</sub>S<sub>2</sub>  
 Molecular Weight: 252,31  
 Rf: 0.23 (PE/EtAc 4:1 v/v)

**(E)-3-((4-hydroxybenzylidene)amino)-2-thioxothiazolidin-4-one (4c).** mp: 190 °C (dec.).

<sup>1</sup>H NMR (400 MHz, DMSO-*d*<sub>6</sub>) δ ppm: 4.34 (s, 2H, CH<sub>2</sub>/H<sub>5'</sub>), 6.93 (dt, *J* = 8.7, 2.7, 2.0 Hz, 2H, H<sub>3,5</sub>), 7.76 (dt, *J* = 8.6, 2.9, 2.0 Hz, 2H, H<sub>2,6</sub>), 8.51 (s, 1H, HC=N), 10.42 (s, 1H, OH).

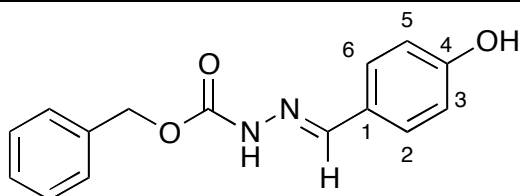
<sup>13</sup>C NMR (101 MHz, DMSO) δ ppm: 35.08 (s, 1C, CH<sub>2</sub>/H<sub>5'</sub>), 116.50 (s, 2C, C<sub>3,5</sub>), 123.23 (s, 1C, C<sub>1</sub>), 131.65 (s, 2C, C<sub>2,6</sub>), 162.55 (s, 1C, C<sub>4</sub>), 170.25 (s, 1C, C=N), 171.04 (s, 1C, C=O), 197.20 (s, 1C, C=S).

FTIR (KBr) ν cm<sup>-1</sup>: 3411 (O-H), 2964 (-CH<sub>2</sub>-), 2914 (C-H), 1701 (C=O), 1607 (C=N), 1573 (C=C ar.), 1512 (C=C ar.), 1167 (O-C), 1031 (C=S);

UV (EtOH, 60.77 μM, 25°C): λ=294 nm, ε=17665 mol<sup>-1</sup>.L.cm<sup>-1</sup>.

MS (ES, TOF, MeOH) m/z: 253.0108 [M+H<sup>+</sup>]

HRMS (ES, TOF) m/z: C<sub>10</sub>H<sub>9</sub>N<sub>2</sub>O<sub>2</sub>S<sub>2</sub> (calc./found) 253.0110/253.0108 [M+H<sup>+</sup>].



Chemical Formula: C<sub>15</sub>H<sub>14</sub>N<sub>2</sub>O<sub>3</sub>  
 Molecular Weight: 270.28  
 Rf: 0.55 (EtAc/PE 1:1 v/v)

**(E)-benzyl 2-(4-hydroxybenzylidene)hydrazinecarboxylate (5c).** mp: 188 °C.

<sup>1</sup>H NMR (400 MHz, DMSO-*d*<sub>6</sub>) δ ppm: 5.17 (s, 2H, CH<sub>2</sub>), 6.80 (dt, *J* = 8.7, 2.7, 2.0 Hz, 2H, H<sub>3,5</sub>), 7.31 – 7.43 (m, 5H, H<sub>ar</sub>), 7.46 (dt, *J* = 8.7, 2.6, 1.9 Hz, 2H, H<sub>2,6</sub>), 7.94 (s, 1H, HC=N), 9.82 (s, 1H, OH), 11.02 (s, 1H, NH).

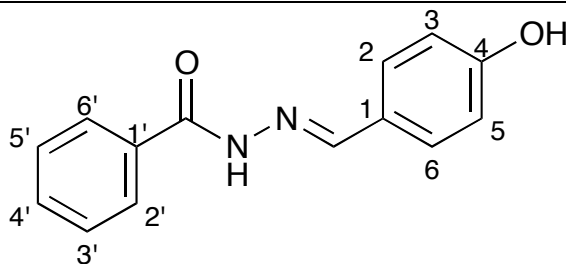
<sup>13</sup>C NMR (101 MHz, DMSO) δ ppm: 66.22 (s, 1C, CH<sub>2</sub>), 116.07 (s, 2C, C<sub>3,5</sub>), 125.82 (s, 1C, C<sub>1</sub>), 128.41 (s, 2C, C<sub>ar</sub>), 128.45 (s, 2C, C<sub>ar</sub>), 128.78 (s, 2C, C<sub>2,6</sub>), 128.88 (s, 1C, C<sub>ar</sub>), 137.17, 159.43 (s, 1C, C<sub>4</sub>).

FTIR (KBr) ν cm<sup>-1</sup>: 3397 (O-H), 3212 (N-H), 3090 (-CH<sub>2</sub>-), 3067 (C-H<sub>ar</sub>), 2949-2825 (C-H), 1693 (C=O), 1674 (C=N), 1607 (C=C ar.), 1513 (C=C ar.), 1269 (C-O-C), 1055 (C-O).

UV (EtOH, 36.99 μM, 25°C): λ=288 nm, ε=25658 mol<sup>-1</sup>.L.cm<sup>-1</sup>; λ=212 nm, ε=19504 mol<sup>-1</sup>.L.cm<sup>-1</sup>.

**MS (ES, TOF, MeOH) m/z:** 271.1082 [M+H<sup>+</sup>]

**HRMS (ES, TOF) m/z:** C<sub>15</sub>H<sub>15</sub>N<sub>2</sub>O<sub>3</sub> (calc./found) 271.1083/271.1082 [M+H<sup>+</sup>].



Chemical Formula: C<sub>14</sub>H<sub>12</sub>N<sub>2</sub>O<sub>2</sub>  
Molecular Weight: 240.26  
Rf: 0.48 EtAc/PE (70/30 v/v)

**(E)-N'-(4-hydroxybenzylidene)benzhydrazide (6c). mp:** 239 °C.

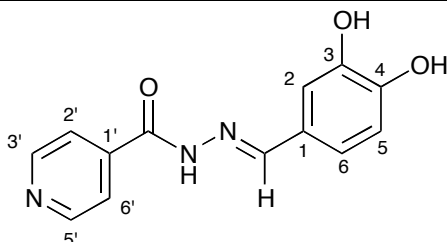
**<sup>1</sup>H NMR (300 MHz, DMSO-*d*<sub>6</sub>) δ ppm:** 6.85 (d, *J* = 8.2 Hz, 2H, H<sub>3,5</sub>), 7.44 – 7.64 (m, 5H, H<sub>2,6</sub> and H<sub>3',4',5'</sub>), 7.90 (dd, *J* = 7.0, 1.4 Hz, 2H, H<sub>2'</sub>), 8.36 (s, 1H, HC=N), 9.94 (s, 1H, OH), 11.65 (s, 1H, NH); **<sup>13</sup>C NMR (75 MHz, DMSO-*d*<sub>6</sub>) δ ppm:** 116.17 (s, 2C, C<sub>3,5</sub>), 125.76 (s, 1C, C<sub>1</sub>), 127.98 (s, 2C, C<sub>2,6</sub>), 128.88 (s, 2C, C<sub>2',6'</sub>), 129.31 (s, 2C, C<sub>3',5'</sub>), 132.01 (s, 1C, C<sub>4'</sub>), 134.11 (s, 1C, C<sub>1'</sub>), 148.57 (s, 1C, C=N), 159.88 (s, 1C, C<sub>4</sub>), 163.31 (s, 1C, C=O).

**FTIR (KBr) ν cm<sup>-1</sup>:** 3405 (O–H), 3182 (N–H), 3069–3020 (C–H), 1629 (C=O), 1605 (C=N), 1581 (C=C ar), 1516 (C=C ar).

**UV (EtOH, 42.79 μM, 20°C):** λ=318 nm, ε=25949 mol<sup>-1</sup>.L.cm<sup>-1</sup>

**MS (ES, TOF, MeOH) m/z:** 241.0977 [M+H<sup>+</sup>], 263.0797 [M+Na<sup>+</sup>]

**HRMS (ES, TOF) m/z:** C<sub>14</sub>H<sub>13</sub>N<sub>2</sub>O<sub>2</sub> (calc./found) 241.0977/241.0977 [M+H<sup>+</sup>].



Chemical Formula: C<sub>13</sub>H<sub>11</sub>N<sub>3</sub>O<sub>3</sub>  
Molecular Weight: 257.24  
Rf: 0.22 (EtAc/PE 1:1 v/v)

**(E)-N'-(3,4-dihydroxybenzylidene)isonicotinohydrazide (1d). mp:** > 260 °C (dec.).

**<sup>1</sup>H NMR (400 MHz, DMSO-*d*<sub>6</sub>) δ ppm:** 5.17 (s, 2H, CH<sub>2</sub>), 6.81 (d, *J* = 8.2 Hz, 1H, H<sub>5</sub>), 6.97 (dd, *J* = 8.2, 2.0 Hz, 1H, H<sub>6</sub>), 7.27 (d, *J* = 2.0 Hz, 1H, H<sub>2</sub>), 7.81 (dd, *J* = 4.4, 1.7 Hz, 2H, H<sub>2',6'</sub>), 8.28 (s, 1H, HC=N), 8.77 (dd, *J* = 6.1, 1.6 Hz, 2H, H<sub>3',5'</sub>), 9.29 (s, 1H, OH – C<sub>3</sub>), 9.44 (s, 1H, OH – C<sub>4</sub>), 11.81 (s, 1H, NH).

**<sup>13</sup>C NMR (101 MHz, DMSO) δ ppm:** 113.25 (s, 1C, C<sub>5</sub>), 116.06 (s, 1C, C<sub>2</sub>), 121.36 (s, 1C, C<sub>2',6'</sub>), 121.93 (s, 1C, C<sub>2</sub>), 125.91 (s, 1C, C<sub>1</sub>), 141.17 (s, 1C, C<sub>1'</sub>), 146.22 (s, 1C, C<sub>3</sub>), 148.74 (s, 1C, C<sub>4</sub>), 150.01 (s, 1C, C<sub>3',5'</sub>), 150.72 (s, 1C, C=N), 161.68 (s, 1C, C=O).

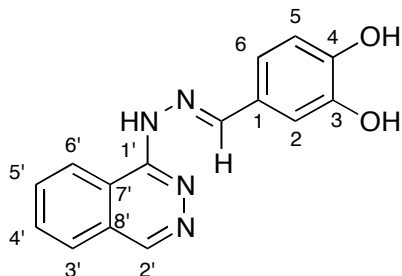
**FTIR (KBr) ν cm<sup>-1</sup>:** 3500–3456 (O–H), 3100–3000 (C–H), 1648 (C=N), 1596 (C=C ar.), 1552

(C $\equiv$ N), 1525 (C=C ar.), 1202 (O-C), 1125 (O-C).

UV (EtOH, 38.86 $\mu$ M, 25°C):  $\lambda$ =336 nm,  $\epsilon$ =18099 mol<sup>-1</sup>.L.cm<sup>-1</sup>.

MS (ES, TOF, MeOH) m/z: 258.0880 [M+H<sup>+</sup>]

HRMS (ES, TOF) m/z: C<sub>13</sub>H<sub>12</sub>N<sub>3</sub>O<sub>3</sub> (calc./found) 258.0879/258.0880 [M+H<sup>+</sup>].



Chemical Formula: C<sub>15</sub>H<sub>12</sub>N<sub>4</sub>O<sub>2</sub>

Molecular Weight: 280.28

Rf: 0.53 (EtAc/PE 1:1 v/v)

**(E)-3,4-dihydroxybenzaldehyde phthalazin-1-ylhydrazone (2d).** Mp: > 260 °C (dec.).

<sup>1</sup>H NMR (300 MHz, DMSO-*d*<sub>6</sub>)  $\delta$  ppm: 6.79 (d, *J* = 8.1 Hz, 1H, H<sub>2</sub>), 7.27 (dd, *J* = 8.2, 2.0 Hz, 1H, H<sub>6</sub>), 7.44 (d, *J* = 1.9 Hz, 1H, H<sub>5</sub>), 7.79 – 7.63 (m, 3H, H<sub>3',4',5'</sub>), 8.02 (s, 1H, H<sub>2'</sub>), 8.24 (d, *J* = 7.9 Hz, 1H, H<sub>6'</sub>), 8.27 (s, 1H, HC=N), 8.91 (br s, 1H, OH – C<sub>3</sub>), 9.44 (br s, 1H, OH – C<sub>4</sub>), 11.84 (s, 1H, NH).

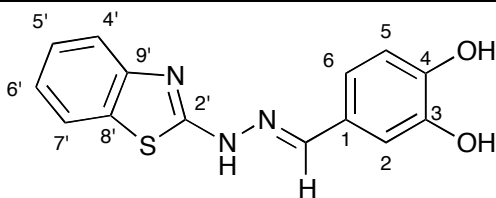
<sup>13</sup>C NMR (75 MHz, DMSO-*d*<sub>6</sub>)  $\delta$  ppm: 115.51 (s, 1C, C<sub>5</sub>), 115.80 (s, 1C, C<sub>2</sub>), 121.23 (s, 1C, C<sub>6</sub>), 123.97 (s, 1C, C<sub>6'</sub>), 126.52 (s, C<sub>7'</sub>), 126.86 (s, 1C, C<sub>3'</sub>), 127.01 (s, 1C, C<sub>1</sub>), 127.43 (s, 1C, C<sub>8'</sub>), 132.14 (s, 1C, C<sub>5'</sub>), 132.63 (s, 1C, C<sub>4'</sub>), 137.92 (s, 1C, C<sub>2'</sub>), 145.78 (s, 1C, C<sub>3</sub>), 148.06 (s, 1C, C<sub>1'</sub>), 153.73 (s, 1C, C=N), 159.68 (s, 1C, C<sub>4</sub>).

FTIR (KBr)  $\nu_{\max}$ /cm<sup>-1</sup>: 3308 (O-H), 2968-2950 (C-H<sub>ar</sub>), 1618 (C=N), 1596 (C=C ar.), 1537 (C $\equiv$ N), 1507 (C=C ar.), 1271 (O-C).

UV (EtOH, 42.53  $\mu$ M, 25°C):  $\lambda$ =374 nm,  $\epsilon$ =25536 mol<sup>-1</sup>.L.cm<sup>-1</sup>;  $\lambda$ =292 nm,  $\epsilon$ =18143 mol<sup>-1</sup>.L.cm<sup>-1</sup>.

MS (ES, TOF, MeOH) m/z: 281.1037 [M+H<sup>+</sup>]

HRMS (ES, TOF) m/z: calcd for C<sub>15</sub>H<sub>13</sub>N<sub>4</sub>O<sub>2</sub> [M+H<sup>+</sup>] 281.1039, found 281.1037.



Chemical Formula: C<sub>14</sub>H<sub>11</sub>N<sub>3</sub>O<sub>2</sub>S

Molecular Weight: 285.32

Rf: 0.35 (EtAc/PE 1:1 v/v)

**(E)-3,4-dihydroxybenzaldehyde-1,3-benzothiazol-2-ylhydrazone (3d).** Mp: > 260 °C (dec.).

<sup>1</sup>H NMR (400 MHz, DMSO-*d*<sub>6</sub>)  $\delta$  ppm: 6.79 (d, *J* = 8.1 Hz, 1H, H<sub>5</sub>), 6.93 (dd, *J* = 8.1, 2.0 Hz, 1H, H<sub>6</sub>), 7.08 (td, *J* = 7.6, 1.2 Hz, 1H, H<sub>5'</sub>), 7.20 (d, *J* = 2.0 Hz, 1H, H<sub>2</sub>), 7.28 (td, *J* = 7.3,



1.3 Hz, 1H, H<sub>6'</sub>), 7.41 (d,  $J = 7.9$  Hz, 1H, H<sub>7'</sub>), 7.75 (d,  $J = 7.5$  Hz, 1H, H<sub>4'</sub>), 7.96 (s, 1H, C=N), 9.21 (s, 1H, OH – C<sub>3</sub>), 9.35 (s, 1H, OH-C<sub>4</sub>), 11.97 (br s, 1H, NH).

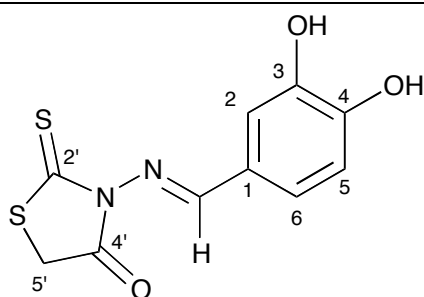
<sup>13</sup>C NMR (101 MHz, DMSO)  $\delta$  ppm: 112.89 (s, 1C, C<sub>2</sub>), 116.08 (s, 1C, C<sub>5</sub>), 120.37 (s, 1C, C<sub>6</sub>), 121.74 (s, 1C, C<sub>7'</sub>), 121.89 (s, 1C, C<sub>6'</sub>), 126.27 (s, 1C, C<sub>1</sub>), 126.32 (s, 1C, C<sub>5'</sub>), 146.15 (s, 1C, C<sub>3</sub>), 148.06 (s, 1C, C<sub>4</sub>), 167.20 (s, 1C, C<sub>2</sub>).

FTIR (KBr)  $\nu$  cm<sup>-1</sup>: 3477 (N-H), 3249 (O-H), 3065 (C-H<sub>ar</sub>), ~2910 (C-H), 1600 (C=N), 1581 (C=C ar.), 1516 (C=C ar.), 1279 (O-C).

UV (EtOH, 24.53  $\mu$ M, 25°C):  $\lambda$ =344 nm,  $\epsilon$ =47216 mol<sup>-1</sup>.L.cm<sup>-1</sup>.

MS (ES, TOF, MeOH)  $m/z$ : 286.0655 [M+H<sup>+</sup>]

HRMS (ES, TOF)  $m/z$ : C<sub>14</sub>H<sub>12</sub>N<sub>3</sub>O<sub>2</sub>S (calc./found) 286.0650/286.0655 [M+H<sup>+</sup>].



Chemical Formula: C<sub>10</sub>H<sub>8</sub>N<sub>2</sub>O<sub>3</sub>S<sub>2</sub>  
Molecular Weight: 268.31  
Rf: 0.12 (PE/EtAc 4:1 v/v)

**(E)-3-((3,4-dihydroxybenzylidene)amino)-2-thioxothiazolidin-4-one (4d). Mp:** > 200 °C (dec.).

<sup>1</sup>H NMR (400 MHz, DMSO-*d*<sub>6</sub>)  $\delta$  ppm: 4.33 (s, 2H, CH<sub>2</sub>), 6.87 (d,  $J = 8.1$  Hz, 1H, H<sub>5</sub>), 7.15 (dd,  $J = 8.3, 2.0$  Hz, 1H, H<sub>6</sub>), 7.38 (d,  $J = 2.0$  Hz, 1H, H<sub>2</sub>), 8.41 (s, 1H, HC=N), 9.50 (s, 1H, OH – C<sub>3</sub>), 9.90 (s, 1H, OH – C<sub>4</sub>).

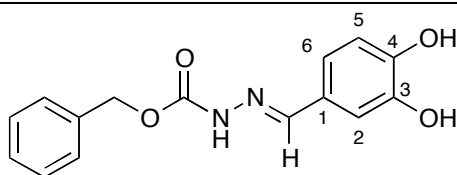
<sup>13</sup>C NMR (101 MHz, DMSO-*d*<sub>6</sub>)  $\delta$  ppm: 35.06 (s, 1C, CH<sub>2</sub>), 114.31 (s, 1C, C<sub>5</sub>), 116.16 (s, 1C, C<sub>2</sub>), 123.59 (s, 1C, C<sub>1</sub>), 124.08 (s, 1C, C<sub>6</sub>), 146.35 (s, 1C, C<sub>3</sub>), 151.34 (s, 1C, C<sub>4</sub>), 170.27 (s, 1C, C=O), 171.18 (s, 1C, C=N), 197.22 (s, 1C, C=S).

FTIR (KBr)  $\nu$  cm<sup>-1</sup>: 3295 (O-H), 2980 (-CH<sub>2</sub>-), 2927 (C-H), 1732 (C=O), 1687 (C=N), 1576 (C=C ar.), 1516 (C=C ar.), 1253 (C-O), 1172 (C-O), 1023 (C=S).

UV (EtOH, 44.52  $\mu$ M, 25°C):  $\lambda$ =292,  $\epsilon$ =23298 mol<sup>-1</sup>.L.cm<sup>-1</sup>.

MS (ES, TOF, MeOH)  $m/z$ : 269.0054 [M+H<sup>+</sup>]

HRMS (ES, TOF)  $m/z$ : C<sub>10</sub>H<sub>9</sub>N<sub>2</sub>O<sub>3</sub>S<sub>2</sub> (calc./found) 269.0053/269.0054 [M+H<sup>+</sup>].



Chemical Formula: C<sub>15</sub>H<sub>14</sub>N<sub>2</sub>O<sub>4</sub>  
Molecular Weight: 286.28  
Rf: 0.52 (EtAc/PE 1:1 v/v)

**(E)-benzyl 2-(3,4-dihydroxybenzylidene)hydrazinecarboxylate (5d). Mp:** 80 °C (dec.).

**<sup>1</sup>H NMR (400 MHz, DMSO-*d*<sub>6</sub>) δ ppm:** 5.16 (s, 2H, CH<sub>2</sub>), 6.75 (d, *J* = 8.1 Hz, 1H, H<sub>5</sub>), 6.83 (dd, *J* = 8.1, 2.0 Hz, 1H, H<sub>6</sub>), 7.14 (d, *J* = 2.0 Hz, 1H, H<sub>2</sub>), 7.29 – 7.47 (m, 5H, H<sub>ar</sub>), 7.85 (s, 1H, HC=N), 9.19 (s, 1H, OH – C<sub>3</sub>), 9.27 (s, 1H, OH – C<sub>4</sub>), 10.97 (br s, 1H, NH).

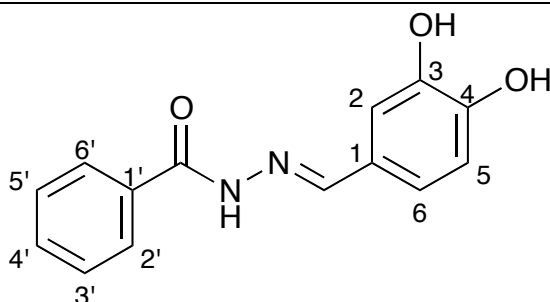
**<sup>13</sup>C NMR (101 MHz, DMSO) δ ppm:** 66.20 (s, 1C, CH<sub>2</sub>), 112.79 (s, 1C, C<sub>5</sub>), 115.96 (s, 1C, C<sub>2</sub>), 120.41 (s, 1C, C<sub>6</sub>), 126.28 (s, 1C, C<sub>1</sub>), 128.40 (s, 2C, C<sub>ortho</sub>), 128.45 (s, 1C, C<sub>para</sub>), 128.89 (s, 2C, C<sub>meta</sub>), 137.17 (s, 1C, C<sub>hypso</sub>), 145.6 (s, 1C, C=N), 146.09 (s, 1C, C<sub>3</sub>), 147.95 (s, 1C, C<sub>4</sub>), 153.76 (s, 1c, C=O).

**FTIR (KBr) ν cm<sup>-1</sup>:** 3447 (N-H), 3342 (O-H), 3195 (H-C=N), 3040 (C-H<sub>ar</sub>), 2960 (C-H), 1702 (C=O), 1686 (C=N), 1596, 1526 and 1449 (C=C), 1270 (C-O ar.), 1252 (C-O-C), 1046 (C-O).

**UV (EtOH, 36.33 μM, 25 °C):** λ = 234 ε = 35676 mol<sup>-1</sup>.L.cm<sup>-1</sup>; λ = 310, ε = 35632 mol<sup>-1</sup>.L.cm<sup>-1</sup>.

**MS (ES, TOF, MeOH) m/z:** 287.1038 [M+H<sup>+</sup>]

**HRMS (ES, TOF) m/z:** C<sub>15</sub>H<sub>15</sub>N<sub>2</sub>O<sub>4</sub> (calc./found) 287.1032/ 287.1038 [M+H<sup>+</sup>].



Chemical Formula: C<sub>14</sub>H<sub>12</sub>N<sub>2</sub>O<sub>3</sub>  
Molecular Weight: 256.26  
Rf: 0.28 EtAc/PE (70/30 v/v)

**(E)-N<sup>1</sup>-(3,4-dihydroxybenzylidene)benzhydrazide (6d). Mp:** 214 °C.

**<sup>1</sup>H NMR (300 MHz, DMSO-*d*<sub>6</sub>) δ ppm:** 6.80 (d, *J* = 8.1 Hz, 1H, H<sub>5</sub>), 6.94 (dd, *J* = 8.1, 2.0 Hz, 1H, H<sub>6</sub>), 7.26 (d, *J* = 2.0 Hz, 1H, H<sub>2</sub>), 7.45 – 7.64 (m, 3H, H<sub>3',4',5'</sub>), 7.90 (dd, *J* = 7.1, 1.9 Hz, 2H, H<sub>2',6'</sub>), 8.28 (s, 1H, HC=N), 9.28 (s, 1H, OH), 9.39 (s, 1H, OH), 11.61 (s, 1H, NH);

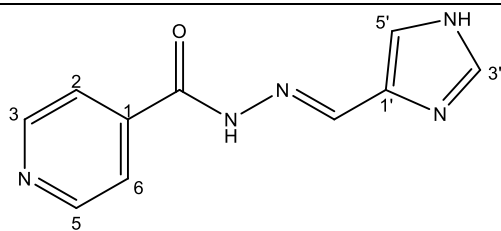
**<sup>13</sup>C NMR (75 MHz, DMSO-*d*<sub>6</sub>) δ ppm:** 113.12 (s, 1C, C<sub>5</sub>), 116.02 (s, 1C, C<sub>2</sub>), 121.05 (s, 1C, C<sub>6</sub>), 126.22 (s, 1C, C<sub>1</sub>), 127.96 (s, 2C, C<sub>2',6'</sub>), 128.87 (s, 1C, C<sub>3',5'</sub>), 131.99 (s, 1C, C<sub>4'</sub>), 134.13 (s, 1C, C<sub>1'</sub>), 146.18 (s, 1C, C<sub>3</sub>), 148.43 (s, 1C, C<sub>4</sub>), 148.77 (s, 1C, C=N), 163.26 (C=O).

**FTIR (KBr) ν cm<sup>-1</sup>:** 3480 (O-H), 3227 (N-H), 3050 (C-H), 1648 (C=O), 1605 (C=N), 1567 (C=C ar), 1448 (N-H bend).

**UV (EtOH, 43.63 μM, 20°C):** λ = 330 nm, ε = 24434 mol<sup>-1</sup>.L.cm<sup>-1</sup>

**MS (ES, TOF, MeOH) m/z:** 257.0926 [M+H<sup>+</sup>], 279.0746 [M+Na<sup>+</sup>]

**HRMS (ES, TOF) m/z:** C<sub>14</sub>H<sub>13</sub>N<sub>2</sub>O<sub>3</sub> (calc./found) 257.0926/257.0927 [M+H<sup>+</sup>].

Chemical Formula: C<sub>10</sub>H<sub>9</sub>N<sub>5</sub>O

Molecular Weight: 215.21

Rf: 0.1 EtAc/MeOH (4:1 v/v)

**(E)-N'-((1H-imidazol-4-yl)methylene)isonicotinohydrazide (7a).** mp: 296.7 °C (dec.).

**<sup>1</sup>H NMR (300 MHz, DMSO-*d*<sub>6</sub>) δ ppm:** 8.15 (d, *J* = 1.4 Hz, 1H, H<sub>5'</sub>), 8.36 (dd, *J* = 6.6, 1.5 Hz, 2H, H<sub>2,6</sub>), 8.52 (s, 1H, H-C=N), 9.10 (dd, *J* = 6.6, 1.5 Hz, 2H, H<sub>3,5</sub>), 9.21 (d, *J* = 1.3 Hz, 1H, H<sub>3'</sub>), 15.67 (s, 2H, N-H).

**<sup>13</sup>C NMR (75 MHz, DMSO) δ ppm:** 122.02 (1C, C<sub>5'</sub>), 125.10 (2C, C<sub>2,6</sub>), 128.25 (1C, C<sub>1'</sub>), 138.37 (1C, C=N), 136.80 (1C, C<sub>3'</sub>), 144.77 (2C, C<sub>3,5</sub>), 146.91 (1C, C<sub>1</sub>), 160.14 (1C, C=O), 126.78 (2C, C<sub>2,6</sub>), 134.36 (1C, C<sub>5'</sub>), 143.08 (2C, C<sub>3,5</sub>).

**FTIR (KBr) ν cm<sup>-1</sup>:** 3193.59 (N-H), 3038.08 (C-H<sub>ar</sub>), 1648.96 (C=O), 1626.02 (C=N-N), 1596.86 (C=C<sub>ar</sub>), 1551.04 (C<sub>ar</sub> = N), 1506.46 (C=N).

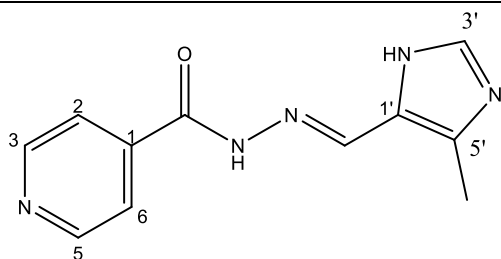
**UV (EtOH, 182 μM, 25°C):** λ=309 nm, ε=5495.05 mol<sup>-1</sup>.L.cm<sup>-1</sup> (very poorly soluble).

**MS(ES, TOF, MeOH) m/z:** 216.0887 [M+H<sup>+</sup>]

**MS (ES, TOF, MeOH) m/z:** 238.0708 [M+Na<sup>+</sup>]

**HRMS (ES, TOF) m/z:** C<sub>10</sub>H<sub>10</sub>N<sub>5</sub>O (calc./found) 216.0885/216.0887 [M+H<sup>+</sup>].

**HRMS (ES, TOF) m/z:** C<sub>10</sub>H<sub>9</sub>N<sub>5</sub>ONa (calc./found) 238.0705/238.0708 [M+Na<sup>+</sup>].

Chemical Formula: C<sub>11</sub>H<sub>11</sub>N<sub>5</sub>O

Molecular Weight: 229.24

Rf: 0.1 EtAc/MeOH (4:1 v/v)

**(E)-N'-((4-methyl-1H-imidazol-5-yl)methylene)isonicotinohydrazide (7b).** mp: 299 °C (dec.).

**<sup>1</sup>H NMR (300 MHz, DMSO-*d*<sub>6</sub>) δ ppm:** 2.43 (s, 3H, CH<sub>3</sub>), 8.42 (dd, *J* = 5.5, 1.8 Hz, 2H, H<sub>2,6</sub>), 8.53 (s, 1H, H-C=N), 9.11 (s, 1H, H<sub>3'</sub>), 9.14 (dd, *J* = 5.5, 1.8 Hz, 2H, H<sub>3,5</sub>), 15.98 (br, 2H, N-H).

**<sup>13</sup>C NMR (75 MHz, DMSO) δ ppm:** 9.38 (1C, CH<sub>3</sub>), 123.60 (1C, C<sub>1'</sub>), 125.38 (2C, C<sub>2,6</sub>), 131.78 (1C, C<sub>5'</sub>), 138.44 (1C, C=N), 142.84 (1C, C<sub>3'</sub>), 144.03 (2C, C<sub>3,5</sub>), 147.78 (1C, C<sub>1</sub>), 159.52 (1C, C=O).

**FTIR (KBr)  $\nu$   $\text{cm}^{-1}$ :** 3194.75 (N–H), 3097.19 ( $\text{C}_{\text{ar}}\text{--H}$ ), 1660.58 (C=O), 1621.45 (C=N–N), 1602.24 ( $\text{C}_{\text{ar}}\text{=C}_{\text{ar}}$ ), 1551.49 ( $\text{C}_{\text{ar}}\text{---N}$ ).

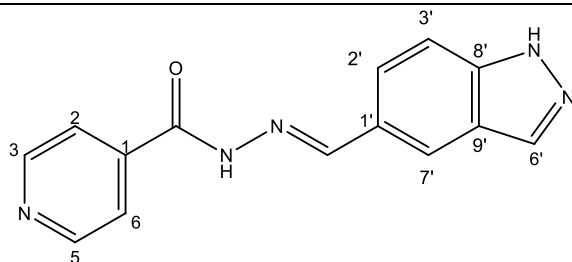
**UV (EtOH, 161.58 $\mu\text{M}$ , 25 $^{\circ}\text{C}$ ):**  $\lambda$ =316 nm,  $\epsilon$ =5551.73  $\text{mol}^{-1}\cdot\text{L}\cdot\text{cm}^{-1}$  (very poorly soluble).

**MS (ES, TOF, MeOH)  $m/z$ :** 230.1049 [ $\text{M}+\text{H}^{+}$ ]

**MS (ES, TOF, MeOH)  $m/z$ :** 252.0866 [ $\text{M}+\text{Na}^{+}$ ]

**HRMS (ES, TOF)  $m/z$ :**  $\text{C}_{11}\text{H}_{12}\text{N}_5\text{O}$  (calc./found) 230.1042/230.1049 [ $\text{M}+\text{H}^{+}$ ]

**HRMS (ES, TOF)  $m/z$ :**  $\text{C}_{11}\text{H}_{11}\text{N}_5\text{ONa}$  (calc./found) 252,0861/252,0866 [ $\text{M}+\text{Na}^{+}$ ].



Chemical Formula:  $\text{C}_{14}\text{H}_{11}\text{N}_5\text{O}$

Molecular Weight: 265.27

Rf: 0.45 PE/EtAc/MeOH (5:5:3 v/v)

**(E)-N'-((3a,7a-dihydro-1H-indazol-5-yl)methylene)isonicotinohydrazide (7c). mp:** 302.5  $^{\circ}\text{C}$ .

**$^1\text{H}$  NMR (300 MHz, DMSO- $d_6$ )  $\delta$  ppm:** 7.63 (d,  $J$  = 8.7 Hz, 1H,  $\text{H}_{3'}$ ), 7.84 (dd,  $J$  = 4.4, 1.6 Hz, 2H,  $\text{H}_{2,6}$ ), 7.90 (dd,  $J$  = 8.8, 1.5 Hz, 1H,  $\text{H}_{2'}$ ), 8.03 – 8.10 (m, 1H,  $\text{H}_{7'}$ ), 8.17 (t,  $J$  = 1.2 Hz, 1H,  $\text{H}_{6'}$ ), 8.57 (s, 1H, H-C=N), 8.79 (s, 2H,  $\text{H}_{3,5}$ ), 12.01 (s, 1H, N-H), 13.31 (s, 1H, N- $\text{H}_{\text{ind}}$ ).

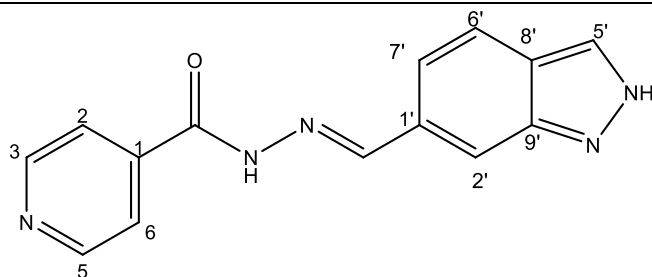
**$^{13}\text{C}$  NMR (75 MHz, DMSO)  $\delta$  ppm:** 111.39 (1C,  $\text{C}_{3'}$ ), 121.98 (2C,  $\text{C}_{2,6}$ ), 122.73 (1C,  $\text{C}_{7'}$ ), 123.35 (1C,  $\text{C}_{9'}$ ), 124.19 (1C,  $\text{C}_{2'}$ ), 127.23 (1C,  $\text{C}_{1'}$ ), 134.99 (1C,  $\text{C}_{6'}$ ), 141.07 (1C,  $\text{C}_1$ ), 141.14 (1C,  $\text{C}_{8'}$ ), 150.31 (1C, C=N), 150.76 (2C,  $\text{C}_{3,5}$ ), 161.87 (1C, C=O).

**FTIR (KBr)  $\nu$   $\text{cm}^{-1}$ :** 3188.96 (N–H), 3027.37 ( $\text{C}_{\text{ar}}\text{--H}$ ), 1652 (C=O), 1622.47 (C=N–N), 1607.84 ( $\text{C}_{\text{ar}}\text{=C}_{\text{ar}}$ ), 1549.40 ( $\text{C}_{\text{ar}}\text{---N}$ )

**UV (EtOH, 38.37 $\mu\text{M}$ , 25 $^{\circ}\text{C}$ ):**  $\lambda$ =234 nm,  $\epsilon$ = 22666.92  $\text{mol}^{-1}\cdot\text{L}\cdot\text{cm}^{-1}$

**MS (ES, TOF, MeOH)  $m/z$ :** 266.1046 [ $\text{M}+\text{H}^{+}$ ]

**HRMS (ES, TOF)  $m/z$ :**  $\text{C}_{14}\text{H}_{12}\text{N}_5\text{O}$  (calc./found) 266,1042/266,1046 [ $\text{M}+\text{H}^{+}$ ].



Chemical Formula:  $\text{C}_{14}\text{H}_{11}\text{N}_5\text{O}$

Molecular Weight: 265.27

Rf: 0.45 PE/EtAc/MeOH (5:5:3 v/v)

**(E)-N'-((2H-indazol-6-yl)methylene)isonicotinohydrazide (7d). mp:** 295.2  $^{\circ}\text{C}$ .

**<sup>1</sup>H NMR (300 MHz, DMSO-*d*<sub>6</sub>) δ ppm:** 7.61 (dd, *J* = 8.5, 1.3 Hz, 1H, H<sub>7'</sub>), 7.84 (m, 4H, H<sub>2,6</sub>, H<sub>2'</sub>, H<sub>6'</sub>), 8.13 (d, *J* = 1.3 Hz, 1H, H<sub>5'</sub>), 8.60 (s, 1H, H-C=N), 8.80 (br, 2H, H<sub>3,5</sub>), 12.12 (s, 1H, N-H), 13.28 (s, 1H, N-H<sub>ind</sub>).

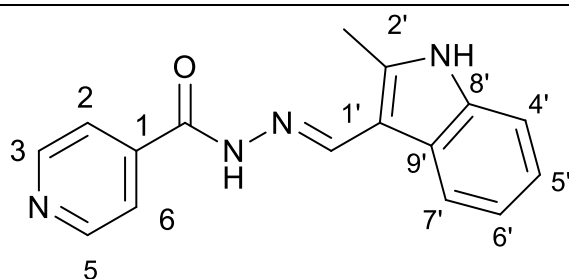
**<sup>13</sup>C NMR (75 MHz, DMSO) δ ppm:** 110.75 (1C, C<sub>2'</sub>), 119.03 (1C, C<sub>7'</sub>), 121.51 (2C, C<sub>2,6</sub>), 122.01 (1C, C<sub>6'</sub>), 124.39 (1C, C<sub>8'</sub>), 132.43 (1C, C<sub>1'</sub>), 134.21 (1C, C<sub>5'</sub>), 140.33 (1C, C<sub>1</sub>), 140.95 (1C, C<sub>9'</sub>), 150.03 (1C, C=N), 150.79 (1C, C<sub>3',5'</sub>), 162.08 (1C, C=O).

**FTIR (KBr) ν cm<sup>-1</sup>:** 3193.59 (N-H), 3038.08 (C-H<sub>ar</sub>), 1648.96 (C=O), 1626.02 (C=N-N), 1596.86 (C=C<sub>ar</sub>), 1551.04 (C<sub>ar</sub> = N), 1506.46 (C=N).

**UV (EtOH, 37.39 μM, 25°C):** λ=313 nm, ε= 25055.1 mol<sup>-1</sup>.L.cm<sup>-1</sup>

**MS (ES, TOF, MeOH) m/z:** 266.1047 [M+H<sup>+</sup>]

**HRMS (ES, TOF) m/z:** C<sub>14</sub>H<sub>12</sub>N<sub>5</sub>O (calc./found) 266.1042/266.1047 [M+H<sup>+</sup>].



Chemical Formula: C<sub>16</sub>H<sub>14</sub>N<sub>4</sub>O  
Molecular Weight: 278.31  
Rf: 0.55 PE/EtAc/MeOH (5:5:3 v/v)

**(E)-N'-((2-methyl-1H-indol-3-yl)methylene)isonicotinohydrazide (7e). mp:** 281.1 °C.

**<sup>1</sup>H NMR (300 MHz, DMSO-*d*<sub>6</sub>) δ ppm:** 2.54 (s, 3H, CH<sub>3</sub>), 7.12 (ddt, *J* = 24.4, 9.3, 1.9, 1.9 Hz, 2H, H<sub>5'</sub>, H<sub>6'</sub>), 7.35 (tt, *J* = 2.4, 1.7, 0.9, 0.8 Hz, 1H, H<sub>4'</sub>), 7.85 (dd, *J* = 4.5, 1.8 Hz, 2H, H<sub>2,6</sub>), 8.16 – 8.32 (m, 1H, H<sub>7'</sub>), 8.71 (s, 1H, H-C=N), 8.78 (dd, *J* = 4.4, 1.6 Hz, 2H, H<sub>3,5</sub>), 11.55 (d, *J* = 7.4 Hz, 1H, N-H), 11.67 (s, 1H, N-H<sub>ind</sub>).

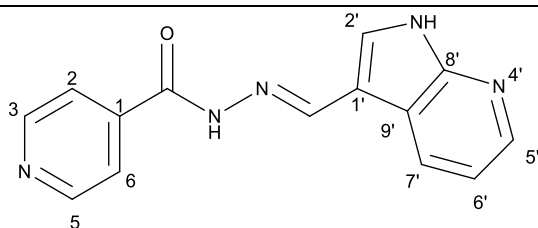
**<sup>13</sup>C NMR (75 MHz, DMSO) δ ppm:** 11.97 (1C, CH<sub>3</sub>), 107.84 (1C, C<sub>1'</sub>), 111.34 (1C, C<sub>4'</sub>), 120.82 (1C, C<sub>7'</sub>), 121.63 (1C, C<sub>5'</sub>), 121.87 (2C, C<sub>2,6</sub>), 122.34 (1C, C<sub>6'</sub>), 125.85 (1C, C<sub>9'</sub>), 136.19 (1C, C<sub>8'</sub>), 141.05 (1C, C<sub>2'</sub>), 141.56 (1C, C<sub>1</sub>), 146.10 (1C, C=N), 150.69 (2C, C<sub>3,5</sub>), 161.00 (1C, C=O).

**FTIR (KBr) ν cm<sup>-1</sup>:** 3385.07 (N-H), 3209.03 (N-H), 3049.08 (C<sub>ar</sub>-H), 1655.09 (C=O), 1626.02 (C=N-N), 1599.50 (C=C<sub>ar</sub>), 1550.60 (C<sub>ar</sub> = N), 1506.46 (C=N).

**UV (EtOH, 57.29 μM, 25°C):** λ=224 nm, ε=21909,58 mol<sup>-1</sup>.L.cm<sup>-1</sup>.

**MS (ES, TOF, MeOH) m/z:** 279.1246 [M+H<sup>+</sup>]

**HRMS (ES, TOF) m/z:** C<sub>16</sub>H<sub>15</sub>N<sub>4</sub>O (calc./found) 279.1246/279.1246 [M+H<sup>+</sup>].



Chemical Formula: C<sub>14</sub>H<sub>11</sub>N<sub>5</sub>O  
 Molecular Weight: 265.27  
 Rf: 0.34 PE/EtAc/MeOH (5:5:3 v/v)

**(E)-N'-((1H-pyrrolo[2,3-b]pyridin-3-yl)methylene)isonicotinohydrazide (7f). mp:**  
 323.2 °C (dec.)

**<sup>1</sup>H NMR (300 MHz, DMSO-*d*<sub>6</sub>) δ ppm:** 77.24 (tt, *J* = 7.8, 4.7, 4.7 Hz, 1H, H<sub>6'</sub>), 7.84 (dd, *J* = 4.2, 1.7 Hz, 2H, H<sub>2,6</sub>), 8.03 (d, *J* = 2.3 Hz, 1H, H<sub>2'</sub>), 8.33 (dd, *J* = 4.7, 1.7 Hz, 1H, H<sub>7'</sub>), 8.58 (d, *J* = 1.6 Hz, 1H, H<sub>5'</sub>), 8.62 (s, 1H, H-C=N), 8.78 (dd, *J* = 4.4, 1.7 Hz, 2H, H<sub>3,5</sub>), 11.86 (s, 1H, N-H), 12.17 (s, 1H, N-H<sub>ind</sub>).

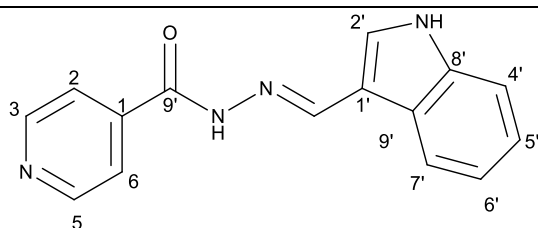
**<sup>13</sup>C NMR (75 MHz, DMSO) δ ppm:** 110.85(1C, C<sub>1</sub>), 117.13 (1C, C<sub>9'</sub>), 117.44 (1C, C<sub>6'</sub>), 121.95 (2C, C<sub>2,6</sub>), 130.56(1C, C<sub>5'</sub>), 131.51 (1C, C<sub>2'</sub>), 141.39(1C, C<sub>1</sub>), 144.56(1C, C<sub>7'</sub>), 146.09 (1C, C=N), 149.84(1C, C<sub>8'</sub>), 150.71 (2C, C<sub>3,5</sub>), 161.49 (1C, C=O).

**FTIR (KBr) ν cm<sup>-1</sup>:** 3454.03 (N-H), 3199.51 (N-H), 3031.09 (C<sub>ar</sub>-H), 1662.68 (C=O), 1611.72 (C=N-N), 1600.48 (C=C<sub>ar</sub>), 1551.26 (C<sub>ar</sub> = N), 1284.78 (C-N).

**UV (EtOH, 58.08 μM, 25°C):** λ=200 nm, ε= 18839.92 mol<sup>-1</sup>.L.cm<sup>-1</sup>, λ=218 nm, ε=17446.62 mol<sup>-1</sup>.L.cm<sup>-1</sup>, λ=322 nm, ε=17193.69 mol<sup>-1</sup>.L.cm<sup>-1</sup>.

**MS (ES, TOF, MeOH) m/z:** 266.1045 [M+H<sup>+</sup>]

**HRMS (ES, TOF) m/z:** C<sub>14</sub>H<sub>12</sub>N<sub>5</sub>O (calc./found) 266.1042/266.1045 [M+H<sup>+</sup>].



Chemical Formula: C<sub>15</sub>H<sub>12</sub>N<sub>4</sub>O  
 Molecular Weight: 264.28  
 Rf: 0.55 PE/EtAc/MeOH (5:5:3 v/v)

**(E)-N'-((1H-indol-3-yl)methylene)isonicotinohydrazide (7g). mp:** 242 °C.

**<sup>1</sup>H NMR (300 MHz, DMSO-*d*<sub>6</sub>) δ ppm:** δ 7.11 – 7.28 (m, 2H, H<sub>5',6'</sub>), 7.47 (dt, *J* = 7.9, 0.9 Hz, 1H, H<sub>4'</sub>), 7.85 (dd, *J* = 4.4, 1.6 Hz, 2H, H<sub>2,6</sub>), 7.88 (d, *J* = 2.8 Hz, 1H, H<sub>2'</sub>), 8.31 (dd, *J* = 6.8, 1.5 Hz, 1H, H<sub>9'</sub>), 8.65 (s, 1H, H-C=N), 8.78 (dd, *J* = 4.4, 1.6 Hz, 2H, H<sub>3,5</sub>), 11.65 (s, 1H, N-H), 11.76 (s, 1H, N-H<sub>ind</sub>).

**<sup>13</sup>C NMR (75 MHz, DMSO) δ ppm:** 111.96 (1C, C<sub>1'</sub>), 112.34 (1C, C<sub>4'</sub>), 120.77 (1C, C<sub>3'</sub>), 121.00 (1C, C<sub>5'</sub>), 121.95 (2C, C<sub>2,6</sub>), 122.44 (1C, C<sub>7'</sub>), 123.17 (1C, C<sub>6'</sub>), 123.35(1C, C<sub>7'</sub>), 124.77 (1C,

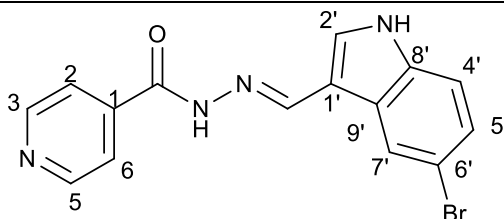
$C_{9'}$ ), 131.36 (1C,  $C_{2'}$ ), 137.53 (1C,  $C_{8'}$ ), 141.54 (1C,  $C_1$ ), 146.63 (1C, C=N), 150.69 (2C,  $C_{3,5}$ ), 161.33 (1C, C=O).

**FTIR (KBr)  $\nu$   $cm^{-1}$ :** 3543.66 (N–H), 3395.82 (N–H), 2886.55 (C–H<sub>ar</sub>), 1656.52 (C=O), 1626.02 (C=N–N), 1598.83 (C=C<sub>ar</sub>), 1550.54 (C<sub>ar</sub>  $\cdots$  N), 1496.83 (C=N).

**UV (EtOH, 40.01  $\mu$ M, 25°C):**  $\lambda=221$  nm,  $\epsilon=22519$  mol<sup>-1</sup>.L.cm<sup>-1</sup>

**MS (ES, TOF, MeOH) m/z:** 265.1092 [M+H<sup>+</sup>]

**HRMS (ES, TOF) m/z:** C<sub>15</sub>H<sub>13</sub>N<sub>4</sub>O (calc./found) 265,1089/265,1092 [M+H<sup>+</sup>].



Chemical Formula: C<sub>15</sub>H<sub>11</sub>BrN<sub>4</sub>O  
Molecular Weight: 343.18  
Rf: 0.61 PE/EtAc/MeOH (5:5:3 v/v)

**(E)-N'-((5-bromo-1H-indol-3-yl)methylene)isonicotinohydrazide (7h).** mp: 309.3 °C (dec.)

**<sup>1</sup>H NMR (300 MHz, DMSO-*d*<sub>6</sub>)  $\delta$  ppm:** 7.35 (dd,  $J = 8.7, 2.1$  Hz, 1H,  $H_{5'}$ ), 7.44 (d,  $J = 8.5$  Hz, 1H,  $H_{4'}$ ), 7.84 (dd,  $J = 4.5, 1.9$  Hz, 2H,  $H_{2,6}$ ), 7.95 (d,  $J = 2.7$  Hz, 1H,  $H_{9'}$ ), 8.48 (s, 1H,  $H_{2'}$ ), 8.62 (s, 1H, H-C=N), 8.73 – 8.89 (m, 2H,  $H_{3,5}$ ), 11.83 (d,  $J = 6.0$  Hz, 2H, N-H).

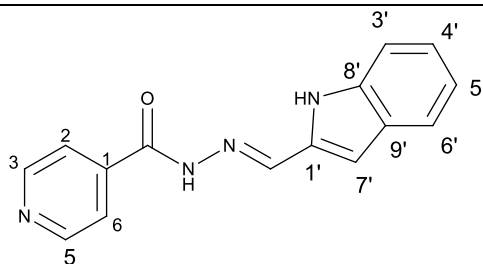
**<sup>13</sup>C NMR (75 MHz, DMSO)  $\delta$  ppm:** 111.59(1C,  $C_{1'}$ ), 113.70 (1C,  $C_{6'}$ ), 114.42 (1C,  $C_{4'}$ ), 121.93 (2C,  $C_{2,6}$ ), 124.60 (1C,  $C_{2'}$ ), 125.71 (1C,  $C_{5'}$ ), 126.42 (1C,  $C_{9'}$ ), 132.71 (1C,  $C_{7'}$ ), 136.27 (1C,  $C_{8'}$ ), 141.38 (1C,  $C_1$ ), 146.13 (1C, C=N), 150.72 (2C,  $C_{3,5}$ ), 161.40 (1C, C=O).

**FTIR (KBr)  $\nu$   $cm^{-1}$ :** 3127.58 (N–H<sub>ind</sub>), 2891.39 (C–H<sub>ar</sub>), 1662.69 (C=O), 1618.34 (C=N–N), 1538 (C=C<sub>ar</sub>), 1552.13 (C<sub>ar</sub>  $\cdots$  N), 1041.12 (C<sub>ar</sub>–Br).

**UV (EtOH, 52.65  $\mu$ M, 25°C):**  $\lambda=201$  nm,  $\epsilon=29890$  mol<sup>-1</sup>.L.cm<sup>-1</sup>,  $\lambda=226$  nm,  $\epsilon=25981$  mol<sup>-1</sup>.L.cm<sup>-1</sup>,  $\lambda=330$  nm,  $\epsilon=18196$  mol<sup>-1</sup>.L.cm<sup>-1</sup>.

**MS (ES, TOF, MeOH) m/z:** 343.0194 [M+H<sup>+</sup>]

**HRMS (ES, TOF) m/z:** C<sub>15</sub>H<sub>12</sub>BrN<sub>4</sub>O (calc./found) 343.0193/343.0194 [M+H<sup>+</sup>].



Chemical Formula: C<sub>15</sub>H<sub>12</sub>N<sub>4</sub>O  
Molecular Weight: 264.28  
Rf: 0.82 PE/EtAc/MeOH (5:5:3 v/v)

**(E)-N'-((1H-indol-2-yl)methylene)isonicotinohydrazide (7i).** mp: 231°C (dec.)

**<sup>1</sup>H NMR (300 MHz, DMSO-*d*<sub>6</sub>) δ ppm:** 76.90 (dd, *J* = 2.1, 0.9 Hz, 1H), 7.02 (ddd, *J* = 8.0, 7.0, 1.1 Hz, 1H), 7.18 (ddd, *J* = 8.3, 7.0, 1.2 Hz, 1H), 7.47 (dq, *J* = 8.2, 0.9 Hz, 1H), 7.58 (dd, *J* = 7.9, 1.1 Hz, 1H), 7.86 (dd, *J* = 4.4, 1.6 Hz, 2H), 8.51 (s, 1H), 8.81 (dd, *J* = 4.4, 1.7 Hz, 2H), 11.65 (s, 1H), 12.05 (s, 1H).

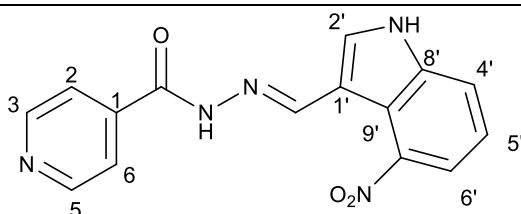
**<sup>13</sup>C NMR (75 MHz, DMSO) δ ppm:** 107.98 (1C, C<sub>2'</sub>), 112.57 (1C, C<sub>3'</sub>), 120.06 (1C, C<sub>4'</sub>), 121.31 (1C, C<sub>6'</sub>), 122.01 (2C, C<sub>2, 6</sub>), 128.05 (1C, C<sub>9'</sub>), 133.28 (1C, C<sub>1'</sub>), 138.47 (1C, C<sub>8'</sub>), 142.16 (1C, C=N), 150.79 (2C, C<sub>3, 5</sub>), 161.84 (1C, C=O).

**FTIR (KBr) ν cm<sup>-1</sup>:** 3250.19 (N-H), 3032.16 (C-H<sub>ar</sub>), 1689.09 (C=O), 1621.50 (C=N-N), 1599.80 (C=C ar), 1548.50 (C<sub>ar</sub> = N).

**UV (EtOH, 52.65 μM, 25°C):** λ=206 nm, ε=27480 mol<sup>-1</sup>.L.cm<sup>-1</sup>, λ=350 nm, ε=33825 mol<sup>-1</sup>.L.cm<sup>-1</sup>.

**MS (ES, TOF, MeOH) m/z:** 265.1090 [M+H<sup>+</sup>]

**HRMS (ES, TOF) m/z:** C<sub>15</sub>H<sub>13</sub>N<sub>4</sub>O (calc./found) 265,1089/265,1090 [M+H<sup>+</sup>].



Chemical Formula: C<sub>15</sub>H<sub>11</sub>N<sub>5</sub>O<sub>3</sub>  
Molecular Weight: 309.28  
Rf: 0.70 PE/EtAc/MeOH (5:5:3 v/v)

**(E)-N'-((4-nitro-1H-indol-3-yl)methylene)isonicotinohydrazide (7j). mp:** 3017.1 °C (dec.)

**<sup>1</sup>H NMR (300 MHz, DMSO-*d*<sub>6</sub>) δ ppm:** 7.36 (t, *J* = 8.0 Hz, 1H, H<sub>5'</sub>), 7.84 (dd, *J* = 4.4, 1.7 Hz, 2H, H<sub>2, 6</sub>), 7.94 (dd, *J* = 11.8, 7.9 Hz, 2H, H<sub>4', 6'</sub>), 8.28 (d, *J* = 2.9 Hz, 1H, H<sub>2'</sub>), 8.78 (dd, *J* = 4.4, 1.7 Hz, 2H, H<sub>3, 5</sub>), 8.91 (s, 1H, H-C=N), 12.00 (s, 1H, N-H), 12.55 (s, 1H, N-H).

**<sup>13</sup>C NMR (75 MHz, DMSO) δ ppm:** 110.29 (1C, C<sub>9'</sub>), 117.59 (1C, C<sub>1'</sub>), 118.94 (1C, C<sub>4'</sub>), 119.92 (1C, C<sub>6'</sub>), 121.50 (1C, C<sub>6'</sub>), 122.01 (2C, C<sub>2, 6</sub>), 131.31 (1C, C<sub>2'</sub>), 139.55 (1C, C<sub>8'</sub>), 141.22 (1C, C<sub>1</sub>), 141.90 (1C, C-NO<sub>2</sub>), 146.43 (1C, C=N), 150.66 (2C, C<sub>3, 5</sub>), 161.56 (1C, C=O).

**FTIR (KBr) ν cm<sup>-1</sup>:** 3156.34 (N-H), 3137.68 (N-H), 3053.25 (C-H<sub>ar</sub>), 1664.06 (C=O), 1628.34 (C=N-N), 1590.99 (C=C ar), 1554.10 (C<sub>ar</sub> = N), 1513.15 (C=N), NO<sub>2</sub>.

**UV (EtOH, 52.64 μM, 25°C):** λ=214 nm, ε=26971,88 mol<sup>-1</sup>.L.cm<sup>-1</sup>, λ=331 nm, ε=17046,35 mol<sup>-1</sup>.L.cm<sup>-1</sup>.

**MS (ES, TOF, MeOH) m/z:** 310.0940 [M+H<sup>+</sup>]

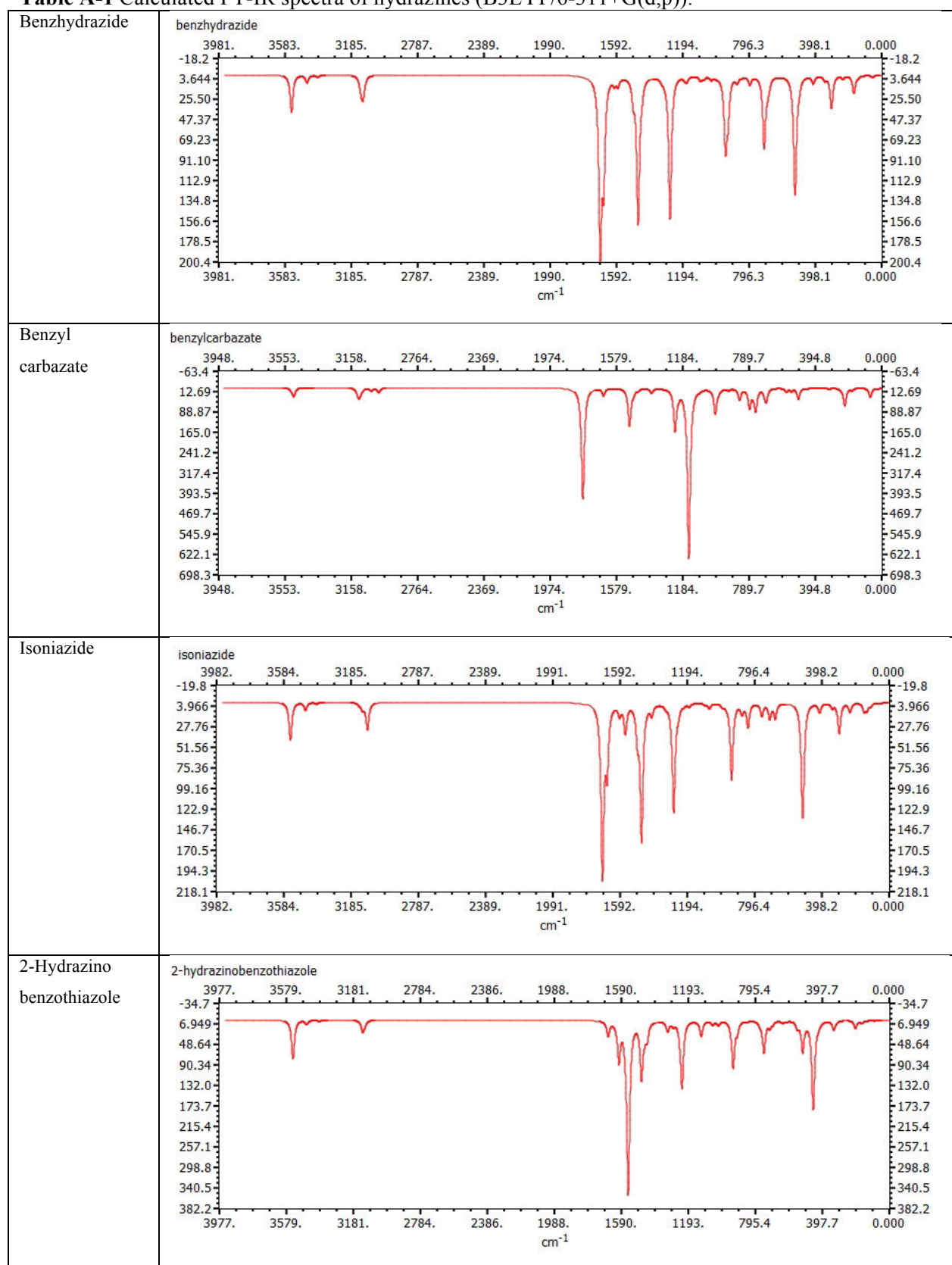
**MS (ES, TOF, MeOH) m/z:** 332.0760 [M+Na<sup>+</sup>]

**HRMS (ES, TOF) m/z:** C<sub>15</sub>H<sub>12</sub>N<sub>5</sub>O<sub>3</sub> (calc./found) 310.0937/310.0940 [M+H<sup>+</sup>]

**HRMS (ES, TOF) m/z:** C<sub>15</sub>H<sub>11</sub>N<sub>5</sub>O<sub>3</sub>Na (calc./found) 332.0752/332.0760 [M+Na<sup>+</sup>].



## APPENDIX III – FTIR STUDIES

**Table A-1** Calculated FT-IR spectra of hydrazines (B3LYP/6-311+G(d,p)).

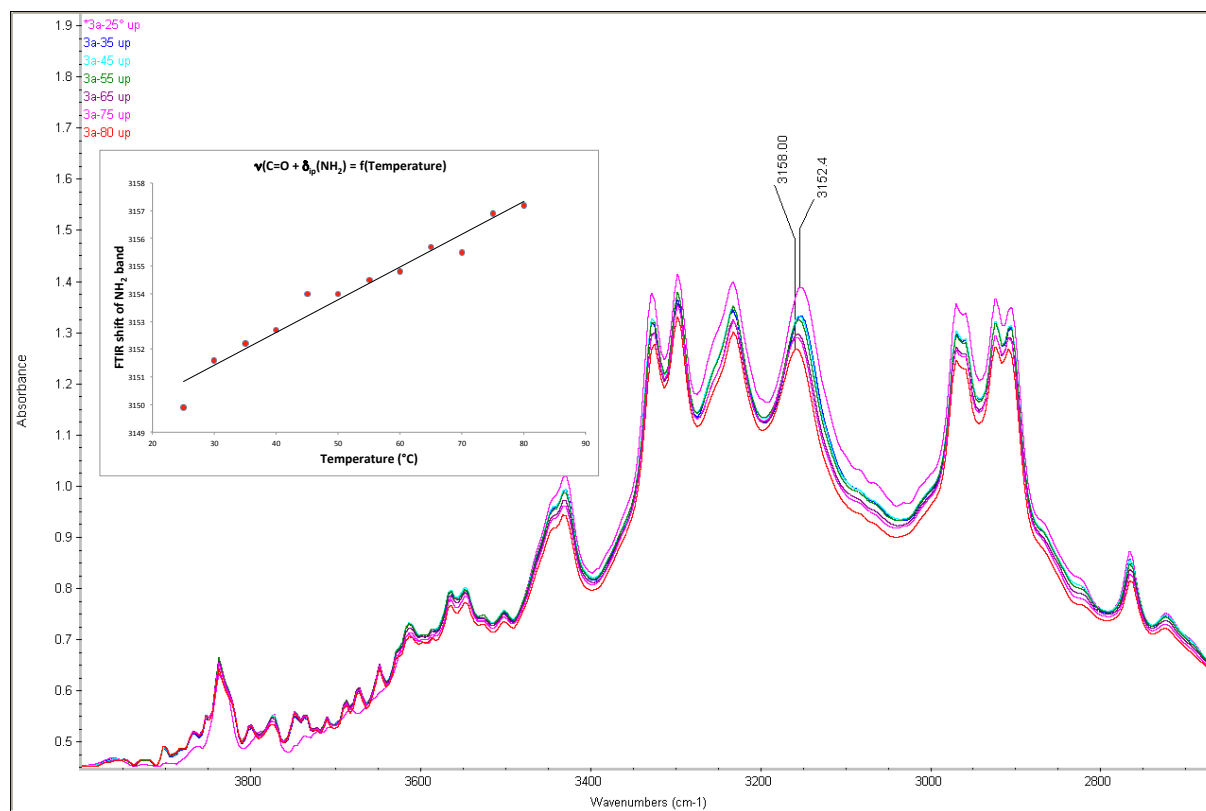
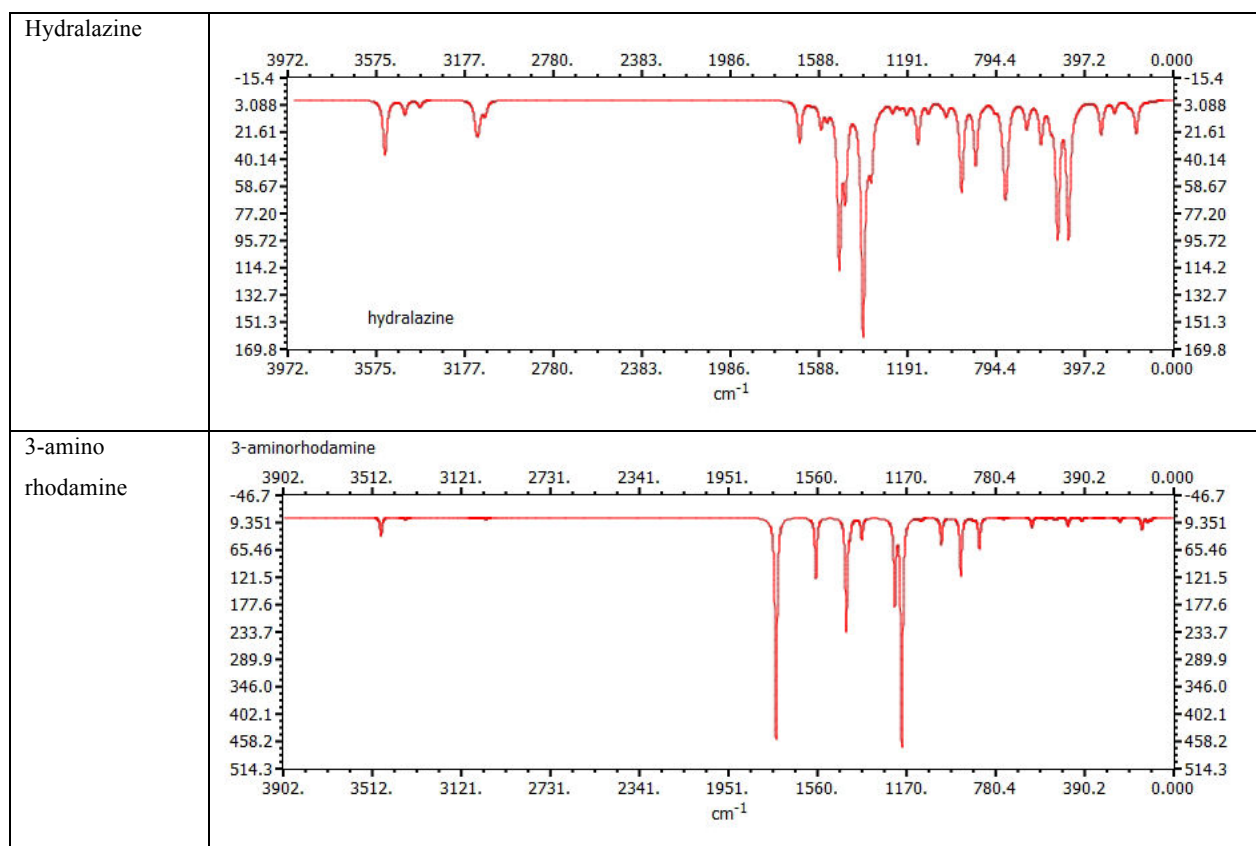


**Figure A-1** Shift of NH<sub>2</sub> band of 3-aminorhodanine as function of temperature.

## ACRONYMS, ABBREVIATIONS AND SYMBOLS

### Acronyms and Abbreviations

AA	anthranilic acid
ACN	acetonitrile
ACP	acyl carrier protein
ACS	American Chemical Society
AFM	atomic force microscope
AG	agate
API	Active Pharmaceutical Ingredient
BCB	benzocyclobutene
Boc	tert-butoxycarbonyl
BPR	ball-to-powder weight ratio
BQ	benzoquinone
BR	brass
BZ	benzil
BZP	benzophenone
CCDC	Cambridge Crystallographic Data Centre
COD	Crystallography Open Database
CP-MAS	Cross Polarization and Magic Angle Spinning
CPX	ciprofloxacin
CU	copper
DABCO	1,4-diazabicyclo[2.2.2]octane
DBPZ	dibenzo[a,c]phenazine
DFT	density functional theory
DLS	dynamic light scattering
DMSO	dimethyl sulfoxide
DPA	diphenylamine
DPQ	2,3-diphenylquinoxaline
DSC	differential scanning calorimetry
EMB	ethambutol
ETH	ethionamide
FAS	fatty acid synthases
Fmoc	9-fluorenylmethoxycarbonyl
FTIR	Fourier Transformed Infrared Spectroscopy
GCI	Green Chemistry Institute
HIm	ZnO-Imidazole
HIV	human immunodeficiency virus
HMeIm	ZnO-Methylimidazole
HOMO	Highest Occupied Molecular Orbital
HPLC	high-performance liquid chromatography
HRMS	high resolution mass spectrometry
HSM	hot-stage microscopy
ILAG	Ion- and Liquid-Assisted Grinding
INCOME	International Conference on Mechanochemistry and Mechanical Alloying
INH	isoniazid
IPTG	isopropyl- $\beta$ -D-galactopyranoside
IUPAC	International Union of Pure and Applied Chemistry

JCPDS	Joint Committee on Powder Diffraction Standards
<i>katG</i>	<i>mycobacterial catalase-peroxidase enzyme</i>
LAG	Liquid-Assisted Grinding
LD <sub>50</sub>	lethal dose to kill 50% of the test population
LUMO	Lowest Unoccupied Molecular Orbital
MIC	minimum inhibitory concentration
MM	mixer mill
MOF	Metal-Organic Framework
MS	Mass Spectrometry
<i>Mtb</i>	<i>Mycobacterium tuberculosis</i>
NAD	nicotinamide adenine dinucleotide
NBO	Natural Bond Orbital
NMR	Nuclear Magnetic Resonance
OD	optical density
<i>p</i> -TSA	<i>p</i> -toluenesulfonic acid
P0	vibratory ball mill Pulversitte 0 – Fritsch
PDA	<i>o</i> -phenylenediamine
PIPES	1,4-Piperazinediethanesulfonic acid
PM	physical mixture
PM	planetary mill
PMI	Process Mass Intensity
PQ	9,10-phenanthrenequinone
PR	Pharmaceutical Roundtable
PSA	<i>p</i> -aminosalicylic acid
PZA	pyrazinamide
RIF	rifampicin
SA	salicylic acid
SD	sulfadiimide
SI	selectivity index
SM	streptomycin
SMD	solvent continuum model
SNOM	scanning near-field optical microscope
SS	stainless steel
TB	tuberculosis
TEA	triethylamine
TGA	Thermogravimetric analysis
TLC	Thin Layer Chromatography
UNCA	urethane-protected $\alpha$ -amino acid <i>N</i> -carboxyanhydride
UV- <i>vis</i>	ultraviolet-visible spectrophotometry
WH	Woodward-Hoffmann
WHO	World Health Organization
XRD	X-ray diffraction
ZIF	zeolitic imidazolate framework

**Symbols**

$\Delta G^\ddagger$	Gibbs free energy of activation
$\Delta H$	enthalpy
$\Delta H^\ddagger$	enthalpy of activation
$\Delta H_{fus}$	enthalpy of fusion
$\Delta H_{sub}$	enthalpy of sublimation

$\Delta S^\ddagger$	entropy of activation
$A$	absorbance
$A$	pre-exponential factor or frequency factor
$d_{MB}$	milling ball diameter
$E^*$	contribution on the activating energy from mechanical action
$E_0$	activation energy in absence of mechanical stress
$E_a$	activation energy
$h$	Planck constant
$k$	reaction rate constant
$k_B$	Boltzmann constant
LogP	Log (partition coefficient)
$m_{MB}$	milling ball mass/weight
pKa	-log (acid dissociation constant)
$R$	universal gas constant
$T$	absolute temperature
$T_b$	bath temperature
$T_c$	coalescence temperature
$T_g$	glass transition temperature
$T_m$	milling temperature
$X_i$	reaction conversion for the compound i
$\alpha$	reaction extent (analogous to $X_i$ )
$\delta$	chemical shift in NMR spectra
$\nu$	vibrational frequency in infrared spectra
$\rho$	absolute density

---

**LIST OF FIGURES, SCHEMES AND TABLES**
**List of Figures**

<b>Figure 1.1.</b> Types of mills for high-energy milling .....	12
<b>Figure 1.2</b> Ball mills used in laboratory for mechanochemistry purpose and their respective milling media.....	13
<b>Figure 1.3.</b> Stretching of a single polysaccharide chain that is covalently attached between an amino-functionalized glass or gold surface and the AFM tip .....	17
<b>Figure 1.4.</b> Paracetamol-theophylline cocrystal formation in ball milling (LAG, MeOH) conditions .....	19
<b>Figure 1.5.</b> The first MOFs mechanochemically synthesized .....	20
<b>Figure 1.6.</b> Softly layered powders: (left) 2,2'-biphenol and benzoquinone; (right) 4,4'-biphenol and benzoquinone.....	38
<b>Figure 1.7.</b> The eutectic melting of benzophenone and diphenylamine crystals .....	40
<b>Figure 1.8.</b> Electrolytic ring opening of cyclobutene.....	44
<b>Figure 2.1.</b> Vibratory ball mill - Pulverisette 0 (Fritsch) (a) picture, (b) simplified scheme of the apparatus.....	58
<b>Figure 2.2.</b> Amplitude display.....	58
<b>Figure 2.3.</b> Picture of the experimental set.....	59
<b>Figure 2.4.</b> Analytical calibration curve and the parameters for benzil .....	62
<b>Figure 2.5.</b> Preparation of the samples for HPLC.....	62
<b>Figure 2.6.</b> Experimental apparatus for simultaneously DSC analysis and visual observation of phase transitions: on the top, general scheme and on the bottom, the hot-stage cell (FP84HT). .....	65
<b>Figure 3.1</b> General scheme for DBPZ stepwise formation .....	72
<b>Figure 3.2.</b> Vibronic coupling densities for effective vibrations of $C_s$ and $C_2$ symmetrical diamine cations and the energy gap between them .....	73
<b>Figure 3.3.</b> Synthesis of dibenzo[a,c]phenazine (DBPZ) by co-grinding. ....	74
<b>Figure 3.4.</b> Kinetic monitoring of PQ transformation for DBPZ synthesis. ....	75
<b>Figure 3.5.</b> Nonlinearized data fit to the generalized Avrami-Erofeev's equation for DBPZ synthesis. ....	77
<b>Figure 3.6.</b> Heat release patterns for the reaction continuation after grinding for DBPZ synthesis. ....	78

<b>Figure 3.7.</b> Heat release and PQ conversion after 30 min of grinding.....	80
<b>Figure 3.8.</b> $^{13}\text{C}$ CP-MAS NMR spectra for different milling times for DBPZ synthesis. The acquisitions were performed immediately after the milling time. ....	82
<b>Figure 3.9.</b> The possible intermediate (AB) containing C-OH. ....	83
<b>Figure 3.10.</b> Energy diagrams representation and the relative energies for the (a) concerted addition mechanisms and (b) stepwise mechanism .....	83
<b>Figure 3.11.</b> $^{13}\text{C}$ CP-MAS NMR spectra after 30 min of grinding for DBPZ synthesis. The acquisitions were performed each hour (20' of integration + 40' waiting) during 24 h. ....	84
<b>Figure 3.12.</b> XRD patterns for solid-state qualitative monitoring of DBPZ synthesis during continuous milling (PQ: black, PDA: red, DBPZ: green).....	86
<b>Figure 3.13.</b> XRD patterns for solid-state qualitative monitoring of DBPZ synthesis after 30 min of grinding.....	87
<b>Figure 3.14.</b> XRD patterns of DBPZ obtained in different conditions.....	88
<b>Figure 3.15.</b> Synthesis of 2,3-diphenylquinoxaline (DPQ) by co-grinding. ....	90
<b>Figure 3.16.</b> Kinetic monitoring of BZ transformation for DBPZ synthesis: concentration and conversion of benzil (top) and moles of product and reactant (down).....	91
<b>Figure 3.17.</b> Heat release patterns for the reaction continuation after grinding for DPQ synthesis. ....	92
<b>Figure 3.18.</b> Heat flow and reaction extent after 15 min of grinding for DPQ synthesis. ....	93
<b>Figure 3.19.</b> $^{13}\text{C}$ CP-MAS NMR spectra for different milling times for DPQ synthesis. The acquisitions were performed immediately after the milling time. ....	95
<b>Figure 3.20.</b> $^{13}\text{C}$ CP-MAS NMR spectra after 15 min of grinding for DPQ synthesis .....	96
<b>Figure 3.21.</b> XRD patterns for solid-state qualitative monitoring of DPQ synthesis during continuous milling (BZ: black, PDA: red, DPQ: green).....	97
<b>Figure 3.22.</b> XRD patterns for solid-state qualitative monitoring of DPQ synthesis after 15 min of grinding.....	98
<b>Figure 3.23.</b> XRD patterns of DPQ obtained mechanochemically, from reaction continuation after grinding and recrystallized.....	99
<b>Figure 4.1.</b> Effect of the milling ball material on the kinetics of transformation for DPQ synthesis. ....	116
<b>Figure 4.2.</b> Pictures of stainless steel ball (SS2 - top) and copper ball (CU - bottom) before (left) and after (right) use. ....	117
<b>Figure 4.3.</b> Effect of the weight of milling ball on the kinetics of transformation for DPQ synthesis. ....	117

<b>Figure 4.4.</b> Effect of the milling ball diameter on the kinetics of transformation for DPQ synthesis. ....	118
<b>Figure 4.5.</b> Effect of the particle size on the kinetics of transformation for DPQ synthesis. ....	120
<b>Figure 4.6.</b> Kinetic curves of DPQ synthesis for different temperatures and weights of the balls: (a) 12 °C, (b) 16 °C, (c) 21 °C, (d) 27 °C, (e) 32 °C and (f) 35 °C. ....	121
<b>Figure 4.7.</b> Kinetic curves for DPQ formation in no grinding state: (a) reactants mixture (they were milled separated before contact) and (b) co-milled during 15 min (red points) and left in static state .....	123
<b>Figure 4.8.</b> Rate constants as function of the milling temperature ( $T_m$ ). ....	125
<b>Figure 4.9.</b> DSC thermogram for reactants mixture in equimolar amounts of PDA and BZ. ....	125
<b>Figure 4.10.</b> Images from the hot-stage cell with BZ (yellow) and PDA (brown-white) crystals under heat (10 °C/min) showing the different stages of the contact melting. ....	127
<b>Figure 4.11.</b> Arrhenius plot with the rate constants and the milling temperature ( $T_m$ ) for DPQ synthesis in P0 with different weights of the balls ( $m_{MB}$ ). ....	129
<b>Figure 4.12.</b> Eyring plot with the rate constants and the milling temperature ( $T_m$ ) for DPQ synthesis in P0 with different weights of the balls ( $m_{MB}$ ). ....	129
<b>Figure 4.13.</b> Proposed scheme of reaction rate for mechanically-induced DPQ synthesis as function of milling temperature and weigh of the milling ball in vibratory ball-mill P0 ....	132
<b>Figure 5.1.</b> Hydrazone structure .....	144
<b>Figure 5.2.</b> Structures of mycolic acids: A – $\alpha$ -mycolic acid; B – <i>cis</i> -methoxy mycolic acid; C – <i>trans</i> -methoxy mycolic acid; D – <i>cis</i> -ketomycolic acid; E – <i>trans</i> -ketomycolic acid. ....	147
<b>Figure 5.3.</b> Synthesis of mycolic acids in <i>M. tuberculosis</i> . ....	148
<b>Figure 5.4.</b> Substrate reduction mechanism catalyzed by NADH-dependent enoyl-ACP reductase (InhA). ....	149
<b>Figure 5.5.</b> First-line antitubercular drugs structures. ....	149
<b>Figure 5.6.</b> Second-line antitubercular drug structures. ....	150
<b>Figure 5.7.</b> Mechanism of action of isoniazid (INH). ....	151
<b>Figure 5.8.</b> General synthesis of hydrazones in solid-state by co-grinding of a hydrazine and an aldehyde. ....	158
<b>Figure 5.9.</b> Raman spectra of hydrazone formation ( <b>5a</b> ) after 1, 2 and 4 hours of grinding. ....	159
<b>Figure 5.10.</b> The electronic and solid-state balance in reactivity of hydrazines .....	165
<b>Figure 5.11.</b> Indole, indazole and imidazole ring structures. ....	167
<b>Figure 5.12.</b> General scheme of isoniazid derivative mechanosynthesis using <i>p</i> -TSA. ....	168
<b>Figure 5.13.</b> Possible forms of <i>N</i> -acylhydrazones. ....	170



<b>Figure 5.14.</b> Optimized geometry for <b>1c</b> <i>E</i> -rotamers and the transition state (TS).....	171
<b>Figure 5.15.</b> <sup>1</sup> H NMR spectra of <b>1c</b> recorded at different temperatures showing the coalescent of the small signals. ....	172
<b>Figure 5.16.</b> <sup>1</sup> H NMR spectra of <b>7d</b> recorded at different temperatures showing the coalescent of the small signals. ....	178
<b>Figure 5.17.</b> Charges of the hydrazone <b>1a</b> as function of pH.....	186
Figure 5.18. Changes on the UV- <i>vis</i> 1a spectra as function of pH variation. ....	187
<b>Figure 5.19.</b> Plots of absorbance at specific wavelengths ( $\lambda$ /nm) as function of pH. ....	187

**List of Schemes**

<b>Scheme 1.1.</b> Aldol condensation of ninhydrin (Kaupp et al., 2002).....	21
<b>Scheme 1.2.</b> Proline-catalyzed asymmetric aldol reaction (Rodríguez et al., 2006). .....	22
<b>Scheme 1.3.</b> Quantitative uncatalyzed Knoevenagel condensation of aldehydes with barbituric acids (Kaupp et al., 2003). .....	22
<b>Scheme 1.4.</b> Michael addition of diethyl malonate to chalcones catalyzed by $K_2CO_3$ (Zhang et al., 2004 <sup>a,b</sup> ). .....	23
<b>Scheme 1.5.</b> Diels-Alder reaction catalyzed by phenol derivatives (Watanabe and Senna, 2005).....	23
<b>Scheme 1.6.</b> Pd-catalyzed Heck-Jeffrey reaction under ball milling conditions (Tullberg et al., 2004).....	24
<b>Scheme 1.7.</b> Pd-catalyzed Suzuki-Miyaura reaction with different aryl halides in the presence of KF- $Al_2O_3$ (32 wt% KF) (Schneider and Ondruschka, 2008).....	25
<b>Scheme 1.8.</b> Sonogashira reaction in high-speed ball milling conditions (Fulmer et al., 2009). .....	25
<b>Scheme 1.9.</b> (a) azine and (b) thiourea formation in ball mills (Kaupp and Schmeyers, 2000). .....	27
<b>Scheme 1.10.</b> Kneading ball milling for the preparation of 2,4-dinitrophenylhydrazones in presence of water (Kaupp et al., 2000).....	27
<b>Scheme 1.11.</b> Azine, formation from the reaction of dicarbonyl compounds and the 'solid-hydrazine' (Lee et al., 2011 <sup>a</sup> ). .....	27
<b>Scheme 1.12.</b> (a) Hydrazone formation (b) and an example of N-alkylation in ball mills (Nun et al., 2011).....	28
<b>Scheme 1.13.</b> Synthesis of dipeptides under solvent-free ball milling conditions (Declerck et al., 2009).....	29
<b>Scheme 1.14.</b> Synthesis of symmetrical and non-symmetrical o-phenylenediamine (thio)urea derivatives by ball milling (LAG) (Štrukil et al., 2012 <sup>b</sup> ). .....	30
<b>Scheme 1.15.</b> Pyrrole derivatives synthesis in ball mill - 4-step reaction (Kaupp et al., 1999). .....	30
<b>Scheme 1.16.</b> Sequential three-component pyrrole synthesis in ball mill (Estévez et al., 2013). .....	31
<b>Scheme 1.17.</b> Cu-catalyzed 1,3-dipolar cycloaddition of alkynes with azides forming substituted 1,2,3-tirazoles in a planetary mill (Thorwirth et al., 2011).....	31

<b>Scheme 1.18.</b> Cu/Al <sub>2</sub> O <sub>3</sub> catalyzed one-pot Click reaction in ball-milling for 1,2,3-triazoles derivative synthesis (Mukherjee et al., 2013). .....	32
<b>Scheme 1.19.</b> Mechanically activated pyrazole and pyridazinone synthesis (Lee et al., 2013). .....	32
<b>Scheme 1.20.</b> Quantitative condensations with o-phenylenediamine with 1,2-dicarbonyl compounds in ball milling conditions: (a) diphenylquinoxalines and (b) benzo[a]phenazin-1-ol (Kaupp and Naimi-Jamal, 2002). .....	33
<b>Scheme 1.21.</b> (a) benzo[a]phenazine and (b) 1-methylnaphth[2,3-d]imidazole obtained under mechanical action (Zefirov et al., 1996). .....	33
<b>Scheme 1.22.</b> Dibenzophenazines obtained by co-grinding of solid 1,2-diamines and 9,10-phenanthrenequinone (Carlier et al., 2011). .....	34
<b>Scheme 1.23.</b> Three-component reaction in milling devices: (a) (M'hamed and Alduaij, 2014); (b) (Mashkouri and Naimi-Jamal, 2009) .....	34
<b>Scheme 1.24.</b> Pyridazine and diazepine derivatives prepared by ball milling (Kaupp and Schmeyers, 2000). .....	35

## List of Tables

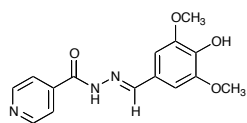
<b>Table 1.1.</b> C-C bond forming reactions reported under ball mills conditions. ....	21
<b>Table 1.2.</b> C-heteroatom bond formation in ball milling conditions. ....	26
<b>Table 2.1</b> HPLC conditions for DBPZ and DPQ kinetic monitoring. ....	61
<b>Table 3.1.</b> Heat released after grinding by the reactant powder mixture for DBPZ synthesis. ....	80
<b>Table 3.2.</b> Heat released after grinding by the reactant powder mixture for DPQ synthesis. ....	93
<b>Table 3.3.</b> Relevant solid phase data of the reactants used for DBPZ and DPQ mechanosynthesis. ....	100
<b>Table 4.1.</b> Mechanochemical systems that studied the kinetic aspects. ....	107
<b>Table 4.2.</b> Milling balls and bowls used for DPQ synthesis in the vibratory micro-mill Pulverisette 0 (P0). ....	114
<b>Table 4.3.</b> Rate constants for zero-order kinetic model as function of milling temperature ( $T_m$ ) and weight of the ball ( $m_{MB}$ ). ....	124
<b>Table 4.4.</b> Activation parameters using Arrhenius ( $E_a$ and $\ln A$ ) and Eyring equations ( $\Delta H^\ddagger$ , $\Delta S^\ddagger$ , $\Delta G^\ddagger$ ) for DPQ synthesis in P0. ....	130
<b>Table 5.1.</b> Reported examples of relevant biologically active hydrazones/hydrazides against <i>M. tuberculosis</i> . ....	153

<b>Table 5.2.</b> Solids aldehydes (column) and hydrazines (line) used for the synthesis of hydrazones and degree of conversion <sup>a</sup> for corresponding hydrazones for 4 hours of grinding as well as the yields <sup>b</sup> from classical method in parentheses. ....	160
<b>Table 5.3.</b> Minimum geometry (B3LYP/6-311+G(d,p)) and charge density of the –NH <sub>2</sub> group (NBO <sup>a</sup> , in brackets) of hydrazines.....	162
<b>Table 5.4.</b> Absolute density (g cm <sup>-3</sup> ) of the solid hydrazines .....	164
<b>Table 5.5.</b> The hydrazones produced by reacting isoniazid as hydrazine and imidazolic, indazolic or indolic aldehydes.....	169
<b>Table 5.6.</b> Energies of minima and transition state for <i>cis/trans-E</i> isomers of <b>1c</b> obtained at B3LYP/6-31+G(d,p) level in the gas phase and using DMSO polarizable continuum model (SMD).....	171
<b>Table 5.7.</b> Determination of activation energy ( $\Delta G^\ddagger$ ) from coalescence temperatures $T_c$ and rate exchange $k_{exch}$ at different chemical shifts for <b>1c</b> conformers.....	173
<b>Table 5.8.</b> Calculated and experimental <sup>1</sup> H chemical shifts for the <i>cis-E</i> and <i>trans-E</i> conformers of <b>1c</b> in DMSO, and the ratio from integration of the minor ( <i>cis-E</i> ) and major ( <i>trans-E</i> ) signals.....	173
<b>Table 5.9.</b> Calculated and experimental <sup>13</sup> C chemical shifts for the <i>cis-E</i> and <i>trans-E</i> conformers of <b>1c</b> in DMSO.....	174
<b>Table 5.10.</b> Geometries, Gibbs free energies and Boltzmann distribution the ( <i>E</i> ) conformers of <b>7d</b> at B3LYP/6-31+G(d,p) level in the gas phase and in the DMSO continuum solvent model (PCM).....	176
<b>Table 5.11.</b> Determination of activation energy ( $\Delta G^\ddagger$ ) from coalescence temperatures $T_c$ and rate exchange $k_{exch}$ at different chemical shifts for <b>7d</b> conformers. ....	177
<b>Table 5.12.</b> Calculated and experimental <sup>1</sup> H chemical shifts for the <i>cis-E</i> and <i>trans-E</i> conformers of <b>7d</b> in DMSO, and the ratio from integration of the minor ( <i>cis-E</i> ) and major ( <i>trans-E</i> ) signals.....	178
<b>Table 5.13.</b> Calculated and experimental <sup>13</sup> C chemical shifts for the <i>cis-E</i> and <i>trans-E</i> conformers of <b>7d</b> in DMSO. ....	179
<b>Table 5.14.</b> Phenolic hydrazones tested as inhibitory agents against <i>M. tuberculosis</i> growth (H <sub>37</sub> Rv strain) .....	181
<b>Table 5.15.</b> MIC of phenolic hydrazones isoniazid derivatives for MDR clinical isolate IC2. ....	182

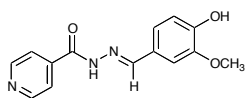
<b>Table 5.16.</b> Isoniazid-nitrogen heterocyclic hydrazones tested as inhibitory agents of <i>M. tuberculosis</i> growth (H <sub>37</sub> Rv strain). .....	182
<b>Table 5.17.</b> Percentage of InhA enzyme inhibition values for the isoniazid derivatives. ....	183
<b>Table 5.18.</b> Cytotoxicity (LD <sub>50</sub> ) and selectivity index (SI) for the most active hydrazones against H <sub>37</sub> Rv <i>Mtb</i> . .....	184
<b>Table 5.19.</b> Stability monitoring of hydrazones. ....	185
<b>Table 5.20.</b> Determine pKa of isonicotinoyl hydrazones .....	188
<b>Table A.I</b> Rate laws for reactions in solids. ....	220



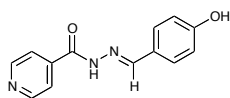
## STRUCTURES OF HYDRAZONES



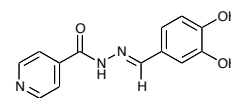
**1a**



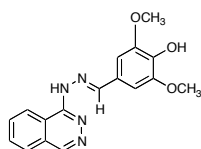
**1b**



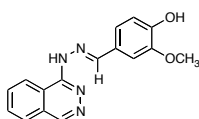
**1c**



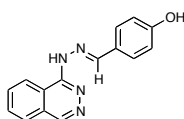
**1d**



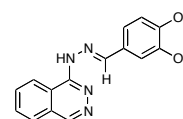
**2a**



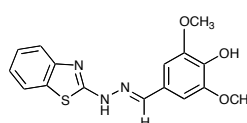
**2b**



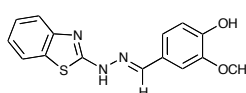
**2c**



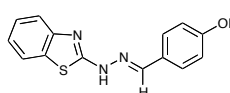
**2d**



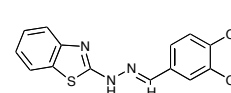
**3a**



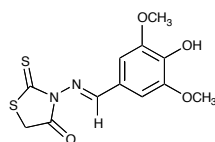
**3b**



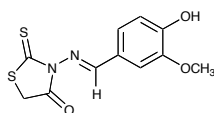
**3c**



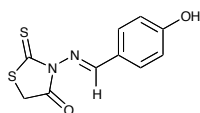
**3d**



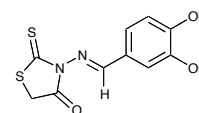
**4a**



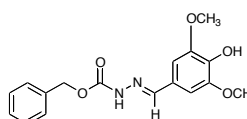
**4b**



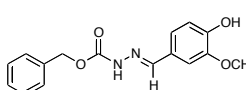
**4c**



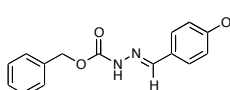
**4d**



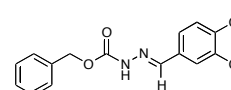
**5a**



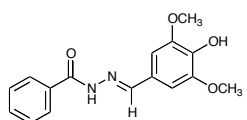
**5b**



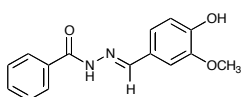
**5c**



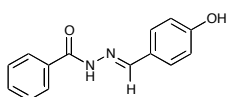
**5d**



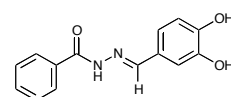
**6a**



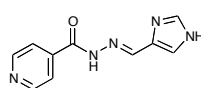
**6b**



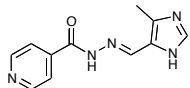
**6c**



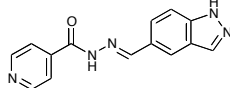
**6d**



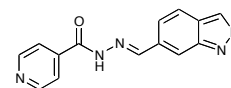
**7a**



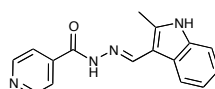
**7b**



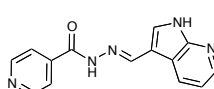
**7c**



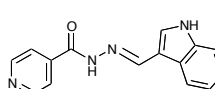
**7d**



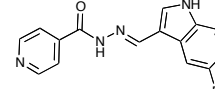
**7e**



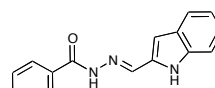
**7f**



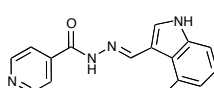
**7g**



**7h**



**7i**



**7j**





## **Investigation of mechanochemical synthesis of condensed 1,4-diazines and pharmaceutically attractive hydrazones.**

**Abstract.** One of the goals of pharmaceutical and chemical industries is the development of green processes that eliminates or reduces the use of solvents. However, avoiding solvents often requires the use of metal catalysts or others, that accelerates chemical reactions, but make the purifications difficult, especially in the case of fine chemical products, such as active pharmaceutical ingredients. The mechanochemistry has emerged as a sustainable way that enables chemical synthesis, including organic molecular transformations, using the mechanical energy. In spite of the recent advances of the methodology, some aspects of the mechanical action still remain to be fully elucidated, mainly concerning the mechanisms. In this thesis, three main axes of mechanochemistry were explored. First, the molecular mechanism of 1,4-diazine mechanosynthesis, mentioning dibenzo[a,c]phenazine (DBPZ) and 2,3-diphenylquinoxaline (DPQ), is investigated by using  $^{13}\text{C}$  CP-MAS NMR that reveals intermediate species for DBPZ, and by calorimetric measurements that show continuation of the reaction after grinding for both reactions. The possibility of a concerted mechanism is considered for dibenzo[a,c]phenazine case. The second focus is on 2,3-diphenylquinoxaline product formation. The process parameters for a vibratory ball mill were studied. Grinding material, size and mass of the balls, granulometry of the starting material were assessed, as well as the temperature of the milling media, providing apparent activation energy ( $E_a$ ). Arrhenius and Eyring-Polanyi plots presented changes in  $E_a$  indicating changes in mechanism, which was attributed to a possible mechanically induced eutectic melting after 30 °C. Finally, after understanding some fundamentals and processes for those model reactions, the mechanochemical route was successfully applied to solid-state synthesis of pharmaceutically attractive phenolic hydrazones and catalyzed isoniazid derivatives synthesis, by reacting solid aldehydes and hydrazines. In general, the products were obtained in shorter times and in higher yields compared to classical thermal route. The roles of electronic and solid-state reactivity of the hydrazines were discussed. Biological assays demonstrated the great activity of isoniazid derivatives in inhibiting *Mycobacterium tuberculosis*. The results presented here cover the mechanochemistry at different levels. The fundamental comprehension is still difficult to access due to the complexity of the system, but some advances could be made such as the detection of intermediate species with significant lifetime. The process parameters are equally important to deduce some mechanism, but also for scale up purposes. At last, the mechanosynthesis of hydrazones showed to be a greener route to produce pharmaceuticals, for high screening of new ones, as well as for the synthesis of others, with great purity and waste reduction.

**Keywords:** Green Chemistry, Mechanochemistry, Mechanism, Kinetics, 1,4-diazine, Hydrazone.